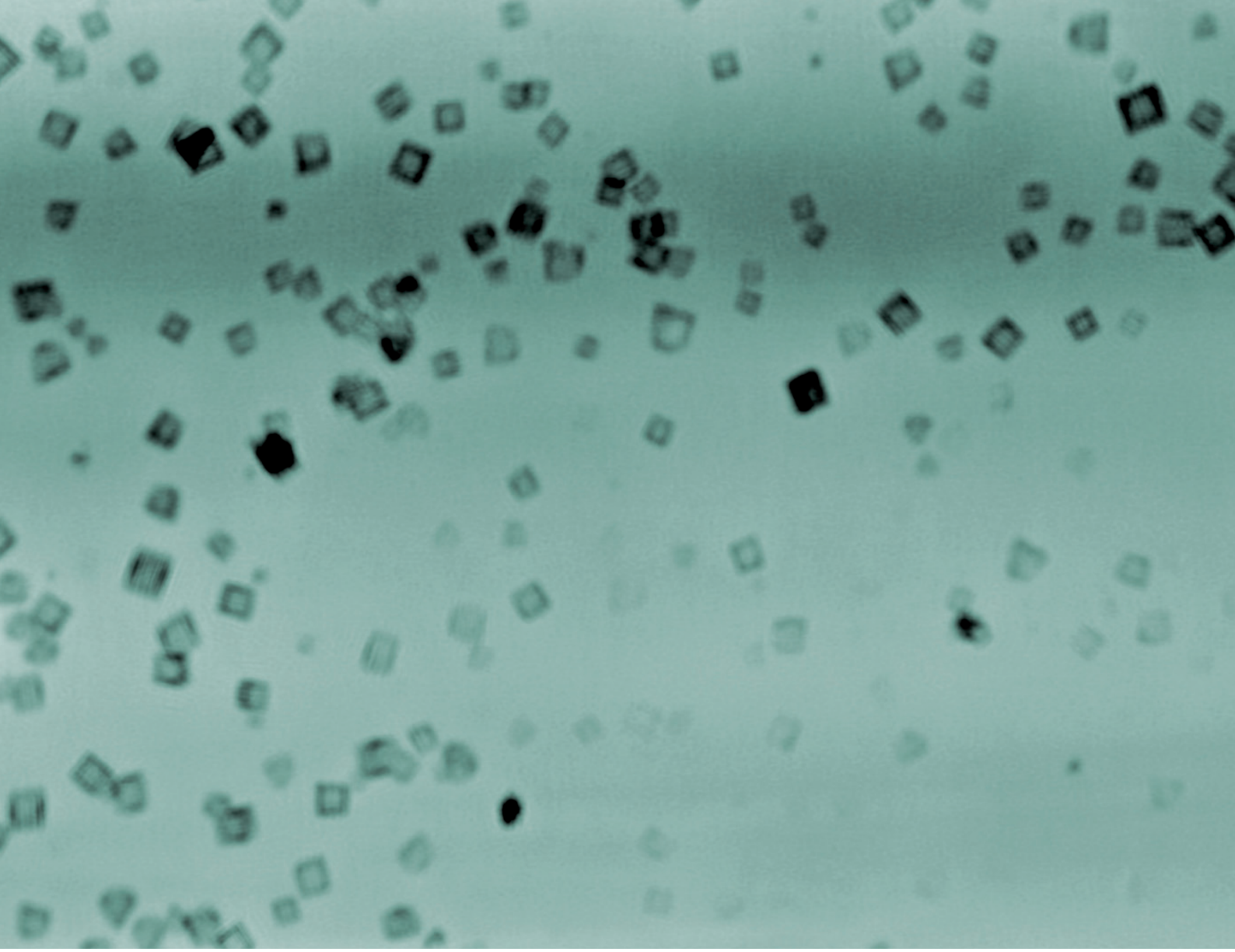

PHOTON SCIENCE 2022.

Highlights and Annual Report

Deutsches Elektronen-Synchrotron DESY
A Research Centre of the Helmholtz Association

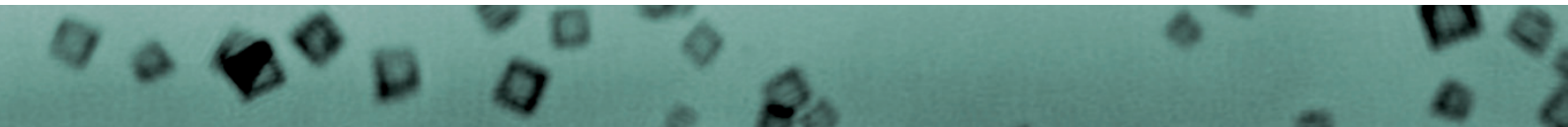

PHOTON SCIENCE 2022.

Highlights and Annual Report

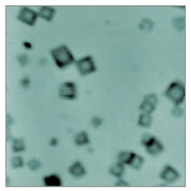

Cover

The cover picture shows hollowing of individual nanocubes at a spatial resolution of 66 nm and with a time resolution of about 20 min. Ptychography allows to reconstruct separate 2D images of nanocubes. These nanomaterials with well controllable shape are of particular interest in several fields of research, and the knowledge on their formation mechanism is essential for developing precise chemical synthesis routes (details see page 22).

Contents

Publications

The list of publications based on work done at DESY Photon Science is accessible online:
http://photon-science.desy.de/research/publications/list_of_publications/index_eng.html

DESY tries to keep this list complete and up-to-date and relies on the support by all users who are kindly requested to register their publications via DOOR (door.desy.de).

The year 2022 at DESY

Chairman's foreword

A look into the future: The DESY campus in Zeuthen with the SDMC building. (Visualisation: Heinle, Wischer und Partner | Freie Architekten)

Dear Colleagues and Friends of DESY,

The geopolitical conflict calls into question much of what we have hitherto taken for granted and poses enormous challenges to us. Our main concerns remain the suffering people in Ukraine and the families who have fled from the war which is now also affecting research at DESY. Our problems at the moment are the general uncontrolled price development on the energy market and in the construction sector and the enormous inflation trend as well as the shaky supply chains worldwide. All of this poses unprecedented challenges for the research centre that we have not previously known on this scale in Europe and beyond.

The DESY management has been working in crisis mode since the outbreak of the Covid pandemic in March 2020. In our current deliberations we assume that we will have another three very difficult years ahead of us and will therefore have to implement massive cost-cutting measures. This includes cuts in the operation of our major research infrastructures, if we do not get financial relief, and painful personnel decisions. Here, the DESY Directorate sees a particularly highly sensitive area in the next generation of scientists and engineers whom we must not abandon under any circumstances. However, we are not giving up hope that the German government will also focus more strongly on rescuing the nation´s future innovation potential. The current signals from politicians to set up a rescue package also for science give us cause for cautious optimism.

The Hamburg Senate had invited DESY to present the PETRA IV project at the city's town hall. Nobel Laureate Stefan Hell (left), Science Senator Katharina Fegebank and DESY Director Helmut Dosch (right).

In a high-tech nation like Germany, research and innovation are the decisive – if not the only – levers to lead us out of the crisis and secure our long-term sovereignty in key technologies. Against the background of the most acute problems in energy supply, we must not forget that the main threat to our survival on this planet is man-made climate change which we have to counter with new energy concepts. Nor must we lose sight of the constant threat of viral or bacterial pandemics. At DESY, we are all working at full steam to play our part in finding solutions to these complex challenges. This is also reflected in our strategy loop, on which we are currently working intensively – in addition to daily crisis management.

We have now identified three pillars for the future development of the research centre:

- the cross-divisional DESY Transformation Project (DTP) which is to prepare the future strategy of our "solution ecosystem" and which requires profound conceptual changes in how we organise research and innovation in the future,
- the National Analytics Center (NAC) with PETRA IV, FLASH2020+ and the Plasma Accelerator as well as an integrated data management structure as the core research infrastructures of the research centre and
- the increased focus in particle physics on medium-sized "dark matter" projects on the DESY campus and the exploration of the new opportunities that the Science Data Management Centre (SDMC) of the Cherenkov Telescope Array Observatory (CTAO) and the German Center for Astrophysics (DZA) offer in the field of astroparticle physics.

Sustainable concepts play a very central role in all planning. The Directorate has a clear vision for DESY's path towards energy-saving and climate-friendly operation. This year, we published our first sustainability report which will appear at regular intervals in the future.

In September, we presented the PETRA IV project, the upgrade of PETRA III to a 3D X-ray microscope, to a broader public with representatives from science, politics and industry at a major event. I was very pleased that the project was also supported by Professor Stefan Hell (MPI Göttingen and Heidelberg), Nobel Laureate and one of the world's most renowned representative of new microscopy concepts. In the evening of that event he gave an impressive talk in the great hall of Hamburg's City Hall, demonstrating the innovative power that new types of high-performance microscopes can unleash.

Under the leadership of Harald Reichert and Riccardo Bartolini, the preparation of the PETRA IV project continues to make great progress. The technical design is essentially complete, and the team is currently working on the application for the national roadmap for research infrastructures. PETRA IV will be a key building block in the transformation process of DESY we have been designing over the past few months. This involves not only the technical design of the facility which will be an interdisciplinary 'discovery and solution engine' that includes AI-assisted operations, an adopted new access model and the comprehensive involvement of the broad user community. Although this will increase construction and operational costs of the facility, the expected socio-economic impact will outweigh this investment many times over. In view of the competing Chinese High Energy Photon Sources (HEPS) project in Beijing for instance, which is already at an advanced stage, we must not lose any valuable time now in implementing it.

We have noted with great pleasure the positive decision from the Federal Ministry of Education and Research (BMBF) to realise the German Center for Astrophysics (DZA) which was prominently promoted by European Space Agency (ESA) and DESY. On the DESY side, Christian Stegmann and Arik Willner were instrumental in the application. This development is a new piece of the puzzle in our 2022/23 strategy loop which fits perfectly into DESY's aspiration to build an international lighthouse in astroparticle physics at its Zeuthen site.

It is gratifying to see that ALPS II is developing very well. We are currently working on implementing the campus projects BabyIAXO and LUXE also for Axion research. Under the given circumstances, this is a major challenge that we hope to master.

We live in difficult times and so does our research centre. Therefore, my special thanks go to the DESY staff and all our national and international users and partners for their reliable support at all times. I hope you can see from reading this annual report that, despite the current challenges that occupy us on a daily basis, we keep DESY on course for a bright future development!

Yours

Helmut Dosch
Chairman of the DESY Board of Directors

Photon Science at DESY

Introduction

In the foreground, the DESY site in Hamburg (September 2021).

Dear Colleagues and Friends of DESY Photon Science,

During the last three years we learned how to carry out experiments under the conditions of a pandemic in a safe and effective manner. I am very grateful to all DESY staff and the entire user community for their efforts to keep our science programs running and to adapt to our safety concepts. However, with the aggression of Russia against Ukraine, the geopolitical and economic situation has changed so dramatically that this might affect DESY's activities much more than the pandemic. Energy costs went up by large factors, such as it will not be possible to operate our facilities for the complete scheduled times for the next years without additional support by our funding bodies. In the meantime, the Federal Ministry of Education and Research (BMBF) has announced special crisis funds to cushion the rise in energy prices and there is some hope that this threat can be brought under control. Nevertheless, DESY might be asked to temporarily reduce its electricity consumption by pausing the operation of its accelerators for the unlikely event that the power grid might become unstable.
The energy price is not the only problem in this crisis. For example, the helium needed for the operation of our superconducting linear accelerator and for many low-temperature experiments has not only become extremely expensive but there are hardly any suppliers, who can deliver the required amounts. The same holds for neon. Furthermore, the price of liquid nitrogen, which is used to cool the X-ray monochromators at PETRA III and samples at the experiments, has also increased significantly, as has the price of many other consumables that we need to run our experiments. These cost increases and the anticipated increase of personnel costs will expose DESY and many other research institutions to severe financial pressure for the next years.

Despite these challenging circumstances, user operation at the synchrotron radiation source PETRA III was running quite smoothly with an availability of more than 98%. After officially finishing the PETRA III extension project in 2021, the design and construction of the remaining free undulator beamlines is still ongoing. Also, during this year for the first time we carried out pilot studies for new access modes. Users had the opportunity to submit proposals for which the immediate socio-economic impact in addition to scientific excellence was evaluated for allocating beamtime. In addition, a call for targeted challenge-driven proposals for molecular water science in the frame of the Center for Molecular Water Science (CMWS) was issued allowing users to apply for cooperative research projects using several different beamlines for a period of two years.

After extensive discussion of the science case and the beamline portfolio with the user community and DESY advisory bodies, the preparation of the proposal for the PETRA IV project, the upgrade of PETRA III, was continuously pushed forward in 2022. Harald Reichert, the former ESRF director for physical sciences, has taken over the project lead. Riccardo Bartolini is acting as deputy project head and is leading the accelerator part of the project. In September, the very successful kickoff meeting for the PETRA IV project took place.

The present timeline foresees to finalise the project proposal in the first quarter of 2023 and to present a full 'Technical Design Report' (TDR) by the end of 2023. The main goal of PETRA IV will be to deliver beams with unprecedented brightness in the hard X-ray regime. In addition, in a so called 'transformation project', DESY will also introduce new modes for the user access. The aim of this transformation is to provide more services to non-expert synchrotron radiation users starting from the planning of the experiment all the way through to the final data evaluation. This should come with a 'rolling access' scheme for faster access for both academic and industrial users during the whole year, which will be explored already at PETRA III in a pilot-phase.

Most of the year 2022, the free-electron laser FLASH was in shutdown for the first phase of the upgrade project FLASH2020+. In this time, two of the superconducting modules of the linear accelerator were replaced by ones with higher gradients. This should bring FLASH up to an electron energy of 1.35 GeV, enabling the produced light beams to cover the nitrogen K-edge with the first harmonic and all L-edges of the transition metals with the third harmonic. Despite the pandemic and supply chain issues, the shutdown work could be completed in time and user operation could start in November as planned. The second upgrade phase of the project is scheduled for mid 2024 to mid 2025. It will comprise the installation of tunable helical undulators and external seeding in FLASH1. Since the beginning of October, Markus Gühr, former Professor at the University Potsdam, has taken over the scientific leadership of the FLASH facility.

In April, the new building for the Center for X-ray and Nano-Science (CXNS) was inaugurated in presence of three German research ministers as well as other distinguished guests. This new office and laboratory building also houses the DESY outstation of Hereon, the Ruprecht-Haensel-Laboratory of the Christian-Albrechts-Universität zu Kiel (CAU Kiel), and colleagues from the Hamburg University of Technology (TU Hamburg) and the Leibniz-Institut für Kristallzüchtung (IKZ) in Berlin.

Scientists from DESY are contributing to three major user consortia at European XFEL. The SFX station has already been very productive for several years. Meanwhile, also the hRIXS and HiBEF experimental stations have started regular operation and are producing first exciting results.

Unfortunately, 2022 turned out to be even more difficult than the years before due to a significant change in the geopolitical and economic situation. Therefore, I would like to sincerely thank all who have contributed to excellent science in many ways for their commitment. Certainly, we still have 2-3 difficult years ahead of us, but I hope that we will manage them together in such a way that our science programs and the development of our young scientists and engineers are not seriously compromised.

Edgar Weckert
Director DESY Photon Science

News and Events

News and Events

A busy year 2022

January

26 January:
DESY Photon Science Users' Meeting 2022 – Online for the second time

From 21 to 28 January 2022, the DESY Photon Science Users' Meeting took place parallel with the users' meeting of the European XFEL. In total, more than 2000 researchers from all over the world registered to join the online event to discuss latest research results and to learn about new developments at DESY Photon Science and its facilities. At the meeting, the directors of the two centres presented a 'Joint Declaration of DESY and European XFEL', with which the two research centres want to put themselves even more at the service of solving acute societal problems, such as climate change or the Corona pandemic.

February

16 February:
Junior professorship for Andrea Trabattoni

There are very few people in the world who take a stab at watching and manipulating nuclear transitions by exploiting the surrounding electrons and tailored lasers. DESY's Helmholtz Young Investigators Group leader Andrea Trabattoni is one of them. He accepted a call as junior professor in Ultrafast Photoelectron Science at Leibniz University Hannover where he will join forces with their Ultrafast Laser Lab at the Institute of Quantum Optics. The research field Trabattoni and his colleagues are working on is extremely ambitious – but very promising. The ultimate goal is to use lasers to control and manipulate electrons in processes connected with atomic nuclei.

March

14 March:
Journal designated Christoph Heyl an 'Emerging Leader'

Christoph Heyl, junior research group leader at DESY and the Helmholtz-Institute Jena, has been identified by the Editorial Board of JPhys Photonics as one of the most exciting researchers in his generation in the field of photonics. Every year the different members of the Journal of Physics group invite works from the best early-career researchers to be published in an 'Emerging leader' special issue. Christoph Heyl's invited contribution, titled 'High-energy bow tie multi-pass cells for nonlinear spectral broadening applications', describes how to overcome pulse energy limitation of novel laser concepts based on multi-pass cells (MPCs) by introducing a novel MPC geometry. Christoph Heyl and his team are using MPCs for spectral broadening and temporal compression of ultrashort laser pulses.

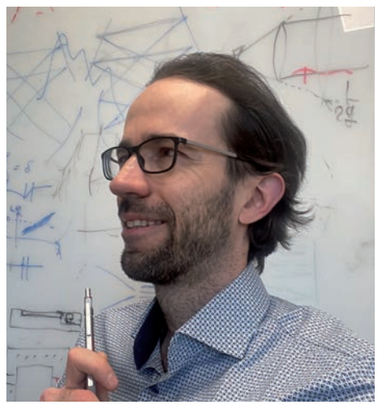

18 March:
WE-Heraeus seminar on Novel Light Sources

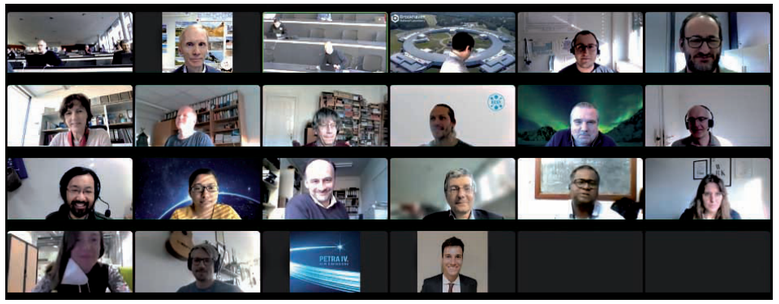

More than 90 researchers from universities and research institutions throughout many countries worldwide attended the 762th WE-Heraeus seminar on 'Diffraction Limited Synchrotron Light Sources and Next Generation Free Electron Lasers'. It took place at the Physikzentrum in Bad Honnef in Germany from 7 to 11 March 2022. This WE-Heraeus seminar – in a hybrid format – addressed the scientific opportunities opened by modern accelerator-based light sources as well as the technical issues, both on the side of the accelerators and the experiments, in order to develop this field even further. The scientific organisers were Robert Feidenhans'l (European XFEL), Wim Leemans and Edgar Weckert (DESY).

28 March:
SRI conference kicks off virtually with more than 1160 participants

The SRI 2021 was back in Hamburg after 40 years, albeit virtually. Scientists from all over the world have been meeting every three years since 1982 for the SRI – the International Conference on Synchrotron Radiation Instrumentation. At one of the largest exchange forums in this field of research, participants discuss the latest developments in technologies, instrumentation, and research. SRI 2021 had originally been scheduled to take place in summer 2021 in Hamburg. However, due to the pandemic, it was postponed until spring 2022. With the pandemic still not over, the organisers and the international conference committee took the difficult decision not to postpone the conference again, but to hold it online instead.

April

6 April:
SAXFELS project receives funding from the Röntgen-Ångström Cluster

Charlotte Uetrecht is an expert in viruses, and on how they assemble and replicate. The new group leader at the Centre for Structural Systems Biology (CSSB) together with collaborators Erik Marklund from Uppsala University and Carl Caleman from Uppsala University and DESY (CFEL) will receive funding from the Röntgen-Ångström Cluster (RÅC), a Swedish-German research collaboration, for their Small Angle X-ray Free Electron Laser Scattering (SAXFELS) project. This four-year project, with a combined funding of 1.75 million Euro, will develop a new method for examining macromolecular structures by integrating and developing powerful techniques for gas-phase sample manipulation with X-ray diffraction imaging.

12 April:
Three research ministers open Centre for X-ray and Nano Science at DESY

A symbol of cutting-edge research: no fewer than three research ministers opened the Centre for X-ray and Nano Science (CXNS) at DESY on 12 April 2022. Federal Research Minister Bettina Stark-Watzinger, Hamburg's Science Senator Katharina Fegebank and Schleswig-Holstein's Minister of Education Karin Prien handed over the keys to the new multistate research building to its new occupants: Kiel University (CAU), the Helmholtz Centre Hereon and DESY. The CXNS is a multi-institutional, interdisciplinary platform for research using X-rays in combination with nano and material sciences and is one of a kind.

14 April:
Nature's handedness in the focus of free-electron lasers

A research collaboration led by Markus Ilchen and Sadia Bari (both DESY) and Swedish researchers Vitali Zhaunerchyk (Gothenburg University) and Mats Larsson (Stockholm University) has received approximately 1.5 million Euro for four years from the Röntgen-Ångström Cluster (RÅC), a Swedish-German science collaboration. The team will use the funding to use free-electron lasers to get closer to the mystery of nature's handedness and its dynamics on timescales of electron movements.

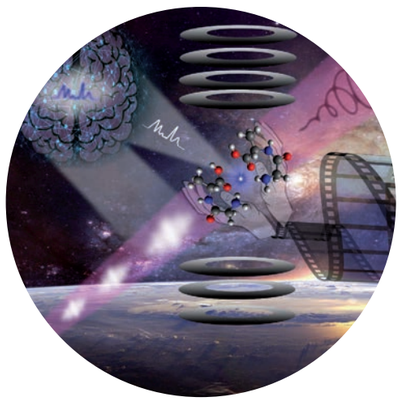

June

13 June:
Royal honour for DESY scientist Henry Chapman

Henry Chapman, DESY lead scientist at CFEL, has received the 2021 Gregori Aminoff Prize for Crystallography from the hands of Sweden's King Carl XVI Gustaf. Aminoff Prize winners from three years were honoured at the ceremony in Stockholm's City Hall, where the annual Nobel Prize banquet is also held. Because of the Corona pandemic, the presentation had to be postponed each time. Henry Chapman, who is also a professor at the University of Hamburg and a member of the Hamburg Cluster of Excellence 'CUI: Advanced Imaging of Matter', was awarded by the Royal Swedish Academy of Sciences together with Janos Hajdu from the University of Uppsala and John Spence from Arizona State University 'for pioneering contributions to the development of structural biology at free-electron X-ray lasers'.

14 June:
Inauguration of the Helmholtz Experimental Station at the X-ray source SESAME in Jordan

A new experimental station has been opened at the SESAME X-ray source in Jordan: the Helmholtz-SESAME Beamline (HESEB) had been designed by five research centres of the Helmholtz Association under the leadership of DESY and considerably extends the experimental possibilities of the facility. It will make so-called soft X-ray light available for research at SESAME, which has less energy than hard X-rays. The project involves Forschungszentrum Jülich, Helmholtz-Zentrum Berlin, Helmholtz-Zentrum Dresden-Rossendorf, Karlsruhe Institute of Technology and DESY.

24 June:
Academy of Sciences and Humanities in Göttingen appoints Melanie Schnell as member

Melanie Schnell, Lead Scientist at DESY and Professor of Physical Chemistry at Kiel University, has been appointed a full member of the 'Mathematical and Natural Sciences Class of the Göttingen Academy of Sciences and Humanities'. She shares this honour with three other scientists from very different disciplines. Every one of them is regarded as a world-wide expert in their field. The ceremony to welcome the new members took place on 24 June 2022 in Göttingen. Melanie Schnell is working to understand chemical processes at the molecular level with the objective to eventually control and manipulate these processes.

August

12 August:
Students from around the world try their hands at real research

After a cancellation in 2020 and one year of a very restricted hybrid summer student programme, a total of 84 students from around the world took part in this year's 'DESY summer student course' – either in person or remotely. The students spent 7.5 weeks working on real research projects with DESY supervisors from different research areas, including particle and astroparticle physics, photon science and accelerator physics.

29 August:
DESY scientist Sebastian Trippel has been awarded the Zdenek Herman MOLEC Young Scientist Prize

Sebastian Trippel has been awarded the 'Zdenek Herman MOLEC Young Scientist Prize' at the 'European Conference on the Dynamics of Molecular Systems' (MOLEC 2022) for his work on 'Electric-field control of molecular clusters and the imaging of their chemical dynamics'. Established in 2016, the prestigious prize is named after the pioneering scientist Zdeněk Herman (1934-2021) and is awarded to the top young scientists in the field of molecular dynamics. At the same event, the 'MOLEC Senior Prize' was awarded to Professor Javier Aoiz from Universidad Complutense de Madrid in Spain for his seminal contributions to the theoretical description of elementary chemical reactions.

September

15 September:
PETRA IV – Setting out into a new era of research and innovation

The world's best X-ray microscope is to be built in Hamburg. The upgrade of PETRA III to PETRA IV will provide 3D images of the nanocosm and offer insights into materials and biological structures with unprecedented precision – from the structure of pathogens, through catalysts, to innovative microchips and quantum materials. The Hamburg Senate had invited DESY to present the project at the city's town hall. Representatives from science, politics and industry attended this major event.

19 September:
Science@FELS 2022 held at European XFEL

The 2022 Science@FELs conference was held at DESY and European XFEL in Hamburg in September 2022 and was attended by more than 100 participants from 12 countries. It is held every two years by FELs of Europe, a collaboration of all free-electron laser facilities in Europe, and has evolved into one of the most important international meetings in FEL science. This year also marks the 10th anniversary of the FELs of Europe collaboration.

October

1 October:
Markus Gühr became Leading Scientist of FLASH

On 1 October 2022, Markus Gühr started as lead scientist of the free-electron laser FLASH. Jointly appointed professor with the Faculty of Chemistry at the Universät Hamburg, the X-ray laser expert will then be in charge as a lead scientist at DESY and responsible for the fortunes of the world´s first SASE X-ray laser, which has been operating as a user facility since 2005 and is currently being made future-proof with the FLASH2020+ expansion project.

10 October:
Official handover finally possible: Francesca Calegari received the ICO prize 2017

Francesca Calegari, lead scientist at DESY and Professor at the Universität Hamburg, received the prestigious ICO Prize 2017 of the International Commission for Optics (ICO). Due to the pandemic, the official handover had to be postponed and could finally take place during the ICO-25-OWLS-16 Congress (5-9 September 2022) in Dresden, Germany. She was awarded the prize 'for her innovative and pioneering research on the generation of isolated XUV attosecond pulses at the nJ-energy level and their application to the study of the electron dynamics in complex molecules'.

November

2 November:
Theory meets FELs workshop

X-ray free-electron lasers (XFELs) offer state-of-the-art capabilities for experimental research with X-rays. Modern theory and simulations play an essential role here as they are not only applied to explain the experimental observations but they are also instrumental to generate new ideas for designing new experiments. The aim of the Workshop 'Theory meets XFELs' held at DESY and European XFEL was to foster collaborations between theorists and experimentalists interested in research with XFELs.

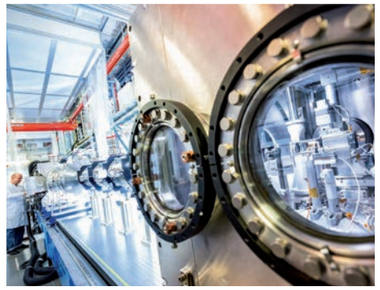

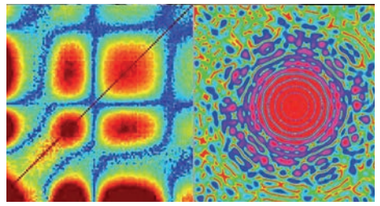

15 November:
Hamburg scientists win the Norddeutschen Wissenschaftspreis 2022

The 'Norddeutscher Wissenschaftspreis' 2022 was awarded on 15 November 2022 in Hamburg. The first prize, worth 150,000 Euro, goes to the 'CIMMS' joint project. The project networks national research in the field of materials science in a research approach that is unique in Germany: scientists from the Technical University of Hamburg, the Universität Hamburg, DESY and the Helmholtz Center Hereon conduct research together. The joint project 'Homeo-Hirn' from the Technical University of Braunschweig received the second prize of 100,000 Euro. The award is presented every two years by the North German Science Ministers' Conference (NWMK).

16 November:
Saša Bajt has been awarded the DESY Innovation Award 2022

DESY researcher Saša Bajt has been awarded the DESY Innovation Award 2022 for her outstanding contributions to extreme ultraviolet and X-ray optics. Already in December 2021, she was awarded one of the highest national prizes of the Republic of Slovenia for her scientific achievements and her intensive collaboration with researchers and students from Slovenia: the title 'Ambassador of Science of the Republic of Slovenia'.

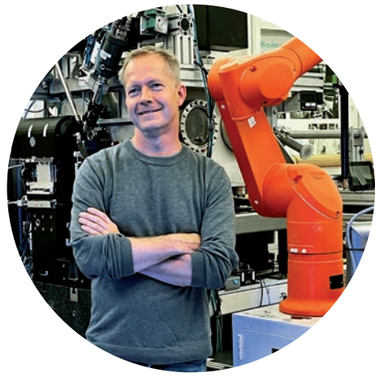

16 November:
Alke Meents has been awarded the Bjørn H. Wiik Prize 2022

During the early stages of the pandemic, the DESY physicist Alke Meents had already launched a promising and internationally acclaimed research project at DESY's X-ray source PETRA III in search of a drug against Covid. This year, Alke Meents is being awarded the Bjørn H. Wiik Prize for his achievement that goes far beyond this project alone.

December

5 December:
Laser Prize for Franz Kärtner

DESY researcher Franz Kärtner has been awarded the Laser Instrumentation Award by the Institute of Electrical and Electronics Engineers (IEEE). The group leader at the Center for Free-Electron Laser Science (CFEL) at DESY is being recognised for his techniques for synchronising large research facilities with femtosecond precision, the IEEE Photonics Society explained.

Science Highlights

Hot electrons driving change in magnetic order

The sub-picosecond metamagnetic phase transition in FeRh

Phase transitions are present in many aspects of condensed matter physics: from water freezing to the formation of Cooper pairs in a super-conductor. Their macroscopic phenomenology is linked to microscopic properties like atomic forces and electronic structure. Magnetism is intrinsically bound to the concept of phase transitions: an established ferromagnetic order can be destroyed simply by increasing the system temperature. In peculiar cases, temperature promotes the change of magnetic order. Metallic FeRh undergoes a metamagnetic first-order phase transition from antiferromagnetic to ferromagnetic order at 360 K, with coupled structural, magnetic and electronic order parameters. We show that the phase transition triggered by ultrafast laser pulses is complete within 300 fs from the electronic structure perspective.

The originality of our approach consists in tracing the antiferromagnetic (AFM) or the ferromagnetic (FM) orders by directly exploiting specific features of the electronic structure. Those manifest in terms of spin unbalance and the appearance of majority and minority spin bands in the electronic structure [1]. This is independent of spin alignment along a particular direction, and thus allows inspecting FM order via valence band photoemission [2]. The fingerprint of the FM phase in FeRh consists of a narrow peak in the electronic density of states, located about 150 meV below the Fermi energy E_F (Fig. 1). We used the state-of-art momentum microscope (HEXTOF end station) to perform pump-probe experiments at the monochromatised PG2 beamline of the FLASH free-electron laser (FEL) using near-infrared (800 nm, 1.55 eV) pulses of 90 fs coupled with 130 fs soft X-ray pulses with a photon energy of $\hbar\omega = 123.5$ eV.

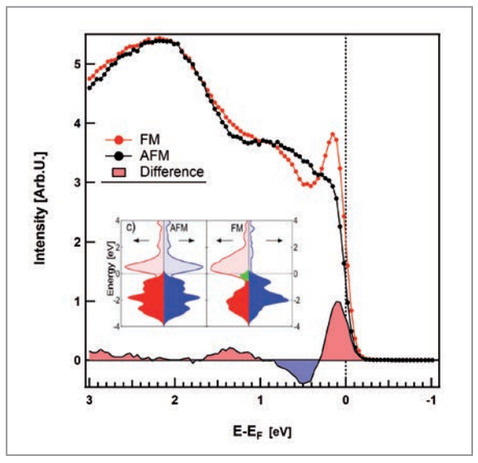

Figure 1

Measured X-ray photoelectron spectra of FeRh in the AFM (black dots) and FM (red dots) phase. The solid curve at the bottom of the graph is the difference between the two spectra which allows to appreciate the relative electron density change across the transition. The data correspond to quasi-static thermal cycling experiments prior to the time-resolved measurements. Inset: Calculated spin-resolved electronic density of states in the AFM and FM phases. The filled areas represent the electronic occupation at thermal equilibrium, with the green area highlighting the position of the Fe minority band.

We measured electron energy distribution curves (EDC) as a function of the delay between the optical pump and X-ray probe pulses (Fig. 2a). One can clearly identify the temporal overlap between the optical and X-ray pulses (about 100 fs around t_0) where the electrons are excited into unoccupied states. The relaxation of electrons toward the Fermi energy and the subsequent changes in the electron density near the Fermi level at different time delays are better identified from the differential matrix, presented in Fig. 2b. We selected three energy ranges marked by the red, blue and black bars placed on the right-hand side of Fig. 2b. The first (red) identifies the total number of electrons injected into the unoccupied states upon photoexcitation. The second (blue) monitors the formation of the Fe-minority peak across the phase transition, and the third (black) follows the modification of deeper bands. The time evolution of the integrated signals in each range is shown in Fig. 2c. The injection of electrons into the unoccupied states takes place near zero delay and then rapidly decays (red empty circles), the process being finished by about 500 fs. The data represented by black diamonds in Fig. 4c nearly mirror the population of the unoccupied levels up to 300 fs, with a fast depletion and recovery. The curve stabilises thereafter at a finite value, implying permanent modifications of the deeper bands after 300 fs, already, during which the Fe minority peak is still shifting toward its final position at 150 meV below E_F. The intensity at the position of the Fe-minority peak starts to grow as early as the laser excitation (filled blue circles), due to both the modification of the electronic structure and the Fermi level smearing. More specifically, this modest intensity growth starting at t = 0 is linked to the presence of an instantaneous increase in the density of states peaking right above the Fermi level and can be considered as a precursor of the FM phase. However, it is only about 300 fs after the excitation that the electronic density corresponding to the minority band peak displays a sharp increase, associated with a persistent band structure modification. So far this established the fastest timescale related to the meta-magnetic phase transition in FeRh.

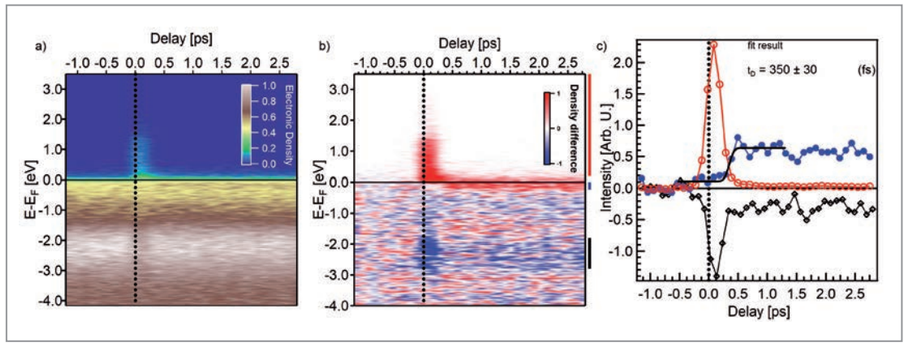

Figure 2

a) Energy- and delay-dependent matrix of the measured spectra. The appearance of electronic density above the Fermi level indicates the laser excitation of hot electrons. b) Energy- and delay-dependent differential matrix. We subtracted the average of unpumped spectra (between −1 ps and −0.5 ps) from each measured spectrum. The laser-induced increase in the electronic density close to the Fermi level is observed at positive time delays. The red, blue and black bars on the right-hand side mark the representative integration regions for tracking the electronic dynamics. c) Temporal evolution of the electronic density in the three characteristic energy regions marked in b). The electronic density slightly below E_F (filled blue circles) shows a pronounced increase due to the change in the magnetic order at a time delay of 350 fs. After this delay the FM phase is established.

Time-dependent density functional theory calculations of the electronic structure of FeRh [3] are used to interpret the laser-induced dynamics near the zero-time delay. In particular, they suggest that a significant charge and spin transfer from the Fe atoms toward the Rh ones, together with intra-atomic electron redistributions, are the ultimate origin of the phase transition. The overall very good agreement between theory and experiment indicates that the changes in the band structure are as important as changes in the electron population for describing ultrafast dynamics of phase transitions.

Our findings supported by theoretical calculations demonstrate that the microscopic manifestation of this magnetic first order phase transition resides in particular features of the electronic structure. During the ultrafast laser pumping, hot electron excitation triggers a significant charge and spin redistribution, resulting in the establishment of the FM phase. Our proposed explanation of this process can potentially be used to interpret similar phase transitions involving a magnetic order change in metallic systems.

Author contact:
Federico Pressacco, federico.pressacco@desy.de
Davide Sangalli, davide.sangalli@ism.cnr.it
Vojtěch Uhlíř, vojtech.uhlir@ceitec.vutbr.cz
Fausto Sirotti, fausto.sirotti@polytechnique.edu

References

1. F. Pressacco et al., 'Stable room-temperature ferromagnetic phase at the FeRh (100) surface', Sci. Rep. 6, 22383 (2016).
2. F. Pressacco et al., 'Laser induced phase transition in epitaxial FeRh layers studied by pump-probe valence band photoemission', Struct. Dyn. 5, 034501 (2018).
3. D. Sangalli and A. Marini, 'Ultra-fast carries relaxation in bulk silicon following photo-excitation with a short and polarized laser pulse', Europhys. Lett. 110, 47004 (2015).

Original publication

'Subpicosecond metamagnetic phase transition in FeRh driven by non-equilibrium electron dynamics', Nature Communications 12, 5088 (2021). DOI: 10.1038/s41467-021-25347-3

Federico Pressacco[1,2], Davide Sangalli[3,4], Vojtěch Uhlíř[5,6], Dmytro Kutnyakhov[2], Jon Ander Arregi[5], Steinn Ymir Agustsson[7], Günter Brenner[2], Harald Redlin[2], Michael Heber[2], Dmitry Vasilyev[7], Jure Demsar[7], Gerd Schönhense[7], Matteo Gatti[4,8,9], Andrea Marini[3,4], Wilfried Wurth[1,2] and Fausto Sirotti[9,10]

1. The Hamburg Centre for Ultrafast Imaging (CUI), Universität Hamburg, Hamburg, Germany
2. Deutsches Elektronen-Synchrotron DESY, Hamburg, Germany
3. CNR-ISM, Division of Ultrafast Processes in Materials (FLASHit), Monterotondo, Italy
4. European Theoretical Spectroscopy Facility (ETSF) https://www.etsf.eu/
5. CEITEC BUT, Brno University of Technology, Brno, Czech Republic
6. Institute of Physical Engineering, Brno Univ. of Technology, Brno, Czech Republic
7. Johannes Gutenberg Universität, Institute of Physics, Mainz, Germany
8. LSI, CNRS, CEA/DRF/IRAMIS, École Polytechnique, IP Paris, Palaiseau, France
9. Synchrotron SOLEIL, L'Orme des Merisiers, Gif-sur-Yvette, France
10. Laboratoire PMC, CNRS and École Polytechnique, IP Paris, Palaiseau, France

Size matters in functional materials

Transition from insulating to metallic phase occurs earlier near the microstructure edges

Smart devices of tomorrow will be small and exploit quantum phenomena for novel functionalities. Promising candidates for these devices are compounds which undergo an insulator-metal transition (IMT). The change of properties accompanying this transition can, for example, be used to switch electric currents or to selectively transmit optical pulses for modern communication. But do the characteristics of the IMT remain the same as those of the bulk if a material is patterned on the micro- or nanoscale? Here, we present an investigation of the IMT of microstructured vanadium dioxide (VO_2) to answer the question whether the transition occurs homogeneously throughout an entire thin-film micro square.

This study exploits a novel experimental setup for imaging soft X-ray absorption spectroscopy with a resolution down to 2 µm at the PETRA III beamline P04 [1]. Incoming X-rays are focused to an approximately 500 µm long line, illuminating several of the VO_2 microsquares (see Fig. 1), each measuring (30 × 30) µm^2. X-ray fluorescence from these squares is imaged and dispersed by an off-axis Fresnel zone plate onto a 2D CCD detector. The zone plate is designed so that it resolves the spatial structure of the sample along the illuminated line onto one dimension of the detector while dispersing the photons emitted from the sample along the orthogonal direction. From the total number of emitted photons per excitation energy, we obtain partial fluorescence yield absorption spectra.

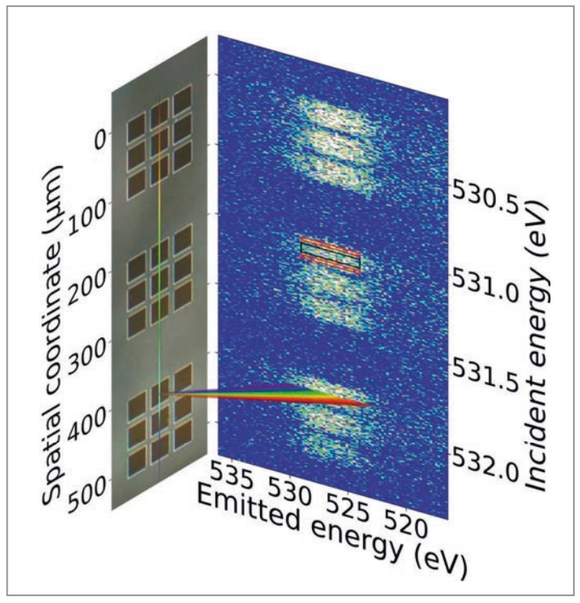

Figure 1

Soft X-ray imaging absorption spectroscopy of VO_2 microstructures. The sample consisting of (30 × 30) µm^2 VO_2 structures on an Al_2O_3 substrate is shown on the left. The vertical rainbow-coloured line symbolises the incident X-ray line focus along which the photon energy varies. The horizontal rainbow fan symbolises X-ray (oxygen *K*-edge) fluorescence from the sample which is dispersed across the detector (shown on the right). The coupling of imaging and spectroscopy is also apparent on the exemplary detector image on the right: spatial information is encoded on the vertical axis, emitted X-ray energy (spectroscopic information) on the horizontal. (Figure adapted from original publication licensed under CC-BY 4.0.)

The IMT in VO_2 occurs at temperatures around 70 °C, which is conveniently close to room temperature for various applications. Upon heating across the transition temperature T_t, the electronic structure around the Fermi level changes which can be tracked with X-ray absorption spectroscopy (XAS): The shift of the π* bands to lower energies can be observed as a red-shift, and the $d_\parallel$ feature disappears [2]. Around the transition temperature T_t, both metal and insulating phases coexist in domains with lateral sizes of a few hundred nanometres [3].

The X-ray absorption spectra acquired from (30 × 30) µm^2 VO_2 squares (see Fig. 2) provide a measure for the average fraction of metallic phase present at a given experimental temperature. Figure 2 shows the spectra extracted from centre and edge regions (highlighted in Fig. 1 with black and red rectangles, respectively). In total, the signal from five different VO_2 microsquares was averaged. Using published data as a reference [4], the characteristic changes in the XAS spectra were related to a metallic fraction at a given temperature. Thus, an average metallic fraction for each temperature could be derived for the centre and edge regions, which is shown in Fig. 3 in black and red, respectively. It is apparent that the metallic fraction in the edge regions is consistently above that in the centre regions of the VO_2 microsquares, proving that the edge regions progress earlier through the phase transition in comparison to the centre regions.

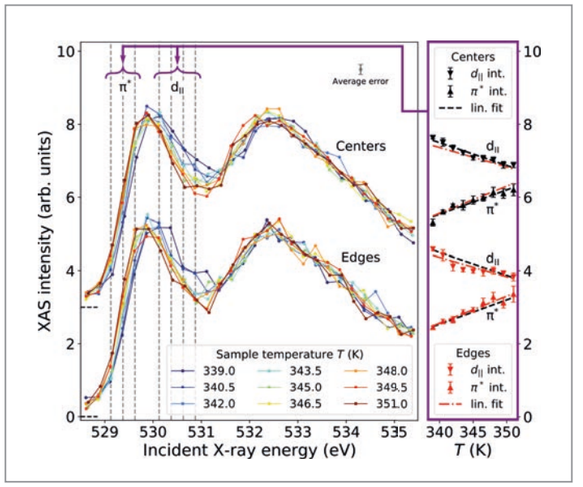

Figure 2

X-ray absorption spectra from VO_2 micro square centre and edge regions allow tracking the progression of the insulator-metal transition with few-micrometre precision. The degree of red-shift of the π* edge and the intensity at the $d_\parallel$ shoulder are a direct measure for how far the phase transition has progressed. (Figure adapted from original publication licensed under CC-BY 4.0.)

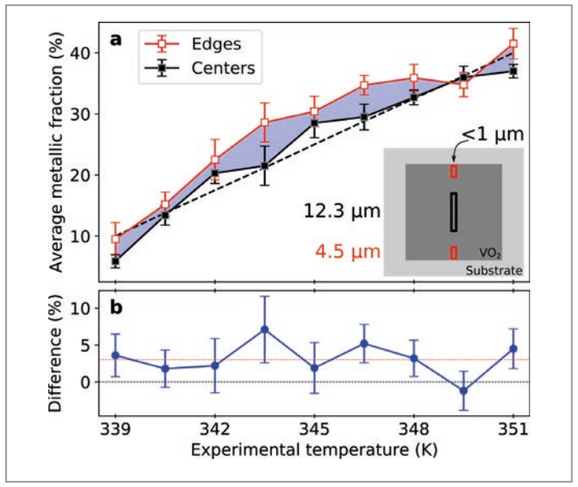

Figure 3

Metallic fraction extracted from edge (red) and centre (black) regions of (30 × 30) µm^2 VO_2 structures at temperatures around the insulator-metal transition (see text). The difference (blue) indicates that the edge regions have on average proceeded further along the phase transition at a given temperature. (Figure adapted from original publication licensed under CC-BY 4.0.)

Importantly, the edge regions of the squares, from which the XAS signal was integrated, measure 4.5 µm. We can thus exclude any effects which are limited to a few layers on the surface, like e.g. increased defect density on the surface. However, during the phase transition, strain builds up due to the lattice rearrangement. We propose that this strain is more easily released close to the edge regions of the microsquares and relaxes the lattice across micrometre dimensions. This might be responsible for promoting the phase transition near the edges at lower temperatures.

To conclude, we found that the IMT in VO_2 proceeds earlier at the edges of thin-film microsquares. This demonstrates that properties of quantum materials may change upon downscaling and highlights the importance of experimental methods which can be conducted to study electronic properties on micrometre length scales.

Author contact: Jan O. Schunck, jan.schunck@desy.de
Martin Beye, martin.beye@desy.de

References

1. J. O. Schunck, F. Döring, B. Rösner, J. Buck, R. Y. Engel, P. S. Miedema, S. K. Mahatha, M. Hoesch, A. Petraru, H. Kohlstedt, C. Schüssler-Langeheine, K. Rossnagel, C. David and M. Beye, 'Soft x-ray imaging spectroscopy with micrometer resolution', Optica 8, 156-160 (2021).
2. M. Abbate, F. M. F. de Groot, J. C. Fuggle, Y. J. Ma, C. T. Chen, F. Sette, A. Fujimori, Y. Ueda and K. Kosuge, 'Soft-x-ray-absorption studies of the electronic-structure changes through the VO_2 phase transition', Phys. Rev. B 43, 7263–7266 (1991).
3. M. M. Qazilbash, A. Tripathi, A. A. Schafgans, B.-J. Kim, H.-T. Kim, Z. Cai, M. V. Holt, J. M. Maser, F. Keilmann, O. G. Shpyrko and D. N. Basov, 'Nanoscale imaging of the electronic and structural transitions in vanadium dioxide', Phys. Rev. B 83, 165108 (2011).
4. P. T. P. Le, K. Hofhuis, A. Rana, M. Huijben, H. Hilgenkamp, G. A. J. H. M. Rijnders, J. E. ten Elshof, G. Koster, N. Gauquelin, G. Lumbeeck, C. Schüßler-Langeheine, H. Popescu, F. Fortuna, S. Smit, X. H. Verbeek, G. Araizi-Kanoutas, S. Mishra, I. Vaskivskyi, H. A. Dürr and M. S. Golden, 'Tailoring Vanadium Dioxide Film Orientation Using Nanosheets: a Combined Microscopy, Diffraction, Transport, and Soft X-Ray in Transmission Study', Adv. Funct. Mater. 30, 1900028 (2020).

Original publication

'Microstructure effects on the phase transition behavior of a prototypical quantum material', Scientific Reports 12, 10464 (2022). DOI: 10.1038/s41598-022-13872-0

Jan O. Schunck[1,2], Florian Döring[3], Benedikt Rösner[3], Jens Buck[4,5], Robin Y. Engel[1,2], Piter S. Miedema[1], Sanjoy K. Mahatha[5,6], Moritz Hoesch[1], Adrian Petraru[6], Hermann Kohlstedt[6], Christian Schüßler-Langeheine[7], Kai Rossnagel[1,4,5], Christian David[3] and Martin Beye[1,2]

1. Deutsches Elektronen-Synchrotron DESY, Hamburg, Germany
2. Department of Physics, Universität Hamburg, Hamburg, Germany
3. Paul-Scherrer-Institut PSI, Villigen, Switzerland
4. Institut für Experimentelle und Angewandte Physik, Christian-Albrechts-Universität zu Kiel, Kiel, Germany
5. Ruprecht Haensel Labor, Christian-Albrechts-Universität zu Kiel, Kiel, Germany
6. Nanoelektronik, Technische Fakultät, Christian-Albrechts-Universität zu Kiel, Kiel, Germany
7. Helmholtz-Zentrum Berlin für Materialien und Energie, Berlin, Germany

Imaging Cu_2O nanocube hollowing in solution

In situ X-ray ptychography reveals the shape of nanoparticles in 3D

Nanomaterials with well controllable shape are of particular interest in several fields of research, and the knowledge on their formation mechanism is essential for developing precise chemical synthesis routes. In many cases, however, understanding and manipulating the course of the underlying morphological changes remains a major challenge. The main difficulty is to observe the latter *in situ* in a bulk solution under relevant conditions, such as high temperature and pressure. Visual insights into the formation dynamics of nanomaterials are thus rare. Even though liquid-cell transmission electron microscopy (TEM) can provide spatial resolution down to the atomic scale, its applicability to solution-based processes is limited to thin layers of liquid. Here, we demonstrate the applicability of X-ray ptychography for in-solution imaging, overcoming the limitations of *in situ* TEM. Using the 'Ptychographic Nanoanalytical Microscope' (PtyNAMi) [1] at the PETRA III beamline P06, we observe the growth and hollowing of Cu_2O nanocubes inside a chemical reactor with a thickness of 1 mm.

The Cu_2O nanocubes [2] nucleate mostly heterogeneously on the walls of the reactor (Fig. 1a) which immobilises them for long-term imaging. Ptychography allows to reconstruct separate 2D images of particles growing on the entrance and exit windows of the reactor by applying the multi-slice model [3]. This way, we track the growth and hollowing of individual nanocubes at a spatial resolution of 66 nm and with a time resolution of 22 min (Fig. 1b). Interestingly, new nanocubes successively appear in the images in addition to those particles that have nucleated on the reactor windows and have thus been visible from the beginning of the reaction. The new particles must have nucleated homogeneously in solution and attached to the windows at some point during their growth process.

To investigate the influence of the nucleation behaviour on the shape of the final nanocubes, we make use of the quantitative information of the ptychographic images which contain the local phase shift induced by the sample. The phase shift gives access to physical parameters such as the area density or thickness of the material, if the composition of the sample is known. We calculate the thickness of the nanocubes by taking the average of the pixel values across individual particles. Since the sizes of the nanocubes vary, we use the aspect ratio rather than the absolute thickness to describe the particle shape (Fig. 1c). This allows us to infer the full growth process in 3D: The aspect ratio of individual nanocubes remains nearly constant. However, a systematic trend is visible with regard to the time a particle attaches to the window which is highlighted by colour in Fig. 1c. Those particles that attach when growth has almost finished at late reaction times (yellow data points) are cubic, while particles growing on the reactor windows (black data points) are cuboids with an aspect ratio of 0.5. Thus, the window material hinders the growth of the particles in the direction perpendicular to the window.

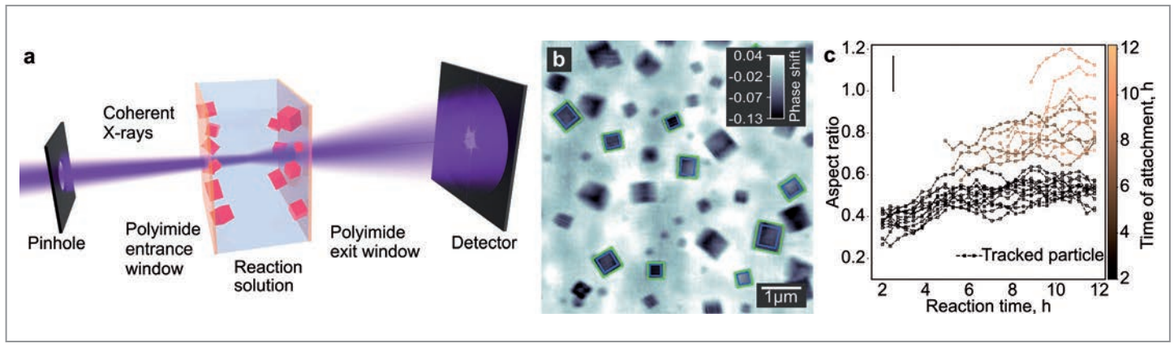

Figure 1

a) Schematic illustration of the experimental setup. b) *In situ* ptychographic image highlighting the in-plane dimension of the nanocuboids by green rectangles. The out-of-plane thickness is calculated from the phase shift within the area highlighted by blue rectangles. The grey scale indicates the quantitative phase shift of the image in radian. c) Evolution of the aspect ratio of the nanocuboids calculated as the quotient of their in-plane dimension and out-of-plane thickness. Yellow color indicates the time when a particle attaches to the substrate. (Adapted from the original publication. Figures from the original publication are licensed under the Creative Commons Attribution 4.0 International License.)

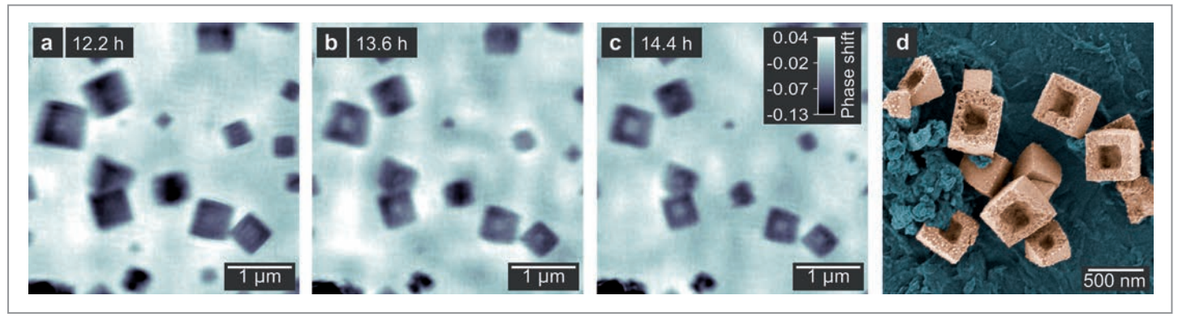

Figure 2

Hollowing process of the nanocuboids. a)-c) Ptychographic images of the hollowing process between 12.2 h and 14.4 h reaction time. The grey scale indicates the phase shift of the images in radian. d) False-coloured SEM image of bowl-shaped hollow nanocuboids (orange) taken from the same sample used for the *in situ* imaging in a)-c). (Adapted from the original publication. Figures from the original publication are licensed under the Creative Commons Attribution 4.0 International License.)

In a second reaction stage, the nanocubes are reduced to metallic copper in a solid-state reaction. Voids form in the centre of the particles and expand towards the surface, resulting in hollow nanocuboids (Fig. 2a-c). We conclude that the mass reduction due to the depletion of oxygen from the crystal lattice and, more importantly, the increase in density from 6.0 g/cm^3 (Cu_2O) to 8.9 g/cm^3 (Cu) are compensated by the formation of a void instead of shrinking of the outer particle dimension. The interaction at the particle-substrate interface and the binding of solvent molecules to the nanocuboids' surface make it energetically favourable to maintain their outer dimensions at the cost of an additional internal surface. The false-coloured SEM image in Fig. 2d shows that the particles in fact have the shape of rectangular bowls, revealing the role of the substrate in the hollowing process. Due to their flatness, it is reasonable to assume that the hollowing starts at the particle-substrate interface, and then carves into the particle in the direction away from the substrate.

Our study demonstrates how imaging in solution with X-ray ptychography enables a direct visualisation of complex transformations of shape and size at the nanoscale. This method can be applied to a wide range of materials and reaction conditions, complementing the capabilities of liquid-cell TEM. Such visual insights into structural changes in solution are important to deepen our understanding of the origins of nanomaterials morphology which is a key factor for the future design of highly active catalysts and functional devices.

Author contact: Dorota Koziej, dkoziej@uni-hamburg.de
Christian G. Schroer, christian.schroer@desy.de
Lukas Grote, lukgrote@physnet.uni-hamburg.de

References

1. A. Schropp et al., 'PtyNAMi: ptychographic nano-analytical microscope', J. Appl. Crystallogr. 53, 957-971 (2020).
2. N. Kränzlin, S. Ellenbroek, D. Duran-Martin and M. Niederberger, 'Liquid-phase deposition of freestanding copper foils and supported copper thin films and their structuring into conducting line patterns', Angew. Chem. Int. Ed. 51, 4743-4746 (2012).
3. M. Kahnt, L. Grote, D. Brückner, M. Seyrich, F. Wittwer, D. Koziej and C. G. Schroer, 'Multi-slice ptychography enables high-resolution measurements in extended chemical reactors', Sci. Rep. 11, 1500 (2021).

Original publication

'Imaging Cu_2O nanocube hollowing in solution by quantitative *in situ* X-ray ptychography', Nature Communication 13, 4971 (2022).
DOI: 10.1038/s41467-022-32373-2

Lukas Grote[1,2], Martin Seyrich[2,3], Ralph Döhrmann[2], Sani Y. Harouna-Mayer[1,4], Federica Mancini[1,5], Emilis Kaziukenas[1,6], Irene Fernandez-Cuesta[3,4], Cecilia A. Zito[1,7], Olga Vasylieva[1], Felix Wittwer[2,3], Michal Kronenberg[8], Natnael Mogos[1], Mirko Landmann[2], Christian G. Schroer[2,3], and Dorota Koziej[1,4]

1. University of Hamburg, Institute for Nanostructure and Solid-State Physics, Centre for Hybrid Nanostructures (CHyN), Hamburg, Germany
2. Centre for X-ray and Nano Science (CXNS), Deutsches Elektronen-Synchrotron DESY, Hamburg, Germany
3. University of Hamburg, Department of Physics, Hamburg, Germany
4. The Hamburg Centre for Ultrafast Imaging (CUI), University of Hamburg, Hamburg, Germany
5. Institute of Science and Technology for Ceramics (ISTEC), National Research Council (CNR), Faenza, Italy
6. Department of Applied Mathematics and Theoretical Physics, University of Cambridge, Cambridge, United Kingdom
7. São Paulo State University UNESP, São José do Rio Preto, Brazil
8. Paul Scherrer Institute (PSI), Villigen, Switzerland

Supported Pd nanoclusters served on a tray

Extraordinary stability of iridium-seeded 1.2 nm Pd clusters

One of today's challenges is to stop global warming and related earth climate change. A possible route is the reduction of greenhouse gases by the establishment of a hydrogen economy accompanied by the use of renewable energy for 'green' hydrogen production [1]. One of the main challenges on the way to substitute conventional fuels by hydrogen is connected to the inconvenience of hydrogen storage. Recent research aiming towards an optimised gravimetric energy density of hydrogen storage media is attributed to palladium nanoparticles on carbon supports. The palladium nanoparticles can provide storage of atomic hydrogen which then can diffuse to the carbon support via so-called spillover. These complex systems are possible candidates for future hydrogen storage solutions.

Among the metal hydrides, the Pd–H system has attracted intense research activities which is attributed to the high hydrogen solubility at convenient pressures and temperatures. Therefore, the Pd–H system serves as an interesting model system in order to understand the relationship between hydrogen solubility and the atomic and electronic structure of the hydrogen hosting crystal lattice and the role of confinement for the case of Pd nanoparticles. The loading and unloading of palladium with hydrogen is accompanied by hysteresis effects which hinder the easy release of hydrogen and are therefore subject of intense research. The microscopic origin of this behaviour is not yet fully understood [2]. A perfect hydrogen storage material should provide high hydrogen storage capacity and easy hydrogen release. To address these needs, palladium nanoparticles have attracted attention, because decreasing particle size leads to reduced hysteresis effects by a reduction of the so-called miscibility gap for H in Pd. In addition, it was reported that the hydrogen solubility is increased for small Pd nanoparticles (NPs).

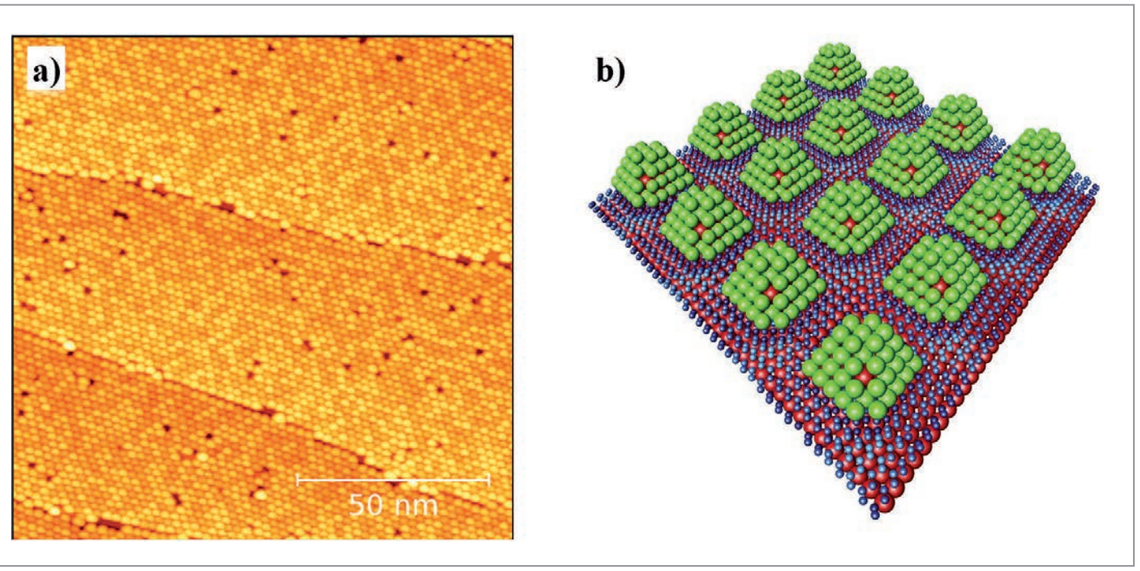

Figure 1

a) High-resolution scanning tunneling microscopy image of iridium-seeded palladium clusters on a graphene/Ir(111) template with 2.5 nm mesh. b) Structural model of the Pd(Ir) nanoparticle superlattice as determined by surface X-ray diffraction.

Furthermore, it was predicted by theoretical calculations that Pd clusters anchored on graphene exhibit extraordinary properties for hydrogen storage. So far it is unclear, if the decrease in hysteresis effects in palladium nanoparticles during hydrogen loading/unloading can be attributed to a different crystal structure and the nanoparticle size. These fundamental questions are strongly connected to the atomic structure of Pd NPs which is a prerequisite for an in-depth understanding of the hydrogen loading mechanisms. In order to address the atomic structure of ultra-small Pd nanoclusters in the 1–2 nm size regime and its evolution under hydrogen exposure, we investigated as a model system Ir-seeded Pd nanoclusters on graphene/Ir(111). This template allows the preparation of a two-dimensional, highly ordered crystalline nanocluster superlattice with a well-defined period of 2.5 nm and a narrow size distribution. Figure 1a shows a scanning tunnelling microscopy image of a nearly perfect Pd nanoparticle array that has been grown by thermal evaporation of Pd after deposition of Ir seed clusters consisting of 12 atoms only. The detailed structural analysis of the surface X-ray diffraction data collected at PETRA III, beamline P09, gives evidence that three atomic layers high nanoparticles with a Pd shell are formed, as pictured in Fig. 1b. Further on, the detailed analysis shows that the nanoparticles are strongly compressed due to the interaction with the graphene support. In addition, we find that the nanoparticles form a crystalline superlattice which can be inferred from the satellite rods at integer reciprocal lattice coordinates H in Fig. 2a. The superlattice formation is the trick to perform in-depth crystallography of the nanoparticles with 1-2 nm size [3]. Under exposure to 1 bar hydrogen, the Ir seeded Pd nanoparticles get unpinned from the graphene/Ir support by the hydrogen interaction with the surface, but they only slightly increase their size. The unpinning can be recognized from Fig. 2b, in which a weakening of the satellite rods is observed together with the appearance of a broad diffraction signal of uncorrelated nanoparticles. Based on the determined nanoparticle lattice parameters, there is evidence for dissolved hydrogen in the correlated and the unpinned clusters during exposure to 10 mbar which gets released when the clusters remain in ultra-high vacuum (UHV) at room temperature. Our detailed structural analysis shows that hydrogen is also dissolved in the Ir seeds, but our analysis is not sensitive enough to address hydrogen enrichment at the Pd–Ir interface. In case of the correlated clusters, only the out of plane lattice parameter increases because of their strong attachment to the substrate. We can, therefore, conclude that small strained Pd nanoparticles represent a system interesting for hydrogen storage, since they provide a large surface area for chemisorbed hydrogen with 71% of the atoms sitting at the surface of the nanoclusters. It can be more rapidly released than hydrogen in the bulk of larger nanoparticles. On the other hand, the compressive strain and finite size suppresses the high hydrogen concentration PdH_x α´ phase formation in the nanoparticle bulk which is at the origin of hysteresis in hydrogen release. Even at 1 bar, we observe only moderate hydrogen-induced sintering of Pd nanoparticles with ~1.2 nm diameter, rendering ultra-small Pd nanoparticles suitable for hydrogen storage applications with fast hydrogen release at room temperature.

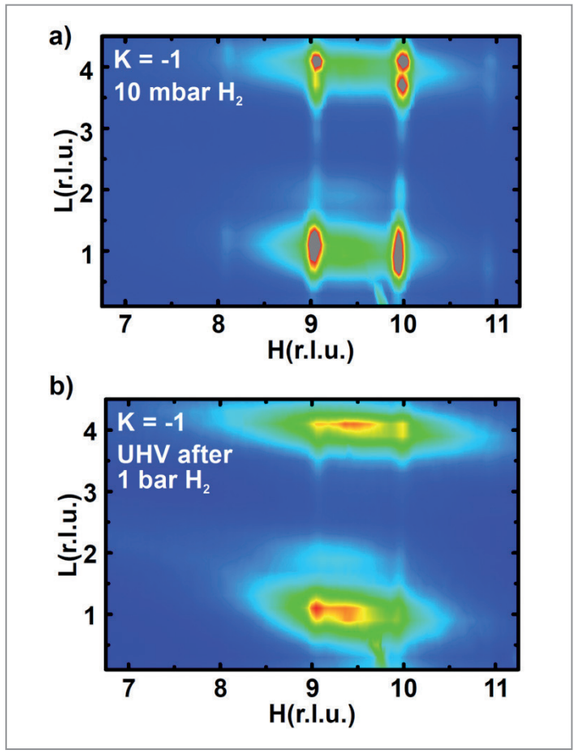

Figure 2

a) Reciprocal space map of the Pd(Ir) nanoparticle superlattice at 10 mbar H_2 pressure and room temperature showing the nanoparticle superlattice reflections. b) After 1 bar H_2 exposure the superlattice signal is strongly reduced, and a broad reflection from small, unpinned nanoparticles appears.

Author contact: Andreas Stierle, andreas.stierle@desy.de

References

1. 'Hydrogen Roadmap Europe', Publications Office of the European Union: Luxembourg, 2, 1–75 (2019).
2. A. Pundt and R. Kirchheim, 'Hydrogen in Metals: Microstructural Aspects', Annu. Rev. Mater. Res. 36, 555–608 (2006).
3. D. Franz, S. Runte, C. Busse, S. Schumacher, T. Gerber, T. Michely, M. Mantilla, V. Kilic, J. Zegenhagen and A. Stierle, 'Atomic Structure and Crystalline Order of Graphene-Supported Ir Nanoparticle Lattices', Phys. Rev. Lett. 110, 065503 (2013).

Original publication

'Hydrogen Solubility and Atomic Structure of Graphene Supported Pd Nanoclusters', ACS Nano 15, 15771–15780 (2021).
DOI: 10.1021/acsnano.1c01997

Dirk Franz[1,2], Ulrike Schröder[3], Roman Shayduk[1], Björn Arndt[1,2], Heshmat Noei[1], Vedran Vonk[1], Thomas Michely[3] and Andreas Stierle[1,2]

1. Deutsches Elektronen-Synchrotron (DESY), Hamburg, Germany
2. Physics Department, University of Hamburg, Hamburg, Germany
3. Institute of Physics II, University of Cologne, Cologne, Germany

X-rays reveal single catalyst nanoparticle at work

How a catalytic converter works in the exhaust systems of cars

Catalysts are materials that promote chemical reactions without being consumed themselves. Today, catalysts are used in numerous industrial processes, from fertiliser production to manufacturing plastics. Because of this, catalysts are of huge economic importance. A well-known example is the catalytic converter installed in the exhaust systems of cars. These contain precious metals such as platinum (Pt), rhodium (Rh) and palladium (Pd) which allow highly toxic carbon monoxide (CO) to be converted into carbon dioxide (CO_2) and reduce the amount of harmful nitrogen oxides (NO_x).

Despite the widespread use and great importance of heterogeneous catalysts, many questions remain regarding how various catalysts work [1]. It is difficult to study real catalysts while in operation as the catalysts are typically used in the form of tiny nanoparticles in order to make the active surface as large as possible and the changes that affect their activity occur on their surface [2]. Here we report X-ray diffraction imaging results of a single catalyst nanoparticle at work, revealing for the first time how the chemical composition of the surface of an individual nanoparticle changes under reaction conditions. This study marks an important step towards a better understanding of industrial catalytic materials.

The experiment is based on a new technique developed at DESY NanoLab for labelling individual nanoparticles and thereby identifying them in a sample. We grew nanoparticles of a PtRh alloy on a $SrTiO_3$ substrate, and we selected one specific particle for characterisation with a $Pt_{60}Rh_{40}$ composition, which was around 100 nm in diameter, similar to the particles used in a car's catalytic converter. We carried out a coherent X-ray diffraction imaging (CXDI) experiment under *operando* CO oxidation reaction conditions (Fig. 1) at beamline ID01 at the European Synchrotron Radiation Facility (ESRF-EBS). From the data analysis we created a detailed image of the nanoparticle morphology, and we determined the mechanical strain within its surface (Fig. 2) [3]. Since the surface strain is related to the surface composition — in particular the ratio of platinum to rhodium atoms — the strain was computed as a function of surface composition by *ab initio* methods. By comparing the observed and computed facet-dependent strain, we could draw, for the first time, conclusions concerning the chemical composition at a single alloy nanoparticle surface.

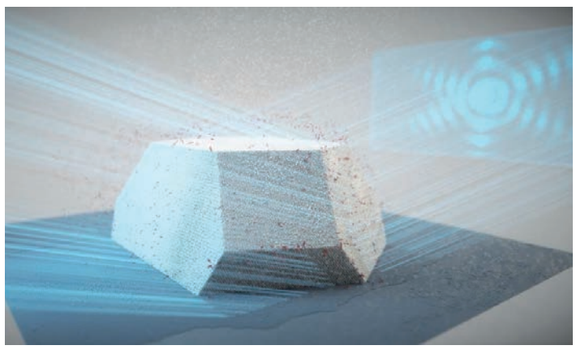

Figure 1

The X-ray investigation not only provided a complete image of a single catalyst nanoparticle, but also shows changes in the chemical composition of its surface during operation.

When the nanoparticle is grown, its surface consists mainly of platinum atoms, as this configuration is energetically favoured under the growth conditions. However, the shape of the particle and its surface strain were studied under different gas conditions, including the operating conditions of an automotive catalytic converter, created by heating the particle to around 430°C and allowing carbon monoxide and oxygen molecules to pass over it. Under these reaction conditions, the rhodium inside the particle becomes mobile and migrates to the surface because it interacts more strongly with oxygen than the platinum. This is also predicted by theory. As a result, the surface strain and the shape of the particle change. We find that a facet-orientation dependent rhodium enrichment takes place, whereby additional corners and edges are formed. The chemical composition of the surface and the shape and size of the particles have a significant effect on their function and efficiency. It is still not completely understood how these are connected and how to control the structure and composition of the nanoparticles. However, CXDI made it possible to detect changes of as little as 0.1 in a thousand in the strain, corresponding to a precision of about 0.0003 nm in this work.

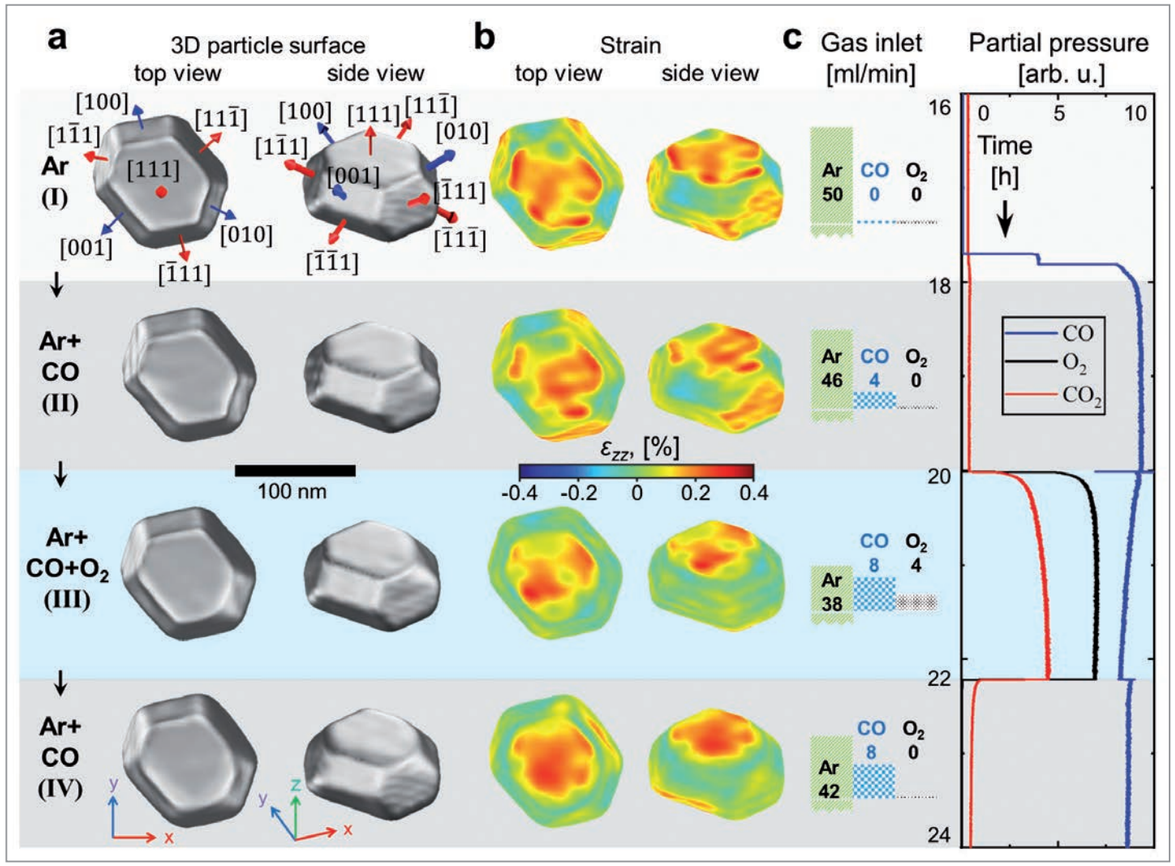

Figure 2

Nanoparticle shape and surface strain for different gas conditions. a) Top and side views of the reconstructed nanoparticle and b) strain field ε_{zz} at the nanoparticle surface for gas conditions (I) to (IV). The position of the surface is defined as a cut at 55% of the reconstructed crystalline electron density from its maximum value. c) Inlet gas composition and mass spectrometer signal during the experiment: CO (blue), O_2 (black), and CO_2 (red). (Adapted from the original publication licensed under the Creative Commons Attribution License 4.0 (CC BY))

Our work shows that the details of the structural changes in such alloy catalyst nanoparticles can be observed while in operation. This is a major step forward in the understanding of an entire class of catalysts, namely, in all reactions that make use of alloy nanoparticles. This investigation is also an important step towards analysing industrial catalytic materials. Until now, model systems have had to be grown in the laboratory in order to conduct such investigations. Future work aims to study individual particles that are ten times smaller – in real catalysts and under reaction conditions.

Author contact: Andreas Stierle, andreas.stierle@desy.de

References

1. K. F. Kalz, R. Kraehnert, M. Dvoyashkin, R. Dittmeyer, R. Gläser, U. Krewer, K. Reuter and J.-D. Grunwaldt, 'Future challenges in heterogeneous catalysis: Understanding catalysts under dynamic reaction conditions', ChemCatChem 9, 17–29 (2017).
2. B. Roldan Cuenya and F. Behafarid, 'Nanocatalysis: Size- and shape-dependent chemisorption and catalytic reactivity', Surf. Sci. Rep. 70, 135–187 (2015).
3. M. Abuin, Y. Y. Kim, H. Runge, S. Kulkarni, S. Maier, D. Dzhigaev, S. Lazarev, L. Gelisio, C. Seitz, M.-I. Richard, T. Zhou, V. Vonk, T. F. Keller, I. A. Vartanyants and A. Stierle, 'Coherent x-ray imaging of CO-adsorption-induced structural changes in Pt nanoparticles: Implications for catalysis', ACS Appl. Nano Mater. 2, 4818–4824 (2019).

Original publication

'Single alloy nanoparticle X-ray imaging during a catalytic reaction', Science Advances 7, 40 (2021). DOI: 10.1126/sciadv.abh0757

Young Yong Kim[1], Thomas F. Keller[1,2], Tiago J. Goncalves[3], Manuel Abuin[1], Henning Runge[1], Luca Gelisio[1], Jerome Carnis[1], Vedran Vonk[1], Philipp N. Plessow[3], Ivan A. Vartanyants[1,4] and Andreas Stierle[1,2]

1. Deutsches Elektronen-Synchrotron DESY, Hamburg, Germany
2. University of Hamburg, Physics Department, Hamburg, Germany
3. Institute of Catalysis Research and Technology, Karlsruhe Institute of Technology, Leopoldshafen, Germany
4. National Research Nuclear University MEPhI, Moscow, Russia

Subducted oceanic crust may weaken in Earth's deep mantle

The strength of subducted oceanic crust has been constrained by novel high-pressure/-temperature experiments at DESY

The movement of tectonic plates on Earth's surface is causing earthquakes and changes the shapes of continents over geological time. A key component of plate tectonics is the subduction of plates at convergent plate margins where the oceanic plate dives deep into Earth's mantle. The subduction of tectonic plates is a major driving force of plate tectonic movements as the descending plate pulls downwards. Subduction is also the key process connecting Earth's inner layers with the surface and atmosphere, facilitating the deep cycling of chemical elements, including those essential for life like H_2O.

A subducting plate contains two major rock types: Oceanic crust sits on top of Earth's mantle rocks. The plastic strength behaviour of the minerals present in both rock types determines the behaviour of the subducting plates in the deeper parts of the Earth's mantle. One of the most important minerals in subducted oceanic crust is a cubic $CaSiO_3$ perovskite, the so-called davemaoite. This mineral's existence has been predicted for decades, although a first natural sample was only found this year. The strength of davemaoite in the deeper mantle, and thus its role in the subduction processes, remained unclear. A common assumption was that davemaoite is a very strong mineral in Earth's mantle which led researchers to think that it plays a minor role for the dynamics of subduction processes. However, the effect of high pressure and high temperature, as present in Earth's interior, on the strength of davemaoite could not be quantified so far, largely due to experimental difficulties in measuring its strength at relevant conditions.

A novel setup (Fig. 1), developed and optimised at the Extreme Conditions Beamline (ECB, P02.2) at PETRA III, DESY [1], has now enabled the first *in situ* measurement of the strength of davemaoite under pressure-temperature conditions expected in a subducting slab at mantle depths of up to 1300 km. The experiments were conducted under the leadership of University of Oxford by an international team of scientists from the University of Bayreuth, DESY and the University of Utah.

To everyone's surprise, the scientists found that davemaoite becomes very weak at temperatures of the deep mantle [2]. In particular, it was found to be much weaker than the mineral (Mg,Fe)O ferropericlase which was previously measured at DESY's ECB [3]. Davemaoite can thus be considered one of the weakest lower mantle minerals (Fig. 2). The weakness of davemaoite could play a decisive role in the subduction process, by strongly decreasing the overall strength of the oceanic crust and thereby allowing it to deform while diving into the mantle. The oceanic crust could behave similarly to a mixture of rock and honey where the strength of the mixture is governed by that of the weak honey rather than the rock.

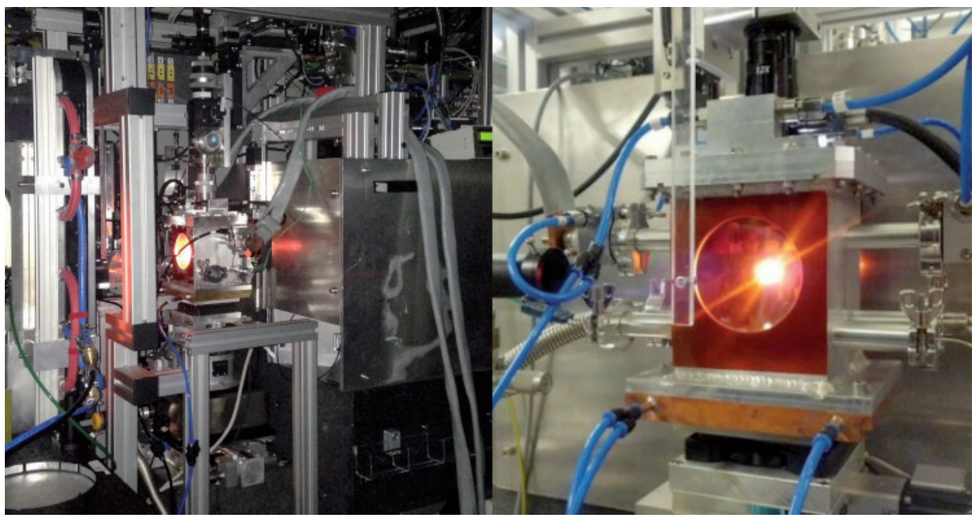

Figure 1
Experimental setup to measure the high-pressure/-temperature strength by synchrotron radial X-ray diffraction at the ECB, DESY. The hot, glowing sample is contained in a water-cooled vacuum chamber while being compressed, deformed and probed by synchrotron X-ray radiation.

The possibility for this type of deformation behaviour has been demonstrated in principle in previous modelling studies focusing on other mineral mixtures [4]. However, the possibility that davemaoite could be such a weak mantle mineral was not considered or anticipated. The novel finding thus sheds a completely new light on deformation processes in subducting plates. A particularly interesting scenario that should be explored in follow-up studies is the possibility that the strength of the oceanic crust decreases abruptly after the formation of davemaoite from the mineral garnet, which occurs at a depth of about 550 km. Thus, it seems possible that the crust is comparatively hard above this transition depth but becomes very weak below it.

The finding has the potential to completely change our understanding of the dynamic behaviour of subducting plates in the deep mantle. In particular, the weakness of the oceanic crust due to the formation of davemaoite could provide an explanation for the long-hypothesised delamination of subducted oceanic crust from the underlying mantle. If the detached crust is less dense than the surrounding mantle, it could accumulate below a depth of about 600-700 km after separating from the mantle. Furthermore, if this crust is denser than the mantle, it could behave as an "upside-down" mantle plume and sink all the way to the core-mantle boundary at 2900 km depths which has been observed in earthquake wave studies.

In either case, it could provide an explanation for physical anomalies observed by the analysis of earthquake waves travelling through Earth's mantle [5-7], and play a key role for the global cycling of geochemical elements. The experimental results promise to have far-reaching geophysical significance, and the findings call for follow-up studies designed to quantify a range of possible geodynamic effects of weak davemaoite on the behaviour of subducting plates in the Earth's mantle and their relevance to understand deep material cycles.

Figure 2
Experimentally measured strength of major lower mantle phases; red: davemaoite, blue: derropericlase, orange: bridgmanite.

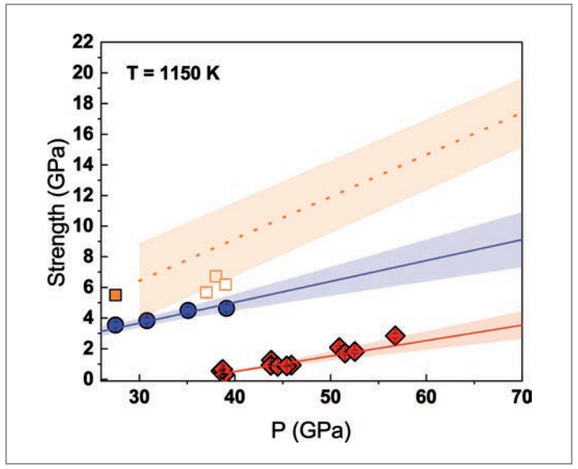

Author contact: Hauke Marquardt, hauke.marquardt@earth.ox.ac.uk

References

1. J. Immoor, H. Marquardt, L. Miyagi, S. Speziale, S. Merkel, I. Schwark, A. Ehnes and H.P. Liermann, ´An improved setup for radial diffraction experiments at high pressures and high temperatures in a resistive graphite-heated diamond anvil cell´, Rev.Sci. Instrumm. 91(4), 045121 (2020).
2. J. Immoor, L. Miyagi, H.P. Liermann, S. Speziale, K. Schulze, J. Buchen, A. Kurnosov and H. Marquardt, ´Weak cubic $CaSiO_3$ perovskite in the earth´s mantle´, Nature 603(7900), 276-279 (2022).
3. J. Immoor, H. Marquardt, L. Miyagi, F. Lin, S. Speziale, S. Merkel, J. Buchen, A. Kurnosov and H. P. Liermann, ´Evidence for {100}<011> slip in ferropericlase in Earth´s lower mantle from high-pressure/high-temperature experiments´, Earth & Planet. Sci. Lett. 489, 251-257 (2018).
4. M. Thielmann, G. J. Golabek and H. Marquardt, ´Ferropericlase control of lower mantle rheology: impact of phase morphology´, Geochem. Geophys. 21(2), e2019GC008688 (2020).
5. M. D. Ballmer, N.C. Schmerr, T. Nakagawa, and J. Ritsema, ´Compositional mantle layering revealed by slab stagnation at ~1000-km depth´, Sci. Adv. 1(11), (2015).
6. A. Thomson, W. Crichton, J. Brodholt, I. Wood, N. Siersch, J. Muir, D. Dobson and S. Hunt, ´Calcium silicate perovskite´s acoustic velocities can explain LLSVPs in Earth´s lower mantle´, Nature 572, 643-647 (2019).
7. T. D. Jones, R. R. Maguire, P. E. van Keken, J. Ritsema and P. Koelemeijer, ´Subducted oceanic crust as the origin of seismically slow lower-mantle structures´, Prog. Earth Planet. Sci. 7(1), 17 (2020).

Original publication

'Weak cubic $CaSiO_3$ perovskite in Earth's mantle', Nature 603, 276-279 (2022). DOI: 10.1038/s41586-021-04378-2

Julia Immoor[1], L. Miyagi[2], Hanns-Peter Liermann[3], S. Speziale[4], K. Schulze[5], J. Buchen[6], A. Kurnosov[1] and Hauke Marquardt[7]

1. Bayerisches Geoinstitut BGI, University of Bayreuth, Bayreuth, Germany
2. University of Utah, Salt Lake City, USA
3. Deutsches Elektronen-Synchrotron (DESY), Hamburg, Germany
4. German Research Center for Geosciences GFZ, Potsdam, Germany
5. Laboratory of Crystallography, University of Bayreuth, Bayreuth, Germany
6. Seismological Laboratory, California Institute of Technology, California, USA
7. University of Oxford, Department of Earth Sciences, Oxford, United Kingdom
4. National Research Nuclear University MEPhI, Moscow

Origin of depressed 660-km discontinuity in cold mantle

Experimental mineralogy explains the structure of Earth's mantle and the geodynamics of subduction zones

The seismic wave velocities abruptly increase at depths around 660 km everywhere in the Earth's interiors, referred to as the 660-km seismic discontinuity (D660) which separates the Earth's upper and lower mantles. From the mineralogical point of view, this discontinuity was commonly interpreted as the dissociation of ringwoodite to bridgmanite plus ferropericlase (RBP transition). Cold subduction zones, however, feature a doubling and significant depression of the D660 down to 750 km, which cannot be explained by the ringwoodite dissociation since it has a minimal temperature dependence. Thus, another strongly temperature-dependent transition should cause this discontinuity.

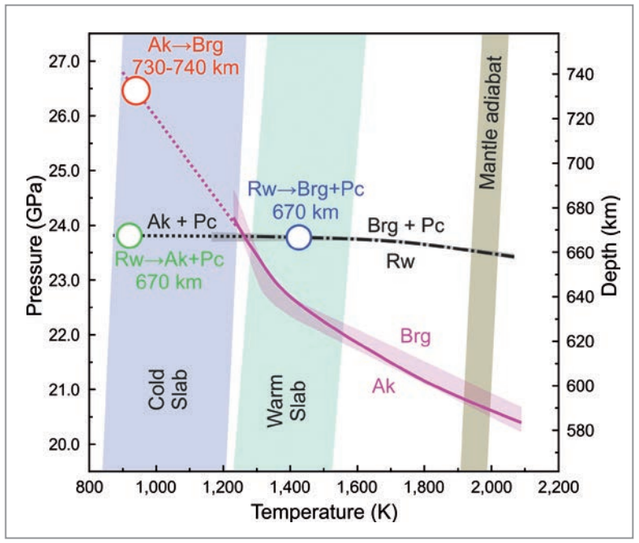

Figure 2

Comparison of the RBP and AB phase transition boundaries. Ak – $MgSiO_3$ akimotoite, Brg – $MgSiO_3$ bridgmanite, Pc – MgO periclase, Rw – Mg_2SiO_4 ringwoodite. Green and red circles indicate Rw→Ak+Pc dissociation at 670 km depth and AB transition at 730-740 km depth, respectively. The blue circle represents the commonly accepted RBP transition causing the D660 in warm slabs. The dotted lines represent a linear extrapolation of the RBP and AB boundaries to lower temperatures. (Figure adopted from the original publication, licensed under CC BY 4.0).

Researchers proposed the akimotoite–bridgmanite (AB) transition as cause of the above-mentioned observations in cold subduction zones where an old oceanic plate sinks into the mantle underneath a continental plate. Akimotoite is supposed to be a major constituent together with ringwoodite in the subduction zones above 660 km depth. Based on recent experimental and computational studies, the AB transition occurs at similar pressures to the RBP transition, i.e. at depths similar to the D660. However, previous experimental studies faced the challenge of accurately determining the transition pressure. Moreover, experimental data were lacking for the AB transition at lower temperatures typical of cold subduction zones. Therefore, we determined both the RBP and AB transitions using advanced multi-anvil techniques with *in situ* X-ray diffraction.

Our advanced techniques include the determination of a stable mineral phase by observing relative changes in the ratio of coexisting higher- and lower-pressure phases at spontaneously and gradually decreasing pressure and at a constant temperature using *in situ* X-ray diffraction (Fig. 1). Our strategy was based on the principle of phase equilibrium, i.e. the balance between forward (akimotoite transforms to bridgmanite) and reverse (bridgmanite transforms to akimotoite) reactions. It avoids problems in phase stability determination caused by sluggish kinetics and excess surface energy.

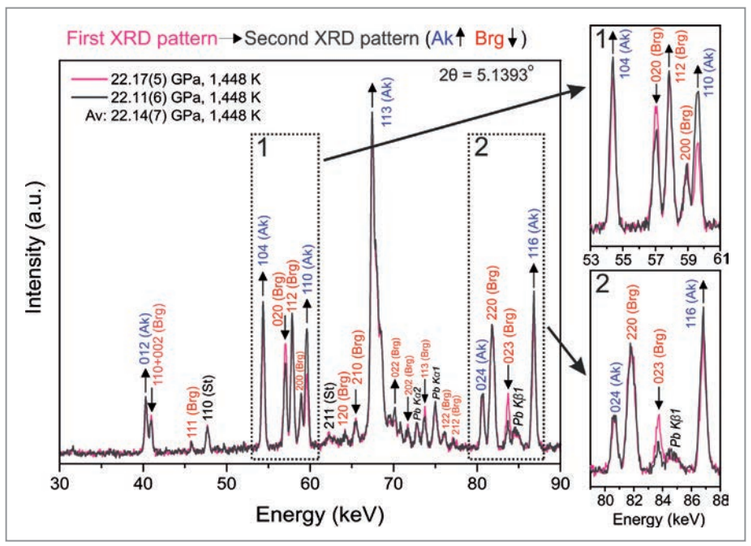

Figure 1

An example of the change of intensity ratio between akimotoite and bridgmanite at 1448 K and 22.14(7) GPa measured at PETRA III beamline P61. The first diffraction pattern is shown in pink and the second pattern in dark grey. The upward and downward arrows indicate the peaks with increased and decreased intensities in the second diffraction patterns, respectively. (Figure adopted from the original publication, licensed under CC BY 4.0).

Our results confirm previous studies showing that the RBP boundary has almost zero temperature dependence at 23.2–23.7 GPa (≈660 km depth). In contrast, our data obtained at PETRA III beamline P61 show that the AB boundary has a steep convex curve with a variable but strong temperature dependence. These results suggest the following explanation of the doubling and depression of the D660 in cold subduction zones: in subducted cold slabs (the main parts of the subducted body), ringwoodite, being most abundant, first dissociates into akimotoite plus periclase at 660–670 km depths which causes the first discontinuity. After the further sinking, this akimotoite transforms to bridgmanite at 680–740 km depth, which causes the second discontinuity (Fig. 2) being far deeper than 660 km depth, thereby producing the depression of the D660. In contrast, the discontinuity at 660 km in warm subduction zones and the ambient mantle results from the RBP transition (Fig. 2).

Seismological observations support our suggestions. For example, in the coldest subduction zone on earth, Tonga slab, seismological studies revealed double discontinuities at depths of 738 km and 669 km [1], which is consistent with our suggestion of ringwoodite → akimotoite + periclase → bridgmanite + periclase transformation. An opposite example is the Peru slab, which is about 300 K warmer and characterised by a single discontinuity at around 656 km depth [2], which can be easily interpreted as the RBP transition.

Our results have significant geodynamic implications, since steep phase-transition boundaries produce large buoyancy forces [3]. When the upward buoyancy produced by a negative phase boundary exceeds the downward force due to thermal expansion, slabs stagnate above the discontinuity. Therefore, the steep negative boundary of the AB transition should result in cold-slab stagnation, whereas the neutral RBP transition should enhance slab penetration deeper into the mantle. These conclusions are also supported by the seismic tomography studies, showing that that cold slabs (for example Izu-Bonin, South Kurile and Japan regions) stagnate above the discontinuities and warm slabs (for example Peru, the Marianas and Central America regions) penetrate the lower mantle.

Author contact:
Artem Chanyshev, artem.chanyshev@uni-bayreuth.de
Takayuki Ishii, takayuki.ishii@hpstar.ac.cn

References

1. S. X. Zang, Y. Z. Zhou, J. Y. Ning and R. Q. Wei, 'Multiple discontinuities near 660 km beneath Tonga area', Geophys. Res. Lett. 33, L20312 (2006).
2. Y. Fukao and M. Obayashi, 'Subducted slabs stagnant above, penetrating through, and trapped below the 660 km discontinuity', J. Geophys. Res. Solid Earth 118, 5920–5938 (2013).
3. G. Schubert, D. A. Yuen and D. L. Turcotte, 'Role of phase transitions in a dynamic mantle', Geophys. J. Int. 42, 705–735 (1975).

Original publication

'Depressed 660-km discontinuity caused by akimotoite–bridgmanite transition', Nature 601, 69-73 (2022).
DOI: 10.1038/s41586-021-04157-z

Artem Chanyshev[1,2], Takayuki Ishii[3,2], Dmitry Bondar[2], Shrikant Bhat[1], Eun Jeong Kim[2], Robert Farla[1], Keisuke Nishida[2], Zhaodong Liu[2,4], Lin Wang[2,5], Ayano Nakajima[6], Bingmin Yan[3], Hu Tang[3], Zhen Chen[3], Yuji Higo[7], Yoshinori Tange[7] and Tomoo Katsura[2,3]

1. Deutsche Elektronen-Synchrotron DESY, Hamburg, Germany
2. Bayerisches Geoinstitut, University of Bayreuth, Bayreuth, Germany
3. Center for High Pressure Science and Technology Advanced Research, Beijing, China
4. State Key Laboratory of Superhard Materials, Jilin University, Changchun, China
5. Earth and Planets Laboratory, Carnegie Institution, Washington D.C., USA
6. Department of Earth Sciences, Graduate School of Science, Tohoku University, Sendai, Japan
7. Japan Synchrotron Radiation Research Institute (JASRI), Hyogo, Japan

Shedding light on Mercury's inner dynamo

Uncovering the structure and melting characteristics of Mercury's core-forming metallic alloys

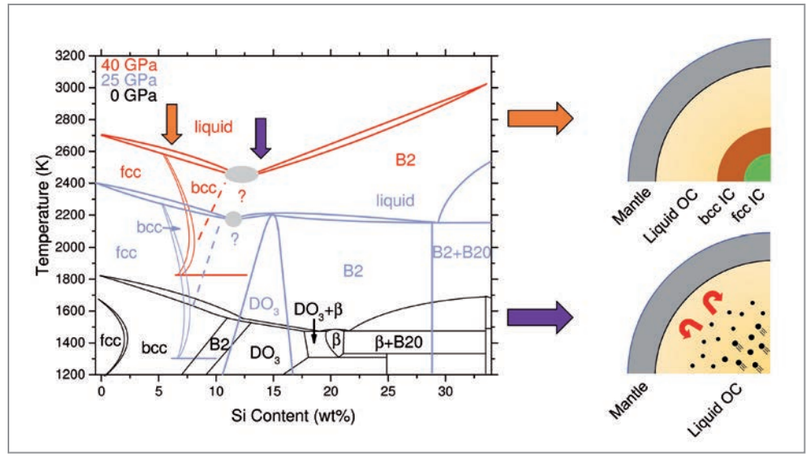

Figure 2

Phase diagram of the iron-silicon system and new crystallisation regimes for a silicon-rich core [4]. It is shown that the effect of silicon abundance leads to a substantially different picture for crystallisation and the dynamo mechanism active in Mercury's core.

Mercury is the only planet of the inner solar system besides Earth to have a global magnetic field whose origins remain enigmatic. As Mercury's iron-alloy core represents nearly 85% of the total radius of the planet, not only the generation of the magnetic field, but also many global aspects of the planet are controlled by the properties of the core. In our study, we have examined the effect of silicon on the melting and stable crystal structures of the iron alloy expected to form Mercury's core over a pressure and temperature range directly pertinent to the deep interior of the planet.

Mercury is an unlikely candidate for an active, dynamic planet. As the planet closest to the sun, its surface exhibits dayside and nightside temperatures of between 430 and -180°C, and the surface itself is largely stagnant, albeit exhibiting evidence for past volcanic activity [1]. However, Mercury has a weak global magnetic field indicating that some part of its core is convecting, likely due to the crystallisation of solid iron alloys [2]. A wealth of different crystallisation regimes have been suggested for Mercury's core, based on various estimates of its composition and temperature and the expected thermodynamic properties of these materials. Depending on the composition and temperature, the core may start to grow solid crystallites from its top near the core-mantle boundary (CMB) or nucleate at the centre of the core to form a solid inner core (IC). Both scenarios are illustrated in Fig. 1. Constraining the structure of the core and its evolution with time is not only important for understanding the properties of Mercury's magnetic field but also to interpret observations of Mercury's surface and data concerning its interior such as those provided by instruments aboard MESSENGER (NASA) and BepiColombo (ESA/JAXA).

While the iron core of Mercury is likely to be enriched with both sulphur and silicon, much of the previous models focused exclusively on the effect of sulphur alloying [e.g. 3]. Indeed, due to the lack of experiments, the effect of silicon on the stable structures and phase relations between solid and liquid iron-silicon alloys was not well understood. In our study, we investigated the structure and phase transformations of iron-silicon alloys at high pressures and temperatures in order to determine the phase diagram of the iron-silicon system at the conditions of Mercury's interior, and by doing so clarify the structure and internal dynamics of Mercury's core.

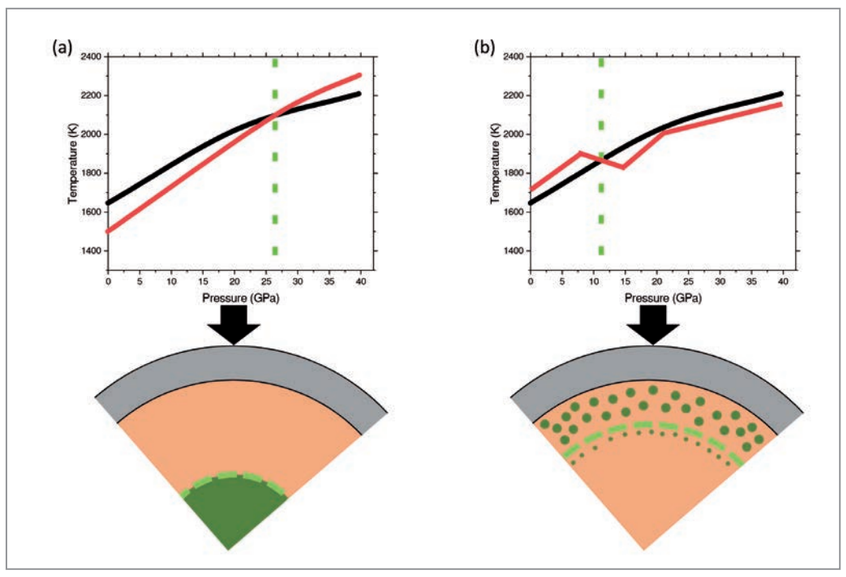

Figure 1

Representative crystallisation regimes for Mercury. Black and red lines indicate a temperature profile for Mercury and representative melting curves for the iron-silicon and iron-sulphur systems after refs. [3,4]. Green dashed lines indicate the crossing point that separates areas of the core where solids are crystallising from areas where they are not. a) An iron-silicon core is shown which results in the growth of an inner core. b) An iron-sulphur core is shown where 'iron snow' forms near the core-mantle boundary and remelts deep within Mercury's interior.

In order to exert pressures of tens of GPa on iron-silicon samples (1 GPa is about 10000 times atmospheric pressure on Earth), samples were compressed between diamond anvils and subsequently heated to temperatures up to 3200 °C using high power infrared lasers. Sample dimensions were on the order of five microns thick and in excess of 100 microns across. Thanks to the high flux and tight focus of the X-ray beam available at beamline P02.2 of PETRA III, it was possible to collect X-ray diffraction patterns from the heated samples. This allowed us to determine the structural evolution of the investigated iron-silicon alloys as a function of pressure, temperature and composition, tracking structural transitions in solid phases and ultimately the melting of the sample. These observations were coupled with chemical analysis of the recovered samples by electron microscopy and used to construct for the first time the phase diagram for the iron-silicon system at conditions encompassing those of Mercury's core (Fig. 2). The so-established phase diagram has unveiled new crystallisation regimes for the core of Mercury. Notably, for relatively low silicon concentration, we observed the formation of a high-temperature body-centred cubic structure stable below melting, indicating that a cooling solid inner core may exhibit internal layering due to structural transitions taking place over geologic time. Alternatively, if the core is more enriched in silicon, the crystallising solid may be more buoyant than the remaining liquid and floats towards the CMB before melting again, providing a new mechanism to drive Mercury's dynamo without actual formation of a solid inner core. Ultimately, this type of laboratory experiment provides one of the few windows available for studying the deep interiors of the planets within the solar system and are a necessary complement to space missions and telescope observations.

Author contact:
Eric Edmund, eedmund@carnegiescience.edu
Daniele Antonangeli, daniele.antonangeli@upmc.fr

References

1. J. W. Head et al., 'Flood Volcanism in the Northern High Latitudes of Mercury Revealed by MESSENGER', Science 333, 1853-1856 (2011).
2. B. J. Anderson et al., 'The Structure of Mercury's Magnetic Field from MESSENGER's First Flyby', Science 321, 82-85 (2008).
3. B. Chen, J. Li and S. A. Hauck II, 'Non-ideal liquidus curve in the Fe-S system and Mercury's snowing core', GRL 35, L07201 (2008).
4. E. Edmund et al., 'The Fe-FeSi phase diagram at Mercury's core conditions', Nat. Comms. 13, 387 (2022).

Original publication

'The Fe-FeSi phase diagram at Mercury's core conditions', Nature Communications 13, 387 (2022).
DOI: 10.1038/s41467-022-27991-9

Eric Edmund[1,2,3], Guillaume Morard[1,4], Marzena Baron[1], Attilio Rivoldini[5], Shunpei Yokoo[6], Silvia Boccato[1], Kei Hirose[6,7], Anna Pakhomova[8] and Daniele Antonangeli[1]

1. Sorbonne Université, Muséum National d'Histoire Naturelle, UMR CNRS 7590, Institut de Minéralogie de Physique des Matériaux et de Cosmochimie, Paris, France
2. Centre for High Pressure Science and Technology Advanced Research, Shanghai, China
3. Earth & Planets Laboratory, Carnegie Institution for Science, Washington, DC, USA
4. Université Grenoble Alpes, Université Savoie Mont Blanc, CNRS, IRD, Université Gustave-Eiffel, ISTerre, Grenoble, France
5. Royal Observatory of Belgium, Brussels, Belgium
6. Department of Earth and Planetary Science, The University of Tokyo, Tokyo, Japan
7. Earth-Life Science Institute, Tokyo Institute of Technology, Meguro, Tokyo, Japan
8. Deutsches Elektronen-Synchrotron DESY, Hamburg, Germany

20 million years to today

X-ray scans reveal extinct ant species in exquisite detail

Fossils provide the only direct insight into the history of evolution. Using the PETRA III beamline P05, an international team of scientists has discovered a new – yet extinct – species of ant from an about 20-million-year-old Ethiopian amber. Named after DESY, this new fossil, *Desyopone hereon*, reveals the past diversity of life in unprecedented detail. The fossil itself required revision to the classification of ants while also providing insight into the deep evolutionary history of phenotypic plasticity. The study, published in the journal *Insects*, shows that the imaging capacity of synchrotron radiation is ushering in a new paradigm for the life sciences, one mediated by genomics and the emerging field of phenomics.

Although ants are ubiquitous and familiar, their diversity and abundance are staggering, with more species than birds (over 14,000 ant species vs about 11,000 bird species [1,2]) and about 2.5 million individuals per each living human, for a total of over 20 quadrillion ants wandering the Earth's surface [3]. The fossil record of ants is also rich, with nearly as many described species as non-avian dinosaurs [4]. Two of the principal limitations of ant and insect palaeontology more broadly are the vagaries of preservation and the technology for observing anatomical detail, as the genomes of multi-million-year-old specimens cannot be sequenced. With the submicron scale resolution of X-rays scans, however, it is possible to document and observe hidden or internal anatomical evidence, allowing researchers to test many evolutionary hypotheses for the first time.

Through direct examination of the new fossils under standard light stereomicroscopes (Fig. 1), the scientists hypothesised that these Ethiopian amber specimens belonged to the relictual ant subfamily Aneuretinae which is represented today by only a single species that is restricted to the island nation Sri Lanka. They then brought the amber piece to DESY for micro-computed tomography (µ-CT) using the PETRA III beamline P05. The resultant 3D reconstructions revealed numerous anatomical details that could not be discerned via traditional light microscopy (Fig. 2). The scientists observed that the waist of the ant was "primitive", having a complex of exoskeletal plates that were lost in the early evolution of the Aneuretinae and their closest relatives. In contrast, the mandibles were found to be rudimentary in form – an evolutionarily derived condition not observed in living or extinct aneuretines. These observations allowed the scientists to reject the hypothesis that these fossil ants were related to Aneuretinae.

Figure 1
The about 20-million-year-old piece of Ethiopian amber that contains 13 individuals of the new fossil ant species *Desyopone hereon*. Direct examination of these extinct insects indicated a relationship with the relictual subfamily *Aneuretinae*, a hypothesis that was tested using the PETRA III beamline P05. (Credit: Vincent Perrichot)

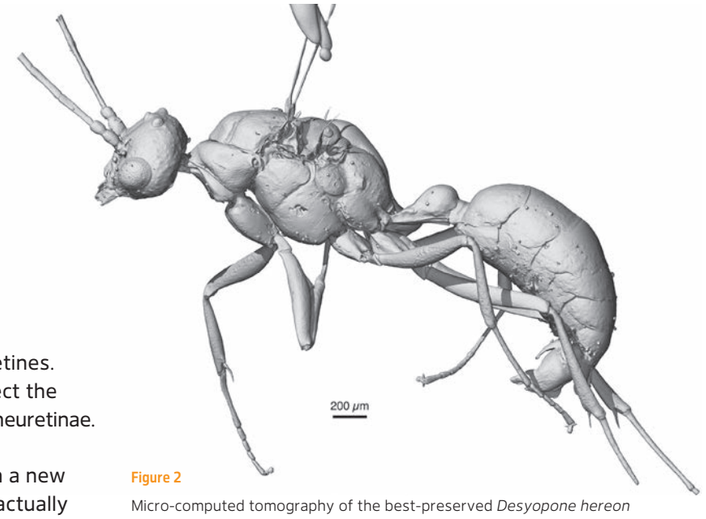

Figure 2
Micro-computed tomography of the best-preserved *Desyopone hereon* specimen revealed anatomical details that were critical for rejecting the hypothesis derived from traditional methodology and for placing the fossil in the correct evolutionary context. (Credit: Brendon Boudinot)

As a consequence, the scientists were faced with a new problem: To which lineage of ants do the fossils actually belong? A special challenge was that all of the fossil specimens are male, while the classification of ants is dependent on workers, which are all female. To resolve this problem, the scientists relied on recent genomic estimates of the branching order of the ant tree of life to trace evolutionary patterns of male anatomy across a representative sample of ant diversity. Between the reciprocally illuminating sources of data, genomics (sequencing) of living species and fossil phenomics (µ-CT), the authors were able to identify the fossils as close relatives of the small, predatory and underground-dwelling ant genus *Cryptopone*. As the fossils also displayed an exceptional combination of ancestral and derived anatomical characteristics, it was clear that they represented an evolutionary excursion that did not survive to the present day, i.e., the 20-million-year-old fossils are an extinct lineage of ants. The scientists, therefore, christened the fossils *Desyopone hereon*, in recognition of the resources and instrumentation provided by DESY and the support of the Helmholtz-Zentrum Hereon which were key for this discovery.

However, the study of *Desyopone hereon* has further evolutionary implications. In addition to requiring a revision of ant systematics, *Desyopone* provides evidence for the developmental decoupling of male and female ants. Since male ants are direct, haploid clones of their diploid mothers, to evolve sexual dimorphism in structures such as the mandibles requires differential regulation patterns of the same genome. The scientists compared male and female ants, including *Desyopone*, finding that while male mandible form usually tracks that of females, there was an apparent parallel series of male-specific evolutionary reductions in the Poneria, a highly diverse lineage of predatory ants, comprising over 1500 species.

Untangling the molecular mechanisms underpinning the development of sexual dimorphism in ants will be a major task in this research field in the coming decades. For nearly the entire history of ant research, males have been ignored because of their distinct morphologies which makes it difficult to identify them. This distinctness itself is a most interesting phenomenon, however, and thanks to *Desyopone*, it is clear that X-ray imaging technologies will provide a meaningful pathway for tracing the evolutionary patterns of development across both living and extinct species. Future work to automate the processing µ-CT data will undoubtedly lead to more breakthroughs. In the meantime, it is imperative to scan more fossils and developmental series of living species.

Author contact:
Brendon E. Boudinot, boudinotb@gmail.com

References

1. B. Bolton, 'AntCat: An online catalog of the ants of the world by Barry Bolton', https://antcat.org, (accessed 5 Nov. 2022).
2. The Cornell Lab of Ornithology, 'Birds of the World', https://birdsoftheworld.org/bow/home, (accessed 5 Nov. 2022).
3. P. Schultheiss, S.S. Nooten, R. Wang, M.K.L. Wong, F. Brassard and B. Guénard, 'The abundance, biomass, and distribution of ants on Earth', Proc. Nat. Acad. Sci. USA 119, e2201550119 (2022).
4. P. Barden, 'Fossil ants (Hymenoptera: Formicidae): ancient diversity and the rise of modern lineages', Myrmecol. News 23, 30 (2017).

Original publication

'Genomic-phenomic reciprocal illumination: *Desyopone hereon* gen. et sp. nov., an exceptional aneuretine-like fossil ant from Ethiopian amber (Hymenoptera: Formicidae: Ponerinae)', Insects 13, 796 (2022). DOI: 10.3390/insects13090796

Brendon E. Boudinot[1], Adrian K. Richter[1], Jörg U. Hammel[2], Jacek Szwedo[3], Błażej Bojarski[3] and Vincent Perrichot[4]

1. Institut für Zoologie und Evolutionsforschung, Friedrich-Schiller-Universität Jena, Jena, Germany
2. Helmholtz-Zentrum Hereon, Geesthacht, Germany
3. Laboratory of Evolutionary Entomology and Museum of Amber Inclusions, Faculty of Biology, University of Gdańsk, Gdańsk, Poland
4. CNRS, Géosciences Rennes, University Rennes, Rennes, France

Steering catalyst's structure and functionality

Operando methods guide the design of dynamic reaction protocols

Structural, chemical and morphological changes in catalysts under actual working conditions pose significant challenges for the experimental and theoretical understanding of their working mechanisms. These alterations of the material hamper our ability to establish the link between the pristine catalyst structure and its functionality (activity, stability, distribution of reaction products). On the other hand, these transformations provide new exciting possibilities to tailor the catalyst properties not through expensive and time-consuming modifications in the catalyst composition and synthesis procedure but through a rational design of dynamic reaction protocols.

In this work we focus on CO_2 electroreduction reaction (CO_2RR) over copper catalysts, derived from size- and shape-selected Cu_2O nanocubes (NCs) (Fig. 1a). Already under static CO_2RR, this catalyst shows good activity for CO_2 conversion to valuable, energy-dense multi-carbon products, such as ethylene and ethanol (EtOH) [1], but the distribution of reaction products is broad. For practical applications, it is important to develop facile approaches for tuning the catalyst selectivity on demand. Furthermore, an ability to tailor the catalyst surface is desirable for fundamental understanding of the electrocatalytic processes and decoupling the roles of structural motifs that coexist in catalysts under reaction conditions. The attempts to control the catalyst composition and structure under operating conditions, however, require validation and guidance from *operando* experimental studies.

Our approach to steer the catalyst functionality relied on a pulsed reaction protocol where the cathodic (working) potential was intermitted with pulses of an anodic potential (Fig. 1b). The latter are expected to perturb the oxidation state and the structure of Cu species on the catalyst surface [2,3]. Such a reaction protocol with pulse durations between 0.5 and 32 s resulted in remarkable changes in the reaction product distribution, such as the suppression of the parasitic hydrogen evolution and an enhancement in CO and methane production. Our most striking observation, however, was that the catalyst selectivity towards EtOH strongly depends on the duration of the applied pulses (Fig. 1c). With anodic pulses longer than 2–3 s, or with cathodic pulses shorter than 1–2 s, EtOH production was suppressed. At the same time, with anodic pulse durations of ca. 0.5–1 s, and cathodic pulse durations of ca. 4 s, the EtOH production was enhanced 1.7 times with respect to that under static CO_2RR.

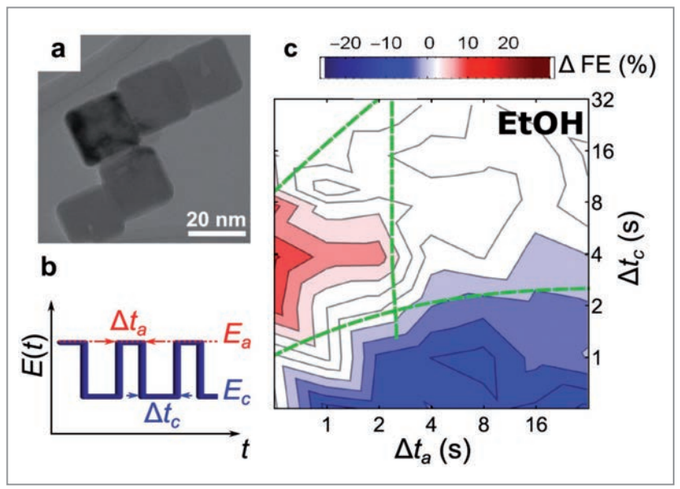

Figure 1
Cu nanocubes (NCs) and their selectivity under pulsed CO_2RR. a) TEM image of the as-prepared Cu NCs. b) Schematic depiction of the applied potential pulse protocol. c) Faradaic efficiency (FE) for ethanol under pulsed CO_2RR with different duration of cathodic (Δt_c) and anodic (Δt_a) potential pulses. The values of cathodic and anodic potentials are E_c = -1.0 V (RHE) and E_a = 0.6 V, respectively. Depicted quantity is the difference between FE values under pulsed CO_2RR and under static CO_2RR at -1.0 V. 0.1 M $KHCO_3$ is used as an electrolyte.

To understand the origins of such intriguing changes, we employed two complementary synchrotron-based approaches: high energy X-ray diffraction (XRD), carried out at beamline P21.2 and *operando* quick X-ray absorption fine structure (QXAFS) spectroscopy, carried out, in part, at beamline P64 at PETRA III. XRD and QXAFS allowed us to track the structural and chemical changes experienced by Cu NCs with subsecond time resolution (Fig. 2a). In particular, QXAFS enabled us to track the periodic oscillations in the Cu oxidation state in response to the changes in the applied potential. Unexpectedly, we have found that not only Cu(I) but also small amounts of Cu(II) species are generated under such a reaction protocol. At the same time, XRD provided key information about the crystallographic structure of the oxide species formed. Taken together, QXAFS and XRD results allowed us to establish characteristic time scales for the formation of different Cu species and, thus, to rationalise the dependency of the catalyst selectivity on the durations of potential pulses (Fig. 2b). In particular, we observed that long anodic pulses result in the formation of a thick bulk-like Cu_2O shell in our catalyst; it is favourable for the CO formation but does not promote multi-carbon products. At the same time, a combination of anodic pulses shorter than 2 s, with cathodic pulses of ca. 4 s results in a formation of unique multivalent surface oxides (as revealed by XAS) with a (not yet) crystalline and distorted Cu oxide phase (as probed by XRD). An optimal balance between these oxide species and the metallic Cu on the catalyst surface favours C–C coupling and explains the observed boost in EtOH production.

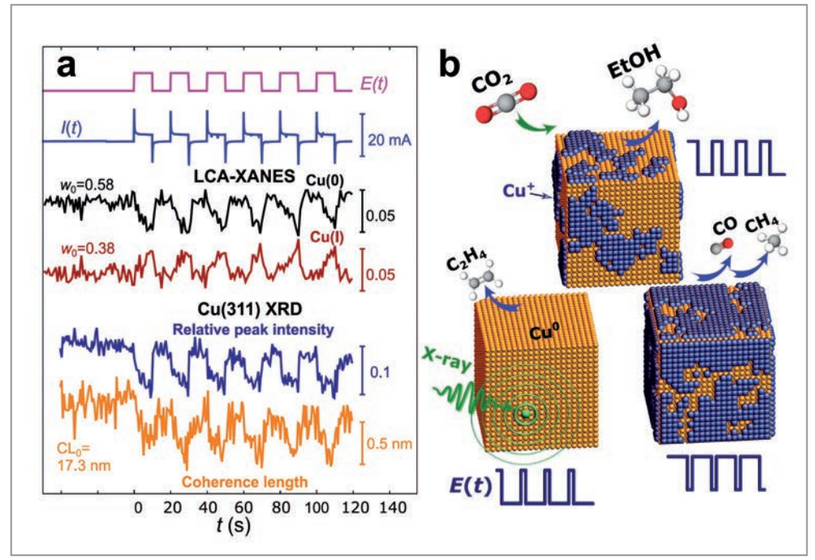

Figure 2
Evolution of the Cu NCs under pulsed CO_2RR. a) Periodic changes in the concentrations of Cu(0) and Cu(I) species, as obtained from linear combination analysis of Cu K-edge XANES data and oscillations of the area of the Cu(3111) Bragg peak (reflecting the amount of metallic copper) as well as in the coherence length of the copper domains (obtained from the Cu(311) Bragg peak widths). The applied potential $E(t)$ and detected current $I(t)$ are also shown. CL_0 and w_0 denote the coherence length (CL) and Cu species concentrations (w) at the beginning of pulse sequence. Here $\Delta t_c = \Delta t_a$ = 10 s. b) Schematic depiction of the catalyst surface structure and composition under potential pulses of different duration as deduced from XAS and XRD data. The main CO_2RR reaction products for each regime are also shown.

Our study is a good example of how *operando* techniques provide insight into the complexity of the processes in the working heterogeneous catalysts. It particularly highlights the importance of non-equilibrium structures and dynamics that are often overlooked in the studies of functional materials. This study showcases an elegant approach for understanding the fundamental aspects of structure-properties relationships in evolving catalytic materials which paves the road toward practical optimisation and rational design of catalytic protocols.

Author contact: Janis Timoshenko, janis@fhi-berlin.mpg.de

References

1. T. Möller, F. Scholten, T. N. Thanh, I. Sinev, J. Timoshenko, X. Wang, Z. Jovanov, M. Gliech, B. Roldan Cuenya, A. S. Varela and P. Strasser 'Electrocatalytic CO_2 Reduction on CuO_x Nanocubes: Tracking the evolution of chemical state, geometric structure, and catalytic selectivity using operando spectroscopy', Angew. Chem. 59, 17974–17983 (2020).
2. R. M. Arán-Ais, F. Scholten, S. Kunze, R. Rizo and B. Roldan Cuenya, 'The role of in situ generated morphological motifs and Cu(I) species in C^{2+} product selectivity during CO_2 pulsed electroreduction', Nature Energy 5, 317-325 (2020).
3. H. S. Jeon, J. Timoshenko, C. Rettenmaier, A. Herzog, A. Yoon, S. W. Chee, S. Oener, U. Hejral, F. T. Haase and B. Roldan Cuenya, 'Selectivity Control of Cu Nanocrystals in a gas-fed flow cell through CO_2 pulsed electroreduction', J. Am. Chem. Soc. 143, 7578–7587 (2021).

Original publication

'Steering the structure and selectivity of electrocatalysts by potential pulses', Nature Catalysis 5, 259–267 (2022).
DOI: 10.1038/s41929-022-00760-z

Janis Timoshenko[1], Arno Bergmann[1], Clara Rettenmaier[1], Antonia Herzog[1], Hyo Sang Jeon[1], Felix T. Haase[1], Uta Hejral[1], Philipp Grosse[1], Stefanie Kühl[1], Earl M. Davis[1], Jing Tian[2], Olaf Magnussen[2] and Beatriz Roldan Cuenya[1]

1. Fritz-Haber Institute of the Max-Planck Society, Berlin, Germany
2. Institute of Experimental and Applied Physics, Kiel University, Kiel, Germany

Observing a Zn/Cu catalyst during methanol production

Live view into catalysis opens a vision for a greener future

Synthetic methanol is believed to be one of the key base chemicals and fuels to mitigate climate change and abolishing the use of fossil fuels. Consequently, the processes of making artificial fuels are at the heart of a change in our society. Industrially, methanol is synthesised over catalyst materials at high pressure and temperature. What exactly happens during this reaction has been unknown. In our contribution we have managed to gain a view into methanol synthesis as the reaction is occurring using PETRA III beamline P22 and the POLARIS instrument. Here, we report about our findings of the promoting mechanism of zinc in methanol synthesis and lay out a vision what questions science needs to address to aid the ongoing transformation of the chemical industry towards a fossil-free future.

Currently, the feedstock for the chemical industry is entirely based on fossil sources with an emittance of 8% of the world's footprint of greenhouse gases (not including when fuel is being burned). There is an urgency to transform the chemical industry away from fossil sources and towards captured CO_2 and H_2 from water electrolysis (see Fig. 1). This might include systems where wind or solar energy drives electrolytic cells for hydrogen production from water. For instance, the annual production of chemical methanol is around 110 million tons [1] which is then transformed to tens of thousands of different products including plastics, pharmaceuticals, fuels or detergents.
Even though methanol production is a century-old reaction, knowledge of the chemical state of the catalysts is sparse, since methods that probe the surface during the reaction have been lacking. One technique that is able to quantify this is photoelectron spectroscopy, traditionally a vacuum-based technique. Therefore, applying this technique in pressures of several hundred mbar has called for significant technological development. To this end, the POLARIS end station has been built by Stockholm University and is operated at the PETRA III beamline P22. Using it, we have enabled *operando* studies of the Zn/ZnO/Cu(211) surface under condition (Fig. 1a) approximating industrial conditions of methanol synthesis [2]. We aim to address the question regarding the state of zinc on the surface under operating conditions and elucidate the role of CO as as admixture. It has been shown in the literature that the reaction progresses more efficiently from CO_2 than from CO but a certain mixture of both yields an optimum.

We show the main results of our study in Fig. 2. The measurements in (b) are taken at a total pressure of 180 mbar at 140 °C with the indicated zinc coverage as Θ while in c) the total pressure is 500 mbar at 230°C. We record the Zn *3d* core-valence electron, the region that is consistently characterised by four peaks at 10.9, 10.3, 9.8 and 9.5 eV throughout the accumulated dataset. The low-binding energy peaks at 9.5 and 9.8 eV (green) correspond to the spin-orbit split states of metallic Zn $3d_{3/2}$ and Zn $3d_{5/2}$. The broad structure at 10.9 eV (gray) is associated with zinc in the +2 oxidation state related to bulk-like ZnO. The component at ~10.3 eV (light blue) is assigned to a $Zn^{\delta+}$ oxidation state species related to zinc interacting with formate and methoxy reaction intermediates as well as ZnOH. Thus, we identify the preferential states of zinc directly from the spectra under gas phase composition-dependent reaction conditions. Under CO-rich conditions, the metallic zinc signal is more dominant, whereas under CO_2-rich conditions, ZnO is strongly enhanced. This trend intensifies at higher pressure as depicted in Fig. 2c.

Taking this evidence and combining it with the information from the observed adsorbed stable reaction intermediates (not pictured), we reach an understanding of the active phase of methanol production on this zinc-promoted Cu catalyst. Balancing CO and CO_2 to stabilise the metallic surface state allows the reaction to progress more rapidly through the availability of surface near Zn-Cu alloy sites for the reduction of CO_2 and thereby optimises the reaction. ZnO is not regarded as an active participant of the reaction, and thus minimising this by the admixture of CO produces the desired effect of preventing the zinc oxidation. In this sense the correct mixing of CO and CO_2 leads to emergent behaviour, as the reaction progresses faster than with any of the two original components alone. Naturally, the catalysts in use today have been developed for over a century with fossil resources in mind. In view of the coming future we expect that the reality of hydrogen production will not allow as high-pressure reactions as methanol synthesis is done today. Instead, the hydrogen pressure from electrolysis cells are expected to be on the scale of ambient conditions (1–10 bar, 300 K). This effort needs to be met with studies of the chemical state of the catalyst material and the reaction intermediates during reaction conditions in order to give feedback for the catalyst development and is partially addressable with the current instrument. In view of the upcoming improvements through PETRA IV, we expect the a smaller beam footprint to enable us to increase the accessible pressures from 1 to at least 10 bar and to meet coming needs efficiently.

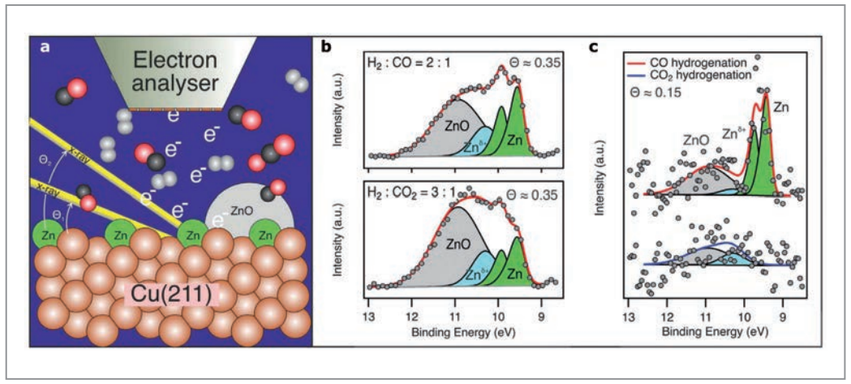

Figure 2
a) X-rays impinge on the Zn/ZnO/Cu surface under grazing incidence conditions (θ_1) and above the critical angle (θ_2), causing electron emission. The surface is kept at elevated temperature and in a virtual pressure cell containing CO, CO_2 and H_2 gas. The emitted electrons are transmitted into the electron analyser and enable a chemical quantification of the surface while methanol synthesis conditions are applied. b) and c) C compare CO and CO_2 hydrogenation conditions at 180 mbar at 140 °C and 500 mbar at 230 °C.

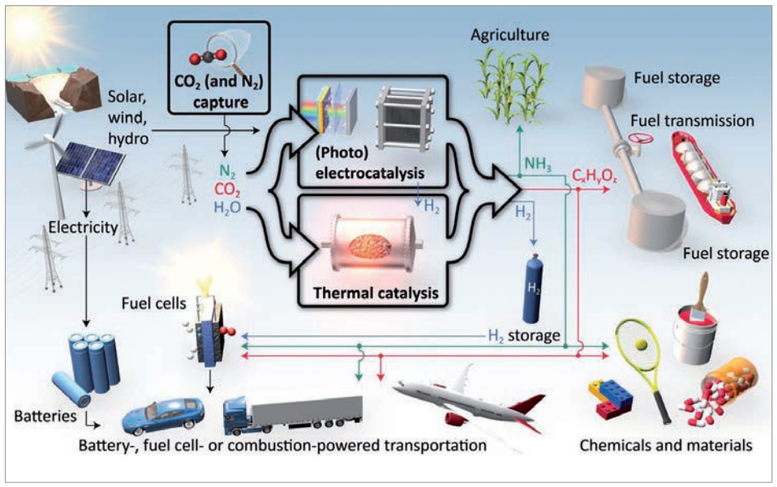

Figure 1
Illustration of a sustainable energy system to produce base chemicals for the industry and transportation fuel based on catalysis. Key processes are electrochemical water splitting and thermal and electrochemical CO_2 and N_2 reduction (Credit: Jakob Kibsgaard, DTU).

Author contact: Patrick Lömker, patrick.loemker@fysik.su.se
Peter Amann, peter.amann@scientaomicron.com
Anders Nilsson, andersn@fysik.su.se

References

1. *The Methanol Industry*, https://www.methanol.org/the-methanol-industry/ (accessed on 15. Dec. 2022).
2. P. Amann et al., *A high-pressure X-ray photoelectron spectroscopy instrument for studies of Industrially relevant catalytic reactions at pressures of several bars*, Rev. Sci. Instrum. 90, 103102 (2019).

Original publication

'The state of zinc in methanol synthesis over a Zn/ZnO/Cu(211) model catalyst', Science 376, 603-608 (2022).
DOI: 10.1126/science.abj7747

Peter Amann[1], Bernhard Klötzer[2], David Degerman[1], Norbert Köpfle[2], Thomas Götsch[3], Patrick Lömker[1,4], Christoph Rameshan[5], Kevin Ploner[2], Djuro Bikaljevic[2], Hsin-Yi Wang[1], Markus Soldemo[1], Mikhail Shipilin[1], Christopher M. Goodwin[1], Jörgen Gladh[1], Joakim Halldin Stenlidv, Mia Börner[1], Christoph Schlueter[4] and Anders Nilsson[1]

1. Department of Physics, Stockholm University, Stockholm, Sweden
2. Institute of Physical Chemistry, University of Innsbruck, Innsbruck, Austria
3. Department of Inorganic Chemistry, Fritz Haber Institute of the Max-Planck Society, Berlin, Germany
4. Deutsches Elektronen-Synchrotron DESY, Hamburg, Germany
5. Institute of Materials Chemistry, Technische Universität Wien, Vienna, Austria

Atmosphere effects on solar cells during degradation process

Revealing the degradation mechanisms of solar cells under operation

Constant research efforts have intensely increased the power conversion efficiencies of perovskite solar cells. This makes this new class of solar cells competitive with single-crystal silicon solar cells. However, today's stability issues are a remaining barrier towards industrialisation. Although scientists established a consensus statement stability assessment and reporting for perovskite cells (PSCs), conflicting results are reported, since a small detail in the experiments may lead to a large discrepancy in the results. For example, most scientists could consider nitrogen and vacuum conditions as similar inert conditions. Typically, researchers select them to avoid the effects of water or oxygen from air. However, our recent results confirm that this simplification is not valid and the effects of the atmosphere should not be overlooked, even if it is inert.

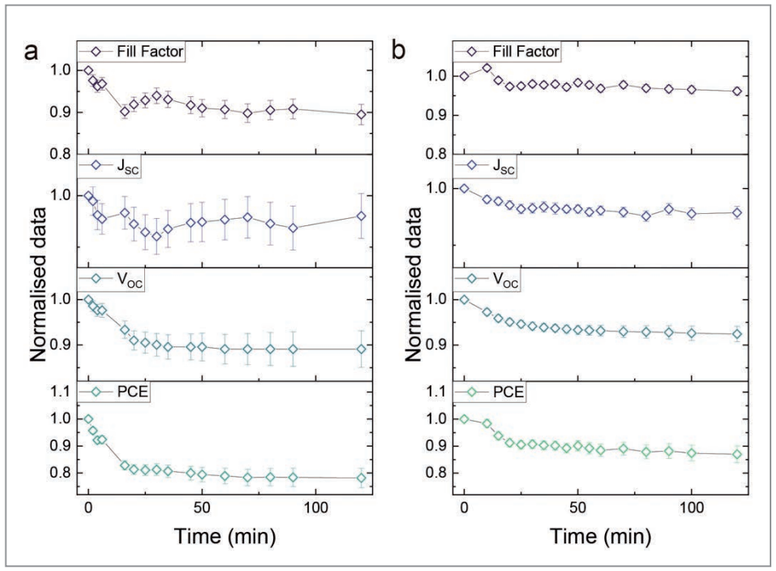

Figure 3
Evolution of Fill Factor, J_{SC}, V_{OC}, and PCE for perovskite solar cells operated under a) vacuum and b) nitrogen.

Solution-processed hybrid halide perovskite materials have attracted high interest for next-generation thin-film photovoltaic applications due to their outstanding power conversion efficiency (PCE) and low fabrication costs compared to silicon photovoltaics [1]. Although there is such a rapid increase in the PCE, more research effort is required on the stability studies of these materials and on the longevity of the devices, since long-term operational stability remains the main challenge for real-world applications [2]. Thus, we investigate the degradation mechanisms of perovskite solar cells under different atmospheres.

Integrating *operando* experiments of solar cells with synchrotron radiation-based grazing incidence X-ray scattering methods at beamline P03 at PETRA III allows for the understanding of the intermediate degradation processes of solar cells under operational conditions [3]. We find that perovskite solar cells experience a significant lattice shrinkage, a phase segregation into a $FAPbI_3$ phase as the minority phase and a large amount of $(MAPbBr_3)_{0.17+x}(FAPbI_3)_{0.83-x}$ (MA, methylammonium; FA, formamidinium) as the majority phase for the perovskite layer under standard one-sun illumination (AM1.5 G) in vacuum. In contrast, continuous operation in nitrogen under the same illumination intensity induces only a slight lattice shrinkage of the perovskite materials (Fig. 1).

Moreover, grazing incident small-angle X-ray scattering technology enables us to discover that crystals inside the perovskite film with diameters lower than 40 nm break into smaller crystals during the operation under vacuum (Fig. 2a). These small crystals act as pinholes in the PSCs which harm the performance of the devices, while, in nitrogen, the morphology of the perovskite layer remains stable. The loose space structure of spiro-OMeTAD offers physical pathways for such results. In vacuum, an outgassing process of MA molecules from the perovskite layer causes broken crystals when the perovskite solar cells are operated. In nitrogen, such a loose space structure allows for the diffusion of nitrogen molecules into the active layer underneath (Fig. 2b). This process can decrease the free energy via an exothermic process. Such physical adsorption of nitrogen could play an important role in reducing the film strain and maintaining the lattice and phase stability which is also related to a larger activation energy barrier for phase segregation.

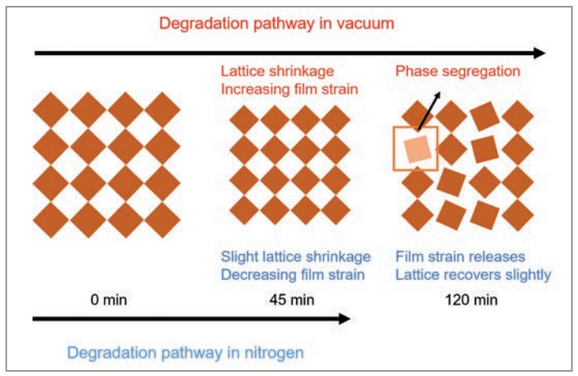

Figure 1
Schematic diagram projecting different lattice dynamics and phase stability when perovskite solar cells are operated under vacuum and nitrogen.

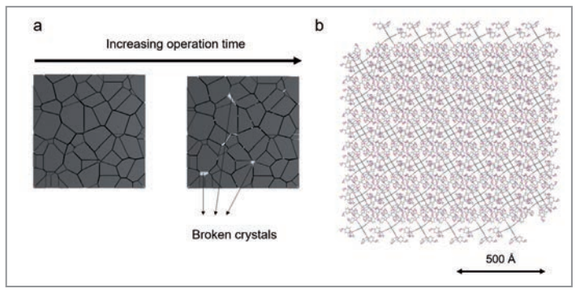

Figure 2
a) Scheme to illustrate the improved strength of the perovskite film to suppress further deformation through the increase of grain boundaries due to broken crystals. b) Schematic diagram of nitrogen molecules diffusing through the spiro-OMeTAD layer expressed by a pink (side chains) and grey (intermolecular π-π stacking) mixed space frame during the operation of solar cells under nitrogen.

The aforementioned different behaviours under vacuum and nitrogen, in turn, cause a different degree of device performance loss. Given that more stable lattice, structure and morphology behaviours when perovskite solar cells are operated under nitrogen, the perovskite solar cells show better stability compared with those solar cells operated under vacuum (Fig. 3).

In summary, our discoveries could offer scientists new insights for degradation studies on next-generation solar cells. Moreover, researchers, who use vacuum or nitrogen to avoid the effects of water and oxygen from air, should care about how a vacuum or nitrogen condition would affect their experimental results obtained from different characterisation methods like scattering, spectroscopy and microscopy.

Author contact: Renjun Guo, renjun.guo@ph.tum.de
Peter Müller-Buschbaum, muellerb@ph.tum.de

References

1. Thomas M. Brenner, David A. Egger, Leeor Kronik, Gary Hodes, David Cahen, 'Hybrid organic–inorganic perovskites: low-cost semiconductors with intriguing charge-transport properties', Nat. Rev. Mater., 1(1), 1-16 (2016).
2. Yaoguang Rong, Yue Hu, Anyi Mei, Hairen Tan, Makhsud I. Saidaminov, Sang Il. Seok, Michael D. McGehee, Edward H. Sargent, Hongwei Han, 'Challenges for commercializing perovskite solar cells', Science 361, 6408, eaat8235 (2018).
3. Adeline Buffet, André Rothkirch, Ralph Döhrmann, Volker Körstgens, Mottakin M. Abul Kashem, Jan Perlich, Gerd Herzog, Matthias Schwartzkopf, Rainer Gehrke, Peter Müller-Buschbaum, Stephan V. Roth, 'P03, the microfocus and nanofocus X-ray scattering (MiNaXS) beamline of the PETRA III storage ring: the microfocus endstation', J. Synchrotron Radiat. 19, 647-653 (2012).

Original publication

'Degradation mechanisms of perovskite solar cells under vacuum and one atmosphere of nitrogen', Nature Energy 6, 977–986 (2021). DOI: 10.1038/s41560-021-00912-8

Renjun Guo[1,10], Dan Han[2,10], Wei Chen[1,3,10], Linjie Dai[4], Kangyu Ji[4], Qiu Xiong[5], Saisai Li[6], Lennart K. Reb[1], Manuel A. Scheel[1], Shambhavi Pratap[1], Nian Li[1], Shanshan Yin[1], Tianxiao Xiao[1], Suzhe Liang[1], Anna Lena Oechsle[1], Christian L. Weindl[1], Matthias Schwartzkopf[7], Hubert Ebert[2], Peng Gao[5], Kai Wang[3], Mingjian Yuan[6], Neil C. Greenham[4], Samuel D. Stranks[4], Stephan V. Roth[7,8], Richard H. Friend[4] and Peter Müller-Buschbaum[1,9]

1. Chair for Functional Materials, School of Natural Sciences, Technical University of Munich, Garching, Germany
2. Department of Chemistry, Ludwig-Maximilians-Universität München, Munich, Germany.
3. Department of Electrical and Electronic Engineering, Southern University of Science and Technology, Shenzhen, China
4. Cavendish Laboratory, University of Cambridge, Cambridge, UK
5. Fujian Institute of Research on the Structure of Matter, Chinese Academy of Sciences, Fuzhou, China
6. Department of Chemistry, Nankai University, Tianjin, China
7. Deutsches Elektronen-Synchrotron DESY, Hamburg, Germany
8. Chemical Engineering and Biotechnology, University of Cambridge, Cambridge, UK
9. Department of Fiber and Polymer Technology, KTH Royal Institute of Technology, Stockholm, Sweden
10. Heinz Maier-Leibnitz-Zentrum, Technical University of Munich, Garching, Germany

From the beamline to the field

Green and solventless synthesis of a stable and efficient urea fertiliser developed with the help of direct synchrotron X-ray monitoring

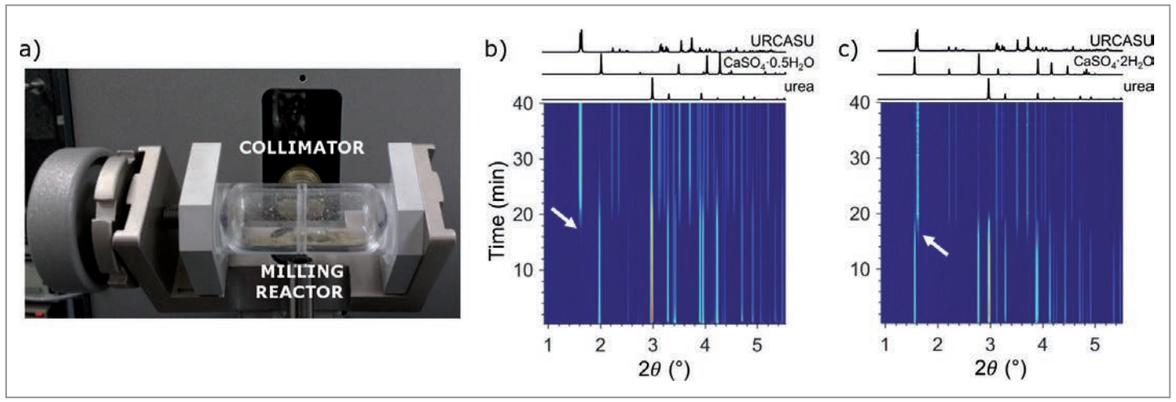

Figure 2

a) The experimental setup for high-energy synchrotron X-ray diffraction (XRD) monitoring of mechanochemical reactions. Reaction profiles obtained from *operando* monitoring by XRD for the reactions of urea with b) calcium sulfate hemihydrate and c) calcium sulfate dihydrate (gypsum). The white arrows indicate the beginning of the conversion from reactants to products.

Artificial fertilisers are crucial for future global food security but present an important sustainability challenge. While sustainably producing enough nitrogen fertiliser to feed the world is already difficult, a lot of it gets lost through decomposition or washing out from the soil. This requires more fertiliser to be added and uses a lot of resources and energy. With the help of direct and real-time monitoring of the mechanochemical synthesis of calcium urea sulfate, we devised a green, solvent-free, economical and scalable procedure for preparing a more efficient and stable fertiliser candidate from gypsum and urea.

Direct *operando* monitoring of mechanochemical reactions by high-energy synchrotron X-ray diffraction (XRD) at beamline P02.1 of PETRA III provided real-time insight into the solvent-free synthesis of a highly potent fertiliser, calcium urea sulfate (URCASU), from gypsum and urea (Fig. 1). *In situ* XRD and variable temperature experiments allowed us to optimise the mechanochemical process and transfer it to large-scale production. The procedure can also be applied to construction gypsum, allowing for the transformation of construction waste into an added-value product.

Urea is one of the most essential and ubiquitous nitrogen fertilisers. However, when used in real-world conditions, its high solubility as well as moisture- and photo-sensitivity result in significant losses. One solution is the preparation of urea-containing compounds that degrade and dissolve more slowly, increasing the retention and availability of urea in the soil. Importantly, these materials must be affordable and accessible at large scales. A good candidate is URCASU [1], an adduct of urea and calcium sulfate whose dihydrate form, gypsum, is a ubiquitous construction material and one of the major components of construction waste. Unfortunately, due to the low solubility of gypsum, an excess of water and urea are needed in the traditional solution synthesis process. At a larger scale, such a solution-based approach is costly, energetically demanding and generates a considerable amount of waste. To address these issues, we devised a robust and efficient green procedure for preparing this fertiliser candidate using mechanochemistry.

In the last two decades, mechanochemistry has developed into a powerful green chemistry alternative to conventional

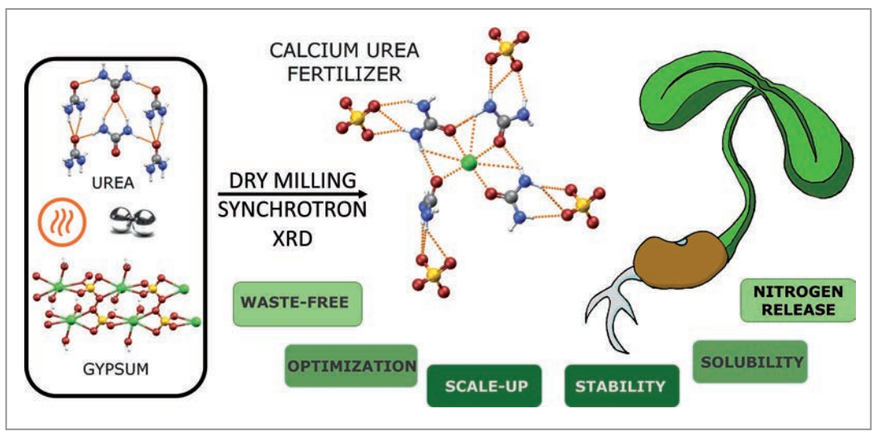

Figure 1

A schematic representation of the mechanochemical synthesis of calcium urea sulfate (URCASU) from gypsum and urea. The fertiliser synthesis is optimised to be efficient, waste-free and applicable on a large scale. The product has better soil retention properties and a beneficial nitrogen release profile compared to pure urea.

synthetic procedures with many advantages, such as higher yields, lower energy and time demands and the stabilisation of some products not available by other techniques [2]. Importantly, mechanochemical reactions are well known for converting poorly soluble reactants into the desired products. However, as mechanochemical processing is conducted in rapidly oscillating vessels containing hard milling media, it is hard to monitor the progress of reactions and optimise them for processing at larger scales. Direct insight into the solid phases occurring during milling was only recently enabled through advanced monitoring techniques such as XRD, sometimes complemented with Raman spectroscopy [3]. P02.1 is one of the few beamlines in the world equipped for *operando* monitoring mechanochemical reactions by X-ray diffraction.

We monitored the mechanochemical formation of URCASU from different forms of calcium sulfate and at different temperatures using XRD (Fig. 2). Combined with Raman spectroscopy, this enabled us to determine that the reaction highly depends on the amount of crystallised water in the calcium sulfate reactant: Only the most hydrated form, gypsum, reacts to the target product quantitatively, and adding external water to the synthesis, inhibits the transformation. The optimised method, therefore, requires no added water and the only 'waste product' is water generated in the reaction.

Based on these results, we transferred the process to larger scales. A large-scale batch synthesis was performed in a planetary mill, producing URCASU in hectogram quantities. A continuous mechanochemical process using a twin-screw extruder enabled the kilogram scale production of the target fertiliser with a much lower relative energy consumption than batch processing. The continuation of this study has shown that construction waste gypsum can be used as a reactant.

The mechanochemically prepared URCASU proved to have superior stability, solubility and release properties compared to urea and other calcium urea adducts, positioning itself as a strong candidate for agricultural applications.

Author contact: Krunoslav Užarević, krunoslav.uzarevic@irb.hr

References

1. C. W. Whittaker, F. O. Lundstrom and S. B. Hendricks, 'Reaction between Urea and Gypsum', Ind. Eng. Chem. 25, 1280-1282 (1933).
2. S. L. James et al. 'Mechanochemistry: opportunities for new and cleaner synthesis', Chem. Soc. Rev. 41, 413-447 (2012).
3. K. Užarević, I. Halasz and T. Friščić, 'Real-Time and *In Situ* Monitoring of Mechanochemical Reactions: A New Playground for All Chemists', J. Phys. Chem. Lett. 6, 4129–4140 (2015).

Original publication

'Scale-up of agrochemical urea-gypsum cocrystal synthesis using thermally controlled mechanochemistry', ACS Sustainable Chemistry & Engineering 10, 6743-6754 (2022), DOI: 10.1021/acssuschemeng.2c00914

Ivana Brekalo[1], Valentina Martinez[1], Bahar Karadeniz[1], Patrik Orešković[2], Donata Drapanauskaite[3], Hein Vriesema[4], Robert Stenekes[4], Martin Etter[5], Igor Dejanović[2], Jonas Baltrusaitis[3] and Krunoslav Užarević[1]

1. Department of Physical Chemistry, Ruđer Bošković Institute, Zagreb, Croatia
2. Faculty of Chemical Engineering and Technology, University of Zagreb, Zagreb, Croatia
3. Department of Chemical and Biomolecular Engineering, Lehigh University, Bethlehem, United States of America
4. ICL Group, Amsterdam, Netherlands
5. Deutsches Elektronen-Synchrotron DESY, Hamburg, Germany

Quasi-atomic behaviour of nanocrystals in superlattices

Variation of optical properties and structure of caesium lead halide perovskite nanoparticles in a supercrystal

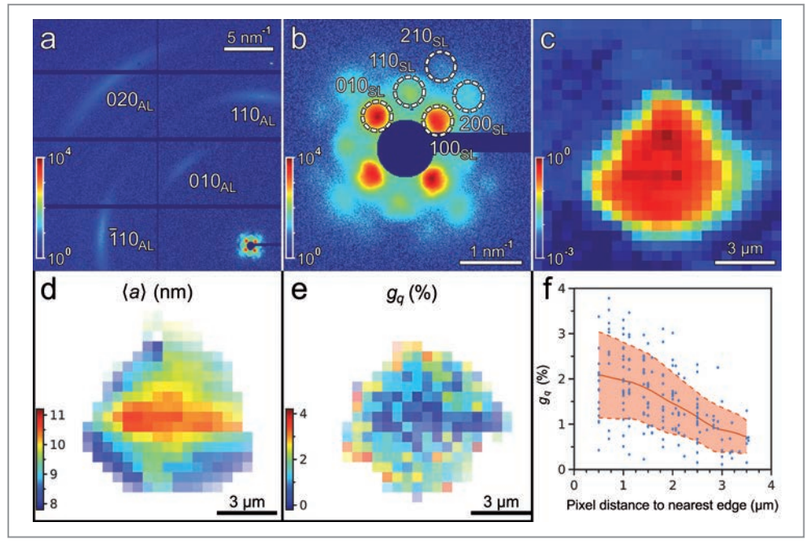

Figure 2

Spatially resolved X-ray nanodiffraction experiment performed on a $CsPbBr_2Cl$ NC supercrystal: a) Average diffraction pattern for a supercrystal. b) Enlarged SAXS region of the averaged diffraction pattern. c) Diffraction map for a scan based on the integrated intensity of the SAXS diffraction patterns at $q < 2\ nm^{-1}$. d) Spatially resolved SAXS. An extracted average unit parameter ⟨a⟩ is shown. e) Atomic lattice distortion g_q extracted from the Williamson–Hall method. f) The same value g_q for each pixel plotted against the distance from this pixel to the nearest edge of the supercrystal. (Adapted from a figure in the original publication licensed under CC BY 4.0.)

Advances of the self-assembly of colloidal nanocrystals (NCs) from solution into three-dimensional arrays with long-range order have enabled the design of microscopic supercrystals that approach the structural precision of atomic single crystals [1]. As the building blocks of a supercrystal, the individual NCs are often regarded as 'artificial atoms'. A large structural coherence of these supercrystals facilitates new collective optoelectronic properties, which makes them prospective materials for electronics and photovoltaics. However, a critical question remains: whether this artificial atom analogy can also be transferred to the corresponding optical properties of NC supercrystals?

To answer the question on these metamaterials and their unique optical properties [2-4], we studied self-assembled supercrystals consisting of perovskite nanocrystals with two different chemical compositions: $CsPbBr_2Cl$ and $CsPbBr_3$. The NCs are monodisperse cubes with a diameter of 7 nm for $CsPbBr_2Cl$ and 9 nm for $CsPbBr_3$. Spatially resolved photoluminescence spectra of the 2.5 µm thick $CsPbBr_2Cl$ NC supercrystal samples on glass substrate under 405 nm excitation in a confocal laser scanning microscope are shown in Fig. 1 (a,b). When approaching an edge of the supercrystal, a continuous blueshift of the emission peak wavelength takes place. This blueshift is strongest for relatively small and highly faceted supercrystals, where it reaches energies up to 20 meV. In the case of supercrystals composed of $CsPbBr_2Cl$ NCs, we measure typical fluorescence lifetimes (τ) around 2.1 ns in the centre which decrease by approximately 20% when scanning from the centre of a supercrystal towards its edges (see Fig. 1 (c,d)).

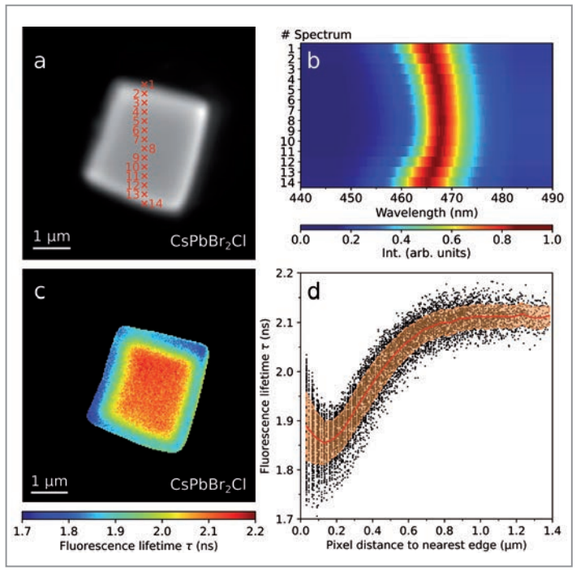

Figure 1

Spatially resolved fluorescence and lifetime imaging. a) Optical micrograph of a $CsPbBr_2Cl$ NC supercrystal. b)The corresponding normalized spectra. c) Fluorescence lifetime τ map of a $CsPbBr_2Cl$ NC supercrystal. d) Fluorescence lifetime values τ obtained at each pixel inside the supercrystal as a function of the distance to the nearest edge. (Adapted from a figure in the original publication licensed under CC BY 4.0.)

To find out the origin of these differences in the fluorescence spectra, which change from the centre of the supercrystal to its edges, we investigated its structure and carried out a synchrotron X-ray diffraction experiment at the PETRA III beamline P10. Using an X-ray beam focused to approximately 400 nm × 400 nm on the sample, we performed a spatially resolved scan of a typical $CsPbBr_2Cl$ NC supercrystal on a Kapton substrate. The averaged wide-angle X-ray scattering pattern (WAXS) is shown in Fig. 2a. The small-angle X-ray scattering (SAXS) region (Fig. 2b) displays several orders of Bragg peaks, corresponding to a simple cubic structure. A real space map of the scan based on the integrated SAXS intensity, corresponding to a single supercrystal is shown in Fig. 2c. Analysing individual SAXS patterns from different locations on the supercrystal, we find that the lattice parameter decreases from the value of $a = 10.7$ nm in the centre of the supercrystal down to $a = 7.8$ nm at the edges (Fig. 2d).

Despite the fact that the atomic average lattice parameter of the NCs a_{AL} is constant throughout the whole supercrystal, we find a difference in the radial width of the WAXS Bragg peaks at different locations. By the Williamson–Hall method, we extract the atomic lattice distortion $g_q = \delta a_{AL}/a_{AL}$ at each spatial point. We find a clear trend of increasing atomic lattice distortion towards the edges of the supercrystal with a maximum of 2% at the edge, as shown in Fig. 2 (e,f). This indicates that, during the process of self-assembly into supercrystals from colloidal solution by slow drying, not only the superlattice exhibits distortions at the edges of supercrystal [5], but also the individual NCs are highly strained at the edges.

To rationalise the experimental trend of increased fluorescence energies at the edges of the supercrystal as compared to its centre, we carried out density functional modeling of the system. Overall, our computational modeling suggests that the spectral blueshift of the fluorescence from the edges of the supercrystal can be caused mainly due to a reduced NC coordination number at the edges as well as the compressive atomic lattice strain.

In conclusion, supercrystals of lead halide perovskite NCs self-assembled from solution exhibit a loss in structural coherence, an increasing atomic misalignment between adjacent NCs and compressive strain near their surfaces. These structural distortions are strongly correlated with a blueshifted fluorescence and decreased radiative lifetimes. Our results emphasise the importance of minimising strain during the self-assembly of perovskite nanocrystals into supercrystals for photovoltaic applications such as superfluorescent emitters. The correlations between structure and fluorescence in supercrystals revealed here are thus another example for the analogy between atoms and NCs as so-called quasi-atoms.

Author contact:
Marcus Scheele, marcus.scheele@uni-tuebingen.de
Ivan Vartaniants, ivan.vartaniants@desy.de

References

1. S. Toso et al., 'Multilayer diffraction reveals that colloidal superlattices approach the structural perfection of single crystals', ACS Nano 15, 6243–6256 (2021).
2. G. Rainò et al., 'Superfluorescence from lead halide perovskite quantum dot superlattices', Nature 563, 671–675 (2018).
3. Y. Tong et al., 'Spontaneous self-assembly of perovskite nanocrystals into electronically coupled supercrystals: toward filling the green gap', Adv. Mater. 30, 1801117 (2018).
4. I. Cherniukh et al., 'Perovskite-type superlattices from lead halide perovskite nanocubes', Nature 593, 535–542 (2021).
5. N. Mukharamova et al., 'Revealing grain boundaries and defect formation in nanocrystal superlattices by nanodiffraction', Small 15, 1904954 (2019).

Original publication

'Spatially resolved fluorescence of caesium lead halide perovskite supercrystals reveals quasi-atomic behavior of nanocrystals', Nature Communications 13, 892 (2022).
DOI: 10.1038/s41467-022-28486-3

Dmitry Lapkin[1], Christopher Kirsch[2], Jonas Hiller[2], Denis Andrienko[3], Dameli Assalauova[1], Kai Braun[2], Jerome Carnis[1], Young Yong Kim[1], Mukunda Mandal[3], Andre Maier[2,4], Alfred J. Meixner[2,4], Nastasia Mukharamova[1], Marcus Scheele[2,4], Frank Schreiber[4,5], Michael Sprung[1], Jan Wahl[2], Sophia Westendorf[2], Ivan A. Zaluzhnyy[5] and Ivan A. Vartanyants[1]

1. Deutsches Elektronen-Synchrotron DESY, Hamburg, Germany
2. Institut für Physikalische und Theoretische Chemie, Universität Tübingen, Tübingen, Germany
3. Max Planck Institute for Polymer Research, Mainz, Germany
4. Center for Light-Matter Interaction, Sensors & Analytics LISA+, Universität Tübingen, Tübingen, Germany
5. Institut für Angewandte Physik, Universität Tübingen, Tübingen, Germany

Magnet for the needle in giant haystacks

A powerful approach to accelerate drug discovery

The initial stage of drug discovery is often compared to the search for a 'needle in a haystack'. The 'haystack' is a library of small molecules which is screened against a protein target. The 'needle' is a molecule that shows activity in an assay against the protein and structural biology is used to confirm its binding on the molecular level. In our work, we turn this paradigm upside down and propose a new strategy to perform fragment-based drug discovery (FBDD). We demonstrate the effectiveness of the approach to retrieve active molecules from vast chemical spaces containing billions of candidate molecules by starting with structural biology first.

The goal of any pre-clinical drug discovery phase is to develop molecules matching the desired properties of a drug. One such property is the strong binding of the molecule to its protein target. To prioritise binding strength, assays have been established in the drug industry in order to detect such strong binders. High-throughput screening (HTS) campaigns test thousands to millions of molecules. Active molecules are named hits. Hits serve as starting points for chemical optimisation. Structural biology is applied afterward and hits are prioritised by their binding strength. Although HTS is a frequently applied method, it has limitations: low hit rates compared to enormous costs and often hits of too large a molecular size. This process is depicted in Fig. 1a.

In our work, we followed a 'crystal structure first' approach instead [1]. Our strategy starts with experimental data from crystallographic screenings of very small probe-like molecules, termed 'fragments', to identify their usually very weak binding. The result is an experimentally validated 3D structure showing the interactions and binding pose. This workflow is depicted in Fig. 1b. Such weak binders can hardly be detected in a binding assay or will not be considered as promising candidates. In addition, our approach provides structural validation at the same time.

We started with four crystal structures of fragment complexes with protein kinase A (PKA). Based on these structures, a virtual library of 2.8 billion synthetically accessible molecules was enumerated by embedding the fragments into bigger molecules. In the next step, the library was subjected to template docking. About two million compounds were scored and filtered. This step is called 'chemical space docking' (Fig. 2). Out of 106 selected compounds, 93 were successfully synthesised and tested for their inhibition of the target protein. Our candidates, resulting from the computational expansion, have the usual size of compounds used in HTS. But the major difference is that our candidates are pre-selected, based on solid data from structural biology.

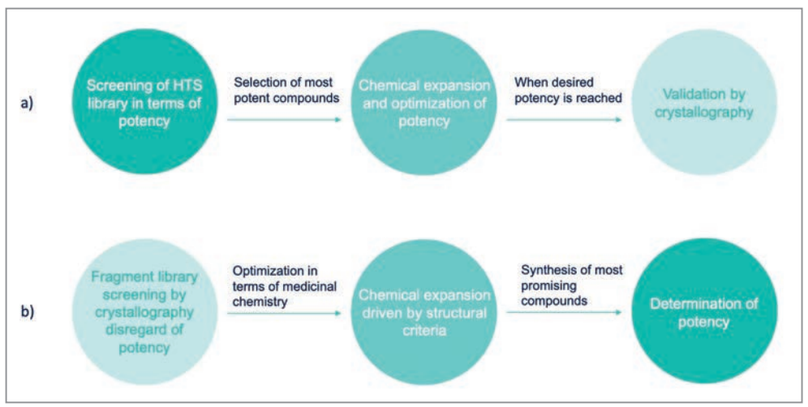

Figure 1

a) Workflow of general HTS drug discovery campaigns. b) Workflow of herein proposed 'crystal-structure first' approach.

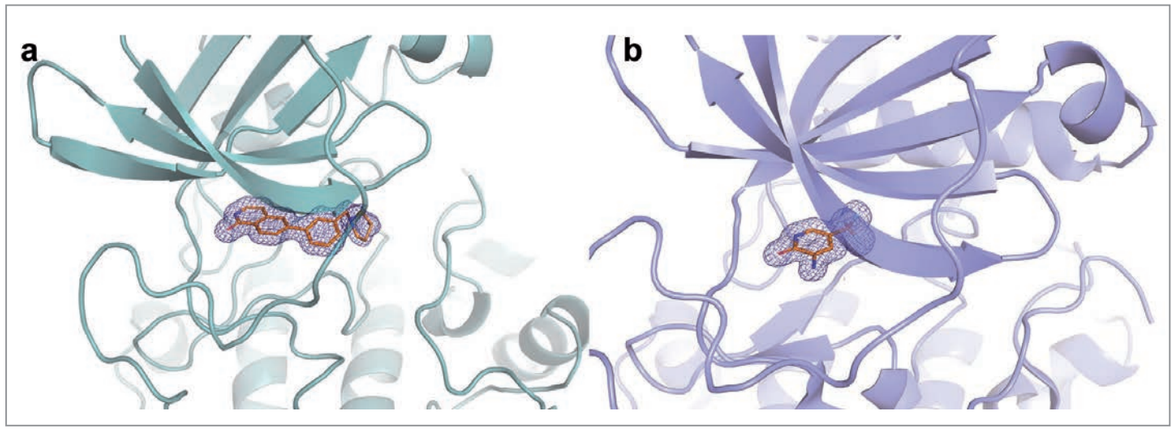

Figure 3

a) Experimentally determined electron density of the most potent compound EN093 (affinity ~ 700 nM). b) The fragment (Frag 2, no significant affinity) which was used as a template.

Overall, about 40% of the 93 compounds exhibited activity in the assays, a hit rate not achievable using HTS. The most potent compounds were co-crystallised and measured at the P11 beamline. The complex structures confirmed that these candidates exhibited the desired binding modes. They aligned well with the binding modes of the starting fragments. Electron densities of the complex structures for the fragment and the most potent compound are shown in Fig. 3.

This campaign was accomplished in nine weeks, highlighting the efficiency and effectiveness of our approach. It also indicates potential deficiencies in HTS-driven approaches: The third most active compound in the assays did not bind to the protein in the crystal structure and represented a false positive. Additionally, the four starting fragments used for the computational expansion did not show any significant activity in either assay. Thus, the screening setup in HTS would have missed these fragments as promising starting points.

Since this approach uses structural data, the determination of crystallographic information is essential. Access to high throughput structure determination at a synchrotron is therefore crucial. P11 at PETRA III provides the possibility to measure crystals in an efficient manner and facilitates such 'crystal structure first' campaigns.

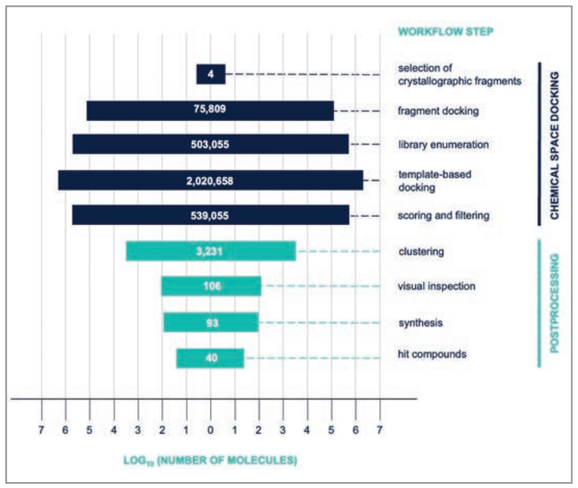

Figure 2

A top-to-bottom overview of the 'chemical space docking' method including the used post-processing exercise and number of enumerated molecules in each step.

Author contact:
Serghei Glinca, serghei.glinca@crystalsfirst.com

References

1. J. Schiebel, N. Radeva, S. G. Krimmer, X. Wang, M. Stieler, F. R. Ehrmann, K. Fu, A. Metz, F. U. Huschmann, M. S. Weiss, U. Mueller, A. Heine, G. Klebe, 'Six Biophysical Screening Methods Miss a Large Proportion of Crystallographically Discovered Fragment Hits: A Case Study', ACS Chem. Biol. 11, 1693-1701 (2016).

Original publication

'Magnet for the Needle in Haystack: "Crystal Structure First" Fragment Hits Unlock Active Chemical Matter Using Targeted Exploration of Vast Chemical Spaces', Journal of Medicinal Chemistry 65, 15663–15678 (2022).
DOI: 10.1021/acs.jmedchem.2c00813

Janis Müller[1], Raphael Klein[2], Olga Tarkhanova[3], Anastasiia Gryniukova[4], Petro Borysko[4], Stefan Merkl[1], Moritz Ruf[1], Alexander Neumann[2], Marcus Gastreich[2], Yurii S. Moroz[4,5], Gerhard Klebe[6] and Serghei Glinca[1]

1. CrystalsFirst GmbH, Hamburg & Marburg, Germany
2. BioSolveIT GmbH, Sankt Augustin, Germany
3. Chemspace LLC, Kyiv, Ukraine
4. Enamine Ltd., Kyiv, Ukraine
5. Taras Shevchenko National University of Kyiv, Ukraine
6. Philipps-University Marburg, Marburg, Germany

How equal charges in enzymes control biochemical reactions

Fundamental principles of enzyme catalysis disclosed

It is a well-established principle in physics and chemistry that equal charges repel each other, whereas opposite charges attract. It was long assumed that this principle also holds when enzymes – the biological catalysts in all living organisms – make or break chemical bonds. Scientists thought that enzymes place charges in their 'active sites', that is where the chemical reactions actually take place, in such a way that they repel similar charges from molecules binding them. This concept is called 'electrostatic stress'. If the substrate (the molecule upon which an enzyme acts) would, e.g. carry a negative charge, the enzyme could use a negative charge to 'stress' the substrate and thus facilitate the reaction.

We analysed the enzyme orotidine-5-monophosphate decarboxylase (OMPDC) which has been studied extensively and actually serves as a textbook example of enzyme catalysis. In the absence of the enzyme, the reaction proceeds extremely slowly: in fact, it would take 78 million years for half of the substrate to react [1]. The enzyme accelerates this reaction by a factor of 10^{17}, just by correctly positioning positive and negative charges in the reaction chamber. Since the substrate contains a negatively charged group that is split off as carbon dioxide, it was assumed for decades that the negative charges of the enzyme serve to stress the substrate, which is also negatively charged and accelerate the reaction [2]. However, this hypothetical mechanism remained unproven because the structure of the reaction was too fast to be observed.

Using protein X-ray crystallography at EMBL beamline P14 at PETRA III, we have now succeeded for the first time to obtain a structural snapshot of the substrate shortly before the chemical reaction takes place. The structure of the enzyme with bound substrate could be captured at the very high resolution of 0.99 Å, allowing us to disclose fine-structural details including bond distortions and protonation states. Unexpectedly, the two negative charges of enzyme and substrate did not repel each other as predicted by the electrostatic stress concept (Fig. 1). Instead, they shared a proton in a low-barrier hydrogen bond in an attractive interaction. Also, the substrate is physically distorted by the enzyme resulting in a selective bond activation of the scissile substrate bond.

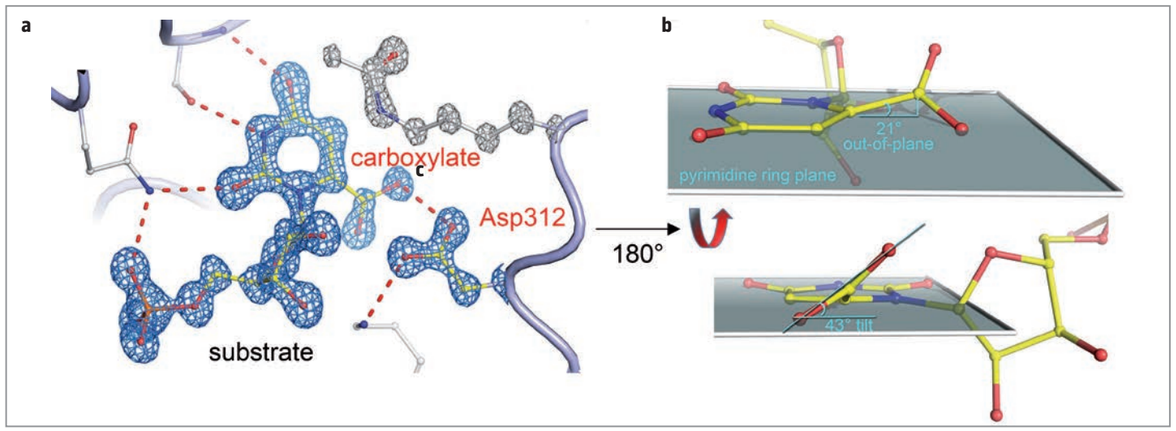

Figure 1

Structural snapshot of substrate binding in the enzyme orotidine-5-monophosphate decarboxylase. a) Structure of substrate OMP (orotidine-5'-monophosphate) bound to human orotidine-5'-monophosphate decarboxylase at 0.99 Å resolution highlighting critical hydrogen bond interactions with protein groups. Note the short, strong H-bond between the substrate carboxylate and residue Asp312 that is incompatible with the proposed electrostatic repulsion between the two carboxylate groups. The structural models of substrate OMP, interacting residue Asp312 and mutated residue 314 are superposed with the corresponding 2mFo-DFc electron density map at a contour level of 3σ. b) Structural features of enzyme-bound substrate highlighting the out-of-plane distortion of the scissile bond and of the substrate carboxylate relative to the pyrimidine ring plane shown in grey, suggesting a selective bond activation of the scissile substrate bond.

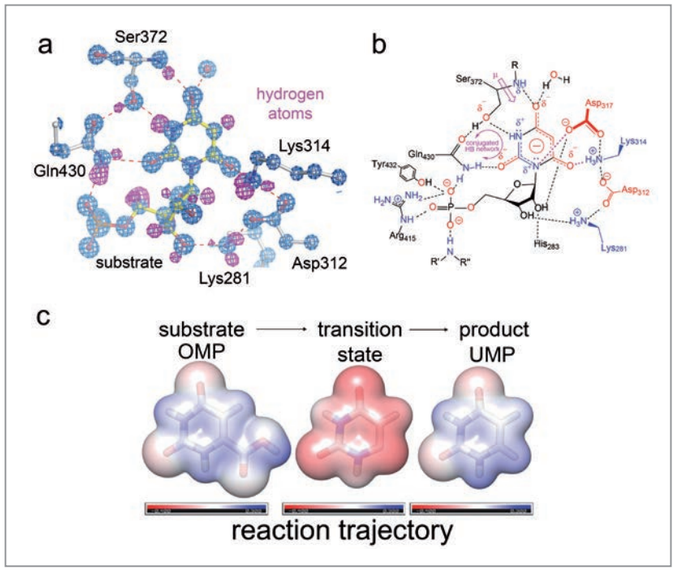

Figure 2

Structure of orotidine-5-monophosphate decarboxylase in complex with a transition-state analogue and implications for the mechanism. a) Structure of transition-state analogue BMP bound to the active site of the human enzyme at a resolution of 0.90 Å highlighting critical H-bonding interactions with protein groups. The structural model is superposed with the corresponding 2mFo-DFc electron density map (blue, contour level 5.3σ). Peaks in the H-omit mFo-DFc difference electron density map (magenta, contour level 3σ) indicate the positions of hydrogen atoms shown in cyan. b) Suggested chemical and electronic structure of the enzyme: transition-state complex showing the corresponding ionisation states as well as H-bond and electrostatic interactions. c) Molecular electrostatic potentials (isosurface value of 0.005 e/Bohr3, colour coding scale in atomic units) for substrate, the genuine transition state and product computed at the B3LYP-D3(BJ)/def2-SVP(IEPFPCM) level of theory suggest that the catalytic prowess of orotidine-5-monophosphate decarboxylase – its preferential binding of the transition state - predominantly results from the development and spread of charge in the transition state.

In addition, we determined a series of structural snapshots along the pathway including enzyme complexes with substrate analogues, transition-state analogues and the product, all at true atomic resolution (Fig. 2). These structural data were combined with extensive quantum chemical calculations and allowed us to define the governing principles of enzyme action. Apparently, OMPDC has evolved an effective transition-state stabilisation by an architecture that provides multiple favourable electrostatic interactions in a network of alternating charges.

Taken together, our structural analysis of OMPDC catalysis has unexpectedly revealed that electrostatic repulsion between substrate and enzyme, as one proposed form of ground-state destabilisation, is not a driving force for this reaction. While enzymes are capable of stressing their substrates by binding them in physically distorted conformations and thus selectively destabilise scissile substrate bonds as also observed in our study, charge-charge interactions are exploited productively and are central to effective transition-state stabilisation. The active site architecture of OMPDC, also referred to as 'the most proficient enzyme' [1], highlights the use of a dedicated network of alternating charges and dipoles that perfectly embrace the reacting substrate and stabilise the charges evolving in the transition state. The enzyme-catalysed decarboxylation is facilitated by hydrogen bond interactions between the substrate carboxylate and acidic side chains of the protein that ensure differential binding of the transition state and reactant state in line with Pauling's famous proposal that enzymes stabilise the transition-state of biochemical reactions.

We are optimistic that these newly described principles of enzyme catalysis will help in the development of new chemical catalysts. Since the enzyme we studied releases carbon dioxide, the most important greenhouse gas produced by human activities, our results could help develop new chemical strategies for carbon dioxide fixation.

Author contact: Kai Tittmann, ktittma@gwdg.de

References

1. A. Radzicka and R. Wolfenden, 'A proficient enzyme', Science 267, 90-93 (1995).
2. N. Wu, Y. Mo, J. Gao, and E. F. Pai, 'Electrostatic stress in catalysis': structure and mechanism of the enzyme orotidine monophosphate decarboxylase, Proc. Natl. Acad. Sci. USA 97, 2017-2022 (2000).

Original publication

'Ground-state destabilisation by electrostatic repulsion is not a driving force in orotidine-5'-monophosphate decarboxylase catalysis', Nature Catalysis 5, 332–341 (2022).
DOI: https://doi.org/10.1038/s41929-022-00771-w

S. Rindfleisch[1], M. Krull[2], J. Uranga[3], T. Schmidt[2], F. Rabe von Pappenheim[1], L. L. Kirck[1], A. Balouri[3], T. Schneider[4], A. Chari[5], R. Kluger[6], G. Bourenkov[4], U. Diederichsen[2], R. A. Mata[3] and K. Tittmann[1]

1. Göttingen Center of Molecular Biosciences, Georg-August University Göttingen, Göttingen, Germany
2. Institute for Organic and Biomolecular Chemistry, Georg-August University Göttingen, Göttingen, Germany
3. Institute of Physical Chemistry, Georg-August University Göttingen, Göttingen, Germany
4. European Molecular Biology Laboratory (EMBL), Hamburg Outstation c/o Deutsches Elektronen-Synchrotron (DESY), Hamburg, Germany
5. Max-Planck-Institute for Multidisciplinary Sciences, Göttingen, Germany
6. University of Toronto, Toronto, Canada

Structural high-resolution X-ray imaging of neurodegenerative diseases

Phase-contrast tomography identifies changes of neuronal structures in Alzheimer's dementia

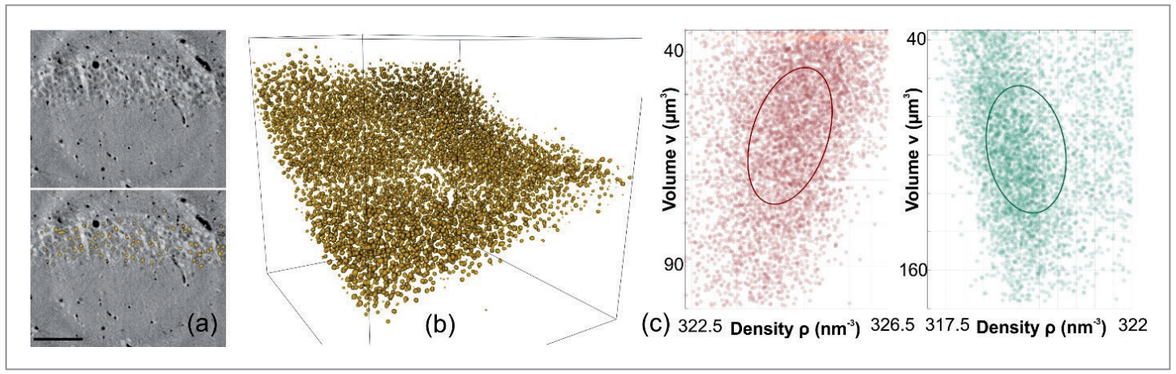

Figure 2

Segmentation of cellular nuclei and feature extraction. (a) Tomographic reconstruction yields 3D maps of the electron density in which the neurons are identified using machine learning. (b) The nuclei of granule neurons in human hippocampus rendered within a volume corresponding to a high-resolution recording. (c) Each neuron corresponds to a point in a higher dimensional feature space. Here, projections into the plane spanned by the parameters volume and density are shown for a sample from the AD group (red) and the control group (green). These distributions differ between patients and shift during disease progression of AD. The following prototypical changes along the transition from physiological to pathological structure are observed: The nuclei become denser, smaller and more heterogeneous in AD.

Which changes in brain tissue are associated with neurodegenerative diseases? How does the structure of the neurons change? Some pathological changes in the tissue are easy to identify using standard microscopy. For example, protein deposits known as 'plaques', which occur in Alzheimer's disease, can be observed with staining techniques. However, pathological changes may also be very subtle and can easily be missed without a complete analysis of the three-dimensional structure. Here, we present a new approach to measure and quantify neuronal tissue architecture in three dimensions at high resolution, which enables us to identify previously unknown structural neuronal changes in Alzheimer's dementia.

Neurons are excitable cells that use electrical impulses and chemical signals to send and process information. In order to understand the physiology and pathologies of the brain, one wants to understand how neurons are located with respect to each other, how they are shaped, and if and how this cytoarchitecture changes in the course of neuro-degenerative diseases such as Alzheimer's dementia (AD). We are asking to which extent the cytoarchitecture of the human brain correlated to its function, and how can we quantify such structure-function relationships? Which morphometric parameters can reveal the pathway from healthy to pathological states of the brain? How do we find these parameters without narrowing our search space to the initial hypothesis? Should we only screen for structural alterations for which we can already formulate a disease-related hypothesis, or should we try to perform a broader structural data mining? And finally, how much inter-subject diversity is found in healthy subjects or patients suffering from neuro-degenerative diseases such as Alzheimer's disease?

In this work, we present methods and workflows to answer these questions. In particular, we use high-resolution and multi-scale phase contrast X-ray tomography to assess the cytoarchitecture of the dentate gyrus of the hippocampus with sub-cellular resolution in *post mortem* brain tissue of AD patients and healthy controls. The hippocampus is known as a brain region where memories are transferred from short-term to long-term memory. Chemically fixed tissue samples were available in paraffin blocks, the standard conservation of tissue in clinical pathology. Pieces with a few millimetres diameter were punched out of the tissue blocks and then scanned by phase-contrast tomography in parallel and in cone beam geometry at the GINIX endstation of beamline P10 at PETRA III [2]. The recordings and phase retrievals were optimised for soft unstained tissue which only weakly absorbs X-rays.

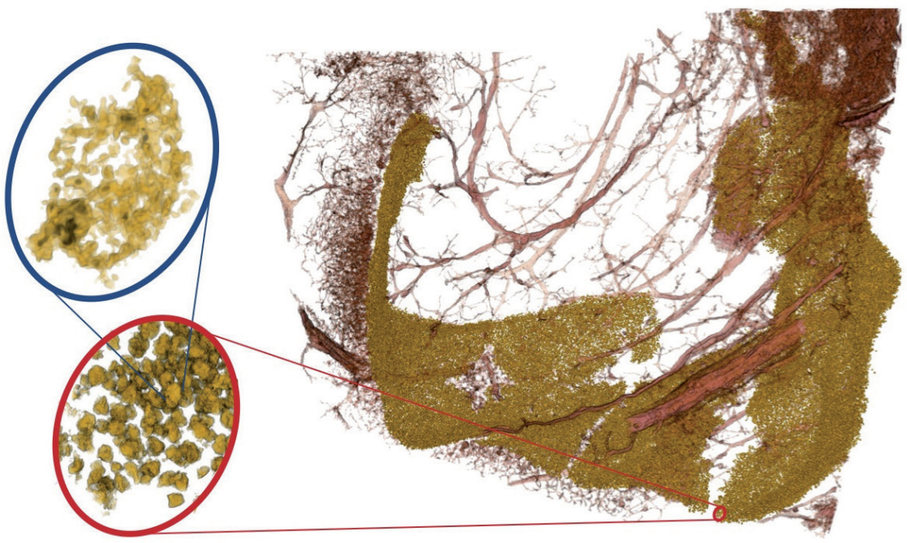

Figure 1

Three-dimensional visualisation of human neuronal tissue reconstructed by multi-scale X-ray phase contrast tomography. Neuronal cell nuclei are shown in yellow for the granule neurons in the dentate gyrus region of the hippocampus. Blood vessels are shown in red. By changing the X-ray optical magnification in the multi-scale recordings, one can zoom into regions-of-interest (red ovals). In these scans the resolution is high enough to resolve sub-structures of the nucleus associated with different DNA packing regimes.

In this way, tissue volumes with millions of neurons can be reconstructed without damaging the samples, in particular, without histological sectioning and without time-consuming preparation. The X-ray projection images are first processed using advanced phase retrieval algorithms. The three-dimensional structure is then tomographically reconstructed at different magnifications, with voxel sizes ranging between 650 nm and 50 nm. Following quantitative phase retrieval and tomographic reconstruction, neuron and nuclei are segmented based on machine learning, and - for each patient - represented as multi-dimensional histograms in a structural 'feature space'. Figure 2 shows an example illustrating the automated segmentation of neurons and their representation in a feature space, which can be regarded as a multi-dimensional histogram over axes representing different structural parameters of the neurons. For visual inspection, only a two-dimensional cross section is depicted, showing volume and density. Within tools of optimal transport theory [3], we use metrics to construct a subject (patient) space for classification and in order to identify prototypical structural variations from healthy to control states. The combination of segmentation by machine learning and methods from optimal transport theory allows us to compare the cell population of different individuals. This can also be done without prior hypothesis and knowledge whether samples belong to a particular patient group. Furthermore, the comparison of the structural features takes every single detected cell of each individual into account and not just the average values of each individual.

We find that the cellular nuclei of specific neurons, the granules in the dentate gyrus region of the hippocampus become more compact and heterogeneous in AD. The more compact structure observed can be explained by an increase of hetero-chromatin to euchromatin in these nuclei, i.e. a higher proportion of densely packed DNA. This happens when transcription, i.e. the read-out of genetic information is down-regulated in these neurons. The findings underline a nuclear involvement or nucleopathic character of AD. Whether the observed changes in the cell nucleus also play a causal role in the development of the disease remains to be investigated.

Author contact: Tim Salditt, tsaldit@gwdg.de
Marina Eckermann, marina.eckermann@esrf.fr

References

1. D. H. Adler et al., 'Characterizing the human hippocampus in aging and Alzheimer's disease using a computational atlas derived from ex vivo MRI and histology', Proc. Natl. Acad. Sci. 115, 4252–4257 (2018).
2. J. Frohn, D. Pinkert-Leetsch, J. Missbach-Güntner, M. Reichardt, M. Osterhoff, F. Alves and T. Salditt, '3D virtual histology of human pancreatic tissue by multiscale phase-contrast X-ray tomography', J. Synchrotron Rad. 27, 1707-1719 (2020).
3. G. Peyré and M. Cuturi, 'Computational optimal transport: with applications to data science', Found. Trends Mach. Learn. 11, 355–607 (2019).

Original publication

'Three-dimensional virtual histology of the human hippocampus based on phase-contrast computed tomography', Proceedings of the National Academy of Sciences 118, e2113835118 (2021). DOI: 10.1073/pnas.2113835118

Marina Eckermann[1], Bernhard Schmitzer[3], Franziska van der Meer[3], Jonas Franz[3], Ove Hansen[1], Christine Stadelmann[3] and Tim Salditt[1]

1. Institute for X-Ray Physics, University of Göttingen, Göttingen, Germany
2. Institut für Informatik, University of Göttingen, Göttingen, Germany
3. Institute for Neuropathology, University Medical Center, Göttingen, Germany

Energising molecular machines

Elucidating the details of homologous recombination in bacteria

Homologous recombination is a fundamental cellular process involved in maintenance of genetic integrity and generation of genetic diversity across all domains of life. One of the first discovered molecular machines contributing to the process of DNA recombination in bacteria was an AAA+ RuvAB Holliday junction branch migration motor. Our work answers long-standing questions about the architecture, oligomeric organisation and underlying mechanisms of this motor. Our data decipher the molecular principles of homologous recombination by the RuvAB complex, elucidate discrete and sequential transition-state intermediates for chemo-mechanical coupling of hexameric AAA+ motors and provide a blueprint for the design of state-specific compounds targeting AAA+ motors.

The key DNA intermediate in homologous recombination is a four-way DNA structure called Holliday junction (HJ) which was discovered by Robin Holliday in 1964 [1]. In bacteria, the HJ is processed by two homo-hexameric AAA+ ATPase RuvB (ATPase associated with various cellular activities) motors which, together with the RuvA–Holliday junction, assemble to energise the ATP-dependent strand-exchange reaction [2]. Prior biochemical and structural evidence suggests that branch migration is facilitated by a tripartite complex [3]. Despite its importance for chromosome maintenance, the structure and mechanism by which this motor complex facilitates branch migration were previously unknown.

To uncover the core mechanisms energising the RuvAB motor, it was essential to decode the molecular dynamics of the process in atomic detail. Using time-resolved cryo-electron microscopy (cryo-EM), we obtained structures of the entire ATP-hydrolysing RuvAB branch complex in seven distinct conformational states at high resolution (~3 A), captured during assembly and actively processing the HJ for the first time. All cryo-EM data were collected at the Cryo-EM Facility at CSSB located at the DESY campus. Using the high-performance computing facility at DESY, we were then able to classify all specific states and combine them together to generate a high-resolution movie detailing how the RuvAB complex functions.

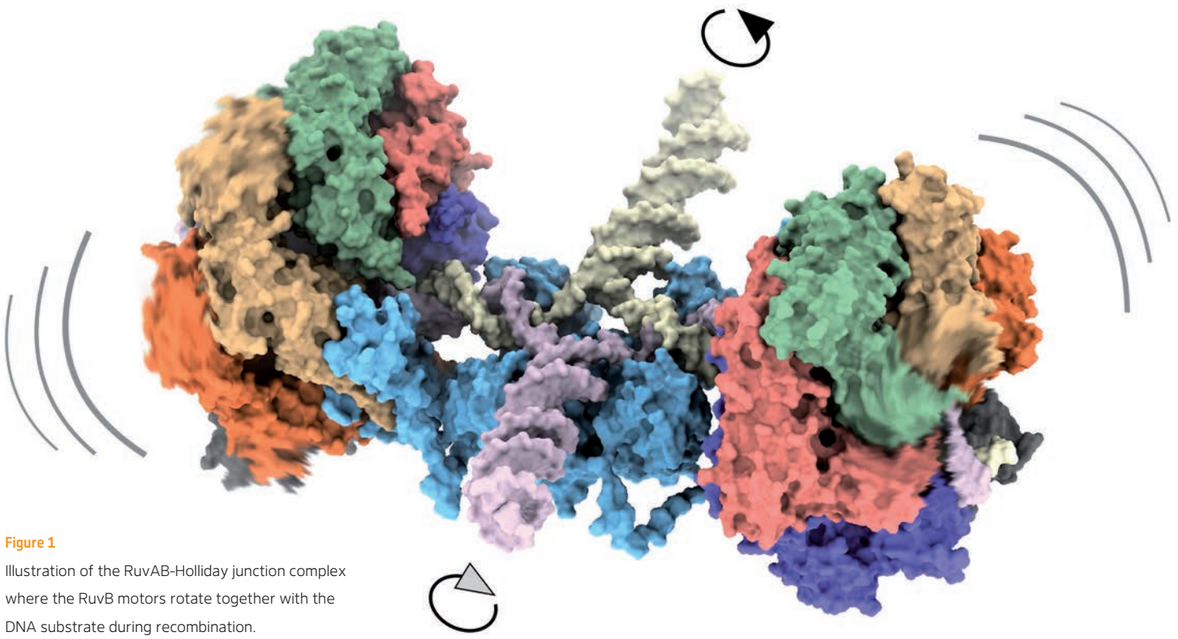

Figure 1
Illustration of the RuvAB-Holliday junction complex where the RuvB motors rotate together with the DNA substrate during recombination.

Five structures together resolve the complete nucleotide cycle and reveal the spatiotemporal relationship between ATP hydrolysis, nucleotide exchange and context-specific conformational changes in RuvB. Our structural data establishes that the nucleotide cycle progresses around the ring in RuvB motors, thus providing proof-of-concept for a conserved core mechanistic principle in hexameric AAA+ translocases. We show, for the first time, the critical role of substrate-disengaged protomers within hexameric AAA+ translocases (a unifying feature across ring-forming AAA+ motors) which form a converter module. Coordinated motions in the converter allosterically stimulate hydrolysis and nucleotide exchange. In addition, we demonstrate that the chemical energy released from ATP hydrolysis is directly transformed through the immobilised converter (through RuvAD3) into a lever action which generates the pulling force driving the branch migration. We establish that RuvB motors rotate together with the DNA substrate, which, together with a progressing nucleotide cycle powering the lever mechanism, forms the mechanistic basis for DNA recombination by continuous branch migration.

In summary, our data decipher the molecular principles of homologous recombination by the RuvAB complex and elucidate discrete and sequential transition-state intermediates for chemo-mechanical coupling of hexameric AAA+ motors. Additionally, the translocation of DNA, RNA and protein substrates is thought to be powered by a common sequential nucleotide cycle. Based on the shared geometrical and mechanistic properties between the ring-shaped ATPase, we suggest that the majority of translocases may function as molecular levers that convert a concerted wave of conformational changes associated with their nucleotide cycles into a defined lift-height of their central pores. These molecular levers are most likely a basic mechanism used to facilitate substrate translocation.

The resolved intermediates covering the full nucleotide cycle of the AAA+ RuvAB provide a critical piece of structural information necessary for understanding a conserved core mechanistic principle in hexameric AAA+ ATPase translocases. By demonstrating how RuvB converts chemical energy into mechanical work and serves as a molecular lever that translocates the substrate, we present the basic principles of AAA+ motors.

Author contact: Jiří Wald, jiri.wald@cssb-hamburg.de
Thomas Marlovits, thomas.marlovits@cssb-hamburg.de

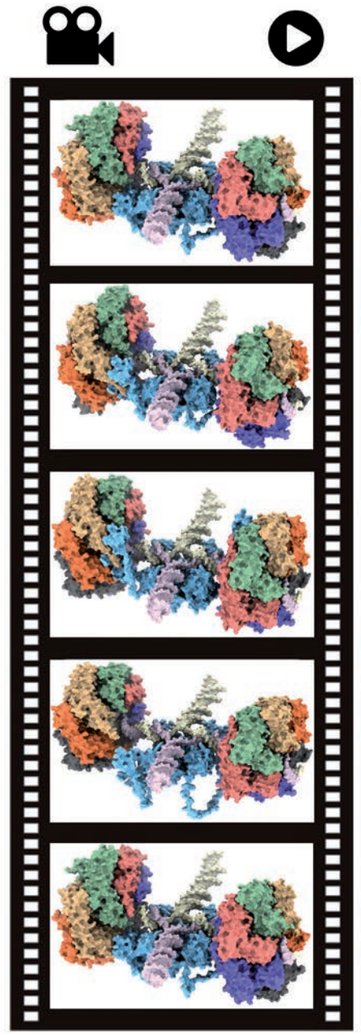

Figure 2
Resolving the RuvAB complex in distinct conformational states describing the entire nucleotide cycle at high resolution allowed us to assemble a 'molecular movie' of the Holliday junction branch migration.

References

1. **R. Holliday, 'A mechanism for gene conversion in fungi', Genet. Res. 5, 282–304 (1964).**
2. **S. C. West, 'Processing of recombination intermediates by the RuvABC proteins', Annu. Rev. Genet. 31, 213–244 (1997).**
3. **K. Yamada et al., 'Crystal structure of the RuvA-RuvB complex: A structural basis for the Holliday junction migrating motor machinery', Mol. Cell 10, 671–681 (2002).**

Original publication

'Mechanism of AAA+ ATPase-mediated RuvAB–Holliday junction branch migration', Nature 609, 630–639 (2022).
DOI: 10.1038/s41586-022-05121-1

Jiri Wald[1,2,3,4,5], Dirk Fahrenkamp[1,2,3], Nikolaus Goessweiner-Mohr[1,2,3,4,5], Wolfgang Lugmayr[1,2,3,4,5], Luciano Ciccarelli[1,2,3,4,5], Oliver Vesper[1,2,3,4,5] and Thomas C. Marlovits[1,2,3,4,5]

1. Institute of Structural and Systems Biology, University Medical Center Hamburg-Eppendorf, Hamburg, Germany
2. Centre for Structural Systems Biology (CSSB) c/o DESY, Hamburg, Germany
3. Deutsches Elektronen-Synchrotron DESY, Hamburg, Germany
4. Institute of Molecular Biotechnology GmbH (IMBA), Austrian Academy of Sciences, Vienna, Austria
5. Research Institute of Molecular Pathology (IMP), Vienna, Austria

Nutrient and drug uptake in stop-motion

Unravelling the structure of the intestinal peptide transporters paves the way for improved drug absorption

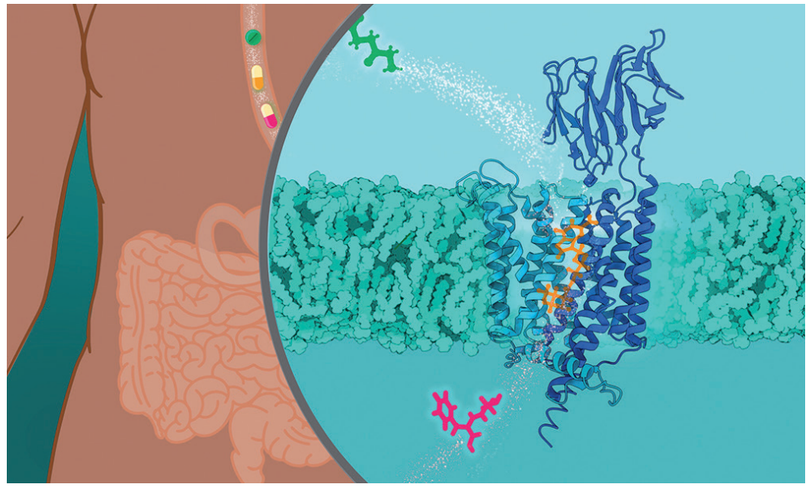

Figure 3
The human peptide transporter PepT1 (shown in blue), mainly expressed in the small intestine, is open to the outside and inside of a cell in an alternating fashion. This allows the bulk uptake of peptide nutrients and selected drug molecules across the lipid bilayer. (Credit: Isabel Romero Calvo/EMBL.)

During digestion, the proteins we eat are broken down into tinier pieces called peptides which consist of amino acids that our body later uses to build its own proteins. Before that happens, peptides must first be taken up from the gut. This task is performed by a protein called peptide transporter 1 (PepT1) which resides in the cell membrane of the intestinal wall and moves small peptides across the cell membrane. This highly promiscuous transporter is also responsible for the uptake of various drug molecules.

There are more than 900 transport systems in the human body dedicated to the uptake of different sorts of solutes and nutrients. Many of them are very specialised. For example, certain sugar transporters can recognise only one type of sugar. However, PepT1 is different – it can transport almost any type of short peptide. This ability is referred to as 'promiscuity'. In a collaborative effort, we determined the molecular structures of human PepT1 and its relative PepT2 which is present mainly in the kidney for nutrient resorption. Since these proteins are hard to crystallise, we used single-particle cryo-electron microscopy (cryo-EM) instead to image individual transport proteins in a thin layer of ice.

The promiscuity of PepT1 enables it to transport not only nutritious peptides but also various types of drugs, including certain antibiotics, antivirals and drugs against hypertension [1, 2]. However, PepT1 transports drugs less efficiently than it shuttles many of the natural peptides across the membrane. As a consequence, often only a fraction of the drugs we take in end up in the human body. The rest is exposed to the microbiome of the human gut which may lead to various side effects. Increasing the dosage of drugs to make up for inefficient transport is particularly dangerous in the case of antibiotics because it may lead to the generation of antibiotic-resistant bacteria.

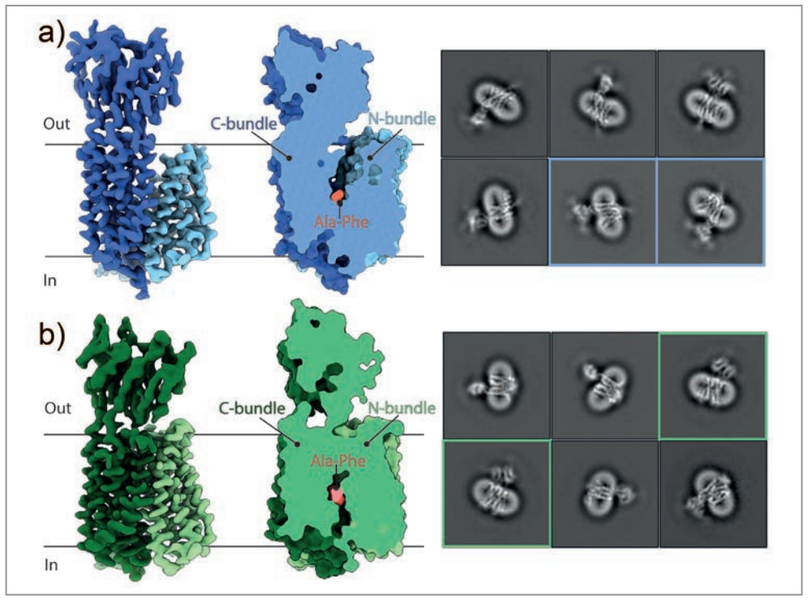

Figure 1
3D reconstructions of a) PepT1 and b) PepT2 with corresponding 2D-class averages and surface representations highlighting the outward and inward facing conformations of the transporter. The bound dipeptide is illustrated in red. (Credit: Maxime Killer/EMBL.)

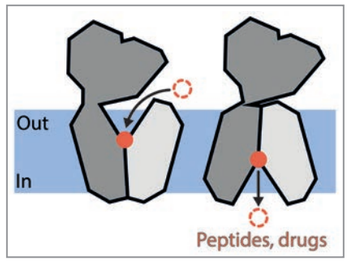

Figure 2
Schematic representation of the alternate transport mechanisms of PepT1 and PepT2. The transporter is open to the intestinal lumen and recognises a short peptide (illustrated as red dot). The nutrient can be released on the other side of the membrane after different conformational changes have taken place. (Credit: Maxime Killer/EMBL.)

The molecular model of the PepT1 structure (Fig. 1) now allows us to design new drugs or modify existing molecules that exploit PepT1 to cross the gut wall much more efficiently than before. Currently, it is almost impossible to predict whether a drug candidate can cross the gut wall via this transport system. Many potentially effective drug candidates have failed in preclinical and clinical studies because they were poorly absorbed. With the help of the structural information for PepT1, some of those failed candidates could be redesigned so they can take the uptake route via PepT1.

To generate an atomic model of PepT1, it was necessary to collect thousands of images of the frozen transporter at the cryo-EM facility at CSSB. Several millions of individual randomly oriented particles needed to be aligned to allow a full 3D reconstruction of the transport molecule. PepT1 is among the smallest monomeric protein structures determined by cryo-EM to date. It resembles a clamp that opens and closes alongside the gut. When a peptide binds to PepT1, the clamp closes around it and then opens to the other side of the membrane to release it (Fig. 1,2) [3]. We did not only determine the structure in a single state but could also freeze the transporter in various states along the transport cycle and determine its structure. This allowed us to stitch the individual structures together and visualise the entire transport cycle in molecular detail, like in a movie.

This work presents a significant step forward in studying membrane transport proteins on a molecular level (Fig. 3). Protocols and techniques developed to study PepT1 and PepT2 will help other scientists to determine structures of similar proteins in the future. Furthermore, our structures create the framework to understand molecular transport mechanism of peptide transporters which in turn will accelerate structure-based design approaches to increase the bioavailability of various compounds in the human body.

Author contact: Maxime Killer, maxime.killer@embl-hamburg.de
Christian Löw, christian.loew@embl-hamburg.de

References

1. M. Brandsch, 'Drug transport via the intestinal peptide transporter PepT1', Curr. Opin. Pharmacol. 13, 881–887 (2013).
2. F. Guettou, E. M. Quistgaard, M. Raba, P. Moberg, C. Löw and P. Nordlund, 'Selectivity mechanism of a bacterial homolog of the human drug-peptide transporters PepT1 and PepT2', Nat. Struct. Mol. Biol. 21, 728–731 (2014).
3. E. M. Quistgaard, C. Löw, F. Guettou and P. Nordlund, 'Understanding transport by the major facilitator superfamily (MFS): structures pave the way', Nat. Rev. Mol. Cell Biol. 17, 123–132 (2016).

Original publication

'Structural snapshots of human PepT1 and PepT2 reveal mechanistic insights into substrate and drug transport across epithelial membranes', Science Advances 7, 45 (2021).
DOI: 10.1126/sciadv.abk3259

Maxime Killer[1,2,3], Jiri Wald[1,4,5], Joanna Pieprzyk[1,2], Thomas C. Marlovits[1,4,5] and Christian Löw[1,2]

1. Centre for Structural Systems Biology (CSSB) c/o DESY, Hamburg, Germany
2. European Molecular Biology Laboratory (EMBL) c/o DESY, Hamburg, Germany
3. Collaboration for joint PhD degree between EMBL and Heidelberg University, Faculty of Biosciences, Heidelberg, Germany
4. Institute of Structural and Systems Biology, University Medical Center Hamburg-Eppendorf, Hamburg, Germany
5. Deutsches Elektronen-Synchrotron DESY, Hamburg, Germany

Ultrafast electron dynamics in space and time

Orbital tomography of a pentacene film using time-resolved momentum microscopy at a FEL

It is a long-standing goal of surface and interface science to visualise electronic dynamics during reactions. Flow of charge and energy across the interface is the driving force of the emergent dynamics that generally involves a complex interplay between the atomic and electronic structure. Here, we are imaging the frontier orbitals with time-resolved momentum microscopy at a free-electron laser and follow the charge and energy flow across the interface at their fundamental dimensions.

In the last decade, orbital tomography has emerged as an exciting extension of the photoemission technique for imaging localised electronic wave functions in thin film molecules [1]. Expanding the orbital tomography technique into the time domain requires XUV or X-ray photon energies and ultrashort pulses with sufficient flux, presently only provided by self-amplified spontaneous emission (SASE) free-electron lasers (FELs) or high harmonics generation (HHG) sources. The common stroboscopic experimental approach to molecular movie making is to switch on the dynamics with a femtosecond laser pump pulse and film the subsequent temporal evolution by taking snapshots with femtosecond probe pulses at specified pump-probe time delays [2, 3].

Here, we investigate the ultrafast charge transfer dynamics between a bilayer of pentacene deposited on Ag(110). Consider a molecule in contact with a surface and charge transfer as a primary fundamental process, as, e.g. in the initial step of a molecule-surface reaction or a molecular electronics device function. Upon receiving a charge from the substrate, the atomic positions as well as electronic orbitals and energy levels of the adsorbed molecule may rearrange significantly, while the local charge build-up will in turn initiate the movement of mobile charge carriers in the substrate and modify the local atomic structure at the adsorption site and its global surface electronic structure by shifting, distorting or splitting of bands.

The pump-probe experiment was performed with a momentum microscope at the PG2 beamline at FLASH. We pumped the organic film with an optical pump laser at 400 nm wavelength and probed the response with FEL at a photon wavelength of 35 nm. Figure 1 displays the experimental and theoretical time-integrated photoelectron momentum maps of the bilayer pentacene film. We can unambiguously identify the molecular orbitals, e.g. $LUMO_{1st}$, $HOMO_{1st}$, $HOMO_{2nd}$ and HOMO-1_{1st} using *ab initio* calculations. In addition to the momentum distribution of molecular orbitals, a feature close to normal emission is present in all experimental measurements. Calculations on a model system of pentacene on a cluster of silver atoms reveals hybridised bonds between the molecule and the substrate.

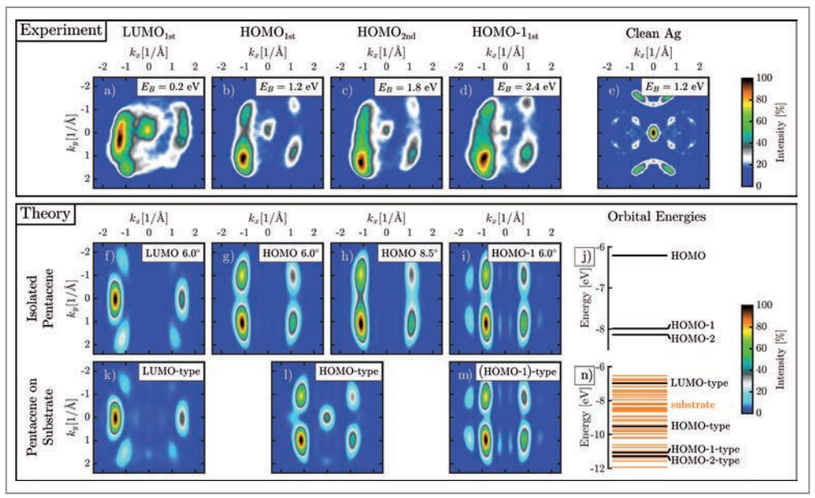

Figure 1
Comparison of experimental and simulated momentum maps of bilayer pentacene on Ag(110). Time-integrated measured a)–d) photoelectron momentum maps (PMMs) for the pentacene valence orbitals. The partly filled $LUMO_{1st}$ a), the $HOMO_{1st}$ b), $HOMO_{2nd}$ c) and the HOMO-1_{1st} d) can be clearly distinguished from one another and identified by comparison to the simulations f)–i) and k)–m). Simulated PMMs for the f) LUMO, g) and h) HOMO and i) HOMO-1 orbitals and j) Hartree-Fock energies of occupied molecular orbitals of isolated pentacene. j)–l) Simulated PMMs for the pentacene on Ag(110) cluster. n) Hartree-Fock energies of the pentacene on Ag(110) cluster. Nature Communications articles are published OA under a CC BY license (Creative Commons Attribution 4.0 International license).

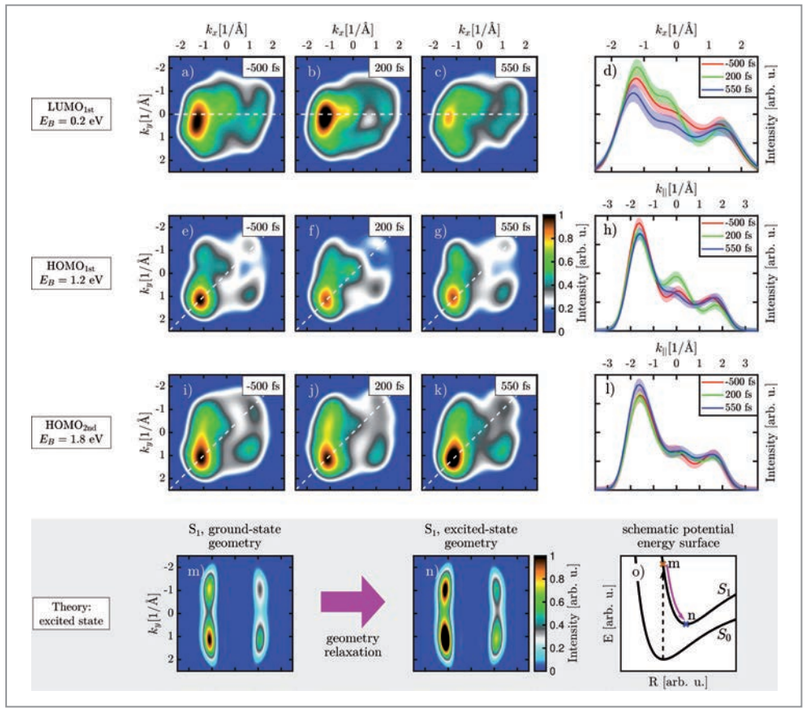

Figure 2
Time evolution of experimental photoelectron momentum maps (PMMs) and comparison to theory. Time evolution of PMMs of pentacene of the a)–c) $LUMO_{1st}$, e)–g) $HOMO_{1st}$ and i)–k) $HOMO_{2nd}$ at E_B =0.2eV, E_B =1.2eV and E_B =1.8eV binding energy, respectively. Momentum distribution curves for (d) $LUMO_{1st}$, (h) $HOMO_{1st}$ and (l) $HOMO_{2nd}$ (bottom) in the direction as indicated by the dashed lines in the corresponding PMMs. Calculated PMMs for a pentacene molecule excited to the first singlet state m) in the ground-state geometry and n) excited-state geometry. o) Schematic representation of the proposed molecular dynamics in the second layer after excitation. Nature Communications articles are published OA under a CC BY license (Creative Commons Attribution 4.0 International license).

In the time-resolved momentum distribution of the molecular orbitals we observe that the intensity around the centre increases after time zero and drops after 200 fs (see Fig. 2). The dynamics can be explained in the framework of charge transfer between molecule and substrate and a charge redistribution from the $HOMO_{1st}$ to the partly filled $LUMO_{1st}$. Due to the strong interaction with the substrate, the molecule can also move relative to the surface after optical excitation which is confirmed by our computational calculations.

Our work shows the feasibility of sub-picosecond time-resolved orbital tomography of molecular thin films at SASE FELs. We identify the molecular orbitals and observe transient changes due to charge transfer between the molecule and the substrate. With the upcoming improvements in the temporal resolution and full polarisation control at FEL light sources alongside with progress in the theoretical framework based on quantum electrodynamics, time-resolved tomography of molecular wave functions during chemical reactions will become feasible [4].

Author contact: Markus Scholz, markus.scholz@desy.de

References

1. **P. Puschnig, S. Berkebile, A. J. Fleming, G. Koller, K. Emtsev, T. Seyller, J. D. Riley, C. Ambrosch-Draxl, F. P. Netzer, M. G. Ramsey, 'Reconstruction of molecular orbital densities from photoemission data', Science 326, 702–706 (2009).**
2. **R. Wallauer, M. Raths, K. Stallberg, L. Münster, D. Brandstetter, X. Yang, J. Güdde, P. Puschnig, S. Soubatch, C. Kumpf, F. C. Bocquet, F. S. Tautz, U. Höfer, 'Tracing orbital images on ultrafast time scales', Science 371, 1056-1059 (2021).**
3. **C. W. Nicholson, A. Lücke, W. G. Schmidt, M. Puppin, L. Rettig, R. Ernstorfer, M. Wolf, 'Beyond the molecular movie: Dynamics of bands and bonds during a photoinduced phase transition', Science 362, 821-825 (2018).**
4. **D. Popova-Gorelova, 'Imaging Electron Dynamics with Ultrashort Light Pulses: A Theory Perspective', Appl. Sci. 8, 318 (2018).**

Original publication

'Ultrafast orbital tomography of a pentacene film using time-resolved momentum microscopy at a FEL', Nature Communications 13, 2741 (2022). DOI: 10.1038/s41467-022-30404-6

Kiana Baumgärtner[1,2], Marvin Reuner[3], Christian Metzger[1,2], Dmytro Kutnyakhov[4], Michael Heber[4], Federico Pressacco[4], Chul-Hee Min[1,5], Thiago R. F. Peixoto[1,4], Mario Reiser[6], Chan Kim[6], Wei Lu[6], Roman Shayduk[6], Manuel Izquierdo[6], Günter Brenner[4], Friedrich Roth[7,8], Achim Schöll[1], Serguei Molodtsov[6], Wilfried Wurth[4,9,10], Friedrich Reinert[1,2], Anders Madsen[6], Daria Popova-Gorelova[3,10] and Markus Scholz[4,6]

1. Experimentelle Physik 7, Julius-Maximilians-Universität Würzburg, Germany
2. Würzburg-Dresden Cluster of Excellence ct.qmat, Julius-Maximilians-Universität Würzburg, Germany
3. I. Institute for Theoretical Physics and Centre for Free-Electron Laser Science, Universität Hamburg, Germany
4. Deutsches Elektronen-Synchrotron DESY, Hamburg, Germany
5. Institut für Experimentelle und Angewandte Physik, Christian-Albrechts-Universität zu Kiel, Germany
6. European XFEL, Schenefeld, Germany
7. Institute of Experimental Physics, TU Bergakademie Freiberg, Freiberg, Germany
8. Center for Efficient High Temperature Processes and Materials Conversion (ZeHS), TU Bergakademie Freiberg, Germany
9. Institut für Experimentalphysik, Universität Hamburg, Germany
10. The Hamburg Centre for Ultrafast Imaging (CUI), Germany

Tracking charge in motion

Femtosecond electronic movies of light-excited nucleobases

Nucleobases are the information carrier of life. Almost contradicting their relevance in nature is their strong absorption of highly energetic UV light. However, the concerted motion of electrons and nuclei quickly funnels the UV energy into heat which contributes to their stability and selection of life's information carrier. Upon substitution of one of the nucleobases' oxygen atoms by sulfur, this mechanism changes drastically, creating molecules that store part of the light energy in the excitation of spins [1]. We investigated the ultrafast dynamics of UV-excited sulfur-substituted nucleobases. The molecules exhibit an efficient and long-lasting population of spin-excited states, determining their behaviour in biochemical and medical applications.

The common medical use of so-called thionucleobases as immunosuppressants is somewhat compromised by the spin-excited states. They create damages in tissue which lead to an increased skin cancer risk. On the other hand, the spin-excitations also lead to further applications as molecular cross-markers and in photodynamic tumor therapy. We shed light on the sulfur-substitution effect that changes the molecular behaviour drastically by studying the ultrafast path of 2-thiouracil into the spin-excited state using X-ray probe photoelectron spectroscopy at the free-electron laser FLASH.

We utilise FLASH as an ultrafast camera providing snapshots of the UV optical laser-triggered electron motion in 2-thiouracil. As shown in Fig. 1, a UV pulse starts the molecular dynamics by inducing electronic motion and coupled changes in the molecular geometry. An X-ray pulse from FLASH probes the electron dynamics by emitting photoelectrons from the sulfur 2p core levels. The energy needed to eject the 2p electrons and thus its kinetic energy is influenced by the local valence electron charge on the sulfur atom [2]. We use an electron spectrometer to determine the 2p electrons' kinetic energy as a function of the delay between UV and X-ray pulse.

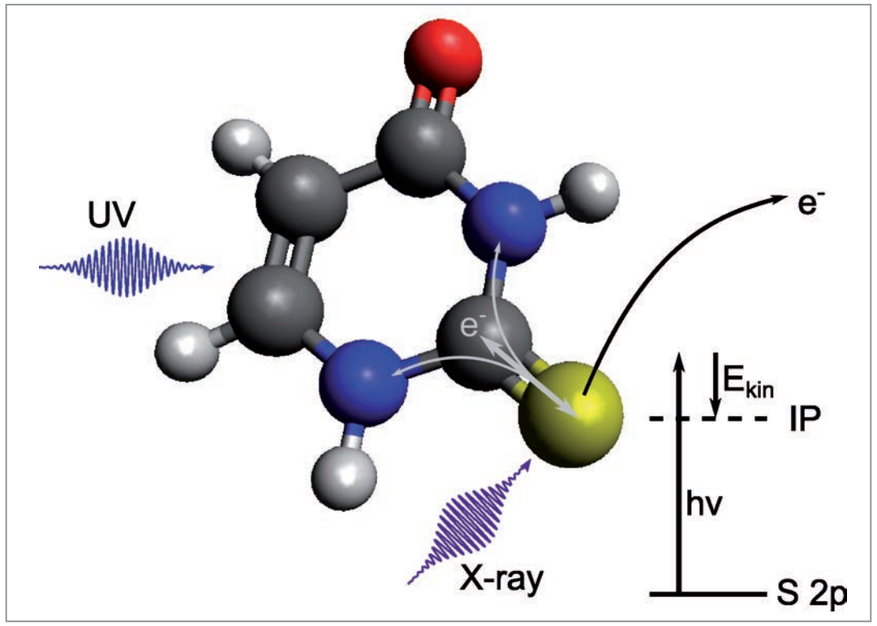

Figure 1
2-Thiouracil is excited with a UV pulse initiating a charge flow away from the sulfur atom (yellow). A soft X-ray pulse tuned on the sulfur 2p core electrons ionises the excited molecule. The electrons are emitted with a distinct kinetic energy which is shifted by the charge sitting on the sulfur atom.

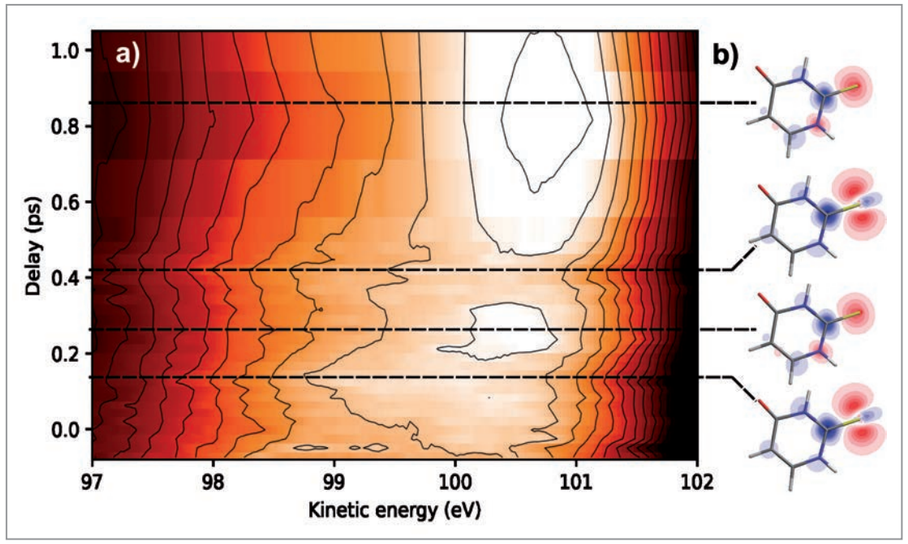

Figure 2
a) The photoelectron spectrum shows a shift to lower kinetic energies indicating a higher binding energy after UV excitation. On top of the signal, small modulations can be seen which we attribute to changes of the electronic state. b) Charge difference map, with and without UV excitation, at different times after UV excitation. Red indicates less electrons, blue more. The charge on the sulfur atom oscillates which leads to oscillations in the core electron kinetic energy.

Figure 2a shows the changes in the kinetic energy of the ejected sulfur core electrons. Right after UV excitation, the electron kinetic energy diminishes. This indicates a UV-induced flow of charge away from sulfur. At about 300 fs after UV excitation, the electrons turn partially back to the sulfur, and the electron kinetic energy shifts again towards higher kinetic energies. The oscillation repeats afterwards. The calculated molecular valence charge maps, showing a difference in charge between UV-excited and non-excited molecules, confirm the observation. The UV irradiation induces a periodic flow of charge from the sulfur to the molecular ring and back with the experimentally observed period. The oscillation of the charge is due to the coupling of electrons and the molecular geometry. As the nuclei change position, the electrons are periodically driven into different states, being more or less localised on the sulfur atom.

Our results show that we are able to image the electronic motion on a femtosecond level from the local perspective of a single atom within the molecule. This information, together with the changes in molecular geometry, is required to fully understand the conversion of light energy within molecules. In the future, we will extend this study to observe several atoms within one molecule, thus obtaining a complete molecular electronic movie.

Author contact:
Dennis Mayer, dennis.mayer@desy.de
Markus Gühr, markus.guehr@desy.de

References

1. S. Arslancan, L. Martinez-Fernandez and I. Corral, 'Photophysics and photochemistry of canonical nucleobases' thioanalogs: from quantum mechanical studies to time-resolved experiments', Molecules 22, 998 (2017).
2. K. Siegbahn, C. Nordling, G. Johansson, J. Hedman, P. F. Hedén, K. Hamrin, U. Gelius, T. Bergmark, L. O. Werme, R. Manne and Y. Baer, 'ESCA applied to free molecules', North-Holland Publishing Company (1969).

Original publication

'Following excited-state chemical shifts in molecular ultrafast x-ray photoelectron spectroscopy', Nature Communications 13, 198 (2022). DOI: 10.1038/s41467-021-27908-y

Dennis Mayer[1], Fabiano Lever[1], David Picconi[1,2], Jan Metje[1], Skirmantas Alisauskas[3], Francesca Calegari[4,5,6], Stefan Düsterer[3], Christopher Ehlert[7], Raimund Feifel[8], Mario Niebuhr[1], Bastian Manschwetus[3], Marion Kuhlmann[3], Tommaso Mazza[9], Matthew S. Robinson[1], Richard J. Squibb[8], Andrea Trabattoni[4], Måns Wallner[8], Peter Saalfrank[2], Thomas J. A. Wolf[10] and Markus Gühr[1]

1. Institut für Physik und Astronomie, Universität Potsdam, Potsdam, Germany
2. Institut für Chemie, Universität Potsdam, Potsdam, Germany
3. Deutsches Elektronen-Synchrotron DESY, Hamburg, Germany
4. Center for Free-Electron Laser Science (CFEL), Hamburg, Germany
5. The Hamburg Centre for Ultrafast Imaging (CUI), Universität Hamburg, Hamburg, Germany
6. Institut für Experimentalphysik, Universität Hamburg, Hamburg, Germany
7. Heidelberg Institute for Theoretical Studies, HITS gGmbH, Heidelberg, Germany
8. Department of Physics, University of Gothenburg, Gothenburg, Sweden
9. European XFEL, Schenefeld, Germany
10. Stanford PULSE Institute, SLAC National Accelerator Laboratory, Menlo Park, USA

Quantum dance of electrons in a biomolecule

Watching the charge density motion in the amino acid glycine with ultrashort X-ray pulses in real time

Intramolecular charge transfer plays a key role in photochemical reactions of biorelevant molecules. Here, we use X-rays to create and monitor the quantum mechanically evolving electron charge distribution in the amino acid glycine via direct real-time measurements. Better knowledge of the quantum effects in the motion of electrons at the molecular level can pave the way to controlling, optimising, and engineering ionising radiation to be used, for example, in radiotherapy for cancer treatment.

Since the pioneering experiments by Weinkauf and Schlag on electron mobility and dissociation in peptide cations [1], the interplay between local ionisation and molecular reactivity is of considerable interest in many areas of physics, chemistry and biology [2]. The amino acid glycine is an abundant basic building block of proteins and plays a part in the recognition sites on cell membranes and enzymes. Due to its compact nature and tendencies to form hydrogen bonds, it facilitates protein folding in biomolecular reactions. Stand-alone, it is utilised as an inhibiting neurotransmitter in the central nervous system.

When energetic radiation hits a glycine molecule, often one of its electrons gets knocked out. In the resulting glycine ion, the remaining electronic charge begins to redistribute itself, resulting in a time-dependent oscillation of the charge density. To ionise glycine, we used the ultrashort soft X-ray pulses from the free-electron laser FLASH, each lasting less than five femtoseconds (fs). With these flashes and by applying sophisticated post-analysis data processing algorithms, we could look at the behaviour of one specific of glycine's 40 electrons from a particular orbital. In the applied experimental scheme depicted in Fig. 1a-d, events featuring electrons from the 10a′ inner-valence orbital are of interest. The 10a′ orbital spans nearly the full molecular backbone, and in consequence, the transient local electron hole density moves to the same extent, thus making this orbital an excellent candidate for the study of charge-induced chemical dynamics [3]. While the initial knockout of the electron results in a positive charge at a specific atom in the molecule, the following charge oscillation creates a force field that makes the nuclei move as well.

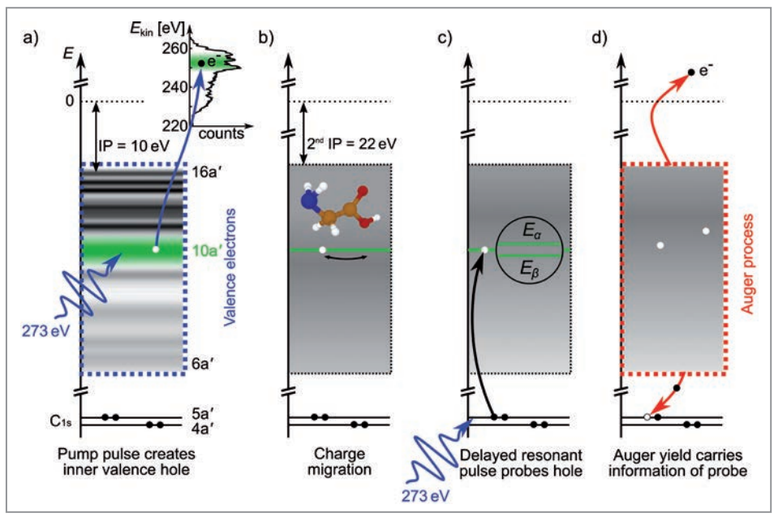

Figure 1
A single-color, X-ray pump-probe scheme is applied to track charge dynamics initiated by photoelectron emission from the 10a′ molecular orbital. The total cascade involves several different processes: a) photoionisation, b) charge migration triggered by coherent population of ionised states during photoionisation, c) resonant carbon 1s core-hole excitation and d) Auger decay.

Figure 2
a) Relative change of the detected correlated yield of 10a′ photoelectrons, Auger electrons and Gly^{2+} ions in relation to the average yield as a function of pump-probe time delay Δt. b) Continuous wavelet transform of the above signal showing the period-resolved magnitude evolution of the nonstationary signal. The 'cone of influence' is given as a darker-shaded area. Here, artificial edge effects disturb the frequency analysis, and therefore, peak structures in the shaded area of the colour plot are likely underestimated. The two dominant oscillation periods identified in the kinematically complete experiment are $19.6^{+1.5}_{-1.4}$ fs and $29.3^{+2.2}_{-2.0}$ fs.

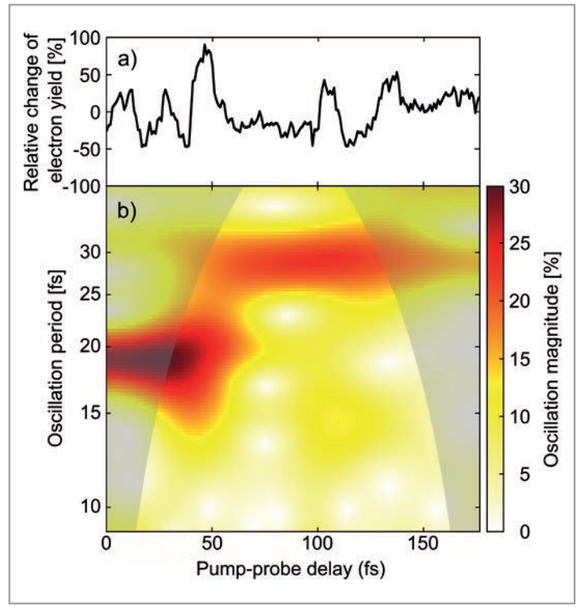

Quantum mechanically, the outgoing electron leaves the molecular ion in a so-called coherent superposition of eigenstates, i.e. an electronic wave packet. The electronic coherence influences the way the molecule reacts chemically. Understanding this quantum behaviour may open a path to make biomolecules act in a desired way. A prerequisite for any control of electronic and nuclear dynamics towards specific molecular reaction pathways is a detailed analysis of structural properties when the molecule is driven out of equilibrium. In particular, the analysis and control of time-dependent electronic structure defining the potential energy landscape in which the nuclei move is of high relevance.

Employing a 'pump-probe' experimental scheme, delayed soft X-ray pulses track the induced wave packet dynamics through resonant X-ray absorption that induces Auger decay. We collect three or more particle events per FEL probe pulse, comprising the photoelectron at the kinetic energy corresponding to valence ionisation of 10a′ under investigation, the final Gly^{2+} parent ion and pump-probe events including Auger decay. Figure 2a shows the result of this kinematically complete experiment, spanning a 175 fs time window. We observed an electronic coherence which is preserved for the first 55 fs after the initial photoionisation with nearly no loss of intensity and an oscillation time period of $19.6^{+1.5}_{-1.4}$ fs. After the first three oscillations, coupling between electronic and nuclear degrees of freedom sets in, slowly destroying the electronic coherence and giving rise to a presumably C-C stretch oscillation with a period of $29.3^{+2.2}_{-2.0}$ fs. The temporal evolution of the two dominant oscillation periods can be seen in Fig. 2b.

Advanced *ab initio* many-electron simulations by collaborative researchers from the Imperial College London allow us to explain the first 25 fs of the detected coherent quantum evolution in terms of the electronic coherence. However, the full coherence brought to life by the few-fs ionisation of glycine in the inner-valence region is, in all probability, of mixed electronic and vibrational character. A full theoretical characterisation of this coherence within the highly computationally demanding inner-valence energy region is currently beyond reach and should be the subject of future theoretical studies.

Author contact: David Schwickert, d.schwickert@desy.de
Tim Laarmann, tim.laarmann@desy.de

References

1. R. Weinkauf, P. Schanen, D. Yang, S. Soukara and E. W. Schlag, 'Elementary processes in peptides: electron mobility and dissociation in peptide cations in the gas phase', J. Phys. Chem. 99, 11255 (1995).
2. H. J. Wörner, C. A. Arrell, N. Banerji, A. Cannizzo, M. Chergui, A. K. Das, P. Hamm, U. Keller, P. M. Kraus, E. Liberatore, P. Lopez-Tarifa, M. Lucchini, M. Meuwly, C. Milne, J.-E. Moser, U. Rothlisberger, G. Smolentsev, J. Teuscher, J. A. van Bokhoven and O. Wenger, 'Charge migration and charge transfer in molecular systems', Struct. Dyn. 4, 061508 (2017).
3. B. Cooper and V. Averbukh, 'Single-photon laser-enabled Auger spectroscopy for measuring attosecond electron-hole dynamics', Phys. Rev. Lett. 111, 083004 (2013).

Original publication

'Electronic quantum coherence in glycine molecules probed with ultrashort X-ray pulses in real time', Science Advances 8, eabn6848 (2022). DOI: 10.1126/sciadv.abn6848

David Schwickert[1], Marco Ruberti[2], Přemysl Kolorenč[3], Sergey Usenko[1,4†], Andreas Przystawik[1], Karolin Baev[1,4], Ivan Baev[4], Markus Braune[1], Lars Bocklage[1,5], Marie Kristin Czwalinna[1], Sascha Deinert[1], Stefan Düsterer[1], Andreas Hans[6], Gregor Hartmann[6], Christian Haunhorst[7], Marion Kuhlmann[1], Steffen Palutkev[1], Ralf Röhlsberger[1,8,9,10], Juliane Rönsch-Schulenburg[1], Philipp Schmidt[6†], Sven Toleikis[1], Jens Viefhaus[11], Michael Martins[4], André Knie[6], Detlef Kip[7], Vitali Averbukh[2], Jon P. Marangos[2] and Tim Laarmann[1,5]

1. Deutsches Elektronen-Synchrotron DESY, Hamburg, Germany
2. Department of Physics, Imperial College London, London, United Kingdom
3. Faculty of Mathematics and Physics, Charles University, Praha, Czech Republic
4. Department of Physics, University of Hamburg, Hamburg, Germany
5. The Hamburg Centre for Ultrafast Imaging (CUI), Hamburg, Germany
6. Institute of Physics, University of Kassel, Kassel, Germany
7. Faculty of Electrical Engineering, Helmut Schmidt University, Hamburg, Germany
8. Helmholtz Institute Jena, Jena, Germany
9. Helmholtz Centre for Heavy Ion Research (GSI), Darmstadt, Germany
10. Friedrich-Schiller-Universität Jena, Jena, Germany
11. Helmholtz-Zentrum Berlin für Materialien und Energie, Berlin, Germany

† Present address: European XFEL GmbH, Schenefeld, Germany

An explosive insight

En route to acquiring movies of photochemical reactions

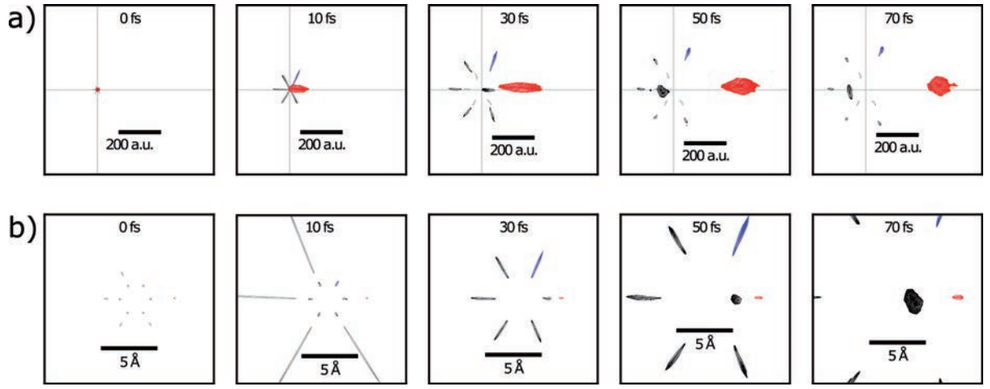

Figure 2
Temporal evolution of the fragmentation of iodopyridine molecules during and after the X-ray pulse, simulated with the XMDYN toolkit. Red: iodine; blue: nitrogen; black: carbon; grey: hydrogen. a) momentum space (representation analogue to Fig. 1). b) position space.

Many different methods to explore the microscopic realm of atoms and molecules exist nowadays. A method, which – compared to other experimental approaches – is still in its infancy, is the so-called Coulomb explosion imaging. As the name already implies, molecules are rapidly charged up, for example via ion bombardment, femtosecond laser pulses, or, more recently, free-electron laser pulses. As a result, the molecules fragment in a violent Coulomb explosion driven by the mutual repulsion of the generated charges. By imaging the momenta of the molecular fragments in a coincidence measurement, the molecule can be studied in great detail.

Coulomb explosion imaging has already come a long way. While initially performed by stripping off electrons from molecular ions by means of thin foils in the 1980's, its next level was achieved when powerful, femtosecond laser sources emerged (see [1] for a recent review). During the last decade, X-ray free-electron lasers have also been used to trigger the charge up via absorption of several photons and subsequent ultrafast Auger-Meitner decay (cascades).

The present study was performed at the European XFEL using the COLTRIMS reaction microscope available at the SQS scientific instrument. Via reaction microscopy, single molecules in the gas phase may be addressed by determining the momenta (and the mass and charge) of reaction products in a coincidence measurement [2]. We employed the intense X-rays provided by the European XFEL to multiply ionise iodopyridine (C_5H_4NI) and molecules (see Fig. 1 top). While the majority of the photoabsorption processes happen at the iodine atom, the charge rapidly spreads to the other atoms and additional charge is created by secondary electron emission. This very rapid charge up yields at least one charge on each atom, thus triggering a rapid fragmentation into atomic ions which already starts during the ultrashort X-ray pulse.

Figure 1 shows the structure of iodopyridine (top) and the momenta of the measured N^+, H^+, and C^+ ions (bottom). Molecules in the gas phase are randomly oriented. Therefore, a molecular frame of reference was constructed from the coincident ion momenta recorded in the laboratory frame. In Fig. 1 bottom left the momenta of the protons and the nitrogen ion are shown in this molecular frame. The distribution shows an astonishing resemblance to the equilibrium structure of the molecule, and the four different hydrogen atoms H3 to H6 can be identified at first glance. However, Coulomb explosion imaging does not map the position space. This becomes clear when inspecting the carbon ion momenta in Fig. 1 bottom right. The five carbon atoms (C2 to C6) can also be clearly assigned, but the C2 ion appears to be 'out of place' at almost zero momentum. This behaviour can be understood with the help of state-of-the-art theoretical modelling of the fragmentation dynamics.

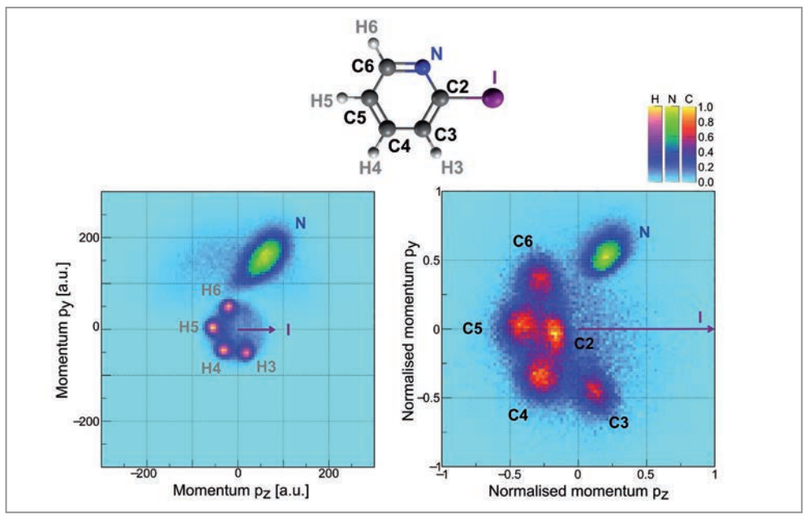

Figure 1
Top: Equilibrium structure of iodopyridine (C_5H_4NI). Bottom: Molecular-frame momentum maps of nitrogen ions (green), hydrogen ions (magenta, left panel), and carbon ions (red, right panel). The emission direction of the iodine ion defines the positive z-axis, and the y/z-plane is spanned by emission direction of the iodine and the nitrogen ion. All ions are singly charged.

Figure 2 shows the temporal evolution of the X-ray induced Coulomb explosion in momentum space (Fig. 2a) and position space (Fig. 2b), calculated with the XMDYN tool kit [3]. This reveals that the C2 ion is temporarily trapped between the heavy iodine ion and the repelling charges of the other atoms of the molecule's ring, which even leads to a significantly reduced C-I distance after ~30 fs and results in almost zero momentum of the C2 atom after the explosion. It also highlights the extremely fast emission of the hydrogen ions, followed by a somewhat slower explosion involving the heavier atoms.

The very clean momentum-space images of the fragmented molecules suggest that Coulomb explosion imaging has huge potential as a tool for studying ultrafast photochemical processes in gas-phase molecules in future pump-probe experiments. In particular, the ability to image every individual hydrogen atom is a key advantage over many other methods. The atomic positions can be determined through comparison with quantitative simulations, such as those provided by XMDYN. In addition, the momentum-space data obtained by Coulomb explosion imaging provides information on the dynamics of the charge up and fragmentation process itself and (as we show in our original publication) even insight into the evolution of molecular charge rearrangement.

Author contact: Rebecca Boll, rebecca.boll@xfel.eu
Robin Santra, robin.santra@cfel.de
Till Jahnke, till.jahnke@xfel.eu

References

1. C. A. Schouder, A. S. Chatterley, J. D. Pickering and H. Stapelfeldt, 'Laser-Induced Coulomb Explosion Imaging of Aligned Molecules and Molecular Dimers', Ann. Rev. Phys. Chem. 73, 323-347 (2022).
2. R. Dörner, V. Mergel, O. Jagutzki, L. Spielberger, J. Ullrich, R. Moshammer and H. Schmidt-Böcking, 'Cold Target Recoil Ion Momentum Spectroscopy: a 'momentum microscope' to view atomic collision dynamics', Phys. Rep. 95, 330 (2000).
3. Z. Jurek, S.-K. Son, B. Ziaja and R. Santra, 'XMDYN and XATOM: versatile simulation tools for quantitative modeling of X-ray free-electron laser induced dynamics of matter', J. Appl. Cryst. 49, 1048-1056 (2016).

Original publication

X-ray multiphoton-induced Coulomb explosion images complex single molecules, Nature Physics 18, 423–428 (2022).
DOI: 10.1038/s41567-022-01507-0

Rebecca Boll[1], Julia M. Schäfer[2,3], Benoît Richard[2,4,5], Kilian Fehre[6], Gregor Kastirke[6], Zoltan Jurek[2,5], Markus S. Schöffler[6], Malik M. Abdullah[7], Nils Anders[6], Thomas M. Baumann[1], Sebastian Eckart[6], Benjamin Erk[7], Alberto De Fanis[1], Reinhard Dörner[6], Sven Grundmann[6], Patrik Grychtol[1], Alexander Hartung[6], Max Hofmann[6], Markus Ilchen[1,8], Ludger Inhester[2,5], Christian Janke[6], Rui Jin[2,9], Max Kircher[6], Katharina Kubicek[1,5], Maksim Kunitski[6], Xiang Li[10], Tommaso Mazza[1], Severin Meister[11], Niklas Melzer[6], Jacobo Montano[1], Valerija Music[1,8], Giammarco Nalin[6], Yevheniy Ovcharenko[1], Christopher Passow[7], Andreas Pier[6], Nils Rennhack[1], Jonas Rist[6], Daniel E. Rivas[1], Daniel Rolles[10], Ilme Schlichting[12], Lothar Ph. H. Schmidt[6], Philipp Schmidt[1,8], Juliane Siebert[6], Nico Strenger[6], Daniel Trabert[6], Florian Trinter[6,7,13], Isabel Vela-Perez[6], Rene Wagner[1], Peter Walter[14], Miriam Weller[6], Pawel Ziolkowski[11], Sang-Kil Son[2,5], Artem Rudenko[10], Michael Meyer[1], Robin Santra[2,3,4,5] and Till Jahnke[1]

1. European XFEL, Schenefeld, Germany
2. Center for Free-Electron Laser Science (CFEL), DESY, Hamburg, Germany
3. Department of Chemistry, Universität Hamburg, Hamburg, Germany
4. Department of Physics, Universität Hamburg, Hamburg, Germany
5. The Hamburg Centre for Ultrafast Imaging (CUI), Universität Hamburg, Hamburg, Germany
6. Institut für Kernphysik, J. W. Goethe-Universität, Frankfurt am Main, Germany
7. Deutsches Elektronen-Synchrotron DESY, Hamburg, Germany
8. Institut für Physik und CINSaT, Universität Kassel, Kassel, Germany
9. Department of Physics and Astronomy, Shanghai Jiao Tong University, Shanghai, China
10. J.R. Macdonald Laboratory, Department of Physics, Kansas State University, Manhattan, KS, USA
11. Max-Planck-Institut für Kernphysik, Heidelberg, Germany
12. Max-Planck-Institut für medizinische Forschung, Heidelberg, Germany
13. Molecular Physics, Fritz-Haber-Institut der Max-Planck-Gesellschaft, Berlin, Germany
14. SLAC National Accelerator Laboratory, Menlo Park, CA, USA

X-ray laser reveals how radiation damage arises

Double bombardment exposes the detailed dynamics of how water molecules break apart

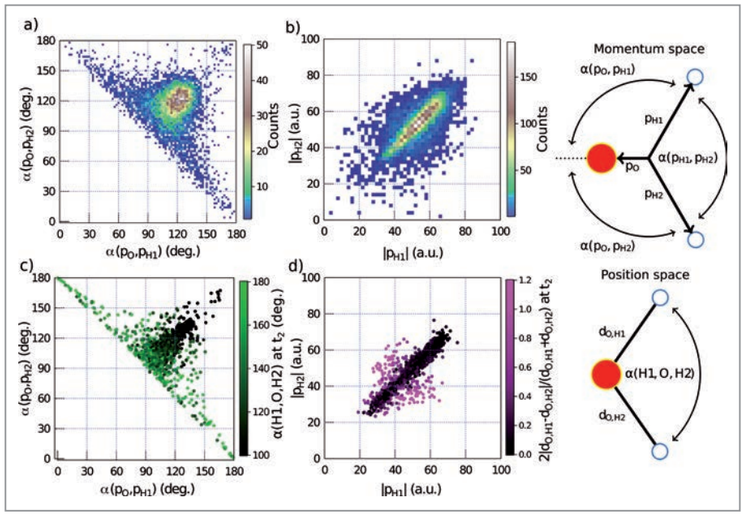

Figure 2
a,c) Scatter plots showing the angles of the final proton momenta with respect to the final oxygen momentum (experiment and simulation). In the simulation scatter plot a large HOH bond angle at the time of the second photoionisation is indicated by green. b,d) Scatter plots showing the magnitudes of the final proton momenta (experiment and simulation). In the simulation scatter plot a large structural asymmetry at the time of the second photoionisation is indicated by pink. The relevant momentum- and real-space coordinates are also shown on the right.

Since water is present in every known living organism, the breakup of H_2O by radiation, i.e. the photolysis of water, is often the starting point for radiation damage. However, the chain of reactions that can be triggered in the body by high-energy radiation is still not fully understood. Even just observing the formation of individual ions and reactive radicals in water upon absorption of high-energy radiation is already very difficult. High-intensity X-ray light generated by X-ray free-electron lasers (XFELs) provides new opportunities to investigate these ultrafast processes.

To study X-ray ionisation-induced dynamics of water, we have exposed water molecules to the very intense and ultrashort light pulses from the European XFEL such that a single water molecule can absorb more than one X-ray photon during a light pulse. In this case, the first photon induces the break-up of the molecule, and the absorption of a further photon shortly afterwards provides a detailed fingerprint of its fragmentation pattern. By carefully analysing this fingerprint in combination with detailed simulations [1,2], we were able to draw conclusions about the ultrafast dynamics of H_2O occurring after X-ray absorption. We captured in a sense a 'film' of the disintegration of the water molecule (which lasted only a few femtoseconds) and found that the breakup process is much more complicated than initially expected.

Figure 1a shows an example of the relevant dynamics of the water molecule. At first, the X-ray light creates a dicationic water molecule by core-shell ionisation and a subsequent Auger decay. The H_2O^{2+} ion starts to deform and break apart, and the evolution of the system continues until a second photon is absorbed. This absorption ionises the molecule further and also triggers a further Auger decay. As the total charge of the molecule is +4 now, the strong Coulomb repulsion induces a violent fragmentation. The momenta of the three ions (O^{2+}, H^+, H^+) preserve information on the structural dynamics undergone in-between the absorptions of the two photons.

By using the COLTRIMS reaction microscope of the SQS instrument at European XFEL [3, 4], these momenta have been measured in coincidence. Figure 1b shows Newton diagrams of the ion momenta with two dominant peaks and pronounced tails. The main peaks result mostly from an almost instantaneous Coulomb explosion, where the final charge of +4 is reached before the dicationic molecular ion has time to undergo a substantial structural rearrangement. In contrast, the pronounced tail in the H^+ momenta pointing towards the emission direction of O^{2+} can be attributed to a scenario where the delay between the two photoabsorption events is sufficiently large to allow the molecule to evolve before being ripped apart by the Coulomb repulsion.

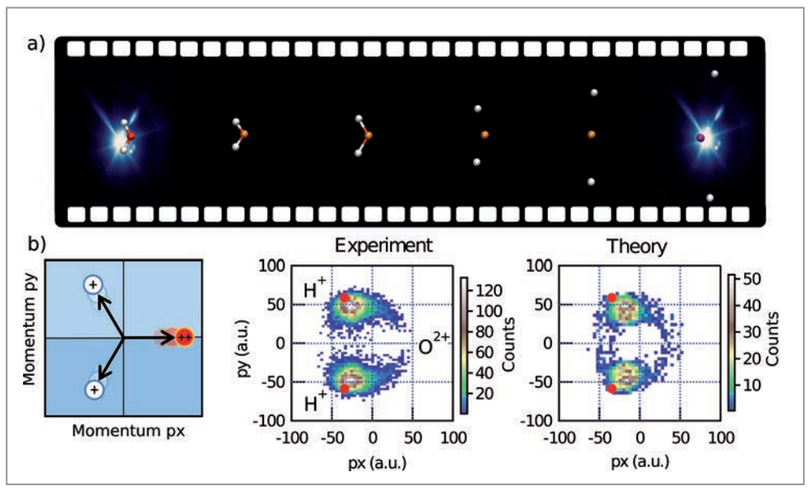

Figure 1
a) After the absorption of an X-ray photon (flash left), the water molecule can bend up so far that after only about ten femtoseconds both hydrogen atoms (grey) are facing each other, with the oxygen atom (orange) in the middle. This motion can be studied by absorbing a second X-ray photon (flash right) which triggers a Coulomb explosion of the molecule. b) Newton diagrams (left to right: scheme, experiment and theory) of the ion momenta for O^{2+} and two H^+ ions detected in coincidence, where the oxygen momentum defines the *x*-axis. On the left, the employed momentum coordinate system is shown. The red dots mark the expected momenta for the case of an instantaneous Coulomb explosion.

Further insight into the underlying dynamics is provided by the scatter plots in Fig. 2. Figure 2a shows that in a number of events the angles of the two H^+ momenta with respect to the O^{2+} momentum are strongly anti-correlated, summing up to almost 180°. Our simulations (Fig. 2c) indicate that this signal must be attributed to an unbending motion, where the water molecule reaches an almost linear geometry before the second photoabsorption triggers the final Coulomb explosion. Absolute momenta of the two H^+ are shown in Fig. 2b. Although most of the H^+ momenta show similar magnitude, a significant fraction is asymmetric. Through the simulations (Fig. 2d), we can clearly assign these cases to asymmetric dissociation of H_2O^{2+} into OH^+ and H^+.

Our simulations reveal that the overall kinetic energy release (KER) decreases when the time delay between the two photoabsorptions is larger. Thus, temporal information is encoded in the KER, and sorting our results according to the KER allows us to inspect the discussed fragmentation patterns as a function of time. Although only based on a single X-ray pulse, this methodology can be hence considered an effective pump-probe method.

Our study succeeded for the first time in taking a closer look at the dynamics of a water molecule after it absorbs high-energy radiation, characterising the formation of the oxygen and hydrogen ions and radicals, as well as the way this process unfolds over time. In particular, we reveal that X-ray irradiation leads to a significant unbending motion that results in the neutral oxygen almost at rest. This finding can have consequences for the radiation chemistry in liquid water, since such a low oxygen momentum may increase the reactivity for further reactions in an aqueous environment.

Author contact: Till Jahnke, till.jahnke@xfel.eu
Ludger Inhester, ludger.inhester@cfel.de
Maria Novella Piancastelli, maria-novella.piancastelli@physics.uu.se

References

1. Y. Hao, L. Inhester, S.-K. Son and R. Santra, 'Efficient electronic structure calculation for molecular ionization dynamics at high x-ray intensity', Struct. Dyn. 2, 041707 (2015).
2. L. Inhester, K. Hanasaki, Y. Hao, S.-K. Son and R. Santra, 'X-ray multiphoton ionization dynamics of a water molecule irradiated by an x-ray free-electron laser pulse', Phys. Rev. A 94, 023422 (2016).
3. R. Dörner, V. Mergel, O. Jagutzki, L. Spielberger, J. Ullrich, R. Moshammer and H. Schmidt-Böcking, 'Cold Target Recoil Ion Momentum Spectroscopy: a "momentum microscope" to view atomic collision dynamics', Phys. Rep. 95, 330 (2000).
4. J. Ullrich, R. Moshammer, A. Dorn, R. Dörner, L. P. H. Schmidt and H. Schmidt-Böcking, 'Recoil-ion and electron momentum spectroscopy: reaction-microscopes', Rep. Prog. Phys. 66, 1463 (2003).

Original publication

'Inner-shell-ionization-induced femtosecond structural dynamics of water molecules imaged at an X-ray free-electron laser', Physical Review X 11, 041044 (2021).
DOI: 10.1103/PhysRevX.11.041044

Till Jahnke, Renaud Guillemin, Ludger Inhester, Sang-Kil Son, Gregor Kastirke, Markus Ilchen, Jonas Rist, Daniel Trabert, Niklas Melzer, Nils Anders, Tommaso Mazza, Rebecca Boll, Alberto De Fanis, Valerija Music, Thorsten Weber, Miriam Weller, Sebastian Eckart, Kilian Fehre, Sven Grundmann, Alexander Hartung, Max Hofmann, Christian Janke, Max Kircher, Giammarco Nalin, Andreas Pier, Juliane Siebert, Nico Strenger, Isabel Vela-Perez, Thomas M. Baumann, Patrik Grychtol, Jacobo Montano, Yevheniy Ovcharenko, Nils Rennhack, Daniel E. Rivas, Rene Wagner, Pawel Ziolkowski, Philipp Schmidt, Tatiana Marchenko, Oksana Travnikova, Loïc Journel, Iyas Ismail, Edwin Kukk, Johannes Niskanen, Florian Trinter, Caterina Vozzi, Michele Devetta, Salvatore Stagira, Mathieu Gisselbrecht, Anna Lena Jäger, Xiang Li, Yubaraj Malakar, Michael Martins, Raimund Feifel, Lothar Ph. H. Schmidt, Achim Czasch, Giuseppe Sansone, Daniel Rolles, Artem Rudenko, Robert Moshammer, Reinhard Dörner, Michael Meyer, Thomas Pfeifer, Markus S. Schöffler, Robin Santra, Marc Simon and Maria Novella Piancastelli

For affiliation details refer to original publication.

Molecular movie with a twist

Revealing the femtosecond dynamics of a photoactive protein traversing a conical intersection

The functional properties of many biomolecules are determined by light-induced structural dynamics. These dynamics often involve conical intersections, defining regions in the space of molecular geometries with divergent coupling between electronic and vibrational degrees of freedom. This enables ultrafast electronic transitions initiated solely by geometric deformations. Experimental investigations, however, are hampered by the required spatial and temporal resolutions. Machine learning techniques can significantly enhance the time resolution of noisy data, providing new insights into femtosecond de-excitation dynamics of photoactive molecules and the topography of the involved conical intersection.

The structural dynamics of a molecule are determined by the underlying potential energy surfaces (PESs), assigning potential energies to all possible geometric configurations of the atomic nuclei. When two PESs intersect, the coupling between the involved electronic states diverges. This precludes a separate treatment of electronic and nuclear degrees of freedom. Instead, dynamical changes of the molecular geometry give rise to an ultrafast, non-radiative transition from one electronic state to another. A conical intersection (CI) is a region of such potential energy degeneracy and concomitant divergent coupling. A prime example of a process predominately determined by a CI is the light-induced trans-to-cis isomerisation, a collective internal rotation, in photoactive yellow protein (PYP).

The level of complexity involved in treating thousands of atoms in a macromolecule such as PYP renders electronic structure calculations for an accurate description of the PESs, on which the structural dynamics unfold, unfeasible. In addition, experimental observation of the ultrafast structural dynamics and electronic de-excitation via CIs has remained elusive due to the required high spatial and temporal resolutions. The latter is limited by uncertainties in the time delay between the excitation pump and the probe pulse, called timing jitter. Machine learning techniques can recover high-resolution dynamics from noisy data with substantial timing uncertainties by incorporating the fact that a system's time evolution is constrained by the underlying laws of motion. Learning these constraints based on experimental data allows highly accurate time-series reconstruction, even for substantial timing uncertainties [1,2].

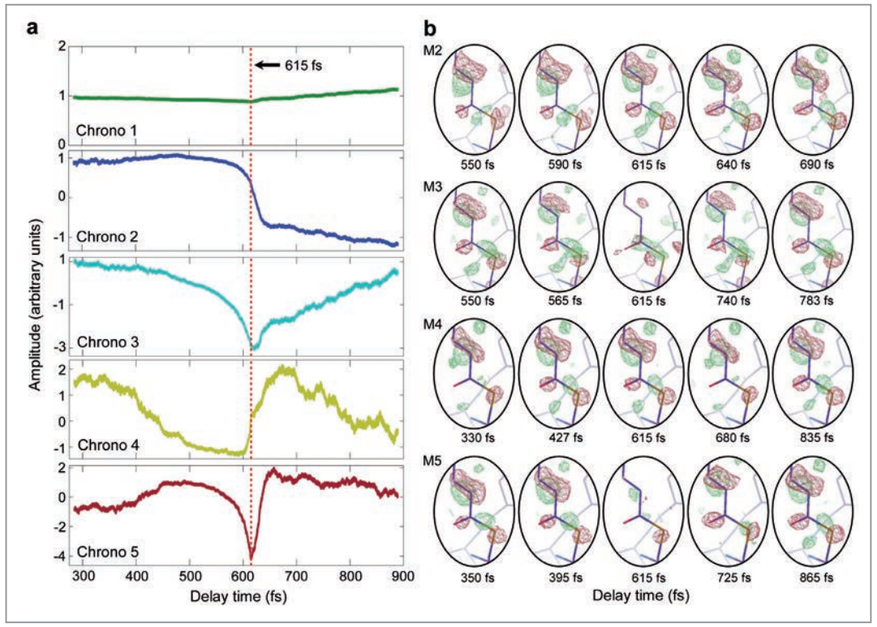

Figure 1

a) Chronograms of the DED dynamics in PYP. The sharp turning point at 615 fs visible in all chronograms coincides with the passage through the conical intersection. b) Time evolution of the DED. Mode 1 (not shown) represents the moving average and has been added to all other modes. The DED maps near the top of the oval region are associated with the trans-to-cis isomerisation. The patterns near the bottom of the oval region show strong oscillatory charge dynamics.
(Copyright © 2021, Springer Nature Limited)

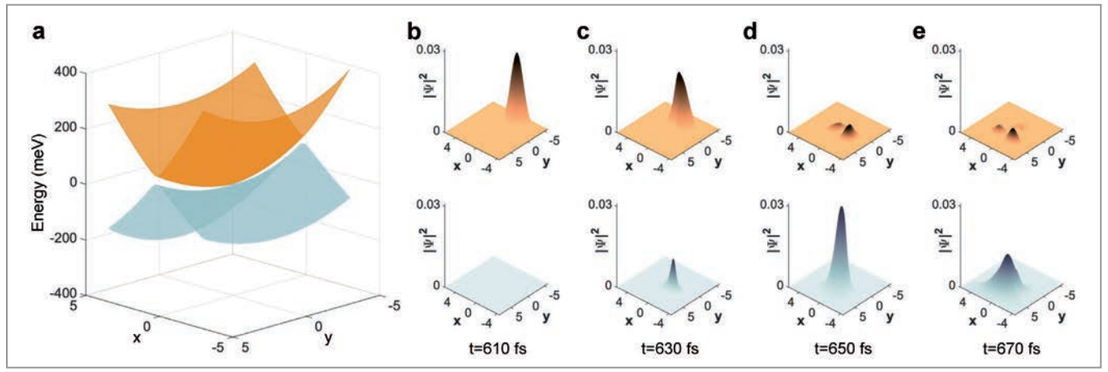

Figure 2

a) Reconstructed local potential energy surface topography in the close vicinity of the conical intersection. Touching of the two PESs constitutes the conical intersection. The normal modes x and y refer to collective modes, each associated with a topogram. b)–e) Time evolution of a Gaussian wave packet on the electronically excited state (top panels) and electronic ground state (bottom panels) in the vicinity of the reconstructed conical intersection.
(Copyright © 2021, Springer Nature Limited)

Applying this technique to a time series of diffraction images with an estimated timing jitter of 100 fs, obtained in a time-resolved X-ray crystallographic study of photo-excited PYP [3], allowed the reconstruction of highly accurate, jitter-suppressed difference electron density (DED) maps, revealing the dynamics of the charge distribution and the underlying atomic structure. Similar to finding a suitable basis in a vector space, the DED dynamics can be decomposed into structure-dynamical modes which, in combination, define the total dynamics. Each mode consists of a characteristic DED map, referred to as topogram, evolving in time as prescribed by a time-dependent weight, called chronogram (Fig. 1). The detection of previously unreported high-frequency oscillations in the chronograms implies a time resolution of the reconstructed DED dynamics of better than 10 fs, much shorter than the timing jitter in the experiment.

The DED decomposition in topograms and chronograms can be used to gain insights into the local CI topography involved in the de-excitation dynamics. The close vicinity of the CI can be considered a 2D subspace of collective modes, each of which is associated with a topogram. Hence, a dynamical trajectory in this subspace, i.e., a time series of 2D position vectors, corresponds to a pairwise combination of chronograms. Incorporating various CI topographies and initial conditions in exact quantum dynamics simulations of de-excitation trajectories, a subsequent comparison with pairwise combinations of experimental chronograms yields direct information on the local topography of the underlying PESs experienced by the structure-dynamical modes when traversing the CI (Fig. 2).

In summary, the presented combination of machine learning to recover dynamics from noisy experimental data with substantial timing uncertainty and quantum dynamical model simulations provides a powerful data-driven route to studying ultrafast processes in complex molecular systems inaccessible by first-principles calculations.

Author contact: Niels Breckwoldt, niels.breckwoldt@cfel.de
Robin Santra, robin.santra@cfel.de
Abbas Ourmazd, ourmazd@uwm.edu
Ahmad Hosseinizadeh, hosseina@uwm.edu

References

1. **D. Giannakis and A. J. Majda, 'Nonlinear Laplacian spectral analysis for time series with intermittency and low-frequency variability', Proc. Natl. Acad. Sci. U. S. A. 109, 2222–2227 (2012).**
2. **R. Fung et al., 'Dynamics from noisy data with extreme timing uncertainty', Nature 532, 471–475 (2016).**
3. **K. Pande et al., 'Femtosecond structural dynamics drives the trans/cis isomerization in photoactive yellow protein', Science 352, 725–729 (2016).**

Original publication

'Few-fs resolution of a photoactive protein traversing a conical intersection', Nature 599, 697–701 (2021).
DOI: 10.1038/s41586-021-04050-9

Ahmad Hosseinizadeh[1], Niels Breckwoldt[2,3,4], Russell Fung[1], Reyhaneh Sepehr[1], Marius Schmidt[1], Peter Schwander[1], Robin Santra[2,3,4] and Abbas Ourmazd[1]

1. University of Wisconsin Milwaukee, Milwaukee, WI, USA
2. Center for Free-Electron Laser Science (CFEL), DESY, Hamburg, Germany
3. Department of Physics, Universität Hamburg, Hamburg, Germany
4. The Hamburg Centre for Ultrafast Imaging (CUI), Universitat Hamburg, Hamburg, Germany

Into the molecule's perspective

Field-free alignment of a prototypical biomolecule

Molecules in the gas phase are oriented isotropically. To fully decipher ultrafast photochemical reactions, the molecules' axes need to be fixed in the laboratory frame. Laser alignment is an established technique to accomplish this [1], requiring TW/cm^2 intensities. However, such intensities can be detrimental to molecular dynamics investigations; suppressing the laser field is highly beneficial. We show that using a sharply truncated laser pulse, a strongly aligned sample of the prototypical biomolecule indole can be prepared and detected in a field-free environment. Our approach is general and can be applied to any molecule.

We studied the prototypical gas-phase asymmetric top-molecule indole, cooled to ~1 K, as our target. Indole consists of only H, C and N atoms, the most common constituents of organic biomolecules. With respect to most experimental investigations aiming to induce and probe field-free alignment of asymmetric-top molecules, indole is missing marker atoms, e.g. halogen atoms or similar ligands which are usually used to determine molecular alignment. Using an off-resonant-wavelength (800 nm) laser pulse of suitable intensity, polarisation and duration, we forced the molecule's axes to align to those of the laboratory frame (Fig. 1). Using phase and amplitude shaping, the laser pulses were rapidly truncated once the molecular alignment reached its maximum. The truncation was more rapid than the rotational dephasing rate, governed by the molecule's inertia, and alignment thus persisted for some time in the absence of significant laser intensity.

To determine the spatial alignment of the indole molecules, we utilised strong-field ionisation, resulting in a Coulomb explosion. Fragment ions were imaged onto a position-sensitive detector using a velocity-map-imaging spectrometer. The projected 2D angular distribution is an easily accessible, but incomplete, measure of alignment. By careful fitting of the velocity maps' temporal evolution to calibrated time-dependent quantum mechanical calculations in the rigid rotor approximation, we determined the true 3D distribution from the measured 2D distributions.

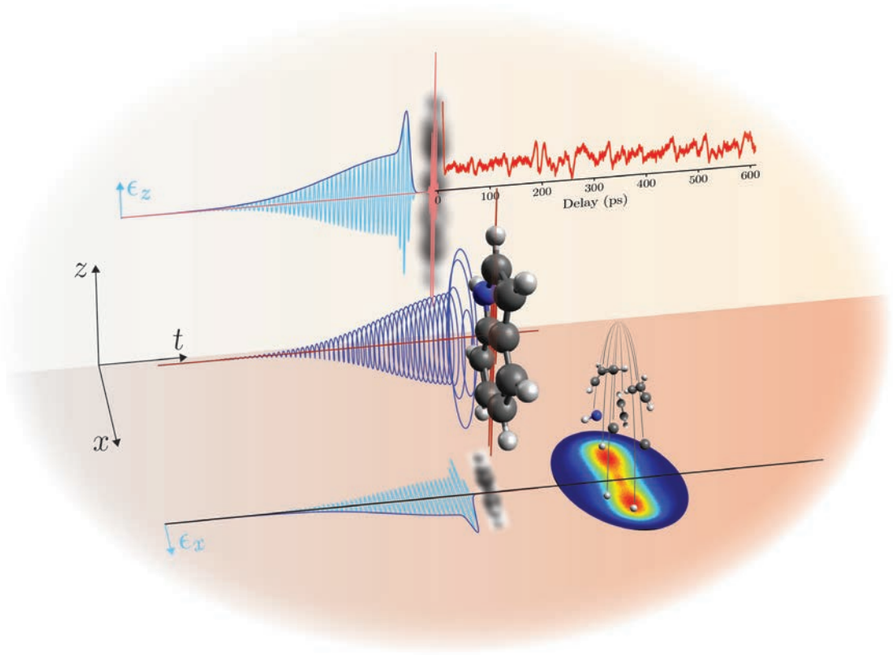

Figure 1

An elliptically polarised laser pulse constrains all three molecular axes to the laboratory frame. The laser pulse is truncated at a fixed time. After truncation, rotational quantum dynamics lead to beats which act as a fingerprint of the molecular wave packet and the alignment. A second short laser pulse, with variable delay, multiply ionises the molecules, leading to Coulomb explosion. Projections of ionic fragments are detected using a velocity map imaging spectrometer.

The alignment dynamics $\langle\cos^2\theta_{eff}\rangle$ extracted from the measured C^{2+} velocity maps, with θ_{eff} as the detected emission angle of the C^{2+} fragments, is shown in Fig. 2 (blue line), together with the temporal profile of the alignment laser pulse (red area). For comparison, the dashed line indicates the extracted alignment without alignment laser pulse, showing the geometric effect of our detection technique. The alignment reached its maximum ~3 ps after the peak laser intensity and persisted for a few picoseconds – more than sufficient for studies on molecular-dynamics timescales – even though the constraining potential of the laser field was no longer present.

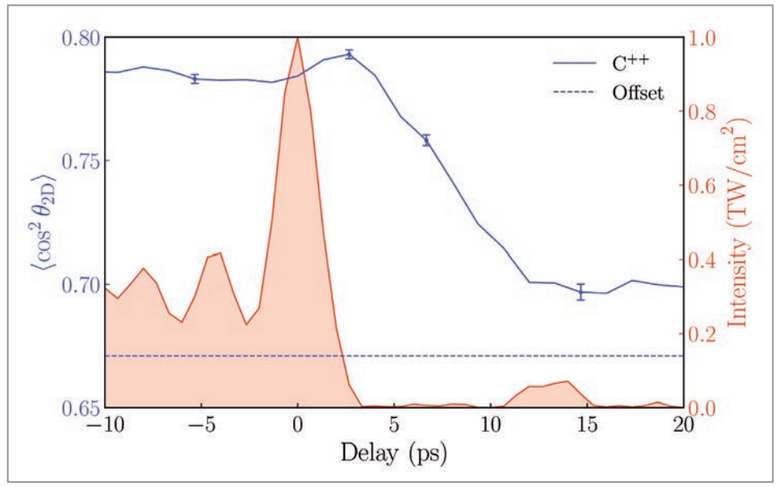

Figure 2

The measured truncation profile of the alignment pulse (red) and the C^{2+} fragment 2D alignment dynamics, $\langle\cos^2\theta_{eff}\rangle$ (blue), in the vicinity of the truncation. Error bars are shown only for selected points for clarity. In the 2D distributions, $\langle\cos^2\theta_{eff}\rangle$ =1 corresponds to a perfectly aligned 2D projection, $\langle\cos^2\theta_{eff}\rangle$ =0.5 corresponds to an isotropic 2D projection. The laser intensity was significantly suppressed at +3 ps, at which time the practically field-free alignment was maximised.

The increased alignment after truncation shows that our exact pulse-shaping method was optimised to even enhance the molecular alignment, compared to standard adiabatic alignment techniques that make use of nanosecond laser pulses [2].

In addition, quantum beats were also observed at longer delays from the coherently populated rotational states. The quantum beat/rotational wave packet dynamics are well reproduced by our 3D quantum mechanical model and allowed us to quantify the alignment of the molecules at the time the laser intensity was truncated, as well as how rapidly the turn-off occurred. The reconstructed 3D alignment values extracted from these simulations were $\langle\cos^2\theta_{zz}\rangle$=0.88, $\langle\cos^2\theta_{yy}\rangle$=0.83, and $\langle\cos^2\theta_{\backslash xx}\rangle$=0.85 at 3 ps after truncation, which indicate the very strong alignment of all three axes.

Our results show that it is possible to both field-free 3D align and characterise the alignment of unadulterated biomolecules in the gas phase for durations suitable for structure determination and dynamics experiments.

Author contact: Jochen Küpper, jochen.kuepper@cfel.de

References

1. **H. Stapelfeldt, 'Colloquium: Aligning molecules with strong laser pulses', Rev. Mod. Phys. 75, 543-557 (2003).**
2. **S. Guérin, A. Rouzée and E. Hertz, 'Ultimate field-free molecular alignment by combined adiabatic-impulsive field design', Phys. Rev. A 77, 041404 (2008).**

Original publication

'Picosecond pulse-shaping for strong three-dimensional field-free alignment of generic asymmetric-top molecules', Nature Communications 13, 1431 (2022). DOI: 10.1038/s41467-022-28951-z

Terry Mullins[1], Evangelos T. Karamatskos[1,2], Joss Wiese[1,3,4], Jolijn Onvlee[1,4,6], Arnaud Rouzée[5], Andrey Yachmenev[1,4], Sebastian Trippel[1,4] and Jochen Küpper[1,2,3,4]

1. Center for Free-Electron Laser Science (CFEL), DESY, Hamburg, Germany
2. Department of Physics, Universität Hamburg, Hamburg, Germany
3. Department of Chemistry, Universität Hamburg, Hamburg, Germany
4. Center for Ultrafast Imaging, Universität of Hamburg, Hamburg, Germany
5. Max Born Institute, Berlin, Germany
6. Institute for Molecules and Materials, Radboud University, AJ Nijmegen, Netherlands

A new mix of extreme ultraviolet and optical light

Probing electron and hole colocalisation by resonant four-wave mixing spectroscopy

Free-electron laser sources are shifting the limits for non-linear spectroscopy into the extreme ultraviolet (XUV) and X-ray spectral ranges, where inner shell electrons become involved in the non-linear processes [1,2]. Exemplarily, we studied the influence of core excitons in a lithium fluoride single crystal on sum- and difference-frequency mixing by employing XUV free-electron and optical laser pulses. This allows probing charge localisation with atomic specificity and gives access to otherwise forbidden, dark transitions.

Lithium fluoride (LiF) is an ionic crystal of cubic symmetry. Photoexciting one of the Li 1s electrons with photons beyond 64 eV can transfer it to the conduction band, where it may freely roam the crystal. Excitation may also form an exciton, with the electron staying colocalised with the core hole at an excitation energy of just 62 eV. This exciton is evidenced by a narrow maximum in linear spectroscopy (Fig. 1b) [3]. The energetically close (1s)(2s) Li+ configuration may also give rise to an exciton but cannot be excited in linear spectroscopy due to dipole selection rules. However, the small shoulder on the low energy side of the pronounced structure in Fig. 1b has been suspected to be based on just this electron configuration, made accessible by breaking the cubic crystal symmetry [4]. Non-linear spectroscopy may help clarify this proposition.

Owing to the symmetry of LiF, the lowest order non-linear process is of third order: four-wave mixing (FWM) governed by the susceptibility $\chi^{(3)}$. Specifically, we studied sum- (SFG) and difference-frequency (DFG) mixing using extreme ultraviolet free-electron (photon energy E_X) and infrared (IR) laser radiation (photon energy E_{IR}). We were then looking for generated radiation at photon energies $E_X + 2E_{IR}$ (SFG) and $E_X - 2E_{IR}$ (DFG), emitted in reflection off the LiF crystal surface as sketched in Fig. 1c.

The measurements were conducted at the FLASH2 beamline FL24 using the MUSIX endstation [5] with the free-electron laser (FEL) photon energy scanned between E_X = 58 eV and 72 eV. The IR laser pulses had a fixed photon energy of E_{IR} = 1.55 eV. The sum- and difference frequency generated in reflection is separated from the driving IR and FEL beams by a grating spectrometer. Please note that this geometry also allows the investigation of thick samples.

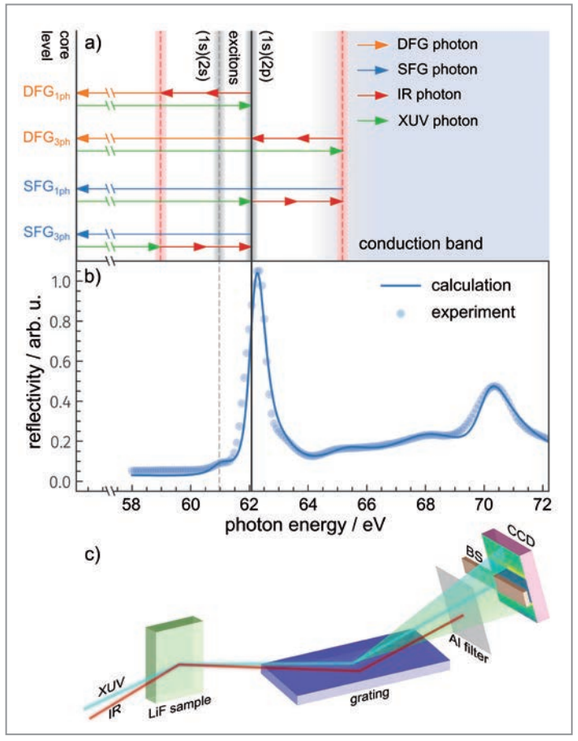

Figure 1

a) Schematic of the LiF energy levels relevant for the FWM experiment. The horizontal arrows represent the SFG and DFG generation if in one- or three-photon resonance with the LiF (1s)(2p) exciton at around 62 eV. b) Linear reflectivity spectrum in the relevant photon energy range. The dots represent the experimental data and the solid line is a calculation based on a linear model for the dielectric constant of LiF. c) Sketch of the experimental setup showing the XUV and IR laser beams impinging nearly collinear on the LiF crystal surface. The reflected IR light is blocked by an Al filter, while the XUV radiation is spectrally dispersed by a grating and detected by a CCD camera. The strong XUV fundamental is blocked by a beamstop (BS) to avoid saturation.

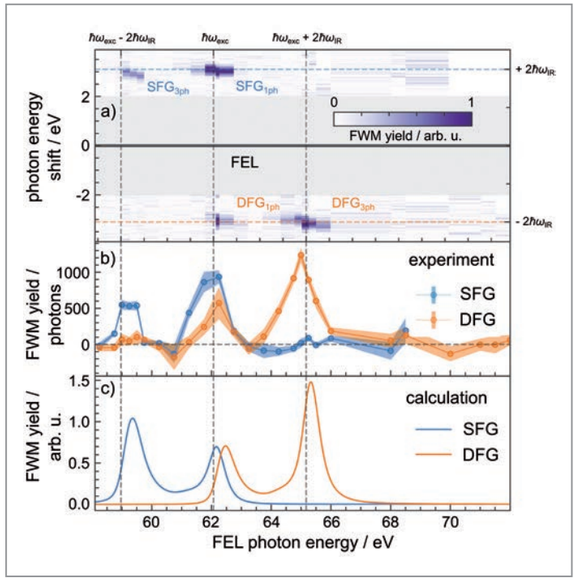

Figure 2

a) Density map of the FWM yield. DFG and SFG signals are only observed when in one- or three-photon resonance with the Li (1s)(2p) exciton at around 62 eV. The corresponding photon energy shift is ± $2E_{IR}$. The experimental SFG and DGF yields shown in b) are in good agreement with the simple atomic model for the non-linear susceptibility $\chi^{(3)}$ of LiF as shown in panel c).

The main experimental result, i.e. the yield of radiation generated by FWM, is shown in Fig. 2a with the FEL photon energy on the horizontal axis and the energy shift of the emitted photons on the vertical axis. A region in the vicinity of the FEL photon energy was blanked out to protect the detector. The integration of the signal over positive (blue) and negative (orange) energy shifts results in the total yield of SFG and DFG, respectively (Fig. 2b).

Significant frequency conversion was only observable with the FEL tuned to the exciton transition (E_{exc} = 62 eV) or offset from E_{exc} by twice the IR photon energy, i.e. ± 3.1 eV (Fig. 2b) and with temporal overlap of both pulses. This verifies the nature of the observed FWM signal. In contrast, no frequency conversion was observed with the FEL tuned to the conduction band, including the 70.5 eV feature, which has been debated to be due to an electron polaron bound to a core hole [6].

The strong influence of the exciton, with its colocalised electron and hole, in the FWM processes suggests a simplified approach to model $\chi^{(3)}$ of LiF. We used an atomic model with two excitons based on the (1s)(2p) and (1s)(2s) electron configurations. It turned out that both excitons, dipole coupled, are necessary to reasonably reproduce the experimental yields (see Fig. 2c). This indicates the presence of an s-type exciton as suspected based on linear spectroscopy [4].

Our work shows that non-linear XUV spectroscopy under resonant conditions is a sensitive probe of charge localisation, enabling atomic specificity even when using wavelengths substantially larger than the unit cell (see also [7]). FWM allows identifying localised excitations, like excitons, even when they are 'optically dark'. More generally, the presence of excited states, inaccessible or suppressed owing to crystal symmetry in linear spectroscopy, can be uncovered. With the FEL pulse widths decreasing, non-linear spectroscopy will soon be able to probe the dynamical evolution of these excitations. As the dynamics of transient localisation and delocalisation of charge at different atomic species is of fundamental importance for a multitude of processes in physics, chemistry and biology, we expect wave mixing processes in resonance with inner shell excitations to become a particularly fruitful approach for future time-domain studies at FELs.

Author contact: Horst Rottke, rottke@mbi-berlin.de
Daniel Schick, schick@mbi-berlin.de
Stefan Eisebitt, eisebitt@mbi-berlin.de
Martin Beye, martin.beye@desy.de

References

1. F. Bencivenga et al., 'Four-wave mixing experiments with extreme ultraviolet transient gratings', Nature 520, 205–208 (2015).
2. J. D. Gaynor et al., 'Solid state core-exciton dynamics in NaCl observed by tabletop attosecond four-wave mixing spectroscopy', Phys. Rev. B 103, 245140 (2021).
3. R. Haensel, C. Kunz and B. Sonntag, 'Measurement of photoabsorption of the lithiumhalides near the lithium *K* edge', Phys. Rev. Lett. 20, 262–264 (1968).
4. W. Olovsson, I. Tanaka, P. Puschnig and C. Ambrosch-Draxl, 'Near-edge structures from first principles all-electron Bethe–Salpeter equation calculations', J. Phys. Condens. Matter 21, 104205 (2009).
5. M. Beye, R. Y. Engel, J. O. Schunck, S. Dziarzhytski, G. Brenner and P. S. Miedema, 'Non-linear soft x-ray methods on solids with MUSIX—the multi-dimensional spectroscopy and inelastic x-ray scattering endstation', J. Phys. Condens. Matter 31, 014003 (2019).
6. X. A. B. Kunz, J. T. Devreese and T. Collins, 'The role of the electronic polaron in the soft X-ray absorption of the lithium halides', J. Phys. C Solid State Phys. 5, 3259–3263 (1972).
7. T. E. Glover et al., 'X-ray and optical wave mixing', Nature 488, 603–608 (2012).

Original publication

'Probing electron and hole colocalization by resonant four-wave mixing spectroscopy in the extreme ultraviolet', Science Advances 8, eabn5127 (2022). DOI: 10.1126/sciadv.abn5127

H. Rottke[1], R. Y. Engel[2,3], D. Schick[1], J. O. Schunck[2,3], P. S. Miedema[2], M. C. Borchert[1], M. Kuhlmann[2], N. Ekanayake[2], S. Dziarzhytski[2], G. Brenner[2], U. Eichmann[1], C. von Korff Schmising[1], M. Beye[2,3] and S. Eisebitt[1,4]

1. Max-Born-Institut für Nichtlineare Optik und Kurzzeitspektroskopie, Berlin, Germany
2. Deutsches Elektronen-Synchrotron DESY, Hamburg, Germany
3. Universität Hamburg, Hamburg, Germany
4. Technische Universität Berlin, Berlin, Germany

Introducing an X-ray polarisation microscope

Precision polarimetry meets microscopy

Polarisation microscopy is a common method in visible optics that has many applications in, e.g. geoscience for the identification of minerals, in biology for the analysis of the organisation of cells and tissues and in materials science for residual stress measurements. Especially in modern fields of optics, such as laser optics, nonlinear optics and ultrafast time-resolved processes of chemical, structural and biological processes, the combination of polarimetry and imaging is the basic method to study fundamental processes in matter and life. Such methods are still missing in modern X-ray techniques but they will become important for future applications of new XFEL sources. We show that an ultra-sensitive X-ray polarimeter with a dynamic range of 11 orders of magnitude can be combined with a refractive confocal X-ray imaging system.

The extreme sensitivity of today's X-ray polarimeters allows to detect tiniest changes of the X-ray's polarisation in materials. At the same time, however, this sensitivity poses a great challenge to any optics which are inserted into the polarimeter. In order to combine X-ray polarimetry with microscopy, it is necessary to introduce focusing and recollimating optics between the polariser and the analyser, as the latter forfeits the extreme degree of polarisation purity with increasing beam divergence. For the realisation of an X-ray polarisation microscope, compound refractive lenses (CRLs) of various materials were used as focussing and collimation elements and tested for their suitability.

The polarisation microscope (Fig. 1) was set up at the PETRA III beamline P01 because this beamline provides a high photon flux and a narrow beam divergence. The heart of the polarisation microscope is the polarimeter, consisting of a polariser and an analyser crystal made of silicon single crystals. These make use of the suppression of the pi-component of the incident radiation at a Bragg reflection angle of 45°. In order to improve the suppression of the pi-component further, a channel is cut into the crystal to realise multiple reflections at 45° (see Fig. 1, polariser). Such a channel-cut crystal enables a suppression of the pi-component versus the sigma-component of up to 11 orders of magnitude [1]. To carry out the polarisation analysis, the analyser can be rotated around the diffraction plane of the first polariser crystal, allowing for an analysis of the X-ray beam which has propagated through a potential sample material. Two-dimensional focusing is achieved by refractive X-ray lenses. Due to the small refractive index decrement, the deflection angles are small, and several lens elements with small radius of curvature have to be aligned in one row to achieve a short focal length.

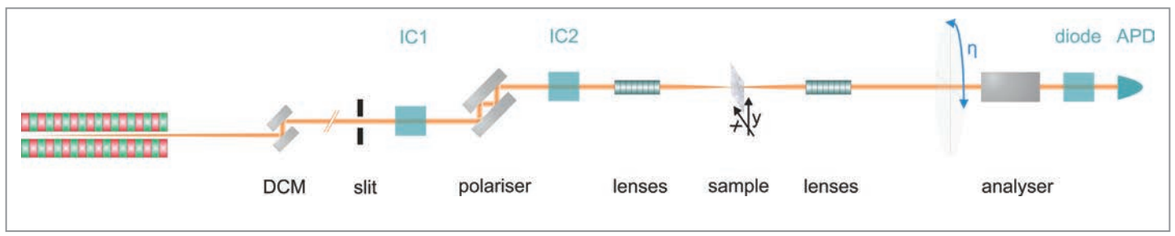

Figure 1

Experimental setup of the X-ray polarisation microscope. The incoming beam from the left is filtered by a double crystal monochromator (DCM) to the photon energy of 12.9 keV. Next, the beam size is restricted by a slit to the aperture of the lenses. Silicon channel-cut crystals are used to polarise and analyse the beam. Two lens stacks are placed in between the crystals before and after the sample to focus and re-collimate the beam. Ionisation chambers (IC), a diode and avalanche photodiodes (APDs) are used for detection.

Figure 2

Result of the polarisation microscopy scan of a 500 µm beryllium foil. The step size was 20 µm × 5 µm in horizontal and vertical direction.

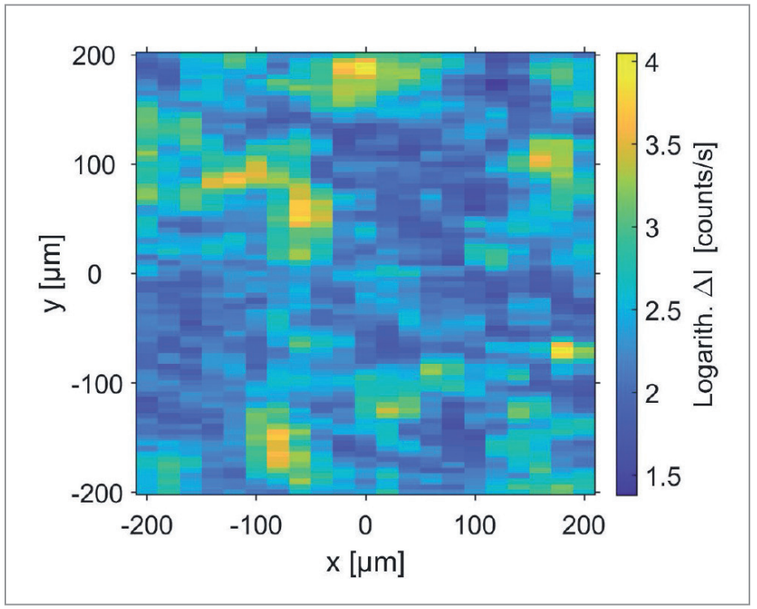

There are several refractive lens materials available. Their manufacturing process and material properties differ which influences the achievable focal sizes and thus the spatial resolution of the polarisation microscope. We tested four different lens materials: single-crystal diamond lenses, polycrystalline beryllium lenses, amorphous polymer lenses (SU-8), and glassy carbon lenses. We succeeded in realising a highly sensitive polarisation microscope with the polymer lenses. With a degree of polarisation purity of 10^{-11} of the incoming beam, no change of the polarisation purity was measurable. The achieved focus size was 7 µm × 28 µm. Both, the spatial resolution and the degree of polarisation purity, can be further improved by reducing the focal length and by using the new ultra-low emittance sources in the future.

The performance of the polarimeter was demonstrated by scanning a beryllium foil of 500 µm thickness through the focus of the polarised beam (Fig. 2). The result shows intensity changes of 2.5 orders of magnitude. The range of intensity change correlates with the crystallite size of the sample material, indicating that the polarisation change is caused by Bragg reflections of the crystallites. Compared to X-ray polarimetry alone, polarisation microscopy makes it possible to observe polarisation changes with high spatial resolution. Knowing the spatial extension of polarisation-changing in a material can strongly facilitate conclusions about their origin.

The successful combination of highly sensitive X-ray polarimeters with polarisation-preserving X-ray lenses is a new method that makes polarisation changes visible on the µm-scale and has the potential to result in new insight in many disciplines like spectroscopic polarimetry [2], nuclear resonant scattering, pump-probe setups for ultrafast time-dependent studies [3] and the detection of the vacuum

Author contact: Berit Marx-Glowna, berit.marx@uni-jena.de

References

1. K. Schulze et al., 'Towards perfectly linearly polarized x-rays', Phys. Rev. Research 4, 013220 (2022).
2. A. Schmitt et al., 'Disentangling x-ray dichroism and birefringence via high-purity polarimetry', Optica 8, 56–61 (2021).
3. D. Diels and W. Rudolph, 'Ultrashort Laser Pulse Phenomena', New York: Academic Press (1996).

Original publication

'Scanning high-sensitive x-ray polarization microscopy', New Journal of Physics 24, 053051 (2022). DOI: 10.1088/1367-2630/ac6e80

B. Marx-Glowna[1,2], B. Grabiger[3], R. Lötzsch[33], I. Uschmann[1,2,3], A. T. Schmitt[3], K. S. Schulze[1,2], A. Last[4], T. Roth[5], S. Antipov[6], H.-P. Schlenvoigt[7], I. Sergueev[8], O. Leupold[8], R. Röhlsberger[1,2,8] and G. G. Paulus[1,2,3]

1. Hemholtz Institute, Jena, Germany
2. Helmholtz Centre for Heavy Ion Research, Darmstadt, Germany
3. Institute of Optics and Quantum Electronics (FSU), Jena, Germany
4. KIT Institute of Microstructure Technology (IMT), Eggenstein-Leopoldshafen, Germany
5. European Synchrotron Radiation Facility (ESRF), Grenoble, France
6. Euclid TechLabs LLC, Bolingbrook, United States of America
7. Helmholtz-Zentrum Dresden-Rossendorf, Dresden, Germany
8. Deutsches Elektronen-Synchrotron DESY, Hamburg, Germany

Sharp X-ray images despite imperfect lenses

Multilayer zone plate objective lenses teamed with advanced phase retrieval enable sub-10 nm resolution in single-shot imaging

X-ray microscopy has evolved into an indispensable tool for materials and life sciences, enabling images at high resolution, in bulk samples and in challenging environments [1]. In the past, progress in X-ray microscopy was driven either by improvements in X-ray optics or by improvements in image reconstruction, notably by algorithms of coherent diffractive imaging which have replaced the lens by numerical computation. In this work we combine both – up to now antagonistic – approaches for full-field X-ray microscopy. We show that an X-ray microscope using both, advanced optics and iterative phase retrieval algorithms, is neither limited by flawed optics nor by constraints imposed by reconstruction algorithms.

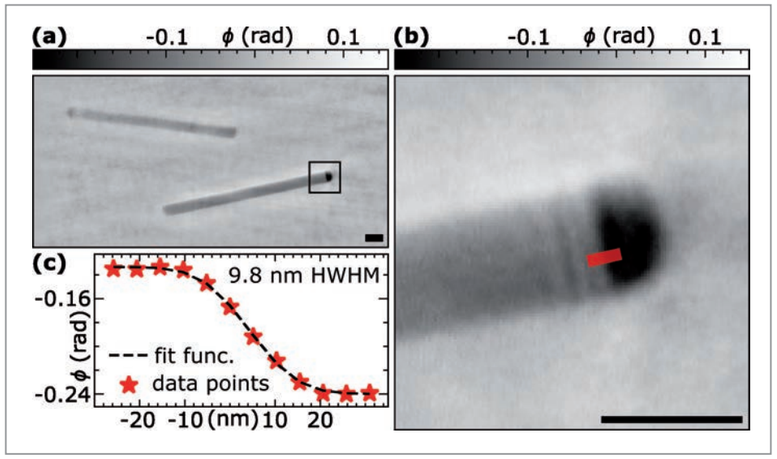

Figure 2

X-ray microscopy results of the nanowire (NW) sample. a) Reconstructed NWs using the detector image shown in Fig. 1(c). The NWs have a 200 nm diameter and an Au tip at one end. b) Enlarged region of one NW tip. c) Error fit of the material edge indicated in b), resulting in a resolution (half-period) of 9.8 nm. Black scale bars: 250 nm.

When larger specimens need to be covered by X-ray microscopy without scanning in a single acquisition, i.e. in a full-field view, one basically has three choices: one can use the classical transmission X-ray microscope (TXM) with Fresnel zone plates (FZP) as objective lenses to directly image and magnify the sample structure. With increasing photon energies, however, the FZPs rapidly lose performance, as low diffraction efficiencies and imperfect FZP lenses deteriorate the image quality. Therefore, lens-based image formation can be replaced by an iterative phase retrieval algorithm which is known as coherent diffraction imaging (CDI). Finally, for a non-compact extended object, single-shot acquisitions are also possible with inline holography in a cone-beam geometry, again without any lenses or optics between object and detector planes.

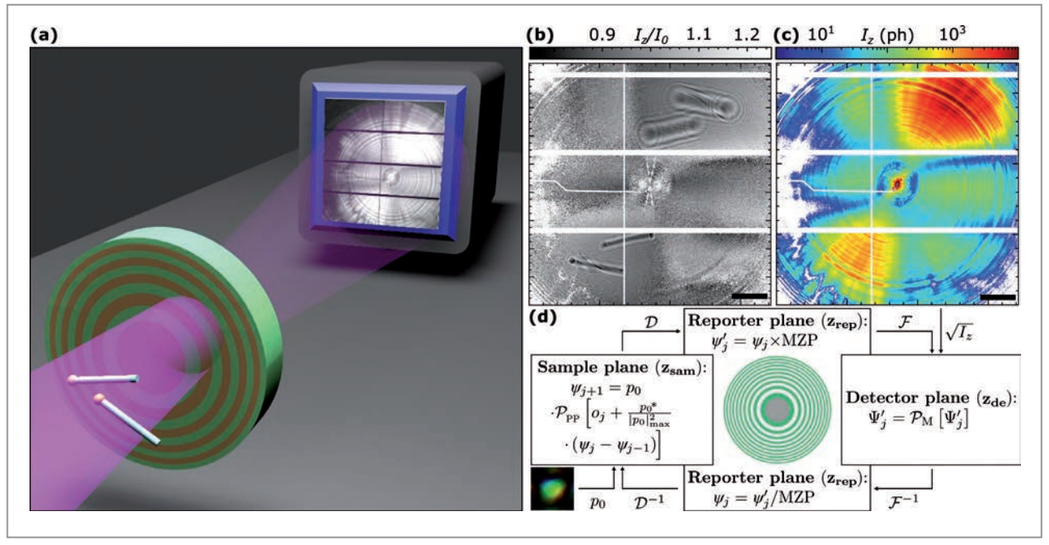

Figure 1

Experimental method. a) Artistic rendering of the experimental setup with nanowires (NW), multilayer zone-plate (MZP) lens used in an off-centre configuration and the pixel detector 5 m behind. b) The empty divided detector image indicating the three different sample (NW) signals: two holograms (top and bottom) and one CDI signal recorded in a single measurement (linear gray scale). The holographic signal components are associated with the +1 and -1 diffraction orders of the MZP. c) The intensity measurement with the sample (NW) in the beam. This single measurement is used for the sample reconstruction (logarithmic color scale). d) Outline of the phase retrieval algorithm with the measured transfer function of the MZP fed into the propagation. Scale bars: 250 pixels, corresponding to a scattering vector of q = 0.15 nm^{-1}.

Notwithstanding the advantages of lensless coherent imaging techniques, nanofabrication has also seen much progress recently, resulting in high-resolution and high-efficiency zone plate optics. In particular, multilayer zone plates (MZPs) and one-dimensional multilayer Laue lenses (MLLs) which can now focus an X-ray beam to a size below 10 nm [2,3]. Unfortunately, however, this focusing capability does not directly translate to an equivalent resolution in full-field imaging due to a number of complications associated with multiple diffraction orders, volume diffraction, remaining aberrations and the need of Zernike phase rings for phase contrast. We have therefore combined conceptional aspects of all three major approaches to full-field X-ray microscopy. We use an MZP as an objective lens to achieve high resolution but do not content ourselves with a sharp intensity image; instead, we use a fully quantitative and iterative phase retrieval scheme to reconstruct the sample transmission function. To this end, we use the measured MZP transfer function. This liberates us from the requirement to use perfectly aligned, aberration- and distortion-free optics, and allows us to exploit the full information and numerical aperture (NA) of the recorded diffraction pattern with the sample encoded in near- and far-field intensity distributions.

The novel scheme has been demonstrated at the coherence beamline P10 at PETRA III by imaging InP-nanowires (NW) which are of particular interest as new materials for photovoltaics. The NWs had a diameter of 200 nm and a length of 2.8 µm, were terminated by an Au tip at one end and deposited on a Si3N4 window. The sample was illuminated by a mildly focused beam (Beryllium CRLs) with an X-ray energy of 8 keV. An MZP was positioned about 900 µm behind the sample - close to the imaging plane, while a photon-counting pixel detector (Eiger 4M, Dectris) was positioned at about 5 m behind the sample. The MZP was composed of 784 zones with a diameter of 16.9 µm, an optical depth of 1.2 µm, an outermost zone width of only 5 nm and a focal length of 530 µm. Using this scheme (see Fig. 1), we experimentally demonstrated a sub-10 nm resolution and a quantitative contrast of the measured sample (see Fig. 2). For this solution to work, it was crucial to precisely measure the MZP lens itself, which was far from perfect, and to completely dispense with the assumption that it could be ideal. The presence of multiple diffraction orders, which is conventionally a nuisance, now came as an advantage for the reconstruction and photon efficiency.

Apart from the resolution, we are emphasising again that the most important advantage of this method is the fact that the object does not have to be scanned. This means that very fast microscopic processes in materials could be recorded, if the scheme is extended to ultrafast X-ray sources, such as the European XFEL.

Author contact: Tim Salditt, tsaldit@gwdg.de
Jakob Soltau jakob.soltau@uni-goettingen.de

References

1. C. Jacobsen, 'X-ray Microscopy', Cambridge University Press (2019).
2. J. Soltau et al., 'Off-axis multilayer zone plate with 16 nm × 28 nm focus for high-resolution x-ray beam induced current imaging', J. Synchrotron Radiat. 28, 1573 (2021).
3. S. Bajt et al., 'X-ray focusing with efficient high-NA multilayer Laue lenses', Light Sci. Appl. 7, 17162 (2018).

Original publication

'Coherent diffractive imaging with diffractive optics', Physical Review Letters 128, 223901 (2022).
DOI: 10.1103/PhysRevLett.128.223901

Jakob Soltau[1], Markus Osterhoff[1], Tim Salditt[1]

1. Institute for X-ray Physics and University of Göttingen, Göttingen, Germany

Fighting noise with noise

Machine learning filter reveals 3D nanostructures in butterfly wings

X-ray imaging is a key technique in various research areas such as medicine, biology and material science. Resolving structures in 3D down to the nanometre scale requires hard X-ray nanotomography. Although the imaging techniques are quite advanced, the acquired images are frequently obscured by noise. While the human eye can still distinguish different features, automated algorithms often fail. This restricts its applicability for automatic image analysis methods which are usually necessary for extracting quantitative information from a 3D volume. Conventional filtering methods for noise reduction often blur the finest structures in the images and decrease the spatial resolution. Here, a machine learning (ML) approach was used to resolve the tiny nanostructures in a butterfly scale which are responsible for the colours of the butterfly wing.

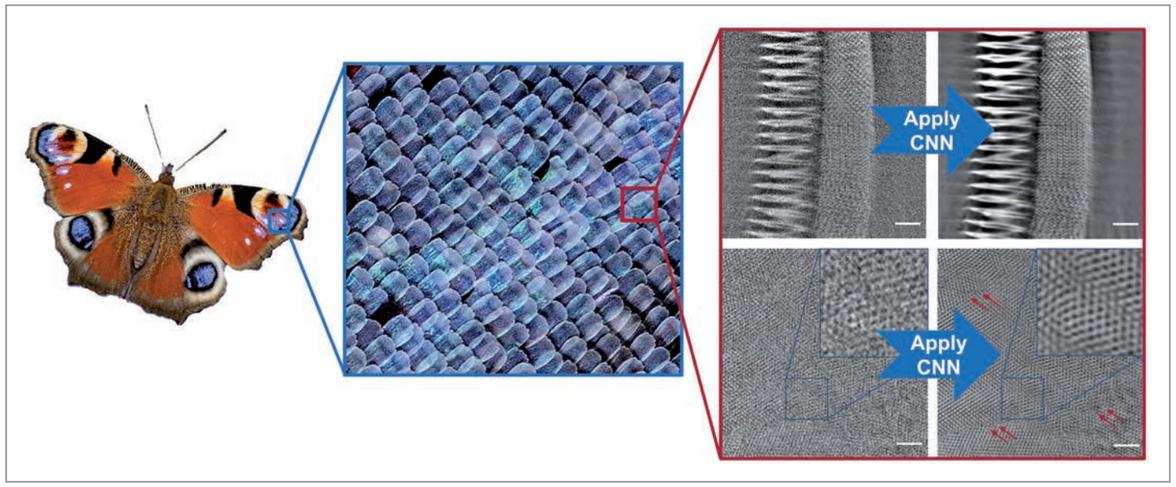

Figure 2

Denoising of a butterfly scale. The nanostructures of the scales on the butterfly wing are responsible for the colour of the wing. After denoising with the ML filter, the fine nanostructures become visible. Arrows point towards orientation changes of different domains. Note: The displayed butterfly species does not correspond to imaged structures. (Butterfly photography by K. H. Diddens)

The nanotomography end station at the PETRA III Imaging beamline P05, operated by Helmholtz-Zentrum Hereon, offers high-performance full-field nanotomography methods with spatial resolutions down to below 50 nm in 3D. A transmission X-ray microscope (TXM) with optional Zernike phase contrast offers high-resolution and high-contrast 3D images which can be acquired within seconds to a few minutes [1]. However, due to the high and often non-uniform noise level in TXM images (e.g. caused by inhomogeneous illumination), standard methods of image noise reduction fail or lead to a loss of spatial resolution. In recent years, there has been a lot of progress in image filtering techniques. In particular, ML approaches optimised for tomography data have a high potential to improve image quality. Several approaches have been made using ML for denoising tomographic data. However, those generally require a high-quality reference, e.g. a certain scanning protocol and cannot be used on data acquired without this protocol [2] or for *in situ* applications where time resolution is an issue.

The presented approach does not rely on a specific scanning protocol. The ML network is tricked: In order to train neural networks, the projections of one tomographic scan are divided into two stacks, each containing every second projection image of the sample. The two stacks of projections are now reconstructed, creating two 3D data sets (tomograms) (Fig. 1). These two tomograms are identical; the only difference between them is the noise, as it occurs randomly [3]. One of the two tomograms is now chosen as the input and the other one as the target for training a convolutional neural network (msdnet, CNN) [2]. If this trained network is then applied to one of the two tomograms, the random noise is completely removed from the tomographic images.

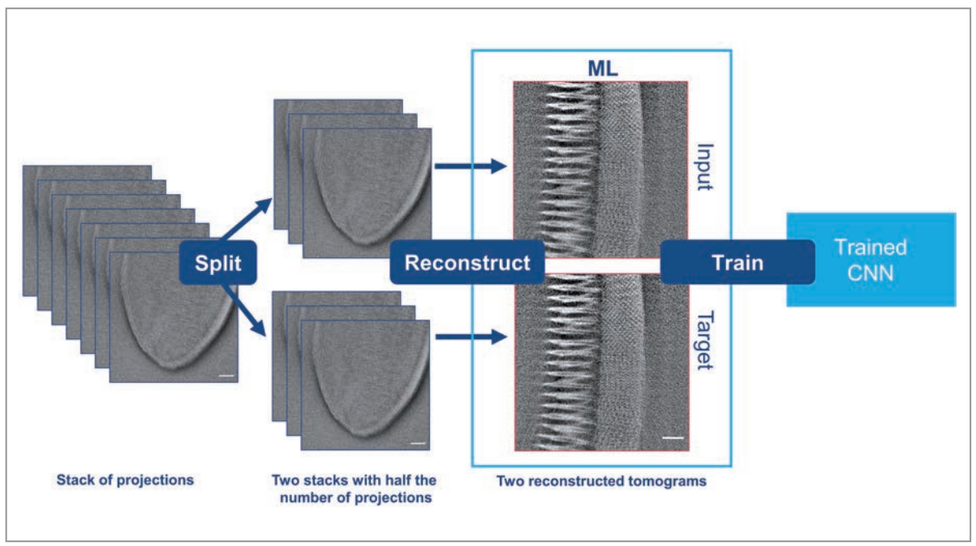

Figure 1

Machine learning denoising approach. A stack of projections is split into two stacks, each containing every other projection. Both stacks are reconstructed separately to gain two independent tomograms. One of the tomograms is then used as an input and the other one as a target for a neural network. The trained network can be applied to one of the two tomograms, yielding a noise-free image.

In this study, the efficiency of the self-supervised denoising ML approach is demonstrated on high-resolution nanotomographic data of a butterfly scale (Fig. 2), acquired using the TXM in Zernike phase contrast mode at the P05 Imaging Beamline. The surface of a butterfly wing is covered with small scales. Each of these scales has a fine periodic structure, diffracting the light in such a way that the scale appears in a certain colour. Depending on the sizes of these nanostructures, the scale appears in a different colour [4]. Due to the presented ML approach it was possible to visualise these photonic crystals in 3D, determining the size of the periodic structure to be in the range of 250 nm. Even differently oriented domains of the 3D lattice become visible (Fig. 2, lower right, indicated by arrows), which results in an average and angle-independent colour.

One advantage of this method is that the trained network can be applied to a range of similar samples measured with the same noise profile. This enables to denoise a whole set of tomographic scans with the same trained network. Since the network needs only half of the acquired projection images for denoising, the scan time can even be reduced, resulting in a higher time resolution. In particular, for *in situ* experiments, this approach is valuable: Here, the network can be trained on a previously recorded scan and applied on shorter scans which are acquired during the *in situ* experiment. Another advantage of this approach is that the ML filter can also be applied retrospectively on previously recorded data, where a sufficient number of projections was acquired. In summary, the ML approach proves to be a very powerful tool that outperforms conventional filters by eliminating noise without blurring relevant structural features, enabling efficient quantitative analysis in different scientific fields.

Author contact: Silja Flenner, silja.flenner@hereon.de
Imke Greving, imke.greving@hereon.de

References

1. S. Flenner, M. Storm, A. Kubec, E. Longo, F. Döring, D. M. Pelt, C. David, M. Müller, I. Greving, 'Pushing the temporal resolution in absorption and Zernike phase contrast nanotomography: Enabling fast in situ experiments', J. Synchrotron Radiat. 27, 1339–1346 (2020).
2. D. M. Pelt, J. A. Sethian, 'A mixed-scale dense convolutional neural network for image analysis', Proc. Natl. Acad. Sci. U.S.A. 115, 254–259 (2017).
3. A. A. Hendriksen, D. M. Pelt, K. J. Batenburg, 'Noise2Inverse: Self-Supervised Deep Convolutional Denoising for Tomography', IEEE Trans. Comput. Imaging 6, 1320–1335 (2020).
4. T. Starkey, P. Vukusic, 'Light manipulation principles in biological photonic systems', Nanophotonics 2, 289–307 (2013).

Original publication

'Machine learning denoising of high-resolution X-ray nanotomography data', Journal of Synchrotron Radiation 29, 230–238 (2022). DOI: 10.1107/S1600577521011139

Silja Flenner[1], Stefan Bruns[1], Elena Longo[1], Andrew J. Parnell[2], Kilian E. Stockhausen[3], Martin Müller[1] and Imke Greving[1]

1. Helmholtz-Zentrum Hereon, Geesthacht, Germany
2. University of Sheffield, Sheffield, United Kingdom
3. University Medical Center, Hamburg, Germany

Parallelising X-ray microscopy using multibeam ptychography

Utilising partial coherence to speed-up microscopy

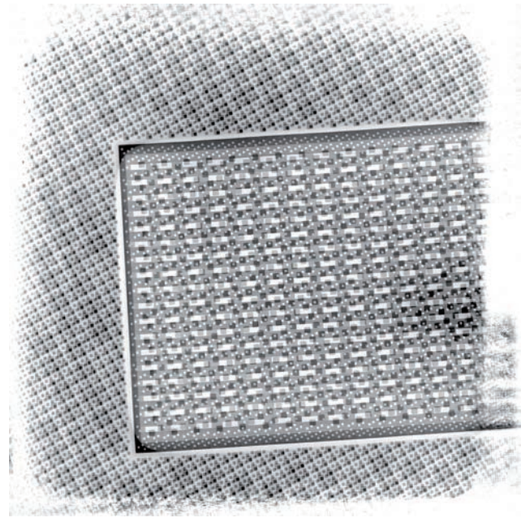

Figure 2
Multibeam ptychography of a microchip. The reconstructed area has a size of 100 × 100 µm².

X-ray microscopy has become an indispensable non-invasive tool for studying objects' internal structures in many science fields from chemistry, catalysis and material science to cultural heritage. With the development of coherent synchrotron radiation sources of the 3rd and 4th generations, ptychography experienced an explosive development and reached nanometre resolution. In practice, one has to find a compromise between the field of view, spatial resolution and acquisition time. Multibeam ptychography can overcome these limitations and look at large samples with a high resolution quickly by parallelising the acquisition using several parallel beams.

The highest resolution in X-ray microscopy is achieved with a scanning method called ptychography [1]. In this technique the sample is raster scanned through a confined beam, recording the far-field diffraction signal at each position. The attenuation and refraction inside the sample can be reconstructed with high resolution from these data. Ptychography has a broad field of application, including multiscale imaging, multimodal imaging and *in situ* and *operando* imaging. Nevertheless, for ptychography to work, only a coherent part of the X-ray beam can be used, e. g. by selecting a small fraction of the beam with narrow slits (Fig. 1 right). In this way, the major part of the beam is wasted. Due to the reduced flux, data accumulation is slow, the field of view is restricted or the spatial resolution is reduced.

Recent improvements in instrumentation and algorithm developments overcome these limitations and allow parallel illumination for ptychography. Using the revolutionising new 3D-printing technique based on two-photon absorption lithography [2], we created an array of lenses to irradiate the sample with several parallel beams (Fig. 1 left). This significantly speeds up the data acquisition, as the sample is scanned in parallel at several positions. The diffraction patterns on the detector overlap and need to be separated by the ptychographic algorithm.

To support the algorithm and improve the reconstructed images' quality, we individually distorted the different beams in a characteristic way by adding special phase plates to each lens. In this way, the individual beams were coded and illuminated the sample differently, resulting in distinctive, unique diffraction patterns that the ptychographic algorithm can separate more easily. This leads to a robust reconstruction of the object without any artefacts.

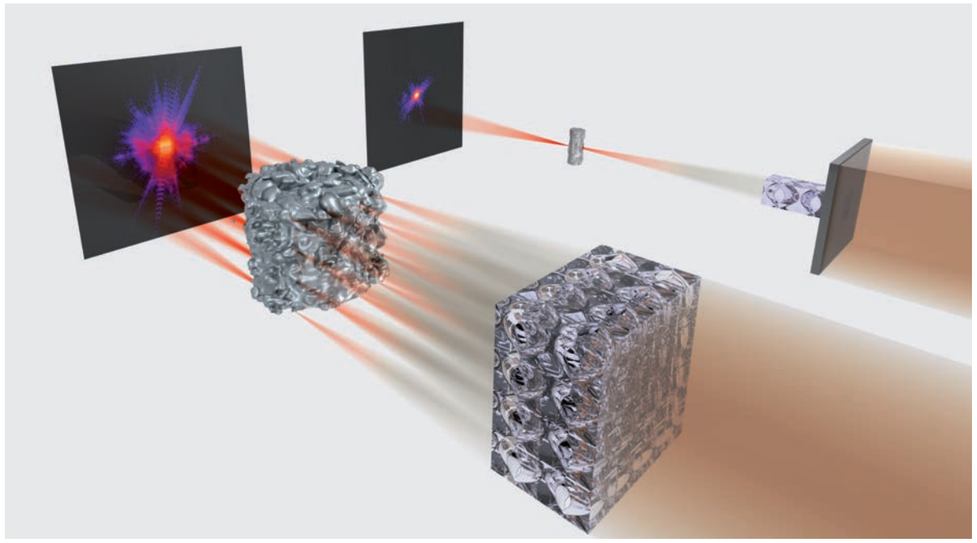

Figure 1
Comparison between state-of-the-art X-ray ptychography (right) and the coded multi-beam ptychography (left). In single beam ptychography, a slit cuts out a tiny fraction of a beam which limits the size of a sample, while with parallel illumination, signals from different parts of a large sample are mixed in the diffraction pattern.

This new method can be applied to fast imaging of a microchip. This sample is very challenging for parallel beam ptychography because of its repeating structures. Thus, separating signals from different areas on the chip is difficult. Using three parallel coded beams, we performed the scan with a field of view of 100 µm × 100 µm and reconstructed it without any noticeable artefacts (Fig. 2).

In this case, parallel illumination with three beams allowed us to extend the field of view on the microchip by almost a factor of three, efficiently using a larger fraction of the beam. Multibeam ptychography with coded beams extends the applicability of ptychography, alleviating the restrictions on field of view, resolution and acquisition time. In terms of multiscale imaging, it extends the excellent spatial resolution achieved with ptychography to larger samples beyond the currently feasible limit. This can be applied, for example, to study pore networks in large solid catalyst bodies on the meso- and macroscale in a single acquisition and in a highly representative manner or to study solid hierarchical samples, e. g. as a microchip.

In terms of chemical *in situ* and *operando* imaging, multi-beam ptychography retains the powerful characterisation potential in recovering the quantitative electron density of the sample but extends this to larger and more representative length scales or relaxes the timeframe in which chemical or structural changes induced in the catalyst can be meaningfully observed. This can potentially be used to study catalyst stability and deactivation processes, including carbon deposition, catalyst poisoning by unwanted elemental deposition or pore structure collapse.

Moreover, the Röntgen-Ångström Cluster, a German-Swedish research collaboration in structural biology and materials science, has supported further development of multibeam ptychography for application to *in situ* imaging of catalysts and funded the project: 'HASTE: High-throughput multibeam ptychography supporting catalytic research'.

Author contact: Mikhail Lyubomirskiy, mikhail.lyubomirskiy@desy.de

References

1. F. Pfeiffer, 'X-ray ptychography', Nat. Photon. 12, 9–17 (2018).
2. M. Lyubomirskiy et al., 'Ptychographic characterisation of polymer compound refractive lenses manufactured by additive technology', Opt. Express 27, 8639-8650 (2019).

Original publication

'Multi-beam X-ray ptychography using coded probes for rapid non-destructive high-resolution imaging of extended samples', Scientific Reports, 12, 1-9 (2022).
DOI: 10.1038/s41598-022-09466-5

Mikhail Lyubomirskiy[1], Felix Wittwer[1,2], Maik Kahnt[3], Frieder Koch[4,5], Adam Kubec[4,6], Ken Vidar Falch[1], Jan Garrevoet[1], Martin Seyrich[1], Christian David[4] and Christian G. Schroer[1,7,8]

1. Centre for X-ray and Nano Science (CXNS), DESY, Hamburg, Germany
2. NERSC, Lawrence Berkeley National Laboratory, Berkeley, USA
3. MAX IV Laboratory, Lund University, Lund, Sweden
4. Paul-Scherrer-Institut (PSI), Villigen, Switzerland
5. GSI Helmholtzzentrum für Schwerionenforschung GmbH, Darmstadt, Germany
6. XRnanotech GmbH, Villigen, Switzerland
7. Fachbereich Physik, Universität Hamburg, Hamburg, Germany
8. Helmholtz Imaging Platform, Deutsches Elektronen-Synchrotron DESY, Hamburg, Germany

Compact, energy-scalable multi-pass cells

Exploring novel regimes for post-compression of high-energy laser pulses towards ultrashort pulse durations.

High peak power, high repetition rate and ultrafast light sources are becoming increasingly important in many scientific fields. They are used, e.g. as drivers for harmonic generation sources, laser-plasma accelerators, for free-electron laser pump-probe studies and many more. However, lasers typically cannot directly provide high average and high peak power simultaneously. Thus, post-compression schemes for temporal compression of ultrashort laser pulses become increasingly attractive, enabling the generation of ultrafast, high-peak power light sources operating at high repetition rates. Common post-compression techniques suffer from the lack of scalability towards high pulse energies. Here we present a new technique for pulse energy scaling of multi-pass cell-based post compression. We numerically demonstrate post-compression of up to 1 Joule pulses in a table-top setup, prospectively achieving multiple terawatts of peak power.

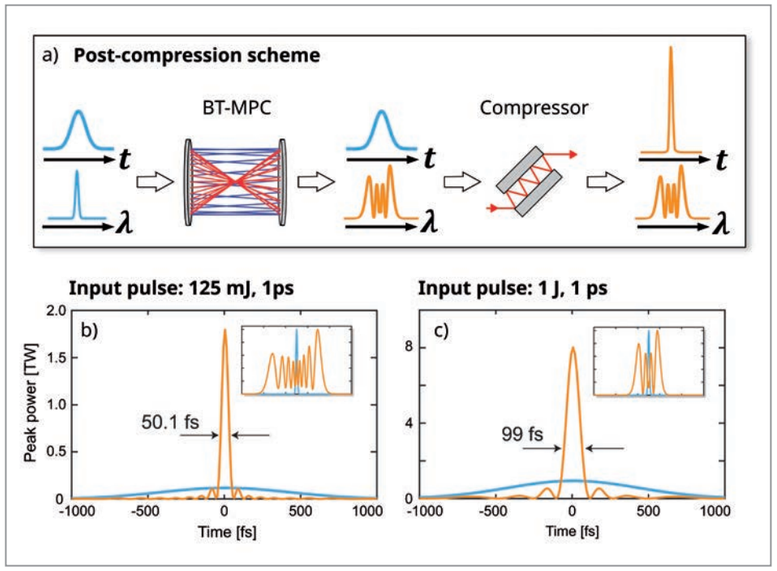

Figure 2

Spectral broadening scheme and results of our numerical study. a) General, simplified MPC post-compression setup consisting of a bow tie MPC used for spectral broadening followed by a compressor. b) Numerical results for input pulses with 125 mJ pulse energy and 1 ps pulse duration. c) Numerical results for pulses with 1 J and 1 ps. The main graphs show the input pulse (blue) and the resulting compressed pulse (orange). The insets show the corresponding initial spectrum (blue) and the spectrally broadened spectrum (orange).

The development of lasers has been an extraordinarily active research field for more than 60 years. Of particular interest for scientific applications are ultrafast coherent light sources, enabling the probing of ultrafast processes occurring in nature. These applications typically require ultrashort femtosecond laser pulses, high pulse energies and high repetition rates; a combination of parameters which is not easy to achieve. For example, ytterbium-based laser systems are becoming increasingly attractive due to their scalability in average power up to the kilowatt range. However, their pulse durations are typically limited to the 100s of fs or even 1 ps range due to the limited gain-bandwidth of the laser medium. The problem of limited gain-bandwidth can, however, be circumvented by employing external spectral-broadening and post-compression techniques.

In recent years, Herriott-type multi-pass cell (MPC) based post-compression has been established as a flexible, efficient and rather simple technique for post-compression of laser pulses. Using bulk materials or gases as the nonlinear medium, pulses of a few µJ up to more than 100 mJ have been successfully post-compressed [1], with compression factors up to about 40 in a single stage [2]. One of the main advantages lies in the scalability of this method: For example, by simply scaling up the size of the setup, higher pulse energies can be coupled into the MPC without damaging the mirror coatings. However, scaling up an MPC setup in size does come with a price: at high pulse energies, the size of the setup can easily become unpractical. As an example, 10 mJ pulses at 1030 nm require an MPC length of about 2 m length. Scaling this up to the 100 mJ regime results in MPC lengths of 10s of metres.

Thus, there is a need for compact MPCs which are pulse energy scalable without the consequence of enormous setup sizes. Our aim here is to explore the possibilities of extending MPC post-compression to novel pulse energy regimes.

MPCs are fundamentally similar to optical cavities but featuring a spatial separation of multiple optical passes. Thus, possible MPC configurations can be characterised by so-called stability diagrams, analogous to optical cavities

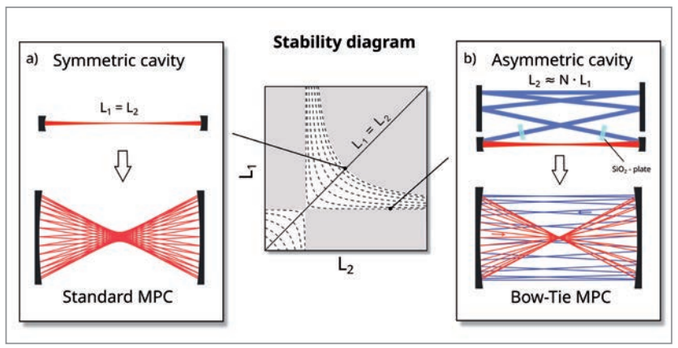

Figure 1

Stability diagram and MPC configurations. The plot in the middle shows the stability regions of optical cavities and MPCs as a function of the optical propagation lengths L_1 and L_2, i.e. the optical path lengths between focusing mirrors. The stable regions, where cavity modes can be formed, are denoted in white, the unstable regions in grey. The dashed lines indicate typical example parameter regions, ensuring input-to-output imaging conditions. a) Symmetric cavity and the corresponding standard MPC configuration. b) Asymmetric cavity and the corresponding bow tie MPC configuration. The positions of the SiO_2 plates, which we use in our simulations as nonlinear media, are indicated in light blue.

(Fig. 1). Typically, MPCs are operated at the stability edge, close to the so-called 4f-imaging condition (Fig. 1a). These standard MPCs are symmetric, meaning that the propagation length in one direction L_1 has the same length as in the reverse direction L_2. If we allow for asymmetric cavity designs, a whole new parameter space opens up. One very promising configuration is shown in Fig. 1b. In this configuration L_2 is larger than L_1, meaning that the propagation in one direction is longer than in the opposite direction. We call it the bow tie MPC. But why do we actually need such asymmetric cavities?

In the configuration shown at Fig. 1b we have a nearly collimated beam in the long arm L_2, rendering the intensity almost constant over the whole propagation length. Using this to our advantage, we can send the beam onto additional flat mirrors in a V-shaped arrangement (Fig. 1b) without the risk of damaging the mirrors. The length L_2 is a parameter we can freely choose and by increasing L_2 to a suitable length, the total cavity length increases and thus the mode size of the beam. This leads to a higher pulse-energy acceptance of the MPC.

In our numerical study, we choose two 1 mm thick SiO_2 plates as nonlinear media used for spectral broadening via self-phase modulation, placed symmetrically in the long MPC arm (Fig. 1b). The simulations of the system show a promising spectral broadening of 125 mJ pulses in a compact 2-metre-long setup (Fig. 2b). Starting from a 1 ps Fourier-transform-limited (FTL) pulse, the output spectrum supports 50 fs FTL. While keeping the setup at 2 m length and increasing the folding ratio, we conduct further numerical simulations for 1 J pulses. Here, the output spectrum supports 100 fs FTL (Fig. 2c). A typical MPC post-compression scheme including an MPC followed by a compressor is shown in Fig. 2a.

Our work shows very promising results employing a novel energy-scalable MPC scheme. Pulse energy up-scaling of MPC post-compression towards the terawatt regime will enable a whole new realm of scientific applications, providing a route to high-field science at multi-kHz repetition rates as demanded, e.g. by laser-driven particle acceleration. The here discussed bow tie MPC may not be the only scalable MPC scheme, and likely there are other configurations to be discovered.

Author contact: Arthur Schönberg, arthur.schoenberg@desy.de

References

1. A.-L. Viotti, M. Seidel, E. Escoto, S. Rajhans, W. P. Leemans, I. Hartl and C. M. Heyl, 'Multi-pass cells for post-compression of ultrashort laser pulses,' Optica 9, 197-216 (2022).
2. P. Balla, A. B. Wahid, I. Sytcevich, C. Guo, A.-L. Viotti, L. Silletti, A. Cartella, S. Alisauskas, H. Tavakol, U. Grosse-Wortmann, A. Schönberg, M. Seidel, A. Trabattoni, B. Manschwetus, T. Lang, F. Calegari, A. Couairon, A. L'Huillier, C. L. Arnold, I. Hartl and C. M. Heyl, 'Postcompression of picosecond pulses into the few-cycle regime,' Opt. Lett. 45, 2572-2575 (2020).

Original publication

'High-energy bow tie multi-pass cells for nonlinear spectral broadening applications', Journal of Physics: Photonics 4, 014002 (2022). DOI: 10.1088/2515-7647/ac483a

Christoph M. Heyl[1,2,3], Marcus Seidel[1], Esmerando Escoto[1], Arthur Schönberg[1], Stefanos Carlström[4,5], Gunnar Arisholm[6], Tino Lang[1] and Ingmar Hartl[1]

1. Deutsches Elektronen-Synchrotron DESY, Hamburg, Germany
2. Helmholtz-Institute Jena, Jena, Germany
3. GSI Helmholtzzentrum für Schwerionenforschung GmbH, Darmstadt, Germany
4. Department of Physics, Lund University, Lund, Sweden
5. Max-Born-Institute, Berlin, Germany
6. Norwegian Defence Research Establishment (FFI), Kjeller, Norway

Tailoring XUV attosecond pulses

Spectral and temporal shapes of isolated attosecond pulses controlled by parametric waveform synthesis

The fastest electronic dynamics occurring in matter can be revealed by probing with attosecond pulses that are flashes of XUV or soft X-ray radiation with duration in the 10^{-18} second range. New developments in the generation of such attosecond pulses via high-harmonic generation (HHG) come through parametric waveform synthesis, a technique that allows to tailor highly energetic light pulses with sub-cycle duration. We demonstrated that central energy, spectral bandwidth/shape and temporal duration of attosecond pulses can be controlled by shaping the optical waveform that drives the HHG process. These results promise to expand the experimental capabilities in attosecond science.

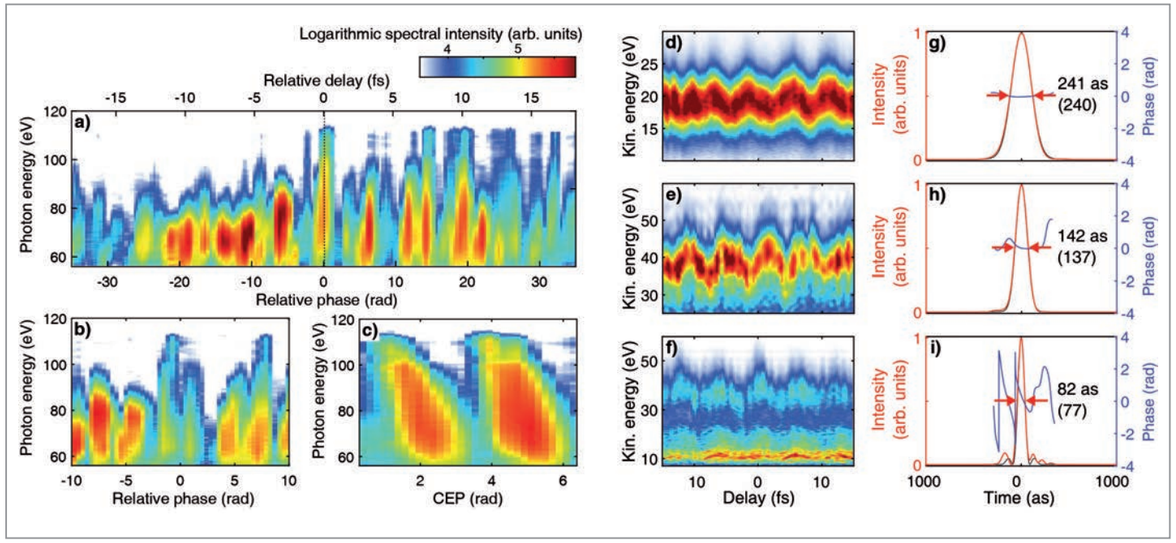

Figure 2

a) HHG emission spectra from argon during a scan of the RP between the NIR and IR pulses. b) Detailed scan around the zero position with the CEP shifted by 180°. c) CEP scan with RP fixed at 0.1 rad. d,e,f) Attosecond streaking traces for three generated pulses from neon. g,h,i) Reconstructed attosecond pulse duration (red/black) and temporal phase (blue). Figure adapted from original publication licensed under CC-BY 4.0.

The generation of attosecond-duration flashes of light is undoubtedly a milestone for the development of time-resolved techniques with sufficient resolution to observe charge dynamics occurring in atoms, molecules and solids on their natural timescale. The shortest man-made light pulses, lasting only few tens of attoseconds, are generated by laser pulses interacting with matter in the strong-field regime (>10 TW/cm^2). This process, called high-harmonic generation (HHG), starts with the tunnel ionisation of a valence electron. This electron, after acceleration in the alternating laser field, recombines with the original atom and emits an attosecond-long flash of coherent radiation.

Depending on the parameters of the driving laser, the attosecond pulses are generated in the XUV or soft X-ray region.

Currently, there are two linked challenges to further develop attosecond sources based on HHG: increasing their photon flux and improving their spectral tunability. With the recently pioneered parallel parametric waveform synthesiser [1], we were able to address the tunability as demonstrated in the original publication. Due to the nature of the HHG process, an ideal laser source for the generation of intense isolated attosecond pulses should provide pulses with only one or even less oscillation of the electric field. Such short pulses in time require a spectral bandwidth significantly exceeding one octave and are often called optical waveforms due to their non-sinusoidal features. Few-cycle pulses over different spectral regions can be generated by using optical parametric amplifiers and coherently combined to yield a multi-octave spanning optical waveform. Such a synthesis scheme was realised with two carrier-envelope-phase (CEP) stable pulses that, once combined, cover an overall bandwidth spanning from 650 nm to 2200 nm (1.7 octaves) with a pulse energy of ~500 µJ (Fig. 1). This synthesis technique allows to modify the overall CEP and the relative phase (RP) between the combined pulses to shape the resulting waveform (Fig. 1 top). With this approach we were able to create a waveform below 3 fs in duration (FWHM) at a central wavelength of 1.4 µm. This corresponds to just 0.6 optical cycles, realising so-called sub-cycle duration.

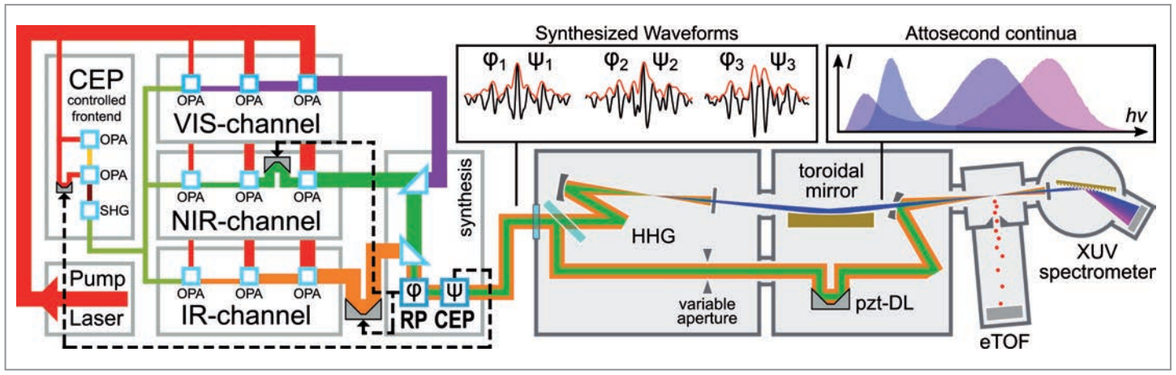

Figure 1

Left: Setup of the synthesiser currently consisting of two spectral (NIR and IR) channels that are coherently combined. With a phase meter at the point of combination, we can control the synthesis parameters (CEP and RP). Right: In the attosecond beamline, the synthesised pulses drive the HH-source while an electron time-of-flight spectrometer and an XUV spectrometer are used to perform attosecond streaking to characterise the isolated pulses and the optical waveform. (Figure adapted from original publication licensed under CC-BY 4.0.)

The emission of HHG from such a pulse is highly dependent on the exact shape of the driving waveform. We observed a significant spectral tunability by performing synthesis scans during which we varied either the CEP of the synthesised pulse or the RP between the two sub-pulses (Fig. 2a–c). In argon as source gas, the generated attosecond pulses can be tuned to cover the spectral region of 35–110 eV with an isolated pulse energy up to 500 pJ. The synthesis setting allows us to generate either narrowband or broadband attosecond pulses. When the source gas is switched to neon, photon energies up to 200 eV were recorded exhibiting a similar tunability. Selected isolated attosecond pulses were temporally characterised by the attosecond streaking technique (Fig. 2d–f) and we retrieved pulse durations tunable between 80 as and 240 as (Fig. 2g–i).

In conclusion, we demonstrated wide tunability of attosecond pulse parameters obtained by HHG. The tunability extends to the centre wavelength, bandwidth and temporal profile of isolated attosecond pulses. This is achieved by the synthesis of pulses generated by optical parametric amplifiers. This represents a significant advance in attosecond source technology since conventional sources do not offer such high degree of tunability that can be exploited in sophisticated attosecond science experiments.

Author contact: Roland E. Mainz, roland.mainz@desy.de

Reference

1. **G. M. Rossi et al., 'Sub-cycle millijoule-level parametric waveform synthesizer for attosecond science', Nat. Photon. 14, 629–635 (2020).**

Original publication

'Strong-field coherent control of isolated attosecond pulse generation', Nature Communications 12, 6641 (2021).
DOI: 10.1038/s41467-021-26772-0

Yudong Yang[1,2], Roland E. Mainz[1,2], Giulio Maria Rossi[1,2], Fabian Scheiba[1,2], Miguel A. Silva-Toledo[1,2], Phillip D. Keathley[3], Giovanni Cirmi[1,2] and Franz X. Kärtner[1,2]

1. Center for Free-Electron Laser Science (CFEL), DESY, Hamburg, Germany
2. Physics Department and The Hamburg Centre for Ultrafast Imaging (CUI), Universität Hamburg, Hamburg, Germany
3. Research Laboratory of Electronics, Massachusetts Institute of Technology, Cambridge, MA, USA

Light Sources and User Infrastructures

FLASH – on its way towards FLASH2020+

Reopening with new features in stock

At FLASH, the FLASH2020+ upgrade programme is in full swing now. For the first long upgrade shutdown, from November 2021 until mid of August 2022, the superconducting linear accelerator of FLASH, normally operating at 2K, had been warmed up to room temperature and is now cold again. FLASH restarted operation with a lot of new features which are expected to further improve the free-electron laser (FEL) performance for our scientific users. Despite the present situation in the world, also causing a shortness in supplies of many technical components, the shutdown was successfully completed, and FLASH was lasing again on 18 October 2022, only ten days later than originally planned in 2021. Thanks to a highly motivated team, performing all the maintenance and refurbishment work at the accelerator and installing many new components within the FLASH2020+ upgrade programme, everything was implemented almost on time. The work completed during the shutdown brought many improvements for the accelerator operation in general and the photon science users in particular. The main ones are listed here:

A machine energy upgrade by installing two modern superconducting accelerator modules with a higher acceleration gradient replacing two old ones (Fig. 1). This will result in about 100 MeV higher maximum electron energy and hence widen the range of FEL tunability at the shortest wavelengths. The goal is to substantially pass the carbon K-absorption edge at 4.4 nm and to get closer to the nitrogen edge at 3 nm wavelength, or even reach this edge at FLASH2. This also particularly extends the range of the FEL harmonics in order to fully cover all the L-edges of the 3d transition metals up to nickel.

Figure 1

One of the two new superconducting accelerator modules (in yellow) installed in the FLASH tunnel replacing two old ones.

Figure 2

Laser heater undulator (yellow circle) and a large box with a laser table for optical components (right of it on green supports) to couple the laser pulses into the electron beamline. In the background at right, the yellow first accelerating module in the FLASH tunnel is visible.

End of October 2022, about four weeks after the start-up of the accelerator, the newly installed modules already operated at their design gradient, boosting the electron beam by additional 100 MeV. This proved to be essential for the first user experiment operating at a fundamental of 3.8 nm at FLASH2 which required an energy of 1280 MeV and thus surpassed the former FLASH maximum (already) by 30 MeV. With some further conditioning of the other five accelerator modules, the expected 1350 MeV maximum electron energy will soon be reached. This additional headroom in energy is also expected to result in about one order of magnitude more FEL intensity at the very short wavelengths (below about 5 nm) on the FLASH2 side and a similar gain in the corresponding harmonics.

In the injector area, or more precisely shortly behind the first accelerator module, a so-called laser heater [1] has been installed (Fig. 2). Intense laser pulses are superimposed with the electron bunches and transfer energy onto the electrons, while these are travelling through an undulator. In doing so, the laser heater smears out the energy distribution of the electrons. Increasing the energy spread of the electrons helps to counteract microbunching instabilities which otherwise would be detrimental, since they lead to a breakup of the charge distribution in the bunch and spoil the FEL amplification process. While keeping the smooth current profile of the electron bunches is also beneficial for the presently used SASE process, the laser heater is of particular importance for the future implementation of external seeding. External seeding – planned to be installed in the next FLASH2020+ upgrade shutdown in 2024/25 – is intended to imprint periodic current modulations on the ideally smooth electron bunch. The early installation of the laser heater provides the opportunity to study beam dynamics and suppression of microbunching instabilities in the machine as of now.

Along with new bunch compressors in the injector area, fast orbit kickers were installed as well. The bunch compressors will enable a more flexible and improved bunching scheme – an advantage for future external seeding and already now offering more options to compress the electron bunches. The fast orbit kickers will allow to precisely steer all electron bunches within a bunch train in order to make them all travel along an almost identical path. That way, intra-train FEL pulse fluctuations in photon energy, intensity and pointing can be substantially reduced.

A set of two new drive lasers for the photocathode electron gun was installed in a new air-conditioned laser building and will be commissioned in spring 2023. The laser systems (Fig. 3) were developed in-house, using a front-end, which is very similar to the one developed for the European XFEL [2], and commercial Yb:YAG gain blocks. Each of the two identical lasers allows flexible control of parameters, such as UV pulse duration, pulse energy, transverse beam size or intra-burst repetition rate. In combination, the systems can provide two individual burst segments, serving the FLASH1 and FLASH2 FEL beamline, respectively, with adjustable segment length and gap in between. The total

Figure 3

Front-end and power amplifier stages of the new photocathode lasers during installation in the laser laboratory adjacent to the FLASH electron gun. In the background, the vacuum beamline tube for transporting the laser pulses towards the electron gun is visible.

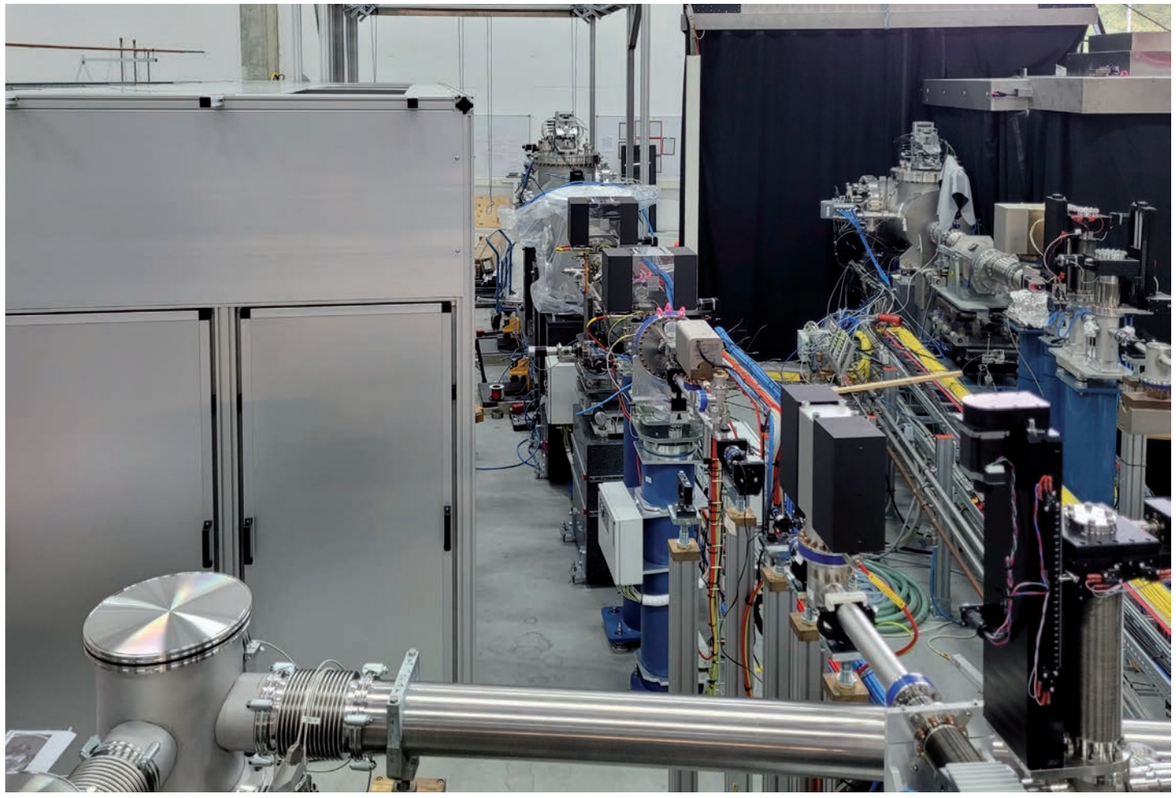

Figure 4

View of the rear section of the new FL23 pulse-length preserving monochromator beamline at FLASH (running from bottom right to top centre), with the frame of the new laser hutch for user experiments in the background and the metal hutch for modular optical delivery (MOD) of the optical laser pulses in the foreground (left).

length of both bursts combined, including gap, can be up to 1 ms. Once the new lasers are fully commissioned, the presently used three different photocathode laser systems will be kept as spares as long as they are operational. It should be noted that these lasers have been in continuous operation for more than ten years.

With all these new features, FLASH will deliver an FEL performance which is more robust, extended towards the short wavelength end, and yields higher intensities at the short wavelengths and in the harmonics. One major item, the installation of the Apple III-type afterburner undulator at the FLASH2 side, had to be postponed into the second half of 2023. Some of its components could not be delivered in time to install it during the recent shutdown. This undulator is supposed to enhance the third harmonic and provide variable polarisation of the FEL. During the shutdown, the last regular (planar) FLASH2 undulator has already been moved to the beginning of the undulator line. At its former position, the beamline vacuum chamber has been exchanged with the new filigree one with 6 mm inner diameter required for the afterburner. Hence, everything is ready for mounting the afterburner in 2023. During the two weeks which are required for the installation in the FLASH2 tunnel, FLASH1 can still be operated for users.

In the experimental hall 'Kai Siegbahn', the new FLASH2 open-port beamline FL23 with its pulse-length preserving monochromator is also nearing completion (Fig. 4). The gratings for both monochromator stages were delivered by the end of November 2022, have been installed and are pre-aligned at the time of writing. After their mounting, the beamline is expected to see its first light in early 2023. In parallel, the FLASH2 optical laser connection to FL23 is being realised. Providing small FEL spectral bandwidth and ultrashort pulses, the new beamline will hence soon complement the other two FLASH2 user beamlines, namely FL24 with its open port and FL26 with the reaction microscope (REMI) end station. Once fully operational, the FL23 beamline with its scientific opportunities will then allow to reduce the load at FL24 and also at the FLASH1 monochromator beamline PG2, which at present are the two mostly booked beamlines at FLASH, hosting about 50-60 % of all user experiments.

The first two FLASH2 beamlines, FL24 and FL26, which started operation in 2016, have been evaluated by external panels in October 2022:
FL24 has been in full swing for a few years, with more than twenty user publications plus numerous in-house publications by now. The panel emphasised the unique beamline capabilities, such as transporting high photon energies at FLASH2, including the FEL harmonics, providing a variable micro-focus and an open port, in combination with FLASH2 features such as NEXAFS-like energy scans and two-colour FEL schemes, owing to the variable gap undulators. FL24 is considered to be the FLASH2 beamline that will take full advantage of the FLASH2020+ upgrades. This is due to the fact that science at FL24 profits from both, the energy upgrade and the push for using the harmonics at variable polarisation with the coming afterburner undulator.
FL26 with the REMI end station is still ramping up features. The combination of down to sub-10 fs extreme-ultraviolet (XUV) FEL pulses with a strong-field high-harmonic generation (HHG) laser source in the vacuum-ultraviolet (VUV) and a recently installed setup for transient absorption spectroscopy by the colleagues from MPIK Heidelberg (see last years' annual reports) was considered by the panel to be unique in the world. It was recommended that the potential of this instrumentation for the AMO and femtochemistry community should be developed further, in particular with respect to the best temporal resolution for pump-probe experiments.

In the year 2023, FLASH will be fully devoted to user experiments again. Instead of the usual 26 to 27 weeks (~4500 hours) of user operation, it is planned to provide even 30 weeks for exciting new science. In parallel, the next big FLASH2020+ upgrade shutdown, starting in the middle of 2024, is being prepared in all its technical aspects. During this shutdown, FLASH1 will be converted into an externally seeded FEL at high repetition rate, including the installation of new variable gap undulators, a new laser system for seeding and new state-of-the-art FEL photon diagnostics.

Contact (FLASH and FLASH2020+):
Rolf Treusch, rolf.treusch@desy.de
Martin Beye, martin.beye@desy.de

References

1. Ch. Gerth et al., 'Layout of the laser heater for FLASH2020+', Proceedings IPAC2021.
2. L. Winkelmann et al., 'Compact Photo-Injector and Laser-Heater Drive Laser for the European X-ray Free Electron Laser Facility', Proceedings CLEO 2018.
3. L. Poletto et al., 'Double-grating monochromatic beamline with ultrafast response for FLASH2 at DESY', J. Synchrotron. Rad. 25, 131-137 (2018).

PETRA III

Last two PETRA III beamlines in planning and automation project funded

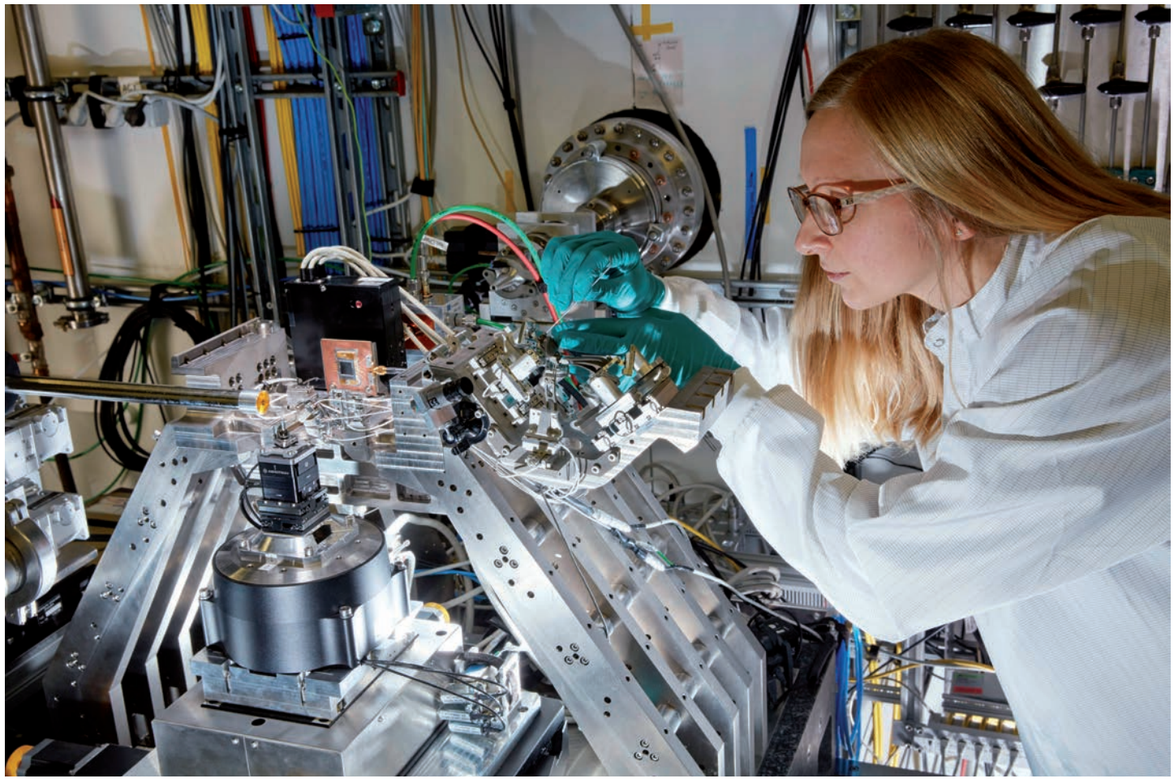

Figure 1

Scientist setting up an experiment at the PETRA III beamline P06 equipped with specially designed nanometer precision positioning mechanics and nano-focusing optics.

During the year 2022, the user operation of PETRA III was still affected by the worldwide SARS-CoV-2 pandemic although international and national restrictions concerning travel and quarantine regulations were lifted to a great extent. In the course of the year, the user access to the beamlines and laboratories basically went back to regular operation and since June 2022 the number of participants for experiments was no longer limited. However, users were still requested to provide a negative antigen test result before starting their experiment and some beamtimes had to be cancelled or were carried out using the mail-in and/or remote options due to infections of the beamline personnel or the users. Experiments within the India@DESY cooperation have been supported by postdoctoral researchers from India permanently located at PETRA III since mid of 2021. This initiative led to a successful continuation of the programme although users from India could not travel as much as before the pandemic and requested the mail-in option for many experiments.

More than 3400 individual users, including mail-in and remote access, performed experiments at PETRA III beamlines, which are even more than before the pandemic in 2019. As usual, the operation time of PETRA III was split in two run periods: one from mid of February until mid of July and a second from mid of August until end of December 2022.

PETRA III – machine operation

During the first run, 2589 hours of machine operation were provided for users at 25 beamlines: P01–P14 in the PETRA III experimental hall 'Max von Laue', P21.1–P24 in the hall 'Ada Yonath', P61–P65 in the hall 'Paul Peter Ewald' and at P66 in building 47K. In total, 4196 hours of user X-ray beamtime were provided at PETRA III (as of 11 November 2022), a total of 4896 hours is envisaged for the entire year which corresponds to about 85000 hours for user proposals.

In 2022, the PETRA III machine has been performing very well with an availability of 98,2% and a mean time between failures of 56 hours (as of 17 November 2022). This is a good result also in comparison to the performance of recent years. The main reasons for the down time in descending order of total down time were a transformer failure, radio frequency issues and external power glitches from the Hamburg power net.

As usual, two different bunch filling modes were offered in the PETRA III storage ring: a 'timing' mode for time resolved experiments with 40 bunches and a 'multi bunch' mode with 480 bunches, both with approximately the same share. This bunch mode distribution has proven to be an optimal scenario to provide a maximum number of 'timing' mode shifts while minimising the radioactive activation of ring components as well as radiation damage of undulators.

PETRA III – new beamlines and endstations in design and automation project funded

Two more new beamlines P25 and P63 are in preparation at the last two remaining slots in the PETRA III experimental halls 'Ada Yonath' and 'Paul Peter Ewald', respectively. The vacuum chambers for the undulators and the front-end hardware for these two beamlines are already installed, and the beamlines will become operational in the next two to three years.

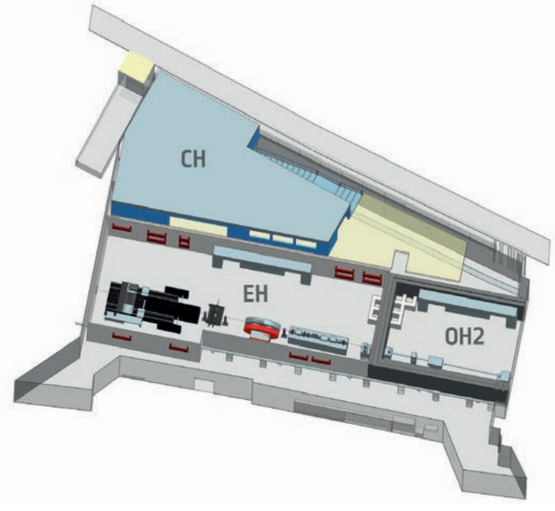

Figure 2

Drawing of the PETRA III beamline P25 design including the control hutch on the 1st floor (CH), the white beam test hutch (OH2) and the experimental hutch (EH) including the automatised powder diffraction station and the imaging station.

Beamline P25 is a cooperation project of PETRA III and the group for Innovation and Technology Transfer (ITT) at DESY, with main funding from ITT. It will be serving customers from industry and academic partners with imaging and powder diffraction applications located in the experimental hutch for monochromatic X-ray beams (EH in Fig. 2). The powder diffraction end station will be designed for fully automated user operation and is expected to serve many industrial clients, e.g. from pharmaceutical industry using the mail-in option. The imaging end station will provide element-specific X-ray fluorescence microscopy and focus on biomedical applications in collaboration with the Medical Center Hamburg-Eppendorf (UKE). In addition, an end station for white and pink beam applications will be constructed in a separate hutch. Among others, this hutch will be used to test and commission components related to PETRA IV. The hutch design has been finished in 2022 (see Fig. 2), and after completion of the call for tender the hutches are envisaged to be built in the summer shutdown in 2023. The final design of the instruments is ongoing and installation can start in late summer of 2023. Beamline operation is planned to start in early 2024.

The plans for beamline P63 at PETRA III became more concrete in 2022. After shifting the shutdown to upgrade PETRA III to PETRA IV by one year to 2027-2028 and realising that the expected beam path in the experimental hutch of P63 at PETRA IV matches the beam path at PETRA III, it was decided to start operation of this beamline still at PETRA III well before the shutdown for the upgrade. Beamline P63 is mainly funded by the Max-Planck-Gesellschaft and planned in very close cooperation with the Fritz-Haber-Institut Berlin and the Max Planck Institute for Chemical Energy Conversion in Mühlheim, which in turn will be granted priority access for a large part of the beamtime provided at P63. It will be dedicated to combined XAS/SAXS/powder diffraction studies and partially adds to XAS capabilities already available at the highly requested XAS beamlines P64 and P65. First components like specialised high performance detectors

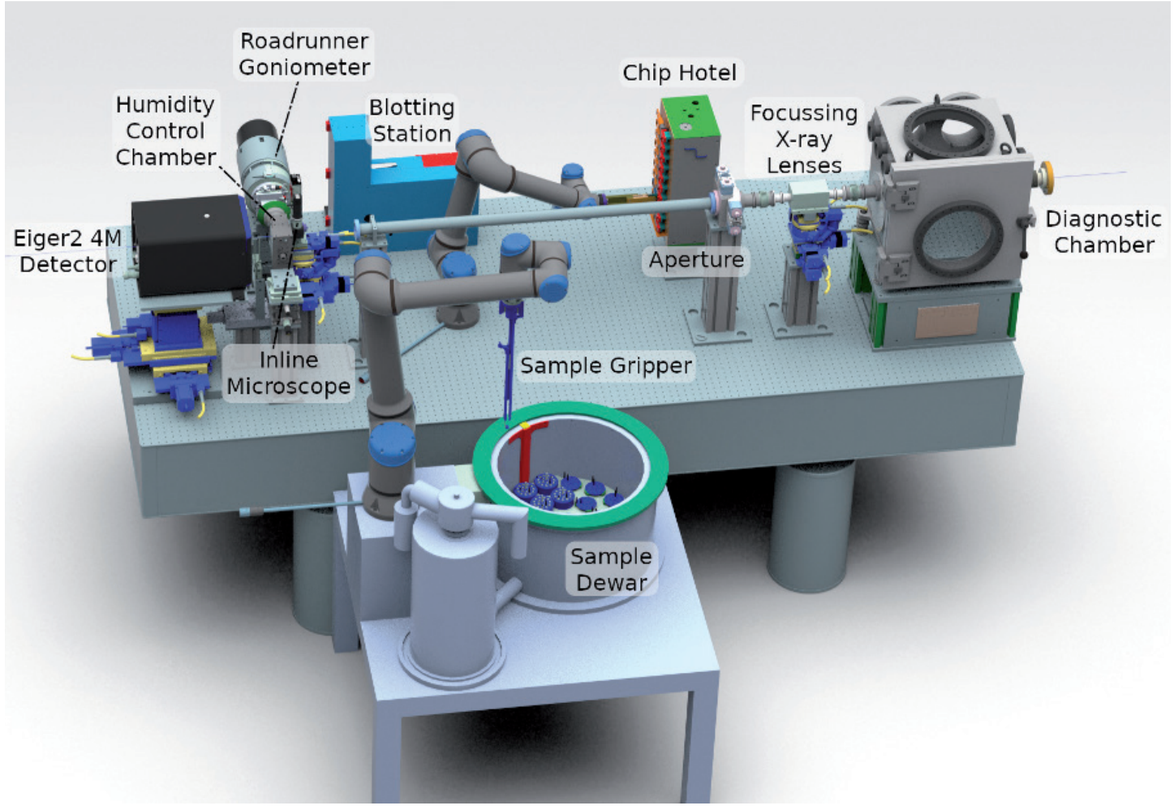

Figure 3

Drawing of the envisaged High-throughput Pharmaceutical X-ray screening' (HiPhaX) setup at the PETRA III beamline P09.

have already been delivered, the design of the experimental hutch is nearly finalised and construction of the beamline is expected in 2024.

In 2023, two new instruments at beamlines P09 and P23 are about to start user operation.

Early in 2022, the setup of a new instrument for 'High-throughput Pharmaceutical X-ray screening' (HiPhaX) at the beamline P09 started. Within the framework of structure-based drug design the X-ray-based structure analysis of proteins plays an important role. The goal of HiPhax is to fully automise the measurements using robotics and artificial intelligence (AI)-based decision processes. In combination with new sample holders, which can host hundreds to thousands of samples, a daily number of scanned samples of about 1000 is envisaged. Furthermore, a newly developed setup at HiPhax (see Fig. 3), which prevents samples from dry-out, will allow to perform measurements at room temperature instead of very low temperatures. During two commissioning campaigns in summer 2022, a roadrunner-goniometer was successfully brought into operation. In November 2022, two screening projects in cooperation with the Bernhard-Nocht-Institut für Tropenmedizin in Hamburg and the Universität Hamburg were successfully performed. In 2023, e.g. on the endonuclease of the Lassa virus, HiPhaX will be upgraded to perform low temperature measurements, and a cryogenic sample dewar will allow storage of about 800 samples at a time (see Fig. 3). After that, the instrument is foreseen to officially serve academic and industrial users.

The operational start of the HIKA end station for hierarchical imaging planned in cooperation with the Karlsruhe Institute of Technology at PETRA III beamline P23 (see last years' report) originally planned for 2022 has been delayed due to technical issues concerning the control hutch installation. First beam and user operation are now expected for early 2023.

In summer 2022, a lift for heavy equipment at P66 ('Superlumi') was installed (Fig. 4). With this final installation, the beamline became fully and efficiently operational as, e.g. the large helium dewars needed for many experiments can now be transported into the experimental hutch without major effort.

Together with partners from the Helmholtz-Zentrum Dresden-Rossendorf, Helmholtz-Zentrum Berlin and the Karlsruhe Institute of Technology, DESY successfully applied for Helmholtz funding for a demonstrator beamline focusing on automation of complex *operando* electrochemical studies, e.g. in catalysis. The 3-year project will start in 2023 and includes automation and remote control of the beamline but also optimisation of the chemical processes of *operando* studies supported by online analysis using AI. In the frame of this project, the PETRA III beamline P65 for X-ray absorption spectroscopy will be upgraded. Besides some new instrumentation the main focus of the project lies on developing new control and analysis software and the AI code.

PETRA III – new beamtime access schemes

Two additional routes for beamtime application have been implemented in 2022. A call for targeted challenge-driven proposals (TCDs) has been launched. Moreover, for regular beamtime proposals the option of claiming socio-economic impact was introduced.

The latter allows to ask for beamtime based on a socio-economic impact rather than on scientific excellence of a project. Practically, this impact is achieved if the project is a pre-commercial development showing a technical readiness level (TRL) of minimum 4. These proposals are reviewed by DESY's Innovation and Technology Transfer Group for the TRL, whereas the impact of the expected results is reviewed by the beamline Project Review Panel (PRP). In case of a positive evaluation, these proposals will receive beamtime. Otherwise the proposals are still reviewed in terms of their scientific excellence and compete with other scientific proposals of the corresponding beamline.

The TCDs offer a new access route for those users who aim at a strategic topic of significant scientific or societal value. The overarching themes are defined by DESY Photon Science management and published on the DESY Photon Science website and communicated along with the related call for proposals. The prerequisite for participation in the new TCD call is a dedicated collaboration of at least three distinct research groups asking for beamtime also at more than one PETRA III beamline for at least three subprojects. It is required that the participating groups address a common scientific question from different angles and that they commit to collaborate, share measurement results and use synergies even before publication. The DESY Photon Science management anticipates that this early collaboration will enable faster progress and greater impact in the scientific field.

The proposals are reviewed by a dedicated PRP depending on the scientific topic of the call. The first TCD call for proposals on 'Molecular Water Science' was opened in summer 2022. Based on the experience collected during this first TDC call, the procedures and regulations of the TDC calls will be carefully reviewed and revised by the DESY Photon Science management.

Figure 4

Experimental hutch of the PETRA III beamline P66 (building 47K) and the recently installed lift for heavy equipment adjacent to the experimental hall 'Max von Laue' on the left side.

Contact: Oliver Seeck, oliver.seeck@desy.de
Hans-Christian Wille, hans.christian.wille@desy.de

PETRA IV – The Ultimate 3D-X-Ray Microscope

Plans for the new light source PETRA IV are taking concrete shape

PETRA IV is the planned upgrade of the PETRA III synchrotron radiation storage ring to the most brilliant high-energy light source which will be diffraction-limited up to a photon energy of to 10 keV (λ = 0.12 nm). It will push imaging techniques into the single-digit nanometre regime with enough brightness to enable time-resolved measurements from nanoseconds to seconds. The extreme brightness will be achieved by introducing a hybrid 6-bend achromat (H6BA) lattice cell for the electron storage ring with a targeted horizontal emittance of 20 pm rad. PETRA IV is a key element in the plan for a unique scientific environment far beyond the current activities on the campus – the Science City Hamburg Bahrenfeld.

In addition to the technical upgrade of the PETRA III facility, the project aims to improve the experimental infrastructure for the full exploitation of the capabilities of the new light source. This includes a new experimental hall (PXW) on the western side of the PETRA IV complex to increase the range of experimental techniques and to expand laboratory space to provide new services to the user community (see Fig. 1).

The new services will increase capacity as well as capabilities for ground-breaking research and innovation not only for the existing large community of academic users but also for non-experts in the use of synchrotron radiation mainly coming from the area of applied and industrial research and development.

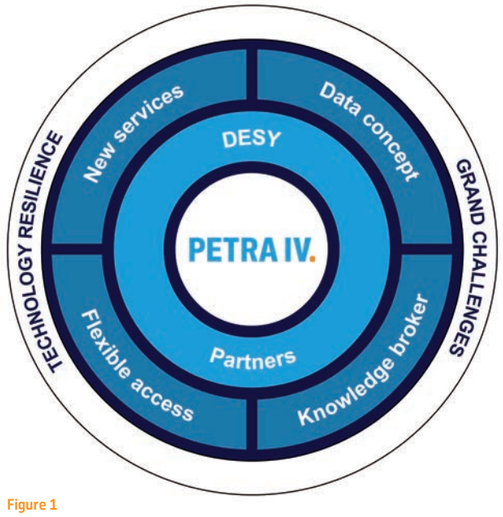

Figure 1

PETRA IV at DESY is conceived as a data-driven solution ecosystem providing, together with its partners, new services for expert users from academia as well as for users from applied and industrial research. In a wider context PETRA IV serves as a key element of a national analytics centre to be established in the planned Science City Hamburg Bahrenfeld.

It is planned to increase the responsiveness to the demands of PETRA IV users by providing faster access to beamtime and dedicated laboratories like, e.g. wet chemistry, nano-sample preparation, cryo-facilities, complementary light and electron microscopes. The other important element is an integrated data handling concept spanning from data acquisition to storage, analysis and archiving. Moreover, this will be complemented by the establishment of a support team to assist non-expert users from the planning of experiments to data analysis and the extraction of solutions to their problems.

In order to work out and test these concepts for large-scale implementation at PETRA IV, it is planned to start pilot projects on a few selected beamlines until the final shut-down of PETRA III.

The planning for the new accelerators and storage ring is already well advanced. The conceptual design of the optical lattice has been 'frozen' in spring 2022. The main activity is now focused on the engineering design for the accelerator complex. In the sector of the beamlines P11-P14 in the experimental hall 'Max von Laue' (each with a total canting angle of 5 mrad) the existing experimental and infrastructure installations could be preserved. Furthermore, this applies also to the Swedish Materials Science Beamline in the experimental hall 'Ada Yonath'. Here, a total canting angle of 1 mrad is required to preserve the current set-up. Since the H6BA lattice cell for the storage ring is very densely packed

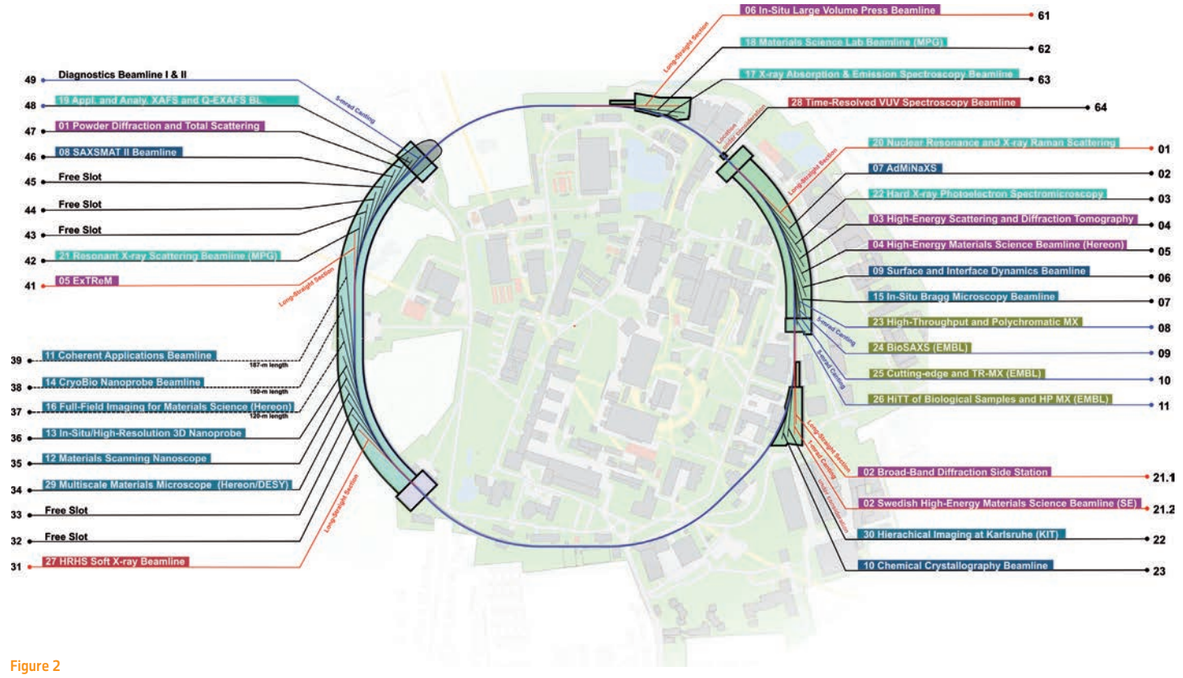

Figure 2

Distribution of the currently planned PETRA IV beamlines in the new experimental hall (in blue-green, left) and in the already existing three experimental halls (in light green, right) in the eastern part of the storage ring (blue line). The beamlines in the eastern halls will be the first to be put back into operation after the PETRA IV accelerator complex is commissioned in 2029.

with magnets and other instrumentation, canting is a task besides that it spoils the emittance of the electron beam.

The design of the optical lattice for the new DESY IV booster synchrotron, part of in the pre-accelerator chain for PETRA IV, has been 'frozen' in 2022. The next steps include the engineering integration into the existing building complex. Owing to its particular topology, the synchrotron DESY IV is planned to be mounted at the ceiling. By keeping it at the same height as the storage ring, unnecessary bends in the transfer line can be avoided which would otherwise spoil the quality of the accelerated electron bunches. DESY II, the current booster synchrotron for PETRA III, will be decommissioned when DESY IV is installed.

In order to achieve the world's smallest horizontal emittance of 20 pm rad of any storage-ring-based source and subsequently a focal spot size of the X-ray beams in the a few nanometre range, all components of the accelerator and photon science complex must be designed for maximum stability. Therefore, a topologically optimised design for the girders of the storage ring cell was chosen to minimise vibrations of the frame and the components mounted on it. This design shows higher stiffness at lower weight. It is also advantageous that this geometry can be readily adjusted to external constraints while maintaining the superior vibrational response of the system. Moreover, this approach is beneficial, e.g. in the northern part of the storage ring where the beamlines of FLASH and the PETRA ring cross each other, and space for the various beam pipes of FLASH has to be provided through the PETRA IV girders.

Starting with ideas collected from the user community via 'Scientific Instrument Proposals' (SIPs), the beamline portfolio for PETRA IV has been further refined in 2022 (see Fig. 2). With the help of the beamline managers of PETRA III, first optical concepts for the new beamlines have been developed and checked for their feasibility and possible performance. Aspects such as the influence of increased thermal load, vibrations of the optical components due to a noisy environment as well as defects in the optical quality have been considered in this design process.

The special characteristics of PETRA IV are the unprecedented brilliance and coherence which will enable the exploration of new scientific territory. For the preservation of these properties from the source to the sample, wave-optical simulations are employed to optimise layout and design of the beamlines for PETRA IV. Wave-optical simulations require a suitable high-performance computing infrastructure which has been made available by the project. In turn, the conceptual and technical design of the beamlines could be well advanced.

For spring 2023, the project team plans to finalise the project proposal for eventual submission to funding agencies. In addition to the accelerator and photon science complex, the

Figure 3

The Hamburg Senate had invited DESY to present the PETRA IV project at the city's town hall to numerous representatives from science, politics and industry (September 2022).

proposal incorporates a full account of the required infrastructure modifications on the DESY campus as well as the logistics required for the realisation of PETRA IV. Plans for new buildings such as the PETRA extension hall West (PXW), the girder assembly building (GAB), a new RF hall and a set of smaller support buildings are being further developed as well as an assessment of the required refurbishment of existing structures like the DESY pre-accelerator complex and its transfer lines. All these activities have to be integrated into the larger campus development plans which include for instance a new visitor centre 'DESYUM' or the new innovation centre 'Integriertes Technologie und Gründerzentrum' (ITGZ), among others. Further elements to be considered in the planning for PETRA IV are parallel upgrade programmes of existing machines: the second shut-down of FLASH in the framework of the FLASH2020+ programme and the maintenance shut-down of the European XFEL. Both are planned for the middle of the decade.

After more than two years of planning in mostly online meetings, it was finally possible to bring together the entire PETRA IV project team on campus for an all-hands meeting in summer 2022. In September 2022, the project team moved to its own office premises, bringing together core members from across many DESY divisions. Being able to work in close contact is crucial for the final stage of producing the PETRA IV Technical Design Report (TDR).

Raising attention for and awareness of PETRA IV is the goal of a campaign which had its kick-off event in September 2022 with a round-table talk on the DESY campus and a subsequent reception of the Senate of the City of Hamburg (see Fig. 3). The Deputy Mayor of Hamburg, Katharina Fegebank, welcomed the project team in the town hall of Hamburg together with representatives from science, politics and industry. The Nobel laureate Prof. Stefan Hell gave a talk on the importance of applied science and research and development for industry and innovation in Germany.

PETRA IV as a key element of the planned Science City Hamburg Bahrenfeld, is set to foster innovation in Germany and contribute to the solution of grand societal challenges as adopted by the Helmholtz Association and the German government. Areas that will particulary benefit from research at PETRA IV are: health and drug development, new materials for catalysis and sustainable energy production and storage or new functional materials for the next generation of hardware for advanced computing and artificial intelligence.

Contact: Harald Reichert, harald.reichert@desy.de
Kai Bagschik, kai.bagschik@desy.de
Stephan Klumpp, stephan.klumpp@desy.de

DESY NanoLab

Strengthening the interconnected approach in nanoscience

The Centre for X-ray and Nanoscience (CXNS), which also houses most of the DESY NanoLab laboratories, was ceremonially opened in April 2022. Already before this date, most of the NanoLab laboratories were operational and in use in the new building on the DESY campus. Looking back to the first year in the new interconnected environment of the CXNS, the DESY NanoLab research has already benefited from the new spacious state-of-the-art laboratories and especially from the short distances to other research facilities (Fig. 1).

The DESY NanoLab offers on-site methods for nanoscience that complement techniques used at PETRA III, FLASH and the European XFEL. The goal is to implement various nanocharacterisation techniques for investigation of the atomic scale structure, chemistry and magnetism as well as nanostructuring and nanosynthesis techniques. It is open for external users from academia in the framework of accepted proposals, supports DESY in-house research as well as European users in the framework of the access programme NEP. Users from industry get access to these facilities via the DESY Innovation and Technology Transfer Department (ITT).

The DESY NanoLab consists of several strong pillars in nanoscience research:
microscopy and nanostructuring, spectroscopy, nanoparticle synthesis, *in situ* and *operando* X-ray diffraction, electrochemistry and magnetic characterisation. Further preparations for the establishment of a laser laboratory for the investigation of dynamics at the nanoscale in cooperation with the Leibniz-Institut für Kristallzüchtung (IKZ) in Berlin, also a partner of the CXNS, are underway. The opening is targeted for the second half of 2023. This laser lab is planned for the preparation of ultrafast pump-probe experiments that complement the existing NanoLab science fields. New instrumentation at the DESY NanoLab includes a scanning Auger microscope with chemical resolution at the nanoscale and e-beam lithography in cooperation with the Center for Hybrid Nanostructures (CHyN) of the Universität Hamburg.

Main research topics of the DESY NanoLab are catalytic reactions on nanomaterials, nanoscale phenomena like oxidation and corrosion and materials research and search for novel, nanostructured materials (Fig. 2), photo-catalytic reactions and research on oxide surfaces and interfaces as well as time- and spatially-resolved investigation of surfaces and nanostructures under *in situ* and *operando* conditions. Future interest of NanoLab research also lies in the development of marker strategy and correlative multimodal imaging.

A detailed overview on the DESY NanoLab instrumentation can be found in the 'Facts and Numbers' section of this DESY Photon Science annual report.

Contact: Andreas Stierle, andreas.stierle@desy.de

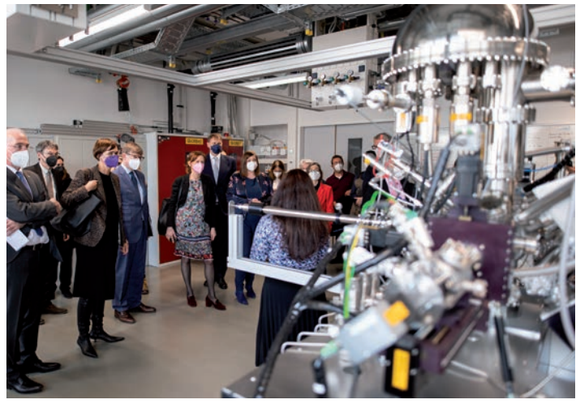

Figure 1

Guided tour through the CXNS laboratories during the opening celebration in April 2022 with three German research ministers: Federal Research Minister Bettina Stark-Watzinger (4th from left), Karin Prien (6th from left) Minister of Science in Schleswig-Holstein and Katharina Fegebank (8th from left), Science Senator of the City of Hamburg as well as other distinguished guests. They visited the NanoLab spectroscopy lab hosting an improved transfer chamber and extended transport facilities under permanent UHV condition. (Image: Daniel Reinhardt DESY)

References

1. **M. Creutzburg et al. 'Adsorption of oleic acid on magnetite facets', Commun. Chem. 5, 134 (2022).**

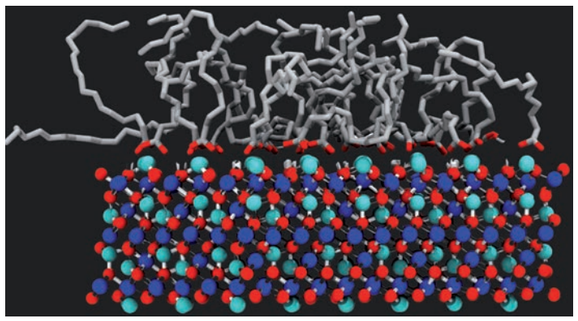

Figure 2

Detailed atomic structure of an oxide/organic acid interface.
(Image: Marcus Creutzburg, DESY)

The European Molecular Biology Laboratory Hamburg Unit

Research and infrastructures for applications in the life sciences

The European Molecular Biology Laboratory Hamburg Unit (EMBL) in Hamburg carries out research with a specific focus on themes in infection biology by mainly applying structural biology and imaging tools at various scales. At present, EMBL Hamburg provides access to three beamlines at the PETRA III storage ring and a dedicated 'Sample Preparation and Characterisation' Facility for external researchers from academia and industry. During the last reporting period, EMBL Hamburg served 566 individual users at the beamlines and the SPC facility. EMBL's portfolio also includes on-site training opportunities for users. External access to EMBL's facilities is supported by a number of European consortia: INSTRUCT, iNEXT-Discovery, MOSBRI, ISIDORe and EOSC4Cancer.

Research infrastructure provision

EMBL's Sample Preparation and Characterisation (SPC) Facility offers a pipeline from the lab bench to the EMBL beamlines, helping optimise and prepare samples for structural studies. The SPC team has recently established a new online platform for analysing data from biophysical experiments (eSPC) [1]. In 2022, a new tool for analysing mass photometry data was added [2].

Beamline P12
for Small-angle X-ray Scattering (BioSAXS) is dedicated to measuring weakly-scattering and low-contrast biological macromolecular samples and bio-composites. These features are combined with high-throughput automated sample delivery [3] and data acquisition/processing and deposition into the EMBL-operated open-access 'Small Angle Biological Data Bank' (SASBDB). SAXS services are spanning fundamental and applied research, such as the interrogation of structured and intrinsically disordered macromolecular systems, biologics/pharmaceutical formulations and delivery, vaccine, infection biology, antimicrobial and anti-inflammatory research.

Together with the company BioNTech and the Mainz University, EMBL is developing a new sample delivery approach at the PETRA III beamline P12. The BMBF-funded project 'Pharma-SAXS' aims to characterise lipid nanoparticles for mRNA vaccines. A recently commissioned in-vacuum sample exposure unit incorporates elements for optical devices and sample environments, such as microfluidic devices and scanning/rastering capabilities for mounted samples (Fig. 1).

Dmitri Svergun, who led EMBL BioSAXS activities for almost two decades, has recently retired. Under his leadership, BioSAXS services and research at EMBL have become a hallmark in modern structural biology. The interim SAXS team under the leadership of Clement Blanchet together with Melissa Graewert and Cy Jeffries ensures that activities at P12 continue and further expand.

Beamlines P13 and P14 for macromolecular crystallography
have witnessed an increasing proportion of users visiting EMBL for in-person data collection. P14 was also used for pilot X-ray imaging experiments. To further improve the beam quality on P14 for crystallographic and X-ray imaging applications, the monochromator crystals were exchanged after more than a decade of continuous operation. After the installation of new beam intensity monitors, precise and accurate estimation of X-ray dose supports the collection of higher quality diffraction data. With next generation inhouse-developed data acquisition software, detectors can now be read out with frame rates above 1 kHz. For data storage, 1.6 PByte of high-performance storage was added to the beamline IT infrastructure in collaboration with the University of Hamburg.

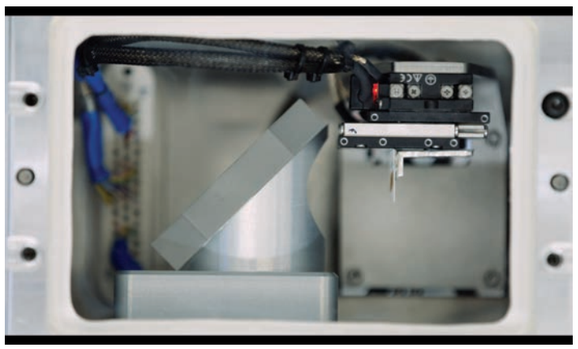

Figure 1
The new in-vacuum sample exposure unit SEU2B has been commissioned at the PETRA III beamline P12. It incorporates elements for optical devices and sample environments, such as microfluidic devices as well as scanning and rastering capabilities for mounted samples. (Credit: Shosho)

Figure 2
EMBL Director General Prof. Edith Heard during a panel discussion at the PETRA IV campaign kick-off event. (Credit: DESY, Daniel Reinhardt)

Plans for EMBL at PETRA IV
EMBL is supporting DESY's efforts related to PETRA IV, the upgrade of PETRA III. At the PETRA IV campaign kick-off event (Fig. 2), EMBL Director General Prof. Edith Heard stressed that PETRA IV will play an important role in the current EMBL programme 'Molecules to Ecosystems 2022-2026' which aims at studying life in its context.

EMBL submitted the conceptional beamline design for three planned EMBL beamlines at PETRA IV which will also offer future opportunities for X-ray imaging of biological specimens. To strengthen joint efforts of EMBL and DESY and to explore future common perspectives, the new coordinator of the PETRA IV project Harald Reichert and leading scientist of PETRA III Christian Schroer visited EMBL's Imaging Centre in Heidelberg in September.

To develop a future joint business case, EMBL and DESY have established a committee to foster innovation which had its first inaugural meeting in October 2022.

Research in X-ray-imaging
The new EMBL team leader Liz Duke is developing a pipeline for high-throughput X-ray imaging of soft biological tissues. Taking advantage of the excellent beam characteristics on P14 and the well-established infrastructure for structural biology, the team is now able to collect, process and reconstruct a 3D data set in less than 10 minutes. Studied samples range from small marine organisms through biopsy samples taken from murine organs to organoids. The ultimate aim of this work is to establish X-ray imaging as one of the user facilities offered by EMBL Hamburg.

AlphaFold: new opportunities for structural biology

AlphaFold2 is an AI-based program that predicts protein structures with unprecedented accuracy. Combining it with their own development for integrated modelling of structures using experimental and computational techniques, scientists at EMBL Hamburg critically contributed to the structure of the human nuclear pore complex's core in unprecedented detail and completeness [4] (Fig. 3).

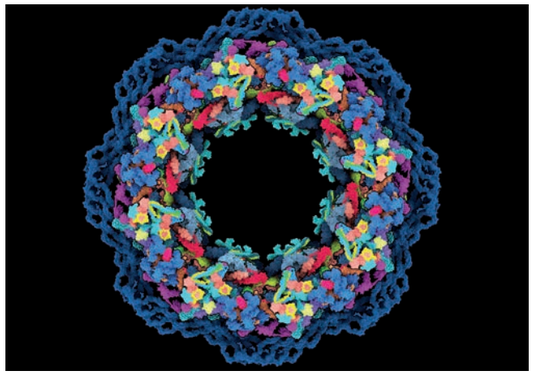

Figure 3
Model of the human nuclear pore complex's core solved by the Kosinski Group at EMBL Hamburg and Beck Lab at Max-Planck Institute of Biophysics. The highest possible level of detail is achieved by combining AlphaFold with techniques such as cryo-electron tomography, single particle cryo-EM and integrative modelling. The complex consists of 1000 pieces - one of the largest complexes in the human body. (Credit: Agnieszka Obarska-Kosińska/EMBL and MPI of Biophysics)

Obituary
The end of the last year brought sad news about the death of Prof. Ken Holmes, the founder of the EMBL Hamburg Unit in 1974. He was a true pioneer in X-ray-based high-resolution molecular structural biology.

Training
In 2022, EMBL Hamburg organised a practical workshop 'Approaches for in cellulo structural biology', practical course 'Membrane Protein Expression, Purification and Characterisation (mPEPC2)', and a MOSBRI course 'ESC3: Quality control for Integral Membrane Proteins' at the SPC Facility.

Contact: Dorota Badowska, dorota.badowska@embl-hamburg.de

References

1. O. Burastero et al., Acta Crystallogr. D 77, 1241–1250 (2021).
2. S. Niebling, et al., Front. Mol. Biosci. 535 (2022).
3. C. Pohl, C. et al., Eur. J. Pharm. Biopharm. 171, 1-10 (2022).
4. S. Mosalagantiet al., Science 376, eabm9506 (2022).

The GEMS branch at DESY

Diffraction and imaging techniques optimised for the needs of materials research

Helmholtz-Zentrum Hereon operates the German Engineering Materials Science Centre (GEMS). In summer 2022, the inauguration of the GEMS wing of the new Centre for X-ray and Nano Science (CXNS) building was celebrated in a GEMS symposium with attendance of the Hereon supervisory board. In addition to office space, the new building provides six new labs which accommodate a suite of X-ray diffraction and imaging instruments as well as a scanning electron microscope (SEM) with a plasma-focused ion beam (FIB). The experimental stations of GEMS at PETRA III are being continuously developed and upgraded for engineering materials and materials science users from institutions in Germany and all over Europe.

GEMS is also preparing to provide cutting-edge instrumentation for new beamlines at PETRA IV, the upgrade project of PETRA III. Without the need for relocation, the new high-energy materials science beamline - now P07 - comes straightforward. On the other hand, the final design of the full-field imaging beamline, the successor to P05 and P07 imaging instruments, is currently being finalised for the location in the new experimental hall. GEMS also pushes for a white-beam beamline at PETRA IV, as there is significant demand for it, and white-beam methods like residual stress analysis have high potential for serving industry. This also applies to high-spatial resolution diffraction, currently offered at the nanofocus endstation of beamline P03, for which GEMS intends to provide a setup at PETRA IV as well.

Diffraction

The engineering materials station P61A as part of the new white beam beamline at PETRA III gained momentum in 2022 with an increasing number of proposals and experiments.

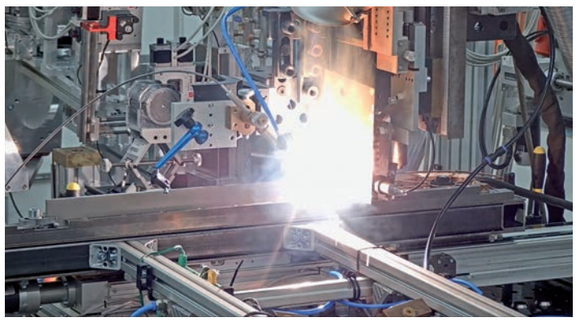

Figure 1

In situ laser welding experiment at PETRA III beamline P61A carried out by scientists from RWTH Aachen. Diffraction patterns are collected in two different directions using two energy-dispersive detectors.

Many experiments focused on residual stress analysis in engineering materials and components, including an *in situ* laser beam welding experiment recording diffraction patterns at a rate of 10 Hz (Fig. 1). The flux up to 200 keV from the damping wiggler allows frame rates above 100 Hz as well as measurements in 4 cm thick steel samples. The group of Elisabeth Schültke from Universitätsmedizin Rostock [1] investigates the microbeam radiotherapy (MRT) technique for cancer treatment which requires an intense white beam. The corresponding experiments were successfully continued with a new roll-in roll-out experimental station (Fig. 2) [2].

At beamline P07, conical slit cells have been extensively used for residual stress analysis within the EU project EASI-STRESS [3]. Conical slit cells define a gauge volume fixed in space and allow spatial resolution in beam direction in a bulk sample. They are used mainly for 3D residual stress mapping. The project EASI-STRESS deals with the standardisation of industrial residual stress characterisation at synchrotrons. Several reference samples were measured at P07 and P61A as part of a round-robin study. Combining both beamlines, four different methods of residual stress analysis can be offered to the scientific community as well as to industry. These methods are: monochromatic beam in transmission geometry (for thin sheets), monochromatic beam with conical slits (in the bulk), white-beam in reflection (near surface stresses) and white beam in transmission (bulk stresses). In addition, Hereon also provides neutron diffraction at the Heinz Maier-Leibnitz Zentrum (MLZ) in Garching as a powerful residual stress analysis tool. These methods cover a wide range of residual stress problems and make Hereon a unique provider of industrial service in this area. A software developed in the project EASI-STRESS will support standardised reporting of results which is essential for industrial customers.

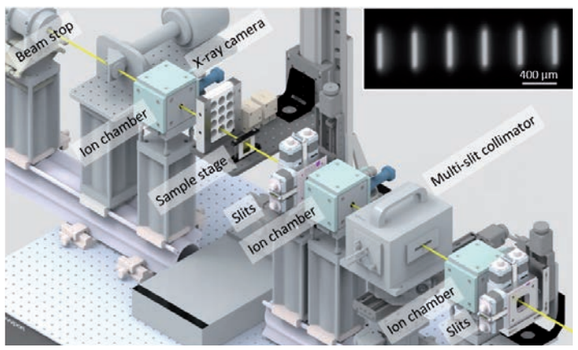

Figure 2

Sketch of the MRT setup at the PETRA III beamline P61A. The inset shows microbeams produced by the multi-slit collimator.

Imaging

Our imaging instruments at the beamlines P03, P05 and P07 provide a combination of high energy, abundant space to house *in situ* sample environments, phase contrast methods and a high range of spatial resolutions. Currently ongoing software developments include implementations of robust phase contrast reconstruction algorithms in order to achieve a high level of automation in the reconstruction of tomographic data. Furthermore, recent developments in applying machine learning for denoising of nanotomography data at P05 were highlighted on the cover of the January issue of the Journal of Synchrotron Radiation. This specifically-trained network is eliminating the noise without changing the structural data of the tomographic scan. Based on these achievements, a network pre-trained on a specific sample type is able to denoise a range of tomographic data sets with the same signal-to-noise ratio, enabling scanning at high temporal resolution [4], (see hightlight section).

High-energy radiography at P07 helped to understand melting and mixing of the melt flow during laser welding of aluminium and copper, as shown in Fig. 3. The results gave valid input for building a model. The industrially relevant process was studied by researchers from the Fraunhofer ILT Institute in Aachen by using the high-energy imaging setup with a time resolution of 1 ms [5]. A high sensitivity with respect to density contrast was essential for the analysis of magnesium degradation under physiological conditions at P05. This helped Hereon researchers to build a computational model for the degradation process which is highly relevant for applications of biodegradable implants [6, 7]. At the P05 nanotomography instrument, the first use of a plenoptic microscope operating with hard X-rays was demonstrated. This proof-of-concept experiment opens new horizons to quasi-3D X-ray imaging without sample rotation at spatial resolution of a few hundred nanometres [8].

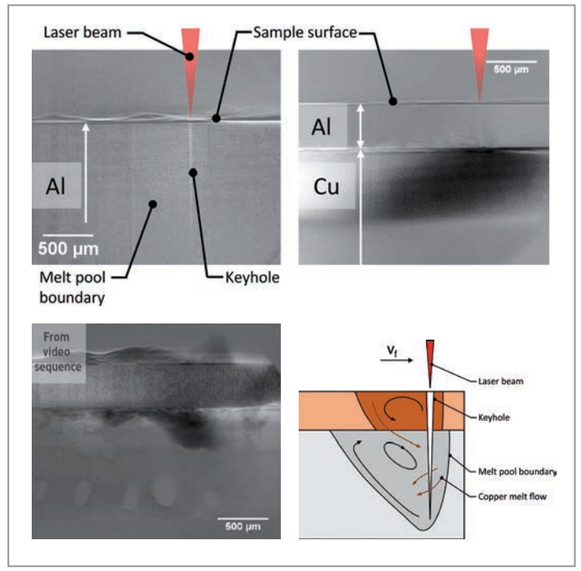

Figure 3

High-energy radiography of a laser beam welding process. Top images: two welding configurations: Al99.5 bead on plate and Al99.5 on CuSn6. Bottom images: The left panel shows the melt pool with intermixing, bubbles and keyhole; the right panel illustrates the derived model of the melt pool flow. (Figures adapted from [5] licensed under CC-BY 4.0.)

Organic semiconductor materials have a great potential for reducing the manufacturing costs of electronic components. Researchers from the University of Siegen examined organic field-effect transistors (OFET) under *operando* conditions at P03 with scanning nanodiffraction. The data obtained from the oligothiophene material indicated a high structural stability under the applied voltage [9]. Also at P03, researchers from the TU München have investigated structure heterogeneity and degradation of hybrid perovskite films, a materials class with a lot of potential for photovoltaics and optoelectronics applications. The data indicates how the spray deposited films bear tensile strains and how moisture-induced degradation is initiated [10].

Author contact:
Christina Krywka, christina.krywka@hereon.de
Peter Staron, peter.staron@hereon.de
Martin Müller, martin.mueller@hereon.de

References

1. https://strahlentherapie.med.uni-rostock.de/forschung/arbeitsgruppe-mikrostrahltherapie (accessed 19 Oct. 2022).
2. E. Schültke et al., Cancer (2022), accepted.
3. https://www.easi-stress.eu/ (accessed 19 Oct. 2022).
4. S. Flenner et al., Journal of Synchrotron Radiation 29, 230 (2022).
5. S. Hollatz et al., Journal of Materials Processing Technology 309, 117738 (2022).
6. B. Zeller-Plumhoff et al., Journal of Magnesium and Alloys 10, 965 (2022).
7. D. Krüger et al., Bioactive Materials 13, 37 (2022).
8. E. Longo et al., Photonics 9, 98 (2022).
9. A. Davydok et al., Nanoscale Research Letters 17, 22 (2022).
10. N. Li et al., Nature Communications 13, 6701 (2022).

DESY Photon Science at the European XFEL

User consortia of the Helmholtz International Beamline

DESY is not only responsible for the construction and the operation of the European XFEL linear accelerator but also plays an important role as user. Moreover, DESY scientists are developing lasers and detectors for usage at the European XFEL and are partners in the largest user consortia: SFX, HIBEF and hRIXS.

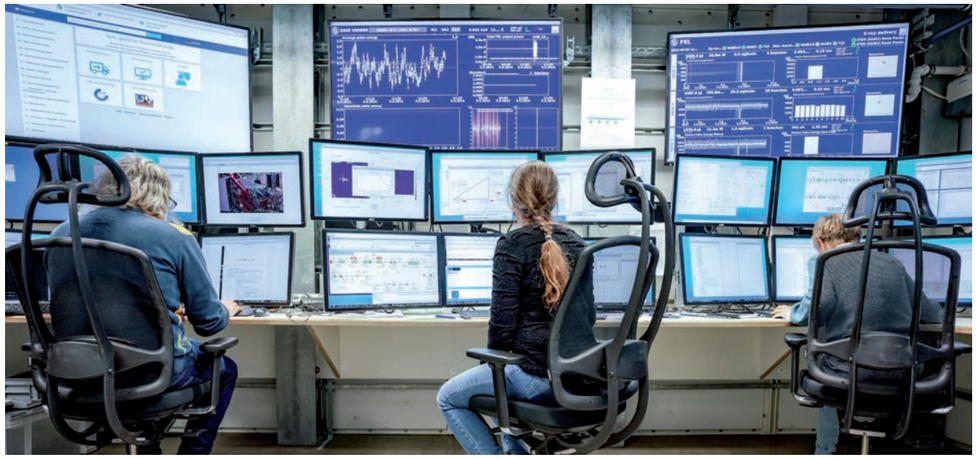

Figure 2
Aligning the hRIXS experiment from the control hutch.

Serial Femtosecond Crystallography (SFX)
The International SFX Consortium contributes experimental instrumentation to the 'Single Particles, Clusters, and Biomolecules and Serial Femtosecond Crystallography' (SPB/SFX) instrument of the European XFEL, to carry out serial femtosecond crystallography and solution scattering for high-throughput determination of macromolecular structures. The SFX Consortium works closely with the SPB/SFX team to achieve higher efficiency and flexibility of serial crystallography (see Fig. 1) and diffraction measurements with the contribution of a second measurement station, collaborates on improved sample delivery systems and diagnostics, and the development of software for data analysis. Members of the SFX Consortium engage with the community across the globe to reduce barriers for new user groups to conduct experiments at the European XFEL and strives to make serial crystallography more accessible to structural biologists. Examples of this are the XFEL Hub at the Diamond Light Source in the UK and the availability of serial crystallography instrumentation at PETRA III. In the last year, a micro-fluidic set up was introduced at the PETRA III beamline P11 consisting of a tape drive to introduce microcrystals to the beam. Using the same small volumes and preparations of crystal slurries as required for liquid-jet experiments at the SPB/SFX instrument, it is now possible to carry out time-resolved measurements of protein reactions over a wide range of time scales addressed with millisecond exposure times at the synchrotron to femtoseconds at the European XFEL. Likewise, the RoadRunner chip scanning system is used at PETRA III and SPB/SFX for low-background fixed-target serial crystallography. A new beam-sweeping device is being investigated that will enable megahertz measurements on extremely small amounts of protein at SPB/SFX.

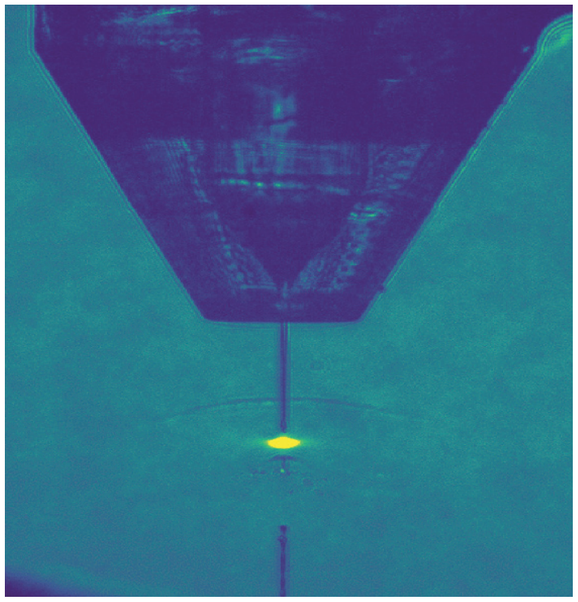

One of the largest upcoming contributions of the SFX Consortium is the 4-megapixel in-vacuum AGIPD detector being constructed at DESY in the group of Heinz Graafsma. This will be delivered and installed next year. In preparation, the data acquisition system and power modules for the detector have been purchased.

Figure 1
View from the nozzle monitoring camera in the SPB/SFX instrument during a serial crystallography experiment. The camera was triggered on the second pulse in the train, and shows the plasma emission (in yellow) resulting from X-ray absorption and the jet explosion. (Credit: SPB/SFX Instrument staff)

Helmholtz International Beamline for Extreme Fields (HIBEF)
The HIBEF user consortium contributes some of the main experimental drivers, scientific and technical personnel and scientific input for experiments at the High Energy Density (HED) instrument of European XFEL. It is led by the Helmholtz-Zentrum Dresden-Rossendorf (HZDR) in collaboration with DESY and the Central Laser Facility (CLF) from Rutherford Appleton Laboratory in the UK as the major consortium partners and founding members.

The high-intensity laser ReLax is available in user operation since 2021. Hereby, relativistic plasma investigation can be performed in combination with several various X-ray based diagnostics like scattering, mainly SAX, spectroscopy and imaging.

Dipole-100X, provided by CLF, is under recommissioning after installation.The velocity interferometer system for any reflector (VISAR) system, contributed by the French HIBEF partner CNRS, is one of the main diagnostics in ramped laser compression experiments and is also under commissioning. More than 80 scientists from different international institutes plan the first community commissioning experiment in the first of 2023.

The design of the pulsed magnetic field setup, generating fields up to 58 T, is almost finalised. The first major components, like the heavy-load goniometer and capacitor bank, are already or will be soon installed. A first on-site test of the complete setup is planned for 2023.

Since Nov 2021, six user proposals were scheduled on the diffraction platform IC2: The experiments included X-ray- and pulsed laser-heating studies at static compression, dynamic compression in piezo-driven dynamic diamond anvil cells and shock compression using the pump–probe laser.

Heisenberg Resonant Inelastic X-ray Scattering (hRIXS)
At European XFEL, commissioning of the Heisenberg RIXS spectrometer was conducted and for both the high resolution grating as well as the transmission-optimised grating design values have been reached. The users assisted commissioning based on community proposals with solids and liquid jet molecular samples; both allowed for first results on static high resolution RIXS and time-resolved experiments. These findings are currently worked out to first scientific publications.

With the successful operation, full users' operation has been started 2022 (Fig. 2), being on time and budget. In the users' proposals, an alternating scheme of calls involving the 'Chem' chamber and the 'solid state sample' environment might be the most efficient use of the hRIXS infrastructure. Funding for hRIXS is provided by the Helmholtz Association via strategic investment in the Helmholtz International Beamline and other national funds (Italy, Germany). The project is partially supported by the ERC Advanced Grant 'EDAX' at Potsdam University. A high-end detector is funded by Finnish partners through a FIRI grant. The hRIXS consortium includes partners from Germany, Switzerland, Finland, France, Sweden, Italy and the UK. The project is coordinated by Potsdam University in close collaboration with DESY and European XFEL.

Contact:
SFX: Henry Chapman, CFEL/DESY and Universität Hamburg, henry.chapman@desy.de
HIBEF: Thomas Cowan, HZDR, t.cowan@hzdr.de
hRIXS: Alexander Föhlisch, Potsdam University and HZB, alexander.foehlisch@helmholtz-berlin.de

Campus and Cooperations

Campus overview

Research centres and cooperations

The research and cooperation landscape at DESY Photon Science involves local, national and international partners with a number of research centres as nuclei for cooperation. All benefit from the excellent scientific environment and research facilities on the Campus Bahrenfeld. The image below highlights the light sources, research centres with involvement of DESY Photon Science as well as associated partner institutions on-site, such as EMBL and Hereon outstations. Some major cooperation activities with universities in networks and the interdisciplinary research platforms on campus are reported on within this chapter.

German universities are also closely involved at PETRA III and FLASH, for example, via BMBF-funded collaborative research. Developments in connection to PETRA III, FLASH and European XFEL are described in the chapter 'Light Sources and User Infrastructures'.

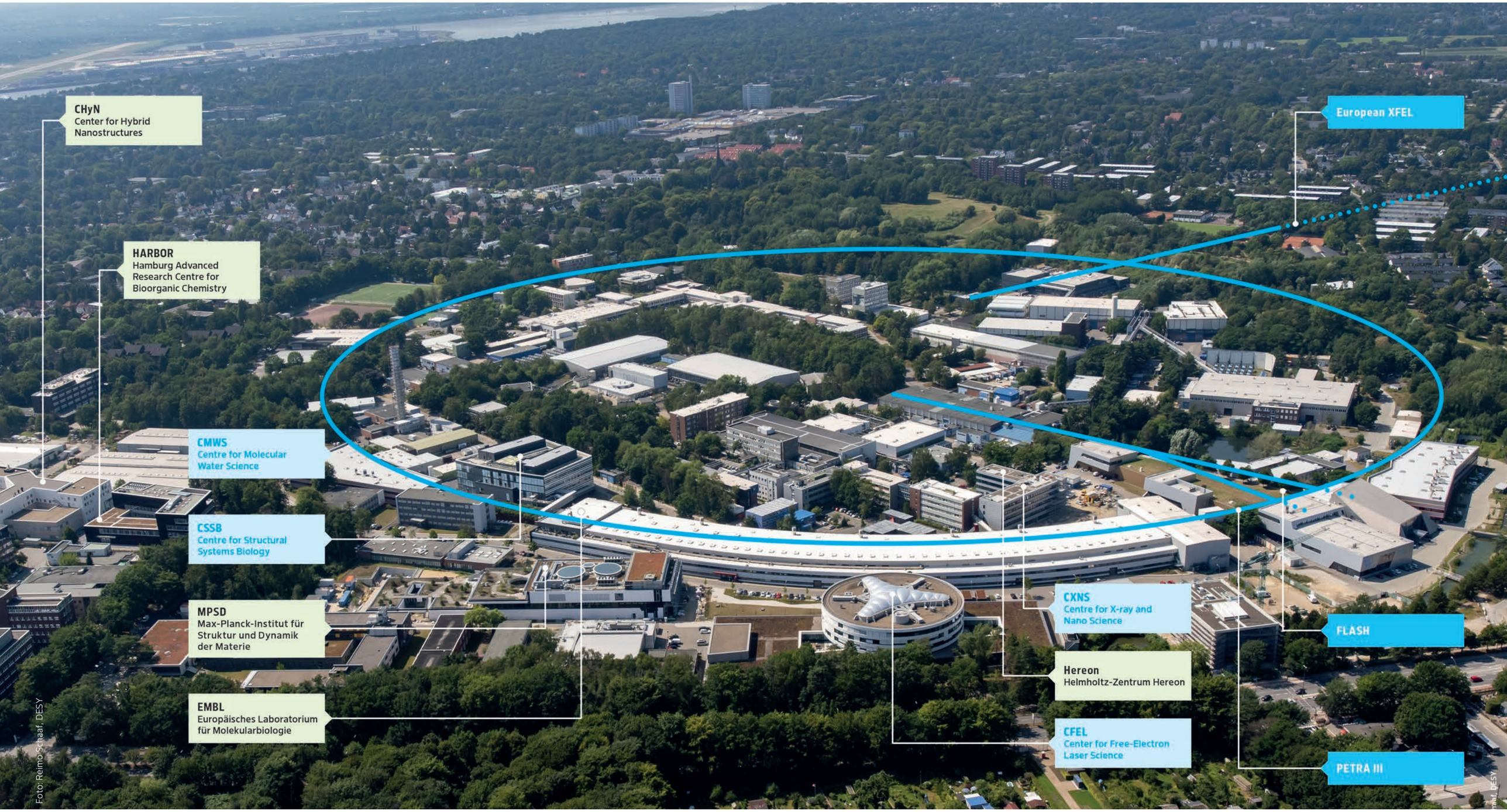

Foto: Reimo Schaaf, DESY

Cooperation in research and education

Universities and networks overview

Graduate Schools

- **PIER Helmholtz Graduate School (PHGS)**
  PHGS is a graduate education programme at DESY in cooperation with Universität Hamburg (UHH). In 2022, almost 300 students are enrolled in PHGS. Doctoral candidates benefit from outstanding research in particle and astroparticle physics, nanoscience, photon science, infection and structural biology as well as accelerators and theoretical physics. PHGS offers numerous research and career skills courses but also supervision and a buddy programme. The annual PIER Graduate Week includes interdisciplinary lectures and workshops to introduce PhD students to the various science fields. During the 2022 PIER PhD reception on 29 June at DESY, about 170 PhD students, supervisors, friends, relatives and staff met to welcome all new doctoral candidates and to honour the 22 graduates present out of a total of 78 graduates from PHGS over the past 16 months.
  graduateschool.pier-hamburg.de

This year's PHGS graduates on site.
(Photo: PHGS, K. Winkler)

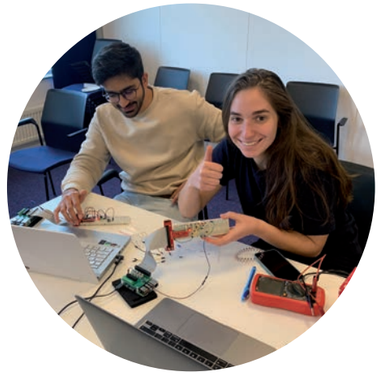

Doctoral students Ammar Bin Wahid and Laura Silletti working on their Raspberry PI project during the 2022 HELIOS retreat. (Photo: HELIOS, S. Tille)

- **The Helmholtz-Lund International Graduate School (HELIOS)**
  HELIOS has been launched in October 2020 and focuses on instrumentation development in the fields of particle physics, molecular physics, nano(bio) science and ultrafast photon science. A major aim is to prepare young scientists for the next generation of instrumentation. The involved partners are UHH, Lund University, City of Hamburg and DESY. Twenty doc-toral candidates are currently enrolled in HELIOS.

  Each year, HELIOS runs a training retreat at Lund University.
  The 2022 retreat was held on 10-14 October and focused on the fundamentals of electronics, detectors, distributed control systems as well as well as CPUs and FPGAs. An integral part of HELIOS is to connect doctoral researchers with industry´, therefore, alumni were invited, now working in the private sector, to meet the doctoral candidates and talk about their careers.
  www.heliosgraduateschool.org

- **Data Science in Hamburg – Helmholtz Graduate School for the Structure of Matter (DASHH)**
  DASHH is a joint project of DESY, Universität Hamburg, Hamburg University of Technology, Helmut-Schmidt-University, Helmholtz-Zentrum Hereon, Helmholtz Centre for Infection Research, Max Planck Institute for the Structure and Dynamics of Matter, European XFEL and Hamburg University of Applied Sciences.

  DASHH's goal is to train the next generation of data and information scientists in the field of novel data acquisition and analysis techniques to meet the challenges posed by the huge data sets generated by experiments at large-scale facilities.

Participants of the first DASHH retreat in the Ostsee-resort Dampland in August 2022. (Photo: DASHH)

At present, 33 interdisciplinary PhD projects are funded by DASHH, mainly in the fields of photon science, particle physics, accelerator science but also structural biology, materials science and ultrafast X-ray science. In August 2022, DASHH organised a first, very successful three-day retreat at the Baltic Sea. The main focus was to foster the exchange among students. Moreover, DASHH regularly organises a PhD seminar and the Data Science Colloquium.
www.dashh.org

Joint laboratories and institutes

- In the Helmholtz International Laboratory on Reliability, Repetition, Results at the most advanced X-ray Sources (HIR^{3}X), DESY and the US National Accelerator Laboratory SLAC in California have joined forces to develop techniques and procedures that enable the reliable application of X-ray lasers.

- DESY is partner of the Helmholtz Institute Jena which is an outstation of the GSI Helmholtz Center for Heavy Ion Research on the campus of the Friedrich Schiller University of Jena. The institute is mainly focused on applied and fundamental research at the borderline of high-power lasers and particle accelerator facilities.

- The Ruprecht Haensel Laboratory is a joint research facility of Christian-Albrechts-Universität zu Kiel and DESY and combines state-of-the-art instruments and methods of nanoresearch, makes new developments available to international cooperation partners and, with joint appointments, ensures that teaching in the field of nanoscience and surface physics is strengthened in a research-oriented manner.

Strategic networks

- **LEAPS**
  is a strategic consortium initiated by the directors of the synchrotron radiation and free-electron laser user facilities in Europe (League of European Accelerator-based Photon Sources).

- **PIER**
  is the strategic partnership between DESY and Universität Hamburg (Partnership for Innovation, Education and Research).

Excellence clusters

DESY Photon Science contributes to two excellence clusters at the Universität Hamburg:

- **'CUI Advanced Imaging of Matter' (AIM)**
  Many of the FS lead scientists are strongly involved in the cluster. Since 1 July 2022, Christina Bömer leads a young investigator group funded within the development programme of AIM.

- **'Understanding Written Artefacts' (UWA)**
  Christian Schroer, leading scientist of PETRA III, is principal investigator of the research project 'Reading Closed Cuneiform Tablets Using High-Resolution Computed Tomography' within UWA.

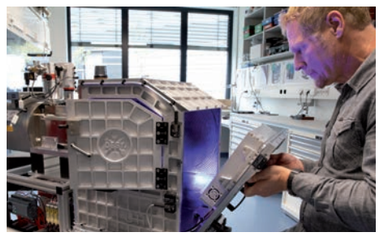

Mobile X-ray tomographic scanner, developed at DESY, is designed to decipher closed cuneiform tablets.

Collaborative research with German universities and institutions

- Tracking the active site in heterogeneous catalysis for emission control (SFB 1441), coordinated by Karlsruhe Institute of Technology (KIT)

- Tailor-made multi-scale materials systems (SFB 986), coordinated by Technische Universität Hamburg (TUHH)

- Atomic scale control of energy conversion (SFB 1073), coordinated by Georg-August-Universität Göttingen (GAU)

- Quantum cooperativity of light and matter (SFB 306), coordinated by Friedrich-Alexander-Universität Erlangen-Nürnberg (FAU)

- Center for Integrated Multiscale Materials Systems (CIMMS), coordinated by TUHH

- Center for Data and Computing in Natural Science (CDCS), coordinated by UHH

- Extreme Light for sensing and driving molecular CHirality (ELCH) (SFB 1319), coordinated by Universität Kassel

- DAta for PHoton and Neutron Experiments for a National Research Data Infrastructure (DAPHNE4NFDI), coordinated by DESY

Center for Free-Electron Laser Science CFEL

Three institutions working successfully together

Laser pulses that briefly grab hold of floating molecules and align them precisely in space – this may sound like an original but academic party trick; however, these are the results which the team led by CFEL's Jochen Küpper is now presenting in the article on *'Picosecond pulse-shaping for strong three-dimensional field-free alignment of generic asymmetric-top molecules'* [1]. The technique has great potential for research, too, because arranging molecules in a precise spatial configuration is an important precondition for observing their extremely rapid behaviour in detail and even filming it. With their latest study, the experts have now managed for the first time to strongly align a relatively complex structure – the biomolecule indole (see Fig. 1.) – without the presence of a laser field. In the future, it should also be possible to use this new method on other complex molecules, such as amino acids, neurotransmitters or vitamins and possibly even entire proteins (see highlight section).

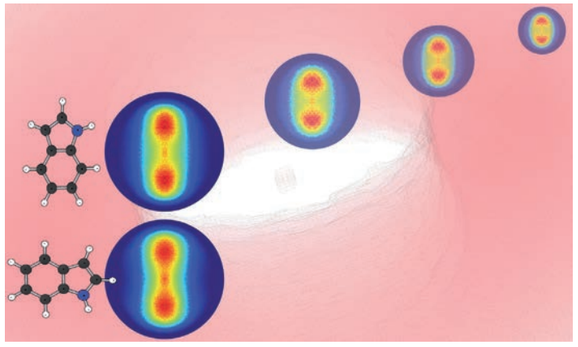

Figure 1
Next to the structure of the biomolecule indole in two selected orientations (left), one can see the measured signals indicating that these molecules are ideally aligned. To the right, one sees one of the molecular orientations during the lapse of time which is determined in the experiment by measuring the momentum of hydrogen ions in the molecule. (Credit: DESY, J. Küpper/C. Lopez Gonzalez)

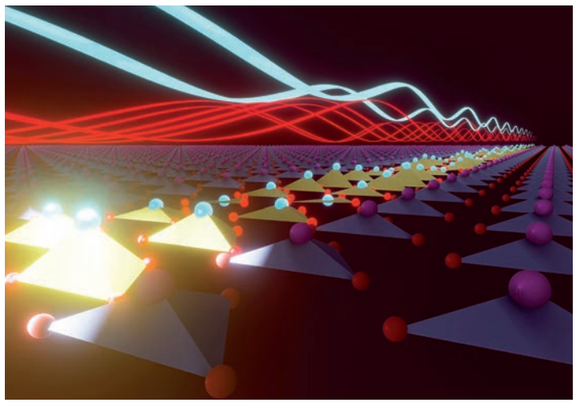

Figure 2
An intense mid-infrared laser pulse hits a ferroelectric $LiNbO_3$ crystal and kicks atomic vibrations only in a short depth below the surface, emphasised by the bright tetrahedra. Through anharmonic coupling, this strong vibration launches a polarisation wave, also called polariton, which propagates throughout the remaining depth of the crystal to modulate the ferroelectric polarisation. (Credit: MPSD, Jörg Harms)

Nonlinear phononics relies on the resonant optical excitation of infrared-active lattice vibrations to induce targeted structural deformations in solids. This form of dynamical crystal structure design has been applied to control the functional properties of many complex solids, including magnetic materials, superconductors and ferroelectrics. However, phononics has so far been restricted to protocols in which structural deformations occur within the optically excited volume, sometimes resulting in unwanted heating. So far, nonlinear phononics has been thought to occur only within the small region of the crystal where the mid-infrared light pulse is present. Now, researchers from MPSD at CFEL have discovered that the ferro-electric polarisation of lithium niobate ($LiNbO_3$) even changes in areas well away from the direct 'hit' of the laser pulse, with the polarisation reversal occurring throughout the entire crystal. The team's study of this hitherto unknown phenomenon – called nonlocal nonlinear phononics – has been published in the article titled *'Nonlocal nonlinear phononics'* [2].

Contact: Ralf Köhn, ralf.koehn@cfel.de

References

1. T. Mullins et al., Nature Communications 13, 1431 (2022).
2. M. Henstridge et al., Nature Physics 18, 457-461 (2022).

CFEL Partner Institutions

- Deutsches Elektronen-Synchrotron DESY
- Max Planck Institute for the Structure and Dynamics of Matter (MPSD)
- Universität Hamburg (UHH)

www.cfel.de

Centre for Structural Systems Biology CSSB

Together we investigate the molecular mechanisms of infections!

Figure 1
CSSB staff in front of the 'Holsten Gate' after teambuilding activities at the CSSB retreat in Lübeck.

After a long period of Corona-related restrictions, operations returned to almost-normal this year, and CSSB staff and scientists focused on reconnecting with one another and fostering a spirit of collaboration. To this end, CSSB held its first all-staff retreat, featuring a science slam and several team-building activities. The retreat was followed by a staff celebration of CSSB's fifth birthday on June 29. During our Scientific Advisory Board meeting in October, CSSB scientific staff contributed to presentations, discussions and a poster session. All these activities have helped to build and strengthen a sense of community at CSSB.

Research highlights

CSSB scientists combined 'AlphaFold2' with experimental and computational techniques to figure out the human nuclear pore complex's architecture in greater detail than ever before [1], deciphered two antimicrobial amyloid structures using cryo-electron microscopy [2], uncovered a novel exit pathway used by the Human Cytomegalovirus (HCMV) to spread infection in human cells [3] and revealed the architecture, complete functional cycle and the mechanism of the RuvAB branch migration complex, a molecular machine involved in homologous recombination and DNA repair processes [4].

Our scientists are also involved in the development of new tools for the infection and structural biology community such as a method to predict the immune system's response to individual peptides [5], a biophysical screening pipeline for cryo-EM grid preparation of membrane proteins [6], StarMap – a user-friendly workflow for computer-assisted molecular structure refinement [7] and AlphaPulldown – a Python package for protein-protein interaction screens using AlphaFold-Multimer [8].

New group leader

Professor Meytal Landau will start her research group at CSSB in spring 2023. She successfully applied for a Helmholtz Distinguished Professorship entitled 'Functional fibrils in the fight against pathogens' and has a joint appointment from DESY and the University Medical Center Hamburg-Eppendorf (UKE). She will lead a group that investigates peptides that are produced across kingdoms of life with a prominent function being antimicrobial protection through their ability to form amyloid fibrils.

Awards

Charlotte Uetrecht (Univ. Siegen, LIV and DESY) was granted the Mattauch-Herzog Award for her development of mass spectrometry methods and technologies. The award is presented by the 'Deutsche Gesellschaft für Massenspektrometrie' (DGMS) and considered one of the most prestigious scientific awards in analytical science. This is only the second time since its establishment in 1988 that the Mattauch-Herzog Award was presented to a woman.

Two postdoctoral scientists working in the Marlovits group have received awards: Jiri Wald was awarded the 'UKE paper of the month' and Catalin Bunduc was granted the 'van Leeuwenhoek Award' for the best publication as first author.

Contact: Kay Grünewald, kay.gruenewald@cssb-hamburg.de

References

1. S. Mosalaganti et al., Science 376, 6598 (2022).
2. R. Bücker et al., Nat. Commun. 13, 4356 (2022).
3. F. Flomm et al., PLoS Pathog. 18(8) e1010575 (2022)
4. J. Wald et al., Nature 609, 630–639 (2022).
5. J. D. Kopicki et al., Commun. Biol. 5, 488 (2022).
6. S. Niebling et al., Front. Mol. Biosci. 9, 882288 (2022).
7. W. Lugmayr et al., Nat. Protoc. (2022).
8. D. Yu et al., bioRxiv 2022.08.05.502961 (2022).

CSSB Partner Institutions

- Bernhard Nocht Institute for Tropical Medicine (BNITM)
- Deutsches Elektronen-Synchrotron DESY
- European Molecular Biology Laboratory (EMBL)
- Forschungszentrum Jülich (FZJ)
- Hannover Medical School (MHH)
- Leibniz Institute of Virology (LIV)
- Helmholtz Centre for Infection Research (HZI)
- Research Center Borstel (FZB)
- Universität Hamburg (UHH)
- University Medical Center Hamburg-Eppendorf (UKE)

CSSB Stakeholders

- Federal Republic of Germany
- Free and Hanseatic City of Hamburg
- Federal State of Lower Saxony
- Federal State of Schleswig-Holstein

www.cssb-hamburg.de

Centre for X-ray and Nano Science CXNS

Official opening ceremony in 2022

On 12 April 2022, the long-awaited CXNS opening celebration took place. It was really satisfying to meet in person for this occasion. We were able to welcome three ministers (Fig. 1): Federal Research Minister Bettina Stark-Watzinger, Schleswig-Holstein's Minister of Education, Science, Research and Cultural Affairs Karin Prien and the Senator for Science, Research and Equalities of the City of Hamburg Katharina Fegebank. The president of the Helmholtz Association (HGF) Prof. Otmar Wiestler, as well as the heads of the CXNS cooperation partners, Prof. Matthias Rehahn from Hereon, Prof. Simone Fulda from Christian-Albrechts-Universität zu Kiel (CAU) and project leader Dr. Peter Gaal from Leibniz-Institut für Kristallzüchtung (IKZ) also joined the event as our guests. Members of the Center for Integrated Multiscale Material Systems (CIMMS) – a joint research group of DESY and the Technische Universität Hamburg (TUHH) – and of course all DESY Photon Science groups linked with the building or its laboratories were present.

From late 2021 until spring 2022 onwards, almost all laboratories in the new CXNS building were brought into working condition. They are now actively used for internal and user research in cooperation with the close-by DESY large-scale facilities PETRA III and FLASH. Interest in all possible options of this interconnected research has already exceeded the capacity of the DESY NanoLab and the other laboratories in the CXNS. Thorough planning of manpower and capacities, especially in combined access of CXNS facilities and the large-scale facilities, is necessary and taken care of by the research teams at the CXNS and the beamlines at PETRA III and FLASH.

Mission of CXNS is to exploit synergies in novel materials, sensor technologies, X-ray based new materials imaging methods, novel catalyst materials for chemical processes and energy conversion as well as time-resolved studies of ultrafast processes on surfaces and nanostructures.

In several mutual activities like joint beamtime proposals as well as nationally funded 'BMBF Verbundforschung' or DFG projects, this valuable interconnection of knowledge and facilities has already been proven to be fruitful and promising.

In 2023, the establishment of a laser laboratory as part of a DESY and IKZ cooperation is planned. It will provide CXNS with a femtosecond laser setup for time-resolved studies of nanomaterials.

Contact: Andreas Stierle, andreas.stierle@desy.de

CXNS Partner Institutions

- **Helmholtz-Zentrum Hereon, German Engineering Materials Science Centre (GEMS)**
- **Christian-Albrechts-Universität zu Kiel (CAU), Ruprecht-Haensel-Labor**
- **Technical University Hamburg (TUHH), Center for Integrated Multiscale Material Systems (CIMMS)**
- **Leibniz-Institut für Kristallzüchtung (IKZ Berlin)**

photon-science.desy.de/research/centres_for_research/cxns

Figure 1
At the opening ceremony (from left to right): A. Stierle (DESY), O. Wiestler (HGF), K. Fegebank (Science Senator City of Hamburg), H. Dosch (DESY), K. Prien (Science Minister Schleswig-Holstein), M. Rehahn (Hereon), S. Fulda (CAU), B. Stark-Watzinger (Federal Research Minister). (Photo: Daniel Reinhardt, DESY)

Centre for Molecular Water Science CMWS

Achieving a detailed molecular understanding of water

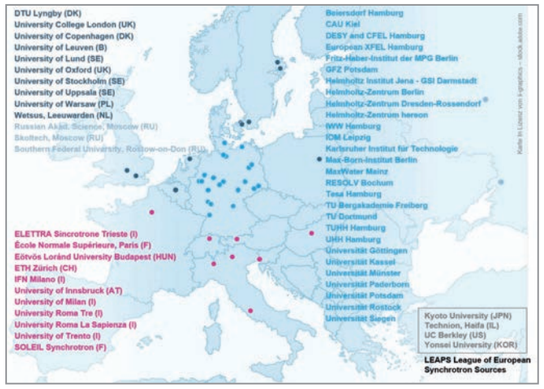

Figure 1
The CMWS network of partners.

The Centre for Molecular Water Science (CMWS) is an international interdisciplinary research centre with a focus on molecular water in a variety of different scientific disciplines and applications. In tight collaboration with partners from all over Europe and beyond, CMWS researchers generate a deep understanding of the role of molecular water in chemistry, physics and biology, and thus provide the knowledge base for future sustainable technologies – a driver for innovation and transfer.

Driving water research forward

Numerous central research foci of the CMWS employ the X-ray methods available at DESY and European XFEL for studying molecular structure and dynamics on different timescales and in various environments. In 2022, targeted challenge-driven calls of the European XFEL and PETRA III were launched for the first time, focusing on 'molecular water science' in close collaboration with the CMWS. The installation of two CMWS laboratories on the DESY campus has been continued, offering for example Raman and FT-IR spectroscopy to CMWS partners.

To further strengthen the common research activities, an Early Science Program (ESP) was launched by DESY in 2019, supporting PhD projects between different CMWS partners. The programme is jointly financed by DESY and CMWS partners with equal contributions. The third call with a focus on the research agenda of the CMWS White Paper [1] was launched in 2022, and ten new projects are about to start. The success of the programme is highlighted by more than twelve publications in peer-reviewed journals in the last two years. Furthermore, the ESP fellow Christina Tonauer (Univ. Innsbruck/DESY) received the prestigious Agnes Pockels Doctoral Award from the Deutsche Bunsen-Gesellschaft for her work on near-infrared spectroscopy on high-density crystalline H_2O ices.

First cooperation agreements for external CMWS hubs were finalised with the Katholieke Universiteit Leuven (Belgium) in the field of nuclear magnetic resonance spectroscopy. CMWS worked on different outreach projects to highlight the relevance of molecular water research and to explain it to a broader audience. In this respect, two articles were published in 'Physik in unserer Zeit' [2] and 'Physik Journal' [3]; also 'FAZ Sonntagszeitung' reported on the CMWS and molecular water research. Furthermore, the CMWS and the special anomalies of water are discussed in a recent Helmholtz resonator podcast.

Events

The CMWS DAYS took place in March 2022 as an all-online event with more than 230 participants. In this meeting, highlights of CMWS research were presented, and the dedicated calls on water research of European XFEL and PETRA III were discussed. The next CMWS Water Days are planned for 21-24 February 2023.

The CMWS Lunch Seminar series, which started during summer semester of 2021 with a focus on water-related science and technology, was successfully continued with more than 80 participants on average. The aim of the series is to intensify the scientific exchange within the network of the CMWS and to introduce students and young scientists to the different research areas of the CMWS.

In the frame of the PIER workshop series, CMWS researchers organised a joint workshop during which researchers from DESY, UHH and TUHH exchanged ideas to explore future possibilities to further strengthen molecular water research in Hamburg.

Contact: Claudia Goy, claudia.goy@desy.de

References

1. G. Grübel, M. Schnell, C. Goy, F. Lehmkühler, S. Bari. (Eds.), 'CMWS – White Paper', Hamburg: DESY, 127 pp. (2021). DOI: 10.3204/PUBDB-2021-01859
2. T. Loerting and H.-P. Liermann, Phys. Unserer Zeit 53, 116 (2022).
3. M. Pfalz, Physik-Journal 21 (3), 14 (2022).
4. C. Tonauer et al., J. Phys. Chem. A, 125(4), 1062-1068 (2021).

CMWS Partner Institutions

60 partner institutions from 16 countries have expressed their support by a Letter of Interest (Fig. 1)

www.cmws-hamburg.de

Facts and Numbers

FLASH

Experimental halls and parameters

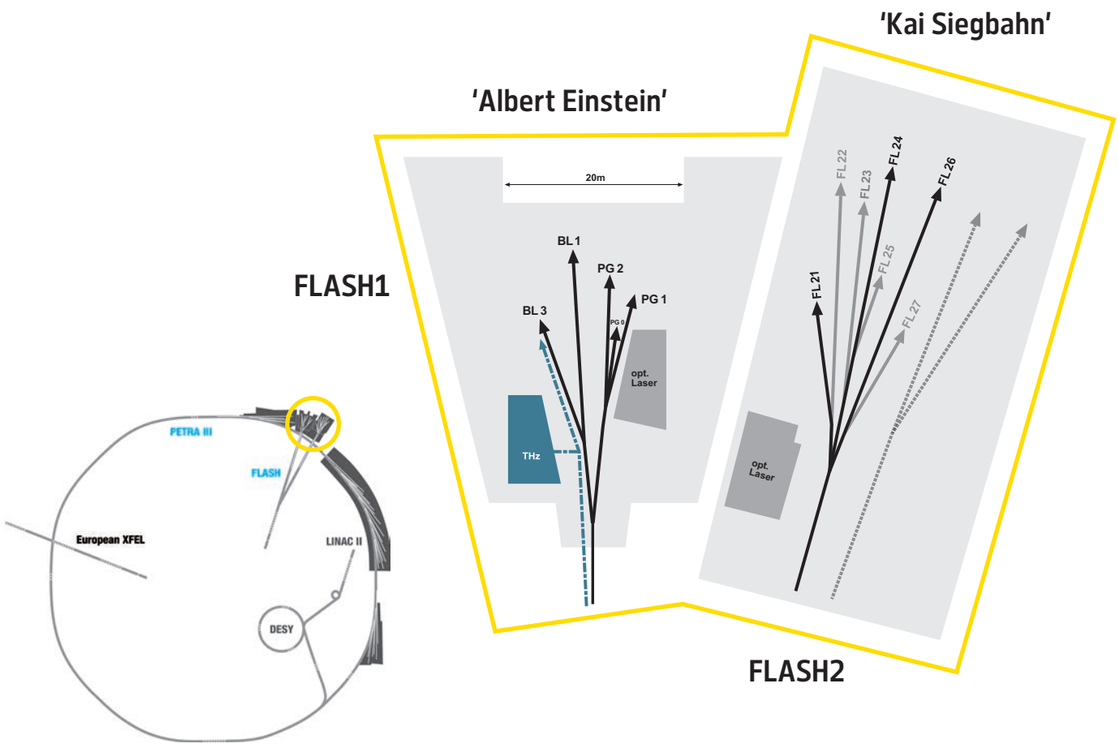

FLASH – machine parameters

	FLASH1	FLASH2
Electron energy range	0.35–1.35 GeV	0.4–1.35 GeV
Normalised emittance at 0.4 nC (rms)	0.4 mm mrad	0.4 mm mrad
Energy spread	200 keV	500 keV
Electron bunch charge	0.01–1.2 nC	0.01–1 nC
Peak current	1–2.5 kA	1–2.5 kA
Electron bunches per second (shared between FL1 and FL2)	5000	5000

FLASH – lasing parameters

	FLASH1	FLASH2
Photon energy fundamental	24–360 eV	14–370 eV
Wavelength fundamental	51–3.4 nm	90–3.3 nm
Photon pulse duration (FWHM)	30–200 fs	10–200 fs
Peak power	1–5 GW	1–5 GW
Single photon pulse energy (average)	1–500 µJ	1–1000 µJ
Spectral width (FWHM)	0.7–2%	0.5–2%
Photons per bunch	10^{11}–10^{14}	10^{11}–10^{14}
Peak brilliance photons/sec/mm²/mrad²/0.1%	10^{28}–10^{31}	10^{28}–10^{31}

PETRA III

Experimental halls and parameters

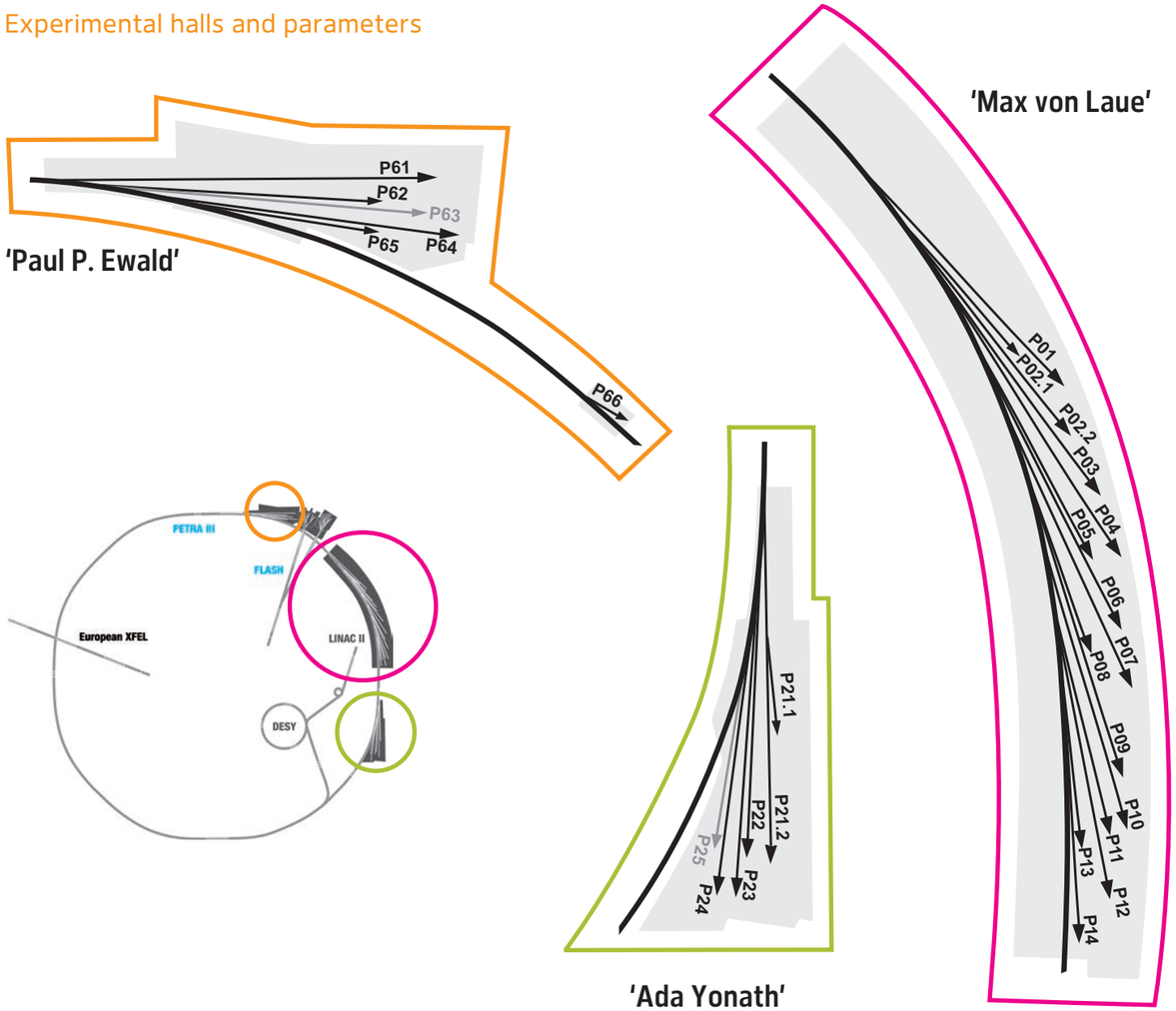

PETRA III – machine parameters

Electron energy	6.08 GeV
Circumference of the storage ring	2304 m
Number of bunches	40 (timing mode) 480 (continuous mode)
Bunch separation	192 ns (timing mode) 16 ns (continuous mode)
Electron beam current	100 mA (timing mode) 120 mA (continuous mode)
Horizontal electron beam emittance	1.3 nmrad
Vertical electron beam emittance	0.01 nmrad
Electron beam energy spread (rms)	0.1%
Horizontal × vertical beam size (rms) at 5 m undulator (high β section) and 10 keV photon energy	141 µm × 5.2 µm
Horizontal × vertical beam size (rms) at 5 m undulator (low β section) and 10 keV photon energy	36 µm × 5.7 µm

FLASH

Beamlines

FLASH1 experimental hall 'Albert Einstein'

BL1	non-monochromatic FEL photons Kirkpatrick-Baez (KB) focusing optics, FEL focal spot of ≈ 7 µm × 8 µm (FWHM)	
	split-and-delay unit for XUV pump – XUV probe experiments (mirrors for 13.57 nm, -30 ps to +650 ps delay)	*TU Berlin*
	optional pump – probe experiments using the FLASH1 optical laser system for BL1 and BL3	
	4-mirror polariser for variable FEL polarisation from 30–70 eV	*TU Berlin*
	permanent end station: multipurpose CAMP chamber with pnCCD detectors, electron and ion spectrometers and collinear incoupling optics for optical laser	
BL3	non-monochromatic FEL photons, spectral range: > 4.5 nm (carbon coated optics) focused to ≈ 20 µm / unfocussed beam size ≈ 5–10 mm (FWHM, depending on wavelength)	
	optional pump – probe experiments using the FLASH1 optical laser system for BL1 and BL3	
	4-mirror polariser for variable FEL polarisation from 30–70 eV	*TU Berlin*
	optional pump – probe experiments using THz radiation: - tunable: 10–230 µm; up to 150 µJ/pulse; ≈ 10% bandwidth - broadband at 200 µm; up to 10 µJ/pulse; ≈ 100% bandwidth - synchronised and phase stable to X-ray pulses (down to 5 fs) - delivered to the experiment via vacuum beamline as: (i) ultra-high vacuum (10^{-8} mbar), shorter delay between THz and X-ray (≈ 4 m path difference); can accommodate up to 0.3 m wide setup (ii) high vacuum (≈ 10^{-6} mbar), longer delay between THz and X-ray (≈ 7 m path difference); can accommodate up to 2 m wide setup - UHV chamber with mounts for refocusing XUV optics to compensate for XUV/THz path delay	
	about 3 × 4 m platform for user-provided end station	
PG1	high resolution plane grating XUV monochromator (SX 700 type, < 10^{-4} bandwidth, carbon coated optics): - variable combination of photon flux and resolution (from high flux to high resolution) - controlled temporal-spectral properties at moderate resolution for pump – probe experiments - high photon flux with harmonic filtering Kirkpatrick-Baez (KB) refocusing optics, FEL focal spot down to 5 µm FWHM (vertically, monochromator exit slit size dependent)	
	permanent end station: - XUV-Raman spectrometer TRIXS for high-resolution and time-resolved RIXS measurements on solid samples (20–400 K, resolving power ≈ 1700, time resolution 170–300 fs FWHM) - optional pump – probe experiments (RIXS; XAS and reflectivity with angular resolution) using the FLASH1 optical laser system for PG1 and PG2	
PG2	uses the same monochromator as PG1 50 µm focus	
	XUV beam splitter with variable time delay (±6 ps) for time resolved studies	
	optional pump – probe experiments using FLASH1 optical laser system for PG1 and PG2	
	about 3 × 4 m platform for user-provided end station	

FLASH1 optical / NIR laser system for pump – probe experiments for beamlines BL1 and BL3

No laser operation in 2022.
Target parameters for the laser available in 2023:

intra-burst repetition rate	single pulse
number of pulses per burst	1
pulse duration	< 60 fs FWHM, ≈ 200 ps FWHM (uncompressed)
timing jitter to FEL	< 60 fs rms
pulse energy	0–10 mJ (before coupling to chamber), 0–7 mJ (at interaction region)
polarisation	flexible
peak intensity	> 10^{14} W/cm²
time delay to FEL	-1 ns to +1 ns, 10 fs resolution
energy stability	< 10% pulse-to-pulse peak (3% rms)

Harmonic generation conversion to 400 nm, 266 nm and 200 nm central wavelength are available with conversion efficiencies of > 30% SHG, > 5% THG at BL1

FLASH1 optical / NIR laser system for pump – probe experiments for beamlines PG1 and PG2

central wavelength	1030 nm
spectral bandwidth	30 to 50 nm (pre-set for experiment)
intra-burst repetition rate	Up to 1 MHz
number of pulses per burst	1–800
pulse duration	60–100 fs FWHM
timing jitter to FEL	< 60 fs rms
pulse energy	0–30 µJ (at interaction point at 1030 nm)
polarisation	flexible
peak intensity	> 10^{14} W/cm²
time delay to FEL	-4 ns to +4 ns, 10 fs resolution, larger delays optional
energy stability	< 10% pulse-to-pulse peak (3% rms)

Harmonic generation conversion to 515 nm, 343 nm or 257 nm central wavelength can be provided

FLASH2 experimental hall 'Kai Siegbahn'

FL24	non-monochromatic FEL photons wavelength range: 4–90 nm fundamental Kirkpatrick-Baez (KB) focusing optics with variable foci down to < 10 µm (FWHM)/unfocussed beam size ≈ 5–10 mm (FWHM, depending on wavelength)	
	optional pump – probe experiments using FLASH2 optical laser system	
	grazing incidence split-and-delay unit with -5/+18 ps time delay	*Univ. Münster*
	about 3 × 4 m platform for user-provided end station	
FL26	non-monochromatic FEL photons wavelength range: 6–90 nm fundamental	
	optional pump – probe experiments using FLASH2 optical laser system	
	Laser-based high harmonic generation VUV source for VUV-XUV pump-probe experiments with up to 50 eV VUV photon energy	*Univ. Hannover*
	permanent end station: - reaction microscope (REMI) for time-resolved AMO spectroscopy - grazing incidence delay-line and refocusing optics: FEL focal spot < 10 µm × 10 µm (FWHM, depending on wavelength) - ±2.7 ps time delay range, 1 fs precision - grating spectrometer for online spectral distribution monitoring and for transient absorption spectroscopy	*MPI-K Heidelberg*

FLASH2 optical / NIR laser system for pump – probe experiments for beamlines FL24 and FL26

central wavelength	700 to 900 nm (fast tuneable)
spectral bandwidth	30 to 100 nm (pre-set for experiment)
intra-burst repetition rate	100 kHz
number of pulses per burst	1–77
pulse duration	15–50 fs FWHM (compressed to 1.1 × bandwidth limit), < 500 fs FWHM (uncompressed)
timing jitter to FEL	typical 190 fs FWHM (typical 35 FWHM with laser arrival monitor)
pulse energy	0–200 µJ (before coupling to chamber), 0–140 µJ (at interaction region)
polarisation	Flexible
focus size (1/e² diameter)	> 50 µm (1/e²)
peak intensity	> 10^{14} W/cm²
time delay to FEL	-1ns to +1 ns, 1 fs resolution, larger delays optional
energy stability	< 10% pulse-to-pulse peak (3% rms)

Harmonic generation conversion to 400 nm and 266 nm central wavelength are available with conversion efficiencies of > 30% SHG, > 5% THG

All FLASH beamlines provide online photon diagnostics for intensity, wavelength and beam position, fast shutter, aperture and filter sets.

PETRA III

Beamlines

PETRA III experimental hall 'Max von Laue'

Beamline and instruments		Operated by
R — *option for remote user operation* M — *option for mail-in service*		
P01	High Resolution Dynamics 10 m U36 | 2.5–80 keV	DESY
	Nuclear resonant scattering	DESY
	Resonant inelastic scattering	DESY | MPI
	X-ray Raman scattering	DESY | MPI
P02.1	Powder Diffraction and Total Scattering 2 m U23 | 60 keV	DESY
M	Standard and *in situ* powder diffraction	DESY
M	Standard and *in situ* total scattering	DESY
P02.2	Extreme Conditions 2 m U23 | 25.6 keV, 42.7 keV	DESY
R	Laser heated experiment for diamond anvil cells (DACs)	DESY
R	General purpose experiment for high pressure DAC applications	DESY
P03	Micro- and Nano-SAXS/WAXS 2 m U29 | 7–21 keV	DESY
	Grazing incidence & transmission micro-beam small and wide-angle scattering	DESY
	Nano-beam scattering and diffraction	DESY | Hereon | collaborators
P04	Variable Polarisation Soft X-rays 5 m UE65 | 250–2800 eV	DESY
	UHV diffractometer and soft X-ray spectrometer	DESY
	Photon-ion spectrometer (PIPE)	DESY | collaborators
	Ultra-high resolution photoelectron spectroscopy (ASPHERE)	DESY | collaborators
	Soft X-ray absorption holographic imaging instrument	DESY | collaborators
	Nano-focus apparatus for spatially resolved spectroscopy	DESY | collaborators
P05	Micro- and Nano-Imaging 2 m U29 | 8–50 keV	Hereon
M	Micro-tomography	Hereon
	Nano-tomography	Hereon
P06	Hard X-ray Micro- and Nano-probe 2 m U32 | 5–45 keV	DESY
	Micro-probe	DESY
	Nano-probe	DESY
P07	High Energy X-ray Materials Science 4 m IVU21 | 50–200 keV	Hereon
	Surface diffraction, grazing incidence total scattering, diffraction tomography	DESY
	Heavy-load diffractometer	Hereon
	Grain mapper	Hereon
	High energy tomography	Hereon
P08	High Resolution Diffraction 2 m U29 | 5.4–29.4 keV	DESY
M	High resolution diffractometer	DESY
	Liquid surface diffractometer	DESY | collaborators
	Langmuir trough in-plane diffractometer	DESY
P09	Resonant Scattering and Diffraction 2 m U32 | 2.7–31 keV	DESY
	Resonant X-ray diffraction at low temperatures (2 K < T < 750 K)	DESY
	Resonant X-ray diffraction in high B-fields (2 K < T < 300 K; B < 14 T, B ⊥ Q)	DESY
	Resonant X-ray diffraction at high pressure (4 K < T < 300 K; p < 30 GPa)	DESY
	X-ray resonant magnetic reflectivity (300 K; B < 0.25 T)	DESY
	Open port	DESY
P10	Coherence Applications 5 m U32 | 4–20 keV	DESY
R	X-ray photon correlation spectroscopy (SAXS/WAXS geometry) (5–15 keV)	DESY
R	Bragg coherent diffraction imaging (5–13 keV)	DESY
R	GINIX — Nano-focusing setup (8 and 13.8 keV)	DESY | collaborators
P11	High-throughput Macromolecular Crystallography 2 m U32 | 2.4–30 keV	DESY
R, M	Macromolecular crystallography (6–26 keV)	DESY | HZI | U Lübeck
M	Serial crystallography (6–26 keV)	DESY

PETRA III experimental hall 'Max von Laue'

Beamline and instruments		Operated by
R — *option for remote user operation* M — *option for mail-in service*		
P12	Bio SAXS 2 m U29 | 4–20 keV	EMBL
R	Small-angle and wide-angle X-ray scattering	EMBL
	Time-resolved X-ray scattering	EMBL
	Anomalous small-angle X-ray scattering	EMBL
P13	Macromolecular Crystallography 2 m U29 | 4.5–17.5 keV	EMBL
R	Macromolecular crystallography	EMBL
P14	Macromolecular Crystallography and Imaging 2 m U29 | 6–20 keV	EMBL
R	Macromolecular crystallography (7–27 keV)	EMBL
R	Serial crystallography (7–18 keV)	EMBL
	High throughput micro-tomography (6–20 keV)	EMBL
	Time-resolved serial crystallography (12.7 keV)	EMBL | U Hamburg

PETRA III experimental hall 'Ada Yonath'

Beamline and instruments		Operated by
R — *option for remote user operation* M — *option for mail-in service*		
P21.1	Swedish Materials Science Beamline side branch: 2 m U29 | 50 keV, 80 keV, 100 keV	Center for X-rays in Swedish Materials Science (CeXS) | DESY
	Diffuse scattering and total scattering	CeXS | DESY
P21.2	Swedish Materials Science Beamline 4 m IVU21 | 40–150 keV	Center for X-rays in Swedish Materials Science (CeXS) | DESY
	Multi-purpose triple-axis diffractometer	CeXS | DESY
	Small-angle scattering	CeXS | DESY (commissioning
	Grain mapper	CeXS | DESY (commissioning)
P22	Hard X-ray Photoelectron Spectroscopy 2 m U33 | 2.4–15 keV	DESY
R	Hard X-ray photoelectron spectrometer (HAXPES)	DESY
R	Ambient pressure XPS (POLARIS)	DESY | collaborators
R	Hard X-ray photoemission electron microscope (HAXPEEM)	DESY | collaborators
P23	*In situ* Nano-Diffraction Beamline 2 m U32 | 5–35 keV	DESY
	XRD and secondary processes, *in situ* and complex environments	DESY
	Hierarchical X-ray imaging	DESY | KIT Start of operation planned for 2023
P24	Chemical Crystallography 2 m U29 | 8 keV, 15–44 keV	DESY
	Single crystal diffraction in complex sample environments	DESY
	Small molecule crystallography	DESY
P25	Beamline for applied bio-medical imaging, powder diffraction and innovation 2m U32 | 8–60 keV	DESY (ITT funded) Start of operation planned for 2024
	X-ray fluorescence imaging (milliprobe) (XFI)	DESY
	Scanning X-ray microscopy (SXRM)	DESY
	High throughput powder diffraction (15–35 keV)	DESY
	PETRA IV test station (white beam)	DESY

PETRA III

Beamlines

PETRA III experimental hall 'Paul P. Ewald'

Beamline and instruments		Operated by
R — *option for remote user operation*	M — *option for mail-in service*	
P61	High Energy Wiggler Beamline 10 × 4 m damping wigglers | white beam btw. 30–250 keV	DESY
	High energy engineering materials science	Hereon
	Large volume press — extreme conditions	DESY
P62	Anomalous Small-Angle X-ray Scattering 2 m U32 | 3.5–35 keV	DESY
	Anomalous small-angle X-ray scattering SAXS tomography	DESY DESY
P63	Material Science Beamline	DESY | MPI Start of operation: not yet defined
	Ex situ and *in situ* XAFS with simultaneous scattering & diffraction	
P64	Advanced X-ray Absorption Spectroscopy 2 m U33 | 4–44 keV	DESY
	Ex situ and *in-situ* XAFS	DESY
	High-resolution X-ray emission spectroscopy (non-resonant and resonant)	DESY
	QEXAFS	DESY
P65	Applied X-ray Absorption Spectroscopy 41 cm U33 | 4–44 keV	DESY
R	*Ex situ* and *in situ* XAFS of bulk samples	DESY
P66	Superlumi *(between PETRA III halls 'Paul P. Ewald' and 'Max von Laue')* Bending magnet | 4–40 eV	DESY
	Time-resolved luminescence spectroscopy	DESY

Beamtime statistics 2022

FLASH

Operation period 2022

During the long FLASH shutdown in 2022, the first FLASH2020+ upgrade was successfully finished (see FLASH article in this report). User operation at FLASH restarted on 7 November 2022 with 5 weeks (≈ 850 h) of user experiments planned in two blocks.

PETRA III

Operation period 2022

	User beamtime	Machine studies and test runs	Maintenance	Shutdown
1 Jan – 9 Dec	4673 h	1432 h	158 h	
planned for 10 Dec – 31 Dec	223 h	61 h		
				2212 h

run periods:
16 Feb – 18 Jul
16 Aug – 19 Dec

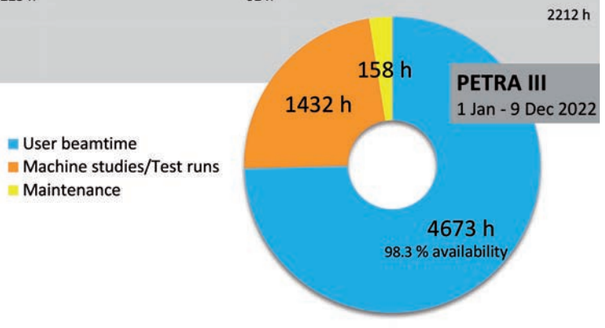

DESY NanoLab

Instruments

DESY NanoLab

Instruments		Operated by
	Sample preparation **(CXNS, ground floor, laboratory 006a and 006b)**	DESY
	2 UHV sample preparation chambers	DESY
	Low energy electron diffraction	DESY
	Zn evaporation chamber	DESY
	Auger electron spectroscopy	DESY
	UHV multi flange tunnel chamber	DESY
	Surface spectroscopy **(CXNS, ground floor, laboratory 006a and 006b)**	DESY
	UHV Infrared reflection absorption spectroscopy (IRRAS)	DESY
	X-ray photoelectron spectroscopy (XPS)	DESY
	Ultraviolet photoelectron spectroscopy (UPS)	DESY
	X-ray diffraction **(building 25, laboratory 023)**	DESY
	UFO chamber, 2 mini reactors, 2 gas mixer	DESY
	2 *in situ* UHV chambers	DESY
	Reflectometer	DESY
	2 six-circle diffractometers	DESY
	Microscopy and nanomanipulation **(CXNS, ground floor, laboratories 001-004, 006a** **PETRA III experimental hall 'Max von Laue', 47c, laboratory L096)**	DESY
	Scanning Auger microscope (SAM)	DESY
	Dual-beam focused ion beam (FIB-SEM)	DESY | Bayreuth University
	High-resolution scanning electron microscope (HR-SEM)	DESY
	Versatile high-resolution atomic force microscope (AFM)	DESY
	UHV scanning tunnelling / atomic force microscope (UHV-STM/AFM)	DESY
	Optical polarisation microscope	DESY
	Sputter coater	DESY
	Physical and magnetic sample characterisation **(CXNS, ground floor, laboratories 014 and 015)**	DESY
	Superconducting magnet	DESY
	Sample cryostat	DESY
	Vibrating sample magnetometer	DESY
	AC Susceptibility	DESY
	AC and DC resistivity and Hall effect	DESY
	AC calorimetry	DESY
	Thermal transport	DESY
	Magnetic microscopy	DESY
	Electrocatalysis and electrochemistry **(building 25b, laboratory 027)**	DESY
	Rotating disc electrode surface X-ray diffraction setup	DESY
	Combined infrared X-ray diffraction setup	DESY | FAU Erlangen-Nürnberg
	Hanging meniscus cell, flow cell	DESY
	Langmuir trough	DESY | CAU Kiel

Acknowledgement
We would like to acknowledge all contributions to the development and operation of FLASH and PETRA III beamlines and instruments provided within the framework of funding from the Federal Ministry of Education and Research (BMBF) 'Verbundforschung/ErUM', and as part of collaborations with the Department of Science and Technology (Government of India) 'India@DESY' and the Ruprecht-Haensel-Laboratory (Christian-Albrechts-Universität zu Kiel).

Committees 2022

Photon Science Committee PSC — advises the DESY Photon Science management

Christian David (chair)	Paul Scherrer Institut, Villigen, CH
Stefan Eisebitt (vice chair)	MBI and Technische Universität Berlin, DE
Serena DeBeer	MPI-CEC, Mülheim an der Ruhr, DE
Kristina Djinovic-Carugo	Universität Wien, AT
Jan-Dierk Grunwaldt	Karlsruher Institut für Technologie, Karlsruhe, DE
Mark Heron	Diamond Light Source Ltd, Didcot, UK
Simo Huotari	University of Helsinki, FI
Oxana Klementieva	Lund University, SE
Sarah Köster	Georg-August-Universität Göttingen, DE
Michael Krisch	ESRF, Grenoble, F
Jan Lüning	Helmholtz-Zentrum Berlin, DE
Edvin Lundgren	Lund University, SE
Thomas Pfeifer	MPI for Nuclear Physics, Heidelberg, DE
Daniela Rupp	Eidgenössische Technische Hochschule Zürich, CH
Bernd Schmitt	Paul Scherrer Institut, Villigen, CH
Thomas Schröder	Humboldt-Universität zu Berlin and IKZ, Berlin, DE
Andrea Somogyi	Synchrotron SOLEIL, Saint-Aubin, FR
Stefan Vogt	Argonne National Laboratory, Lemont, US
Nele Müller, Hermann Franz (PSC secretaries)	DESY, Hamburg, DE

Laser Advisory Committee LAC — advises DESY and European XFEL

Jonathan Zuegel (chair)	Laboratory for Laser Energetics, Rochester, US
Miltcho Danailov	Elettra-Sincrotrone, Trieste, IT
Thomas Dekorsy	Deutsches Zentrum für Luft- und Raumfahrt e.V., Stuttgart, DE
Alan Fry	SLAC, Menlo Park, US
Catherine Le Blanc	Ecole Polytechnique, Laboratoire LULI, FR
Emma Springate	STFC Rutherford Appleton Laboratory, UK
William White	SLAC National Accelerator Laboratory, Menlo Park, US
Andreas Galler (LAC secretary)	European XFEL, Schenefeld, DE
Nele Müller (LAC secretary)	DESY, Hamburg, DE

DESY Photon Science User Committee DPS-UC — represents the user community

Peter Müller-Buschbaum (chair)	Technische Universität München, DE
Natalia Dubrovinskaia	Universität Bayreuth, DE
Markus Mezger	MPI für Polymerforschung, Mainz, DE
Daniela Rupp	Eidgenössische Technische Hochschule Zürich, CH
Gregor Witte	Ludwig-Maximilians-Universität München, DE

Komitee Forschung mit Synchrotronstrahlung KFS — representative body of the German SR and FEL user community

Jan-Dierk Grunwaldt (chair)	Karlsruher Institut für Technologie, Karlsruhe, DE
Sarah Köster (vice chair)	Georg-August-Universität Göttingen, DE
Taisia Gorkhover	Universität Hamburg, DE
Christian Gutt	Universität Siegen, DE
Birgit Kanngießer	Technische Universität Berlin, DE
Dirk Lützenkirchen-Hecht	Bergische Universität Wuppertal, DE
Bridget Murphy	Christian-Albrechts-Universität zu Kiel, DE
Andrea Thorn	Universität Hamburg, DE

The European Synchrotron and FEL User Organisation ESUO (Executive Board)

Cormac McGuinness (ESUO President)	Trinity College Dublin, IE
Carla Bittencourt	Université de Mons, BE
Wojciech Gawelda	Universidad Autónoma de Madrid, ES
Tom P. Hase	University of Warwick, UK
Rainer Lechner	Montanuniversität Leoben, AT
Derek Logan	Lund University, SE
Bridget Murphy	Christian-Albrechts-Universität zu Kiel, DE
Moniek Tromp	Rijksuniversiteit Groningen, NL

For national delegates please see: www.esuo.eu/user-representation/user-delegates-representatives/

Project Review Panels 2022

Bulk and surface diffraction — P08 | P23 | P24

Derek (Del) Atkinson	Durham University, UK
Jan Ingo Flege	Brandenburgische Tech. Univ. Cottbus-Senftenberg, DE
Michael Hanke	Paul-Drude-Institut für Festkörperelektronik, Berlin, DE
Christiane A. Helm	Universität Greifswald, DE
Beate Kloesgen	Syddansk Universitet Odense, DK
Fouad Maroun	Ecole Polytechnique Palaiseau, FR
Reinhard Neder	Friedrich-Alexander-Universität Erlangen-Nürnberg, DE
Beatriz Noheda	Universiteit Groningen, NL
Oliver Oeckler	Universität Leipzig, DE
Sander van Smaalen	Universität Bayreuth, DE
Hans-Georg Steinrück	Universität Paderborn, DE
Chandan Upadhyay	Indian Institute of Technology, Varanasi, IN
Matthias Zschornak	Technische Universität Bergakademie Freiberg, DE
Florian Bertram, Dimitri Novikov, Martin Tolkiehn (PRP secretaries)	DESY, Hamburg, DE

Coherent applications — P10

Sylvain Bohic	Research Centre INSERM, Grenoble, FR
Manfred Burghammer	ESRF, Grenoble, FR
Ralf Busch	Universität des Saarlandes, Saarbrücken, DE
Birgit Hankiewicz	Universität Hamburg, DE
Michael Paulus	Universität Dortmund, DE
Ullrich Pietsch	Universität Siegen, DE
Beatrice Ruta	Université Claude Bernard, Lyon, FR
Jesper Wallentin	Lund University, SE
Michael Sprung (PRP secretary)	DESY, Hamburg, DE

EXAFS — P64 | P65

Dmitry Doronkin	Karlsruher Institut für Technologie, Karlsruhe, DE
Stephan Klemme	Westfälische Wilhelms-Universität, Münster, DE
Dorota Koziej	Universität Hamburg, DE
Aleksej Kuzmin	University of Latvia, Riga, LV
Dooshaye Moonshiram	Materials Science Institute of Madrid, ES
Christina Roth	Universität Bayreuth, DE
Karel Saksl	Slovak Academy of Sciences, Kosice, SK
Claudia Schnohr	Universität Leipzig, DE
Roland Schoch	Universität Paderborn, DE
Kajsa Sigfridsson Clauss	MAX IV Laboratory, Lund, SE
Andrea Zitolo	Synchrotron SOLEIL, Gif-sur-Yvette, FR
Wolfgang Caliebe, Edmund Welter (PRP secretaries)	DESY, Hamburg, DE

Extreme conditions — P02.2 | P61 LVP

Martin Bremholm	Aarhus University, DK
Daniel Errandonea	Universitat de València, ES
Nadège Hilairet	Université des Sciences et Techniques, Lille, FR
Holger Kohlmann	Universität Leipzig, DE
Sergey Lobanov	Deutsches GeoForschungsZentrum, Potsdam, DE
Paolo Lotti	Università degli Studi di Milano Statale, Milano, IT
Sergey Medvedev	MPI für Chemische Physik fester Stoffe, Dresden, DE
Marco Merlini	Università degli Studi di Milano Statale, Milano, IT
Hauke Marquardt	University of Oxford, UK
Guillaume Morard	Sorbonne Université, Paris, FR
Chrystele Sanloup	Sorbonne Université, Paris, FR
Bjoern Winkler	Goethe-Universität Frankfurt am Main, DE
Tony Withers	Universität Bayreuth, DE
Hanns-Peter Liermann, Robert Farla (PRP secretaries)	DESY, Hamburg, DE

HAXPES — P22

Maria Hahlin	Uppsala Universitet, SE
Martina Müller	Universität Konstanz, DE
Christian Papp	Friedrich-Alexander-Universität Erlangen-Nürnberg, DE
Christoph Rameshan	Technische Universität Wien, AT
Anna Regoutz	University College London, UK
Vladimir N. Strocov	Paul Scherrer Institut, Villigen, CH
Christoph Schlüter (PRP secretary)	DESY, Hamburg, DE

Project Review Panels 2022

High energy diffraction — P07 (DESY) | P21.1 | P21.2

Frauke Alves	Georg-August-Universität, Göttingen, DE
Emil Bozin	Brookhaven National Laboratory, Upton, US
William Brant	Uppsala Universitet, SE
Olaf Borkiewicz	Argonne National Laboratory, Lemont, US
Per-Anders Carlsson	Chalmers Tekniska Högskola, Gothenborg, SE
Magnus Colliander	Chalmers Tekniska Högskola, Gothenborg, SE
Margit Fabian	Centre for Energy Research, MTA, Budapest, HU
Jens Gibmeier	Karlsruher Institut für Technologie, Karlsruhe, DE
Julia Herzen	Technische Universität München, Garching, DE
Kirsten Marie Jensen	University of Copenhagen, DK
Simon Kimber	Université Bourgogne Franche-Comté, Dijon, FR
Matt Miller	Cornell University, Ithaca, US
Herbert Over	Justus-Liebig-Universität, Gießen, DE
Tobias Ritschel	Technische Universität Dresden, DE
Joachim Wollschläger	Universität Osnabrück, DE
Ann-Christin Dippel, Martin von Zimmermann, Ulrich Lienert (PRP secretaries)	DESY, Hamburg, DE

Imaging — P05 | P06

Matthias Alfeld	Delft University of Technology, NL
Martin Bech	Lund University, SE
Ulrike Boesenberg	European XFEL, Schenefeld, DE
Asuncion Carmona	Centre d'Etudes Nucléaires de Bordeaux Gradignan, FR
David Fenning	University of California, San Diego, US
Frank Friedrich	Universität Hamburg, DE
Sebastian Kalbfleisch	MAX IV Laboratory, Lund, SE
Florian Meirer	University of Utrecht, NL
Bert Mueller	Universität Basel, Allschwil, CH
Guillermo Requena	RWTH Aachen, DE
Jürgen Thieme	Brookhaven National Laboratory, Upton, US
Katarina Vogel-Mikus	University of Ljubljana, SI
Ulrich Vogt	Royal Institute of Technology, Stockholm, SE
Benjamin Wipfler	Zool. Forschungsmuseum Alexander Koenig, Bonn, DE
Fabian Wilde, Gerald Falkenberg (PRP secretaries)	DESY, Hamburg, DE

Inelastic, magnetic and resonant scattering — P01 | P09

Manuel Angst	Forschungszentrum Jülich GmbH, DE
Elizabeth Blackburn	Lund University, SE
Kristina Kvashnina	Helmholtz-Zentrum Dresden-Rossendorf (HZDR), DE
Catherine McCammon	Universität Bayreuth, DE
Daniel Merkel	Wigner Research Centre for Physics, Budapest, HU
Marco Moretti	Politecnico di Milano, IT
Valerio Scagnoli	ETH Zürich, CH
Volker Schünemann	Technische Universität Kaiserslautern, DE
Joachim von Zanthier	Friedrich-Alexander-Universität Erlangen-Nürnberg, DE
Ilya Sergeev, Sonia Francoual (PRP secretaries)	DESY, Hamburg, DE

Materials science (Hereon) — P07 (Hereon) | P61 (Hereon)

Jeremy Epp	Leibniz-IWT, Bremen, DE
Guillaume Geandier	Institut Jean Lamour, Nancy, FR
Astrid Haibel	Beuth Hochschule für Technik, Berlin, DE
Christian Krempaszky	Technische Universität München, DE
Ingo Manke	Helmholtz-Zentrum Berlin f. Materialien und Energie, DE
Thomas Niendorf	Universität Kassel, DE
Wolfgang Pantleon	Technical University of Denmark, Lyngby, DK
Walter Reimers	Technische Universität Berlin, DE
Georg Schulz	Universität Basel, CH
Carsten Siemers	Technische Universität Braunschweig, DE
Dieter Lott (PRP secretary)	Helmholtz-Zentrum Hereon, DE

Powder diffraction — P02.1

Dorthe Bomholdt Ravnsbæk	Syddansk Universitet, Odense, DK
Gregor Kieslich	Technische Universität München, Garching, DE
Michael Knapp	Karlsruher Institut für Technologie, Karlsruhe, DE
Daria Mikhailova	Leibniz-Institut für Festkörper- und Werkstoff-forschung, Dresden, DE
Martin Sahlberg	Uppsala Universitet, SE
Anatoliy Senyshyn	Technische Universität München, Garching, DE
Florian Spieckermann	Montanuniversität, Leoben, AT
Claudia Weidenthaler	MPI für Kohlenforschung, Mülheim a.d. Ruhr, DE
Mirijam Zobel	Universität Bayreuth, DE
Martin Etter (PRP secretary)	DESY, Hamburg, DE

SAXS/WAXS/GISAXS — P03 | P62

Alexander Gerlach	Universität Tübingen, DE
Thomas Hellweg	Universität Bielefeld, DE
Marianne Liebi	Chalmers Tekniska Högskola, Gothenborg, SE
Fredrik Lundell	Royal Institute of Technology, Stockholm, SE
Giuseppe Portale	Universiteit Groningen, NL
Konrad Schneider	Leibniz-Institut für Polymerforschung Dresden e.V., DE
Qi Zhong	Zhejiang Sci-Tech University, Hangzhou, CN
Stephan Roth, Sylvio Haas (PRP secretaries)	DESY, Hamburg, DE

Soft X-ray and VUV — P04 | P66

Yves Acremann	ETH Zürich, CH
Paola Bolognesi	CNR-ISM, Istituto di Struttura della Materia, Roma, IT
Arno Ehresmann	Universität Kassel, DE
Mark Golden	Universiteit van Amsterdam, NL
Aleksandr Luštšik	University of Tartu, EE
Jan-Erik Rubensson	Uppsala Universitet, SE
Yasmine Sassa	Chalmers Tekniska Högskola, Gothenborg, SE
Emma Sokell	University College Dublin, IE
Anna Vedda	Università di Milano-Bicocca, Milano, IT
Moritz Hoesch, Aleksei Kotlov (PRP secretaries)	DESY, Hamburg, DE

Soft X-ray FEL experiments — FLASH

Christoph Bostedt	Paul Scherrer Institut, Villigen, CH
Majed Chergui	École Polytechnique Fédérale de Lausanne, CH
Hermann Dürr	Uppsala Universitet, SE
Irene Groot	Universiteit Leiden, NL
Marion Harmand	Sorbonne Université, Paris, FR
Michael Meyer	European XFEL, Schenefeld, DE
Robert Schoenlein	SLAC National Accelerator Laboratory, Menlo Park, US
Christian Schüssler-Langeheine	Helmholtz-Zentrum Berlin, DE
Marc Simon	Sorbonne Université, Paris, FR
Julia Stähler	Humboldt-Universität zu Berlin, DE
Martin Weinelt	Freie Universität Berlin, DE
Philippe Wernet	Uppsala Universitet, SE
Elke Plönjes-Palm, Rolf Treusch (PRP secretaries)	DESY, Hamburg, DE

PEC: EMBL Life Science beamlines P12–P14 / PRP Bio-crystallography at P11

Savvas Savvides	Ghent University, BE
Pau Bernadó	CBS/CNRS, Montpellier, FR
Gwyndaf Evans	Diamond Light Source, Didcot, GB
Robert Fischetti	Argonne National Laboratory, Lemont, US
Mariusz Jaskolski	Adam Mickiewicz University of Poznan, PL
Gergely Katona	University of Gothenburg, SE
Annette E. Langkilde	University of Copenhagen, DK
Javier Pérez	Synchrotron SOLEIL, Saint-Aubin, FR
Teresa Santos-Silva	Universidade NOVA de Lisboa, PT
Zehra Sayers	Sabanci University, Istanbul, TR
Joel L. Sussman	Weizmann Institute of Sciences, Rehovot, IL
Maria A. Vanoni	Università degli Studi di Milano, IT
Mark J. van Raaij	Centro Nacional de Biotecnologia, Madrid, ES
Gregor Witte	Ludwig-Maximilians-Universität München, DE
Christian Schroer (DESY observer)	DESY, Hamburg, DE

Photographs and Graphics

Franziska Ahnert, HPI
BWFGB Hamburg
Christian-Albrechts-Universität zu Kiel
CFEL
CMWS
Marcus Creutzburg, DESY
CSSB
DASHH
DESY
K.H. Diddens
EMBL
European XFEL
Heinle, Wischer + Partner
Axel Heimken, Kiel
Helmholtz-Zentrum Hereon
IEEE Photonics Society
Markus Ilchen, DESY
Jakob Kibsgaard, DTU
Maxime Killer, EMBL
Jochen Küpper, DESY
Adrienne Lochte, Academy of Sciences
C. Lopez-Gonzalez, DESY
Christina Mänz, DESY
Markus Marcetic, KVA,
Marta Mayer, DESY
MPG
Heiner Müller-Elsner, Hamburg
Jörg Harms, MPSD,
MST/TU Dresden
Daniel Novakovič, STA
Agnieszka Obarska-Kosińska, EMBL
Markus Osterhoff, Universität Göttingen
Vincent Perrichot
Daniel Reinhardt, DESY
Isabel Romero Calvo, EMBL
Reimo Schaaf, Hamburg
SESAME Synchrotron, Jordan
Shosho
Stefanie Tille, HELIOS
Diana von Ilsemann, DESY
Universität Hamburg
K. Winkler, PHGS

Acknowledgement
We would like to thank all authors and all who have contributed to the realisation of this Annual Report.

Imprint

Publishing and Contact:
Deutsches Elektronen-Synchrotron DESY
A Research Centre of the Helmholtz Association

Hamburg location:
Notkestr. 85, 22607 Hamburg, Germany
Tel.: +49 40 8998-0, Fax: +49 40 8998-3282
desyinfo@desy.de

Zeuthen location:
Platanenallee 6, 15738 Zeuthen, Germany
Tel.: +49 33762 7-70, Fax: +49 33762 7-7413

Photon Science at DESY
Tel.: +49 40 8998-2304, Fax: +49 40 8998-4475
photon-science@desy.de
photon-science.desy.de

www.desy.de

ISBN 978-3-945931-43-1
DOI 10.3204/PUBDB-2022-07678

Online version:
photon-science.desy.de/annual_report

Realisation:
Wiebke Laasch, Daniela Unger

Editing:
Sadia Bari, Krishnayan Basuroy, Lars Bocklage, Christina Bömer, Günter Brenner, Thomas Keller, Dmytro Kutnyakhov, Wiebke Laasch, Britta Niemann, Christoph Schlüter, Markus Scholz, Sang-Kil Son, Sebastian Trippel, Daniela Unger

Layout: Sabine Kuhls-Dawideit, Büro für Grafik und Design, Halstenbek

Printing and image processing: EHS Druck GmbH, Schenefeld

Copy deadline: December 2022

HELMHOLTZ
RESEARCH FOR GRAND CHALLENGES

Deutsches Elektronen-Synchrotron DESY
A Research Centre of the Helmholtz Association

The Helmholtz Association is a community of 18 scientific-technical and biological-medical research centres. These centres have been commissioned with pursuing long-term research goals on behalf of the state and society. The Association strives to gain insights and knowledge so that it can help to preserve and improve the foundations of human life. It does this by identifying and working on the grand challenges faced by society, science and industry. Helmholtz Centres perform top-class research in strategic programmes in six core fields: Energy, Earth & Environment, Health, Aeronautics, Space and Transport, Matter, and Key Technologies.

www.helmholtz.de